

Real-time Integrity Monitoring of High Pressure Membranes

Eddy Ostarcevic

**A thesis submitted in fulfilment of the requirement
for the degree of Doctor of Philosophy**



**Institute for Sustainability and Innovation
College of Engineering and Science
Victoria University**

February 2016

ABSTRACT

Growing water scarcity and deteriorating quality is forcing the re-evaluation of the single use nature of water consumption. Consequently, water reclamation, or the multiple use of a water resource, is considered an effective way to extend resource availability. Multiple use of a water resource for direct potable water production requires the use of reverse osmosis (RO) membrane systems to reject the passage of microbiological contamination including pathogens such as virus. The performance of membrane systems as a barrier to protect public health must be routinely challenged using a surrogate for the smallest pathogen by integrity tests.

The aim of this research was to develop a new integrity monitoring technique that could identify the rejection capacity for pressure driven membrane systems in real-time. The research objectives included the development of a suitable non-microbial virus surrogate and an integrated quantification technique that identified the rejection performance across a membrane system in real-time with high resolution and reliability. Sensitivity and precision are critical to the successful application for any new membrane system challenge test.

Ideally, pressure driven membranes such as RO, should provide a complete physical barrier to the passage of pathogens, such as enteric viruses. In reality, manufacturing imperfections combined with membrane ageing and damage can result in breaches as small as 20 to 30 nm in diameter, sufficient to allow enteric viruses to contaminate the treated water compromising public health.

Existing membrane integrity monitoring systems are limited and health regulators credit RO systems with only $2 \log_{10}$ rejection, well below their capability. A reliable real-time method that can recognise the true rejection potential of membrane systems greater than $4 \log_{10}$ rejection has not yet been established.

Fluorescence and light scattering measurement techniques were identified and assessed using a selection of commercially available non-microbial surrogate dyes and a synthesised polymer nanoparticle. Membrane integrity challenge tests using these non-microbial surrogates were undertaken to determine the potential to measure the rejection capacity at $4 \log_{10}$ or better at bench, pilot and full-scale. These integrity tests were compared against conventional microbial surrogate challenge test using MS2 bacteriophage at full-scale and an assessment of LRV and variability was determined.

A new membrane integrity monitoring technique based on a synthesised 30 nm diameter polymer nanoparticle integrated with light scattering intensity measurement was shown to provide high sensitivity and better than $4 \log_{10}$ rejection with low variability. Synthesised nanoparticle measurements were shown to be more representative of concentration gradients across a membrane array when compared to fluorescent dyes such as Rhodamine WT. Nanoparticle measurements were also shown to be more stable than the variable nature of fluorescence measurements of applied dyes at LRV greater than $4 \log_{10}$ rejection. While microbial surrogates such as MS2 bacteriophage offered the potential for higher LRV credits the use of a nanoparticle as a non-microbial surrogate was able to be detected in real-time, online; a response that microbial surrogates are unable to provide. Real-time measurement and monitoring of membrane integrity

and LRV performance using the optical properties of nanoparticles has been shown to provide greater precision compared to fluorescent dyes and microbial surrogates. The technique has the potential to provide greater confidence in high pressure membrane system performance and move closer to recognising their true performance capability.

ACKNOWLEDGEMENTS

This research would not have been possible without the long-term patience, encouragement, enthusiasm, guidance, humour and gentle, but persistent prodding, provided by my mentors, supervisors and friends Professor Stephen Gray and Dr Marlene Cran. The knowledge they willingly shared and the kindness shown to this student was, and continues to be, an amazing gift that will remain with me for a lifetime. I firmly believe that during this research I have stood on the shoulders of giants such as Rayleigh, Planck and Bohr and certainly contemporary giants Professor Stephen Gray and Dr Marlene Cran who as Principal Supervisor and Co-Supervisor have shaped and guided my research pathway.

I acknowledge and thank my darling wife, Diane, who has now experienced two of these events and has endured the experience for such a long time. Her patience and support have endured for over three decades and continues to be my rock and anchor. My previous acknowledgement to my wife stated that “*We enter a new phase of life – A.T. (After Thesis)*”, well we can now extend that to a newer phase we will call “life after thesis eventually”, or L.A.T.E. Our children, Claire and Angus, have been ever so patient and have willingly supported my drive to reach the end of this work, now it is your time to enjoy unlimited attention, for better or for worse!

I am grateful for the financial support provided by Water Research Australia with substantial financial contributions from Grampians Wimmera Mallee Water (GMMWater) and Coliban Water. Thanks and appreciation goes to my friends and colleagues Mr Paul Atherton (formerly from GMMWater) and Dr Dharma

Dharmabalan (formerly Coliban Water now with TasWater) for their enthusiastic support.

Special thanks go to Dr Stuart Rumble who was able to shine a light on the physics behind light scattering and who was able to educate me in the ways of light energy very much like a modern Jedi. Dr Rumble continues to be a beacon in the world of classical and quantum physics with particular focus on the light scattering phenomenon.

My thanks go to undergraduate students Will Collins, Robin Degginger, Chathuri Piyadasa, David Terrien, and Celine Zaetta that visited ISI as interns, for the support provided during the data collection phase of the research. I am sure that David in particular enjoyed his sheep shearing experience at our farm where he literally rode on the sheep's back.

My gratitude goes to Mrs Elizabeth Smith who looked after me and always provided sound advice. I could always sense the smile when we spoke and her quick responses ensured that my enrolment was current or progress reports were delivered. Thank you Liz for going above and beyond to help a student in rural Victoria continue towards completion.

My thanks go to Dr Jianhua Zhang for providing an opportunity to test the capability of the integrity test at pilot scale for an extended period of time. In addition, Mrs Catherine Enriquez and the members of the ISI team who always encouraged me to develop and complete this research, the light at the end of the tunnel was sunshine indeed!

DECLARATION BY AUTHOR

I, Eddy Ostarcevic, declare that the PhD thesis entitled “Real-time Integrity Monitoring of High Pressure Membranes” is no more than 100,000 words in length including quotes and exclusive of tables, figures, appendices, bibliography, references and footnotes. This thesis contains no material that has been submitted previously, in whole or in part, for the award of any other academic degree or diploma. Except where otherwise indicated, this thesis is my own work.

Signature: 

Date: 26/02/2016

NOMENCLATURE

Acronyms

ASTM	American Society for Testing and Materials
AWRCoE	Australian Water Recycling Centre of Excellence
AWWA	American Water Works Association
AwwaRF	American Water Works Association Research Foundation
CRMWD	Colorado River Municipal Water District
ISO	International Organisation for Standardisation
UNESCO	United Nations Educational, Scientific and Cultural Organisation
UNWWAP	United Nations World Water Assessment Programme
UOSA	Upper Occoquan Service Authority
USEPA	United States Environment Protection Authority

Abbreviations

ATR	attenuated total reflectance
BGIT	binary gas integrity test
BOD	biochemical oxygen demand
CBMS	chemical biological mass spectrometer
CFU	colony forming units
COD	chemical oxygen demand
DNA	deoxyribonucleic acid
DPR	direct potable reuse
EC	electrical conductivity ($\mu\text{s}/\text{cm}$)
EEM	emission excitation matrix
EWFOs	evanescent wave fiber optic sensors
fDOM	fluorescent dissolved organic matter
FNP	fluorescent nanoparticles
FRET	fluorescence resonance energy transfer
FTIR	Fourier transform infrared spectroscopy
IPR	indirect potable reuse
LRV	log reduction value
LSC	laser scanning cytometry
MF	microfiltration
MP	mixed permeate

MR	magnetic resonance
MWCO	molecular weight cut-off
NF	nanofiltration
NOM	natural organic matter
NTA	nanoparticle tracking analysis
PAC	powdered activated carbon
PDT	pressure decay test
PFU	plaque forming units
PIT	pulsed integrity monitoring
QD	quantum dot
RNA	ribonucleic acid
RO	reverse osmosis
RS	Rayleigh scattering
RT-PCR	real-time polymerase chain reaction
SEM	scanning electron microscope
SGAW	surface generated acoustic wave biosensors
SIM	spiked integrity monitoring
SPR	surface plasmon resonance biosensors
TDS	total dissolved salts
TMP	transmembrane pressure
TOC	total organic carbon
TOC	total organic carbon
UF	ultrafiltration
VDT	vacuum decay test
WGM	whispering gallery mode
ZAPS	zero angle photo-spectrometry

Chemicals

APS	ammonium persulphate
BSA	bovine serum albumin
MMA	methyl methacrylate
PEI	polyethyleneimine
PMMA	poly(methyl methacrylate)
PS	polystyrene
PVC	poly(vinyl chloride)

Symbols (dyes)

BB	Brilliant Blue
FG	Fast Green
FL	Fluorescein
QN	Quinine
RB	Vitamin B12
RWT	Rhodamine WT
UR	Uranine
PyTS	1,3,6,8 pyrenetetrasulphonic acid tetrasodium salt (TRASAR)

Measurement, Units

λ	wavelength (nm)
C_f	concentration of challenge species in RO feed
C_p	concentration of challenge species in RO permeate
c	speed of light (2.998×10^8 m/s)
Da	Dalton
E	energy (eV)
h	Planck's constant (6.626×10^{-34} Joule.s)
kPa	pressure unit
nm	Nanometres
mg/L	milligrams per litre
$\mu\text{g/L}$	micrograms per litre
pH	measure of acidity or alkalinity [$-\log_{10}(\text{H}^+)$]

TABLE OF CONTENTS

Abstract	i
Acknowledgements	iv
Declaration by Author	vi
Nomenclature	vii
List of Figures	xvi
List of Tables	xxi
Chapter 1 Introduction	1
1.1 Water Reuse and Recycling	5
1.1.1 Uses and Benefits of Recycled Water	6
1.1.2 Recycled Water Production, Classification and Challenges	7
1.2 Public Perceptions of Recycled Water	8
1.3 Significance of this Research	11
1.4 Research Objectives	12
1.5 Thesis Outline	13
Chapter 2 Current and Emerging Membrane Integrity Tests	17
2.1 Introduction	17
2.2 The Target - Poliovirus	19
2.3 The “Ideal” Integrity Test	22
2.4 Direct Integrity Monitoring	23
2.4.1 Vacuum Decay Testing	25
2.4.2 Pressure Decay Testing	28
2.5 Indirect Integrity Monitoring	28
2.5.1 Challenge Testing	29
2.5.2 Particle Monitoring	30
2.5.3 Turbidity Monitoring	31
2.5.4 Sulphate Monitoring	31
2.5.5 Conductivity Monitoring	32
2.5.6 Total Organic Carbon Monitoring	34
2.5.7 Periodic Testing	35
2.5.8 Dye Testing	37
2.5.9 Microbial Surrogates	39

2.5.10	Non-microbial Surrogates	40
2.5.11	Spiked Integrity Monitoring	42
2.5.12	Pulse Integrity Test	42
2.5.13	TRASAR® Testing.....	43
2.6	Integrated and Multi-Parameter Monitoring Systems	44
2.6.1	Small Sensor Cell Membrane Testing	44
2.6.2	Binary Gas Integrity Testing.....	45
2.6.3	ZAPS LiquiD Station.....	45
2.7	Pathogen Detection Systems	46
2.7.1	BioSentry Device	47
2.7.2	Real-time Polymerase Chain Reaction Monitoring	47
2.7.3	Evanescent Wave Fiber Optic Sensors	48
2.7.4	Surface Generated Acoustic Wave Biosensors	48
2.7.5	RAPTOR Fiber Optic Biosensors.....	49
2.7.6	Block II Chemical Biological Mass Spectrometer	49
2.7.7	Miniaturised Portable Biosensors	50
2.7.8	Microarray Biosensors	50
2.7.9	Surface Plasmon Resonance Biosensors.....	50
2.7.10	Quantum Dot Based DNA Nanosensors.....	51
2.7.11	Laser Scanning Cytometry.....	52
2.7.12	Microfluidic Biochip Systems	52
2.8	Emerging Techniques	53
2.8.1	NanoSight Particle Tracking	53
2.8.2	Online Chemical Oxygen Demand.....	54
2.8.3	Whispering Gallery Microlasers	55
2.8.4	Fluorescence Emission Excitation Matrices.....	55
2.8.5	Quantum Dots.....	57
2.9	Patented Integrity Monitoring Techniques	58
2.10	Discussion – Potential Techniques for Further Development	59
2.11	Towards a New Membrane Integrity Monitoring Technique	65
Chapter 3 Screening Food Grade Dyes and Fluorescent Compounds		66
3.1	Preamble.....	66
3.2	Introduction.....	66

3.3	Fluorescence.....	68
3.4	Screening Methods	70
3.4.1	Potential Surrogates	70
3.4.2	Surrogate Detection Limit and Calibration	70
3.4.3	Effect of Temperature	76
3.4.4	Effect of Sample pH.....	76
3.4.5	Effect of UV Light Exposure.....	76
3.4.6	Effect of Water Chemistry	77
3.4.7	Bench-scale Continuous Dose Dye Testing.....	77
3.4.8	Bench-scale Pulsed Dose Dye Testing.....	78
3.4.9	Dye Absorbance	80
3.5	Results and Discussion	80
3.5.1	Food Dye Screening.....	80
3.5.2	Fluorescent Dye Screening.....	86
3.6	Bench-scale Challenge Test Results.....	96
3.6.1	Continuous Dosing Challenge Test	97
3.6.2	Pulsed Dosing Challenge Tests.....	98
3.6.3	Pulsed Dosing on Applied Defects.....	102
3.6.4	Dye Adsorption	105
3.7	Conclusions.....	108
Chapter 4 Fluorescent Polystyrene Nanoparticles		111
4.1	Preamble	111
4.2	Introduction.....	112
4.3	Materials and Methods	116
4.4	Results and Discussion	119
4.4.1	Calibration and Screening.....	119
4.4.2	Toxicity and Costs	128
4.4.3	Screening Summary	129
4.5	Conclusions.....	130
Chapter 5 Synthesis of PMMA Nanoparticles.....		133
5.1	Preamble	133
5.2	Introduction.....	133
5.2.1	Poly(methyl methacrylate) (PMMA)	134

5.2.2	Synthesis of PMMA	135
5.2.3	Free Radical Polymerization	139
5.2.4	Surfactant Aided Emulsion.....	141
5.3	Aims	142
5.4	Materials and Methods	143
5.4.1	Materials	143
5.4.2	Preparation of PMMA Nanoparticles.....	143
5.4.3	PMMA Characterization	145
5.5	Results and Discussion	146
5.5.1	General PMMA Synthesis.....	147
5.5.2	Effect Polymerization Time	148
5.5.3	Effect of Processing Temperature	151
5.5.4	Effect of Flask Volume and Stirring.....	154
5.5.5	Effect of Initiator.....	155
5.5.6	Effect of Monomer Concentration	156
5.5.7	Effect of Surfactant	158
5.5.8	Effect of Acetone Co-solvent	161
5.5.9	Effect of Nitrogen Purge	165
5.5.10	Addition of Fluorescent Dyes	166
5.5.11	Light scattering of PMMA.....	170
5.6	Conclusions.....	172
Chapter 6 Rayleigh Scattering as a Membrane Integrity Monitoring Tool.....		175
6.1	Preamble	175
6.2	Introduction.....	176
6.2.1	Light Scattering.....	178
6.2.2	Rayleigh Scattering.....	180
6.2.3	Blue Light Scattering.....	181
6.2.4	Resonant Rayleigh Scattering, or is it?	182
6.3	Research Objectives	187
6.4	Materials and Methods	188
6.4.1	Synthesis of PMMA	188
6.4.2	Wastewater Sampling.....	189
6.4.3	Measurement of Rayleigh Scattering.....	189

6.4.4	Bench-Scale Challenge Testing.....	190
6.4.5	Pilot-Scale Challenge Testing.....	190
6.4.6	Full-scale Challenge Testing.....	191
6.4.7	Challenge Tests.....	193
6.4.8	Dye Analysis.....	195
6.4.9	PMMA Analysis.....	195
6.4.10	MS2 Bacteriophage Enumeration.....	196
6.5	Results and Discussion.....	197
6.5.1	Secondary Spectral Lines.....	197
6.5.2	Analysis of Class A Water.....	200
6.5.3	Scattered Light Response.....	207
6.5.4	Bench-scale Detection of Applied Defects.....	211
6.5.5	Pilot Testing.....	213
6.5.6	Full-Scale Challenge Testing.....	215
6.5.7	Full-scale Nanoparticle Challenge Test.....	216
6.5.8	Full-scale Mixed Tracer Dye Test.....	218
6.5.9	Full-scale MS2 Challenge Test.....	221
6.5.10	Full-scale Salt Rejection.....	225
6.5.11	Commercial Instruments.....	227
6.5.12	Costs to Implement at Full-scale.....	230
6.6	Conclusions.....	234
Chapter 7 Conclusions and Recommendations.....		238
7.1	The Target.....	238
7.2	Implications from the Findings.....	240
7.2.1	Chemical Dyes.....	241
7.2.2	Fluorescent Dyes and Chemicals.....	242
7.2.3	Pulsed Integrity Test.....	248
7.2.4	Fluorescent Nanoparticles.....	249
7.2.5	New Membrane Integrity Monitoring Technique.....	251
7.3	Limitations.....	257
7.3.1	Laboratory Scale Synthesis.....	257
7.3.2	Error Analysis.....	257
7.3.3	Integrity Monitoring.....	258

7.3.4	Instrumentation	259
7.3.5	MS2 Bacteriophage Integrity Test.....	260
7.4	Recommendations for Future Directions	261
7.4.1	Low Pressure Membrane Integrity Monitoring	262
7.4.2	Particle Size Identification.....	262
7.4.3	Hydraulic Modelling for Integrity Breach Identification	263
7.4.4	Use and Interpretation of Integrity Challenge Test Results.....	263
7.5	The End.....	264
	Bibliography.....	266
	Appendix A	293

LIST OF FIGURES

Figure 1.1: Cartoon showing public perception towards recycled water	9
Figure 2.1: Schematic representation of membrane barrier performance	18
Figure 2.2: An image of the poliovirus capsid and RNA	22
Figure 2.3: Schematic illustration of VDT apparatus.	26
Figure 2.4: VDT results from two different RO membranes.....	27
Figure 2.5: Calculated LRVs as a function of feed/permeate concentration.	30
Figure 2.6: Example of conductivity monitoring for RO systems	33
Figure 2.7: Schematic representation of conductivity probing setup	36
Figure 2.8: Conductivity probing of breached pressure vessel	36
Figure 2.9: Permeate EC profile from a fourth stage RO.....	37
Figure 2.10: Examples of EEMs from RO feed and permeate.....	56
Figure 3.1: Energy interaction with a molecule creating fluorescence	69
Figure 3.2: Interaction of light with a molecule or particle.....	69
Figure 3.3: Schematic diagram of continuous dose dye challenge test.	78
Figure 3.4: Schematic diagram of pulsed dye challenge test.	79
Figure 3.5: Optimal wavelengths for selected food grade dyes.	81
Figure 3.6: Calibration curves for selected food grade dyes.....	82
Figure 3.7: Calibration curve of FG and BB dyes.	82
Figure 3.8: Effect of pH on FG and BB dyes.	83
Figure 3.9: Effect of temperature on FG and BB dyes.....	84
Figure 3.10: Effect of UV exposure on FG and BB dyes.	85
Figure 3.11: Effect of oxidants on FG and BB dyes.....	85
Figure 3.12: Effect of environmental conditions on FG and BB dyes.	86
Figure 3.13: Calibration curves of fluorescent dyes.....	87
Figure 3.14: Effect of temperature on dye fluorescence.	88

Figure 3.15: Effect of pH on dye fluorescence.....	89
Figure 3.16: Effect of NaCl on dye fluorescence.	90
Figure 3.17: Effect of CaCl ₂ on dye fluorescence.....	91
Figure 3.18: Effect of residual chlorine on dye fluorescence.	92
Figure 3.19: Effect of chloramine on dye fluorescence.....	93
Figure 3.20: Effect of UV exposure on dye fluorescence.	94
Figure 3.21: Change in fluorescence of dyes in RO feedwater.	95
Figure 3.22: Concentration of RWT with time for 10 mg/L pulsed dose.....	99
Figure 3.23: Concentration of UR with time for 10 mg/L pulsed dose.	100
Figure 3.24: Concentration of PyTS with time for 10 mg/L pulsed dose.....	101
Figure 3.25: Comparison of pulsed and continuous dose LRVs.....	102
Figure 3.26: Pulse dose curves for (a) RWT, (b) UR, and (c) PyTS.	103
Figure 3.27: Photograph of (a) stained and (b) new reference membrane.	106
Figure 3.28: Concentration of RWT over 3 hours continuous dosing.	107
Figure 4.1: SEM image of PR microspheres.	118
Figure 4.2: Calibration curves of Sigma nanoparticles.	119
Figure 4.3: Calibration curves of Polysciences nanoparticles.....	120
Figure 4.4: Calibration curves of UR dye and YG nanoparticles.	121
Figure 4.5: Effect of pH on nanoparticle fluorescence.....	122
Figure 4.6: Effect of pH on nanoparticle surface charge.....	123
Figure 4.7: Effect of temperature on nanoparticle fluorescence.	124
Figure 4.8: Effect of salts on nanoparticle fluorescence	125
Figure 4.9: Effect of UV exposure on fluorescence intensities.	126
Figure 4.10: Effect of acetic acid exposure on fluorescence intensities.	127
Figure 4.11: Effect of interfering agents on fluorescence intensities.	128
Figure 5.1: Structures of (a) MMA and (b) PMMA.	135
Figure 5.2: Radical initiator attack on a monomer to start a polymer chain. ...	139

Figure 5.3: Termination by the combination of two polymers.	140
Figure 5.4: Termination by disproportionation of PMMA.....	140
Figure 5.5: Termination of PVC by reaction with radical initiator.	141
Figure 5.6: Schematic representation of a stabilised surfactant emulsion.	142
Figure 5.7: PMMA polymerization apparatus.....	144
Figure 5.8: SEM image of typical PMMA sample.	147
Figure 5.9: SEM image of sample polymerised for 40 min	148
Figure 5.10: SEM image of sample polymerised for 90 min	149
Figure 5.11: SEM image of sample polymerised for 120 min	149
Figure 5.12: SEM image of sample polymerised for 180 min	150
Figure 5.13: SEM image of PMMA polymerised for 120 min	151
Figure 5.14: SEM image of PMMA polymerised at 60°C.....	152
Figure 5.15: SEM image of PMMA polymerised at 80°C.....	152
Figure 5.16: SEM image of PMMA polymerised at 70°C.....	153
Figure 5.17: SEM image of PMMA polymerised in a 100 mL flask.....	155
Figure 5.18: Effect of monomer concentration on particle size.....	157
Figure 5.19: Effect of monomer concentration on particle charge.	158
Figure 5.20: SEM image of particles formed in the presence of surfactant. ...	159
Figure 5.21: Effect of surfactant concentration on particle size.	160
Figure 5.22: Effect of surfactant concentration on particle charge.....	161
Figure 5.23: Effect of acetone concentration on particle size.	162
Figure 5.24: SEM image of PMMA formed using 10% acetone.....	163
Figure 5.25: SEM image of PMMA formed using 40% acetone.....	164
Figure 5.26: Effect of acetone concentration on particle charge.....	165
Figure 5.27: FTIR spectra of samples formed with and without nitrogen.....	166
Figure 5.28: SEM image of PMMA polymerised with Quinine	167
Figure 5.29: SEM image of PMMA successfully polymerised with Quinine ...	168

Figure 5.30: SEM image of PMMA polymerised with RWT	169
Figure 5.31: Fluorescence of Quinine and Quinine/PMMA copolymer.	169
Figure 5.32: EEM contour plot of 27 nm PMMA sample.....	170
Figure 5.33: EEM contour plot of 16 nm PMMA sample with surfactant.....	171
Figure 6.1: Typical light scattering phenomena	178
Figure 6.2: Rayleigh scattering phenomenon	179
Figure 6.3: A comparison between Rayleigh and Mie scattering.....	180
Figure 6.4: Visible light spectrum wavelengths.....	182
Figure 6.5: EEM contour plot of dilute PMMA sample.	184
Figure 6.6: Schematic representation of pilot scale test rig.	191
Figure 6.7: Schematic diagram of the AAD pilot plant in Hobart.....	192
Figure 6.8: Schematic diagram of the RO array.	193
Figure 6.9: EEM matrix without the compensating filter.....	198
Figure 6.10: EEM matrix with the compensating filter.....	199
Figure 6.11: EEM plot of ATP RO feed.	201
Figure 6.12: EEM plot of ATP 1st stage RO permeate.	203
Figure 6.13: EEM plot of ATP 2nd stage RO permeate.....	203
Figure 6.14: EEM of WTP raw water.	205
Figure 6.15: EEM of coagulation treated WTP water.	205
Figure 6.16: EEM plot of Melton's Class A water.	206
Figure 6.17: EEM plot of RO treated Class A water.	207
Figure 6.18 : EEM plot of permeate spiked with PMMA.	210
Figure 6.19: Calibration curve of 30 nm PMMA in MilliQ water.	210
Figure 6.20: Calibration curve of 300 nm PMMA in MilliQ water.	212
Figure 6.21: Calibration curve of 90 nm PMMA in MilliQ water.	213
Figure 6.22: LRVs for 4" BW30 intact element.	214
Figure 6.23: RS calibration curve for 30 nm PMMA.	217

Figure 6.24: Geometric average LRVs for the nanoparticle challenge test.....	217
Figure 6.25: UV absorbance of mixed dye solution at 1 ppm each dye.....	219
Figure 6.26: Calibration curves for fluorescent tracer dyes	219
Figure 6.27: Geometric average LRVs for the mixed dye challenge test.....	221
Figure 6.28: Geometric average LRVs for the MS2 challenge test.....	222
Figure 6.29: Geometric average LRVs for the three challenge tests.	223
Figure 6.30: LRV standard deviations for the three challenge tests.	224
Figure 6.31: Geometric average salt rejection LRVs.	226
Figure 6.32: Comparison of concurrent LRVs for salt rejection and RS.	227

LIST OF TABLES

Table 2.1: Criteria for ideal integrity monitoring systems or devices.....	23
Table 2.2: Summary of reported RWT integrity tests.....	39
Table 2.3: Example COD results of 1st and 2nd stage RO permeates.	54
Table 2.4: Summary of current and emerging integrity monitoring methods. ...	60
Table 3.1: Properties of food and fluorescent dyes selected for screening	71
Table 3.2: Interfering agents used for surrogate screening	77
Table 3.3: Summary of screening results.	96
Table 3.4: Average LRV for continuous dosing of fluorescent dyes	97
Table 3.5: LRVs calculated from pulse dose tests.....	104
Table 3.6: Specific flux values for pulse dose tests.	104
Table 3.7: Average dimensions of fluorescent dyes.	105
Table 4.1: Characteristics of nano/microspheres studied.....	117
Table 4.2: Summary of screening results.	130
Table 5.1: Methods to produce PMMA micro- and nano-particles.....	136
Table 6.1: LRVs for RO membranes with defects.	212
Table 6.2: Average normalised flux values.....	215
Table 6.3: Membrane integrity performance for different surrogates	224
Table 6.4: Potential field instruments for RS detection.....	228
Table 6.5: Cost analysis of PMMA synthesis.....	231
Table 6.6: Challenge test comparison.	237
Table 7.1: Research Objectives versus Outcomes	256

Chapter 1 Introduction

Direct or indirect potable reuse of reclaimed sewage is developing quickly as the security of water supplies nationally and internationally diminishes through human activity. The growth of this type of water substitution is increasing and applications of this approach to water management is becoming evident in the national context by the Queensland Government's Western Corridor Recycled Water Project (Seqwater 2013) operating from 2009 and internationally by Singapore's Public Utility Board approach to securing water supplies for the island state (Singapore PUB 2010).

Applications of reclaimed water treatment are evident throughout the United States of America with the most recent direct potable reuse (DPR) scheme, reusing treated wastewater as drinking water without an environmental buffer, operating at Big Spring, owned and operated by the Colorado River Municipal Water District (CRMWD). The Big Spring DPR plant was opened in mid-2013 and provides 7.5 ML/d of reclaimed water to augment dwindling water supplies. The CRMWD started investigating the opportunity to reclaim wastewater in 2002 and that led to the full-scale development over a decade later. Wichita Falls, a town located around 400 km from Big Spring has also developed a DPR scheme that produces 40 ML/d that started operating during mid-2014 (Martin 2014).

Development of new indirect potable reuse (IPR) and DPR projects continues with the El Paso Water Utility already operating an IPR by injecting the treated water into a local aquifer and is seeking approval from the state regulator to build the full scale facility expected to go online in 2018 (Australian Water Recycling

Centre of Excellence 2015). Indirect potable reuse in the US has been used for over 40 years at the Upper Occoquan Regional Water Reclamation Plant operated by the Upper Occoquan Service Authority. The plant, located in Virginia, started reclaiming water in 1978 at a production capacity of 40 ML/d and was upgraded to treat 120 ML/d and then 205 ML/d. The reclaimed water is discharged into Bull Run and then onto the Occoquan Reservoir that supplies Washington D.C. (Ostarcevic 1991). The demand for additional water supplies from alternative sources continues to expand.

The United Nations World Water Assessment Programme (UNWWAP), reports that all sectors of production will have a greater demand for water (WWAP 2015). Most significantly, the UNWWAP states that a global water deficit of 40% is likely by 2030 under the business as usual climate scenario. The ever increasing pressure on fresh water resources through population growth, urbanization, migration and industrialization, coupled with production and consumption increases, are issues that are forcing the re-evaluation of the single use nature of consumption. Consequently, water reclamation, or the multiple use of a water resource, is considered as an effective way to extend the use of the resource and modify consumption dynamics by better resource utilisation.

A paradigm shift is underway with a new emphasis on the use of high pressure membrane systems that include nanofiltration (NF) and reverse osmosis (RO) systems for their microbiological removal rather than the traditional applications to remove salts and organic material (Texas Water Development Board 2015). A much greater and sustained focus on treatment efficacy by health regulators occurs when these unit operations are employed to reclaim water resources for

a diverse range of end uses such as indirect and direct potable water substitution (Victorian Government Department of Health 2013).

Currently, the true barrier potential of high pressure membranes is not recognised by health regulators and that results in additional process complexity necessary to provide the level of security required by health regulators to mitigate real or perceived risks to public health. This condition is a consequence of the lack of a real-time, online membrane integrity testing regime that can readily validate the performance of a functioning high pressure membrane system on demand with greater than 99% removal ($2 \log_{10}$ reduction) of microbiological contamination by virus. Membrane integrity systems to validate the performance of microfiltration (MF) and ultrafiltration (UF) systems exist (Victorian Government Department of Health 2013) and are extensively employed in the water and food industries but the same cannot be said for NF and RO high pressure membrane systems that are limited to less than $2 \log_{10}$, well below their potential of $4 \log_{10}$ and beyond.

There is limited published information that provides methods to evaluate high pressure membrane integrity or the efficacy of NF or RO to remove microbiological contaminants. Several integrity testing protocols that can be conducted offline include the vacuum hold test and Dow's sulphate test (Jons *et al.* 2005), however, none of these provide real-time membrane integrity monitoring.

Adham *et al.* (1998a) considers that one of the risks associated with reclaiming treated sewage for either direct or indirect water substitution is the inability to quantify the integrity of the high pressure membrane barrier. The ability to assess the integrity of the principle barrier and the associated interconnections used to

treat water to the standards required to satisfy health regulators and consumers online in real-time is generally limited to conductivity and total organic carbon (TOC). These instrument based monitoring techniques can provide feedback on membrane integrity up to 2 log₁₀ reduction, well short of the 4 log₁₀ or greater removal potential of high pressure membrane systems. The national and international water industry, consumers and health regulators struggle with the issue of membrane security and the risk to public health. A number of guidelines that mandate membrane validation processes have been established such as those produced by the Department of Health, Victoria, Australia (Victorian Government Department of Health 2013) and the United States Water Environment Federation (WaterReuse 2015) to reduce risks to consumers.

Although there are currently no clear protocols developed for online, real-time membrane integrity there are several discrete testing regimes that have been developed recently. Generally, the testing regimes have relied on destructive testing by autopsy, or offline testing to determine whether the membrane element is compromised. Destructive testing and offline testing such as vacuum hold testing do not provide the necessary security required. Destructive testing is a measure of last resort and is performed on membranes that are known to be compromised rather than identifying compromised membranes in an array during operation. In addition, these tests consider the performance of individual components rather than the complete operating system that include piping and membrane interconnections, valves and pumping elements.

The consequence of treatment barrier failure by breaches in membrane integrity and system component failure may lead to unacceptable exposure of consumers

to viruses and bacteria. This type of exposure is currently considered an unacceptable risk by most health regulators.

Production of safe drinking water from sources such as brackish water harvested from groundwater, reclaimed sewage and challenged natural surface water treated using NF can also benefit from real-time integrity monitoring. Water reclamation is the principle area of application as health regulators and water providers require real-time monitoring to mitigate the potential risks associated with membrane failure.

A report published by the American Water and Wastewater Research Foundation (AwwaRF) (Lozier *et al.* 2003) recommended, “*Research should be devoted to identifying a more suitable non-biologic, particulate viral surrogate for cost effective, routine use with full scale RO/NF systems.*” The present study aims to deliver a surrogate that can be measured in real-time.

1.1 Water Reuse and Recycling

As countries continue to develop and cities expand, few new water resources are available to support daily fresh water needs. As a result, solutions such as water re-use and salt water desalination have emerged as the keys to sustaining future generations across the globe (Greenlee *et al.* 2009). Water reuse is typically utilised to provide water for irrigation, power plant cooling water, industrial process water, and groundwater recharge and has been accepted as a method for indirect drinking water production (Greenlee *et al.* 2009). In 2007, the major use of recycled water world-wide was for agricultural purposes (Hurlimann 2007).

1.1.1 Uses and Benefits of Recycled Water

Numerous applications can benefit from water recycling and re-use with its own particular water quality requirements to ensure that the use is sustainable and that no adverse effects result from the re-use (Dettrick and Gallagher 2002).

Possible uses of recycled water include (Land & Water Australia 2009):

- Agriculture – to grow crops, pastures, fruit, vegetables, wine grapes and plantation timber
- Amenity horticulture – for watering parks, golf courses, gardens
- Heavy industry – for washing and cooling in manufacturing, mineral processing and power generation plants
- Other industries – fire-fighting, dust control, road-making, building and construction
- The environment – for recharging groundwater, enhancing environmental flows, watering amenity landscapes, and sustaining wetlands and ponds
- Domestic uses – flushing toilets and watering gardens
- Drinking water – for direct or indirect potable re-use.

Water recycling and re-use provides numerous benefits to consumers, industry and the environment (Land & Water Australia 2009). These include:

- Potable water availability: recycling can reduce the demand for high-quality potable water by using alternative supplies for activities that do not require such a high standard of water. The 'freed-up' water can then be put to better use. The amount of water extracted from the natural environment for human use can be reduced, decreasing the stress on rivers, wetlands and aquifers.
- Additional, more secure water: in cases such as the recycling of treated effluent, it is possible that the users of the recycled water receive a further benefit – gaining a more secure and reliable supply of water that is independent of rainfall.

- Increased water use efficiency on local, regional and national scales: recycling means that communities and countries get more use, more production and more economic value from scarce water resources.

1.1.2 Recycled Water Production, Classification and Challenges

Potential sources of recycled water include, but are not limited to (Government of Western Australia 2010): untreated sewage; grey water; industrial process water; and stormwater. Sewage includes waste water sourced from grey water and black-water sources (Northern Territory Government 2009). These include toilet discharges (Tjandraatmadja and Diaper 2006) and other household wastewater from the kitchen, laundry and bathrooms. These liquid wastes are normally collected in a sewer system and processed in a treatment plant (ACT Environment and Health 1997). Stormwater is generally not designated as wastewater (Northern Territory Government 2009).

Each individual source of recycled water will have different quality characteristics and different contaminants. In recycled water, contaminants are identified as a potential hazard to the environment and/or people that come into contact with the recycled water and may include: biological contaminants (e.g. pathogens); chemical contaminants (e.g. insecticides, cleaning products, endocrine disruptors); physical contaminants (e.g. debris); and heavy metals (NSW Government 2008; Northern Territory Government 2009).

The major acute potential hazard of human contact with recycled water is infection and illness caused by bacteria, viruses and other pathogenic microorganisms. If not correctly managed, exposure to recycled water has the potential to adversely impact on the health of people and the environment (NSW

Government 2008). Direct ingestion, spray inhalation and hand to mouth contact are the most hazardous routes of exposure (Gold Coast City Council 2008). Whereas both chemical and microbiological aspects can influence human health, waterborne enteric diseases are more common and are the focus of most management strategies to minimise the risks to public health (Dettrick and Gallagher 2002). A review and discussion of the microbial pathogens in addition to chemical contaminants that can be used to define a non-microbial surrogate that can be used to determine membrane integrity is presented in the following chapter.

1.2 Public Perceptions of Recycled Water

Domestic and international researchers and water authorities report that there is no scientific or health reason that recycled wastewater cannot be safely used as part of drinking water supplies if it is treated properly (Australian Academy of Science 2006). In Victoria, Australia, the Department of Health and Human Services claims that the levels of heavy metals in recycled water are safe and endocrine disrupting chemicals in recycled water are not a risk to human health (Department of Health & Human Services Victoria 2015). This is because the amounts of these substances entering sewage are highly diluted and because sewage treatment processes are very effective in removing the endocrine disrupting chemicals that are present (Department of Health & Human Services Victoria 2015).

Similarly, the levels of pharmaceuticals in recycled water are extremely low and are therefore not hazardous to humans. Health experts have calculated the highest possible levels of pharmaceuticals that could be present in recycled water

based on their use within our communities. Of these, the contraceptive pill and the painkillers paracetamol and aspirin will be present at much higher concentrations than any other pharmaceutical (Department of Health & Human Services Victoria 2015).

Although the public is aware that recycled water is safe for many purposes, there is a formidable psychological reason behind the reluctance to accept it for drinking water. Termed the '**yuk factor**' and depicted humorously in Figure 1.1, this perception is based on the thinking that the water in the glass in your hand might have started off in someone's toilet bowl (Australian Academy of Science 2006).

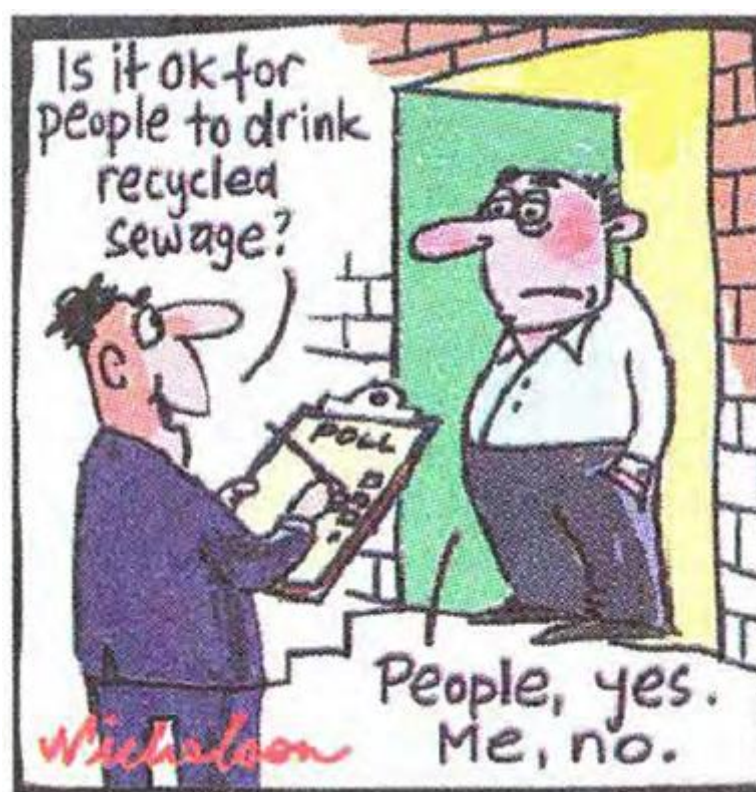


Figure 1.1: Cartoon showing public perception towards recycled water (Radcliffe 2008).

In the past decade, Dolnicar and Schäfer (2006) reported that the Australian population clearly discriminated between desalinated and recycled water with the quality of the latter a concern as the primary source is municipal wastewater. As such, it carries human excretions and household discharges from sources such as the kitchen and laundry and can also contain miscellaneous dumps of household/garden toxins and pharmaceuticals. In the survey-based study conducted by Dolnicar and Schäfer (2006), respondents clearly showed their understanding that recycled water is the more environmentally sustainable, whereas desalinated water is perceived as less risky from a public health point of view.

Control of microorganisms in drinking water treatment and water re-use has always been, and continues to be, a major concern to public health and water treatment professionals (Adham *et al.* 1998a; Causserand *et al.* 2002). A number of surveys have shown that acceptance of recycled water use varies across communities. Generally, there is widespread support for recycling water but the closer the water comes to personal contact, the less acceptable the re-use option (Horticulture Australia Limited 2006). Positive community perceptions of recycled water schemes can only be achieved through wide-spread trust in the relevant authorities, technologies, regulatory arrangements and compliance measures underpinning such schemes (Natural Heritage Trust 2010). Consequently, a robust, reliable real-time online membrane integrity monitoring program has the potential to increase the trust in membrane performance and subsequent adoption and use of high pressure membrane water reclamation systems.

1.3 Significance of this Research

Water quality security is the key outcome of an effective and timely membrane integrity monitoring system for wastewater recycling schemes that utilise membrane systems. This research can therefore mitigate the risks associated with the provision of direct or indirect potable water for substitution or supplementation of current domestic water sources. In addition, real-time integrity monitoring has the potential to provide greater public confidence in the treatment and subsequent distribution of reclaimed wastewater.

Real-time membrane integrity monitoring can deliver service providers and health regulators access to a tool that enables performance of systems to be closely monitored, scrutinised and more importantly verified in real-time. Performance validation in real-time of reclaimed water systems as well as surface water treatment where NF membranes are employed, particularly in catchments with elevated risk factors, can significantly reduce the potential for exposing consumers to microbial contamination. Facility operators can then have the capability to maintain very high quality assurance and control over the complete production process, not just the membranes, and promptly identify and isolate compromised elements as well as other system components as a result of the real-time information provided by online membrane integrity monitoring.

Membrane integrity can be classified into two broad categories that relate to the target components to be excluded, namely, chemical and microbiological contaminants. Chemical contaminants include compounds such as pharmaceutical products that can affect the human endocrine system whereas

virus is a microbiological contaminant. This research is specifically focussed on microbiological pathogens and targets the smallest virus.

1.4 Research Objectives

The objective of this research was to develop and test a real-time membrane integrity monitoring protocol that has the capacity to identify breaches in membranes and their associated system components small enough to allow passage of the smallest virus, the poliovirus, with an approximate diameter of 30 nm (Schijven and Hassanizadeh 2000).

Identifying a non-microbial surrogate and appropriate instrumentation to continuously monitor, in real-time, the integrity of high pressure RO and NF membranes is the cornerstone of this research and includes the following features:

- Target the smallest virus, i.e. poliovirus with a diameter of 30 nm to define the size and nature of the surrogate,
- A reliable and easy method of detection that can be used online and provide real-time feedback,
- Is non-toxic and environmentally degradable,
- Utilise a relatively inexpensive surrogate that may contribute less than \$0.02/kL of the water treated,
- Can be incorporated into new system designs (greenfield) and existing (brownfield) operational platforms,
- Identify detection devices available in the market such as fluorometers, scanning spectrophotometers, light scattering devices, etc. that will achieve surrogate detection at the desired sensitivity.

Overcoming these challenges will lead to a robust and reliable membrane integrity and surveillance technique. Pre-treatment using low pressure membrane

filtration greatly reduces the protozoan load and therefore virus rather than protozoan removal will be the key measure of this research due to the significantly smaller size and subsequent greater integrity challenge for size exclusion processes.

An additional challenge for this research program was to determine whether real-time integrity monitoring can be used to determine the log removal of RO and NF membranes. The capability to measure at least 4 log₁₀ virus removal will indicate that detection sensitivity is within a suitable range (Lozier *et al.* 2003).

1.5 Thesis Outline

This introductory chapter outlined the importance of membrane integrity monitoring of membrane systems, not just the membrane elements by themselves. Membrane integrity surveillance is a critical aspect when considering the application of high pressure membrane systems for water reclamation and advanced water processing for sensitive applications.

A comprehensive review of the literature is provided in Chapter 2 that identified current and potential membrane integrity systems to verify pathogen removal performance. The verification approach required to meet the demands of regulators and operators is examined and how these key issues define system development. This chapter also identified and discussed the key measure of membrane integrity, the log removal value (LRV) with its inherent limitations and provided a review of current membrane integrity surveillance techniques including fluorescence. New and innovative techniques that can be applied to monitor membrane integrity were critically examined with an assessment of their benefits and limitations. A comparison of each technique identified will be

compared against an 'ideal' membrane integrity technique and the features defined by the selection matrix. Chapter 2 sets the scene for chemical and non-microbial surrogates described in Chapters 3 and 4 by addressing the key issues that were used in subsequent experimentation.

Chapter 3 interprets the data collected from experiments developed to establish the effectiveness of a range of dyes and fluorescent chemicals selected as potential surrogates. The results of a series of methods developed to assess the performance and efficacy of these compounds to meet the features defined as the objectives of this research are reported and assessed against the criteria identified. A discussion of the outcomes and limitations of the screening process and a conclusion on the performance of the compounds is provided in this chapter.

A similar approach was adopted to assess commercially available fluorescent nanoparticles (FNPs) to follow on from the screening of dyes and fluorescent compounds. Chapter 4 reports the results of the screening assessments of various FNPs in the laboratory including their sensitivity and environmental stability in order to measure their effectiveness as non-microbial surrogates for membrane integrity monitoring. A nexus to Chapter 5 where nanoparticles were fabricated and assessed is provided.

Assessing the performance of nanoparticles synthesised in the laboratory is the cornerstone of Chapter 5. This assessment led to the development of nanoparticles without a fluorescent tag to determine whether they could naturally fluoresce to reduce the complexity and cost of production. Consequently, poly(methyl methacrylate) (PMMA) nanoparticle spheres were synthesised in the

laboratory. Additional experiments were conducted to control particle diameter to closely replicate the target virus size to develop a suitable non-microbial surrogate. This chapter provides the synthesis pathway and characterisation of the untagged PMMA nanoparticles and identifies the detection capacity of these particles. The potential to tag the PMMA nanoparticles to enhance fluorescence was also explored and these efforts are reported. Analysis of an observed light scattering phenomenon was examined and found to be the result of Rayleigh scattering (RS). The implication of RS to membrane integrity surveillance is discussed and leads to the next chapter on light scattering and detection.

The phenomenon of RS is reported using the classical electromagnetic wave and quantum physics to describe the dual behaviour of light in Chapter 6. The move from fluorescence to light scattering to develop a sensitive and stable membrane integrity technique is discussed with a focus on RS as a potential analytical tool and monitoring technique. An important and useful feature of spectrofluorometry used to detect RS is addressed as it relates to the ability to monitor the fluorescence of natural organic matter (NOM) and use the signature as an early trigger for membrane integrity surveillance. Results from experiments were analysed to determine whether RS can satisfy the selection matrix requirements and compared favourably against the 'ideal' membrane integrity technique.

Evaluating the PMMA non-microbial surrogates and measuring the concentration using the RS response at bench, pilot and full-scale after the screening conducted previously is also presented in Chapter 6. The methods developed to determine the efficacy of the synthesised non-microbial surrogate coupled with the use of RS to determine concentration and the results obtained from the experiments

using flat sheet and 4 inch membranes are reported in this chapter. The results are critically examined and discussed to determine whether the technique based on PMMA nanoparticles and RS measurements can deliver or exceed the desired sensitivity and stability on a consistent basis. The ability to determine the level of rejection by the entire membrane system in terms of log removal is discussed as this is one of the key outcomes required from a membrane integrity monitoring technique.

Chapter 7 provides an opportunity to draw the research to a conclusion to determine whether the objectives of the research were achieved. Limitations from potential scope, methodological restrictions, and practical realities are discussed. Recommendations for future research are identified and include the use of the monitoring technique in other applications in addition to the use of hydraulic modelling to accurately predict where the integrity breach is within the membrane array. Chapter 7 represents the culmination of this work and reports on the success and limitations of the research program.

Chapter 2

Current and Emerging Membrane Integrity Tests

2.1 Introduction

High pressure nanofiltration (NF) and reverse osmosis (RO) membranes are widely used for water reclamation and desalination (Bartels *et al.* 2005; DeCarolis *et al.* 2005; Greenlee *et al.* 2009). The mechanism of water transport in these high pressure membrane systems is based on solute transport by diffusion through the nonporous active membrane layer (Paul 2004; Ridgway *et al.* 2013). These membranes are, therefore, capable of rejecting particles including pathogens, and in the case of RO membranes, dissolved ions including salts illustrated in Figure 2.1.

In reality, however, NF and RO membranes are not complete barriers to these contaminants (Adham *et al.* 1998a) and over time the integrity of membrane systems may be compromised due to a range of breaches that can develop in the system. These breaches can include the following modes:

- Damage to the membrane layer as a result of chemical or biological degradation and particulate abrasion,
- Delamination of the membrane supporting layers, and
- Failures of O-rings, gaskets, connectors and other fittings (Crozes *et al.* 2002; Kitis *et al.* 2003b; Lozier *et al.* 2003).

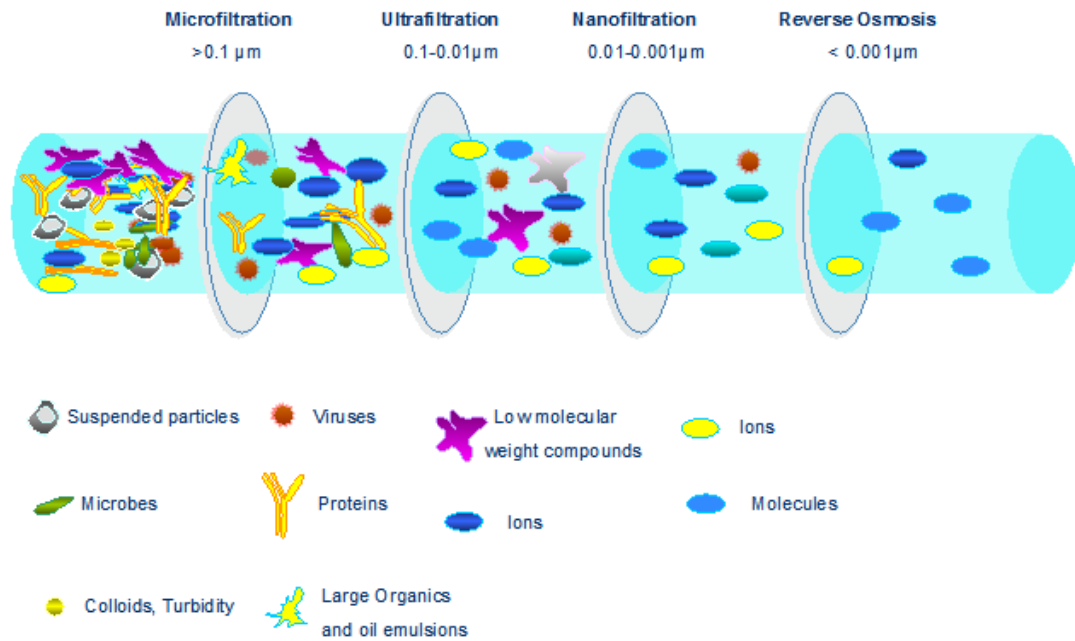


Figure 2.1: Schematic representation of membrane barrier performance
 (Modified from: <http://www.hydrogroup.biz/areas-of-use/water-treatment/membrane-filtration.html>; <http://www.degremont.com/en/news/special-topics/micropollutants-in-water-treatment-processes/> for Ostarcevic, 2005 Kwatye Water Prize).

In addition to these ‘in service’ failure modes, manufacturing defects such as incomplete glue-lines can affect the integrity of membrane elements and depending on the quality control processes employed are usually detected before membranes are shipped to customers.

In order to ensure the quality and safety of water treated by NF or RO membranes, the integrity of the entire system must remain intact over the service life of the elements. Moreover, system operators must be able to provide evidence of the integrity to satisfy regulatory requirements on a regular basis (Victorian Government Department of Health 2013). Several integrity monitoring techniques have been developed for these systems and they are broadly classified into direct and indirect techniques (Adham *et al.* 1998a; Kumar *et al.* 2007). In general, direct methods assess the integrity of membrane elements by

the application of a pressure-based test whereas indirect methods use a surrogate parameter measured in the permeate for assessing the integrity of the whole membrane system (Adham *et al.* 1998a; Gitis *et al.* 2002; Casani *et al.* 2005). Direct tests are usually performed offline on individual elements but indirect tests can be performed on membranes during service and have a wider scope for online continuous monitoring. Challenge tests are a type of indirect technique where a surrogate species is introduced into the feed water and the removal efficiency is determined by the measurements of the surrogate species in the permeate (Gitis *et al.* 2002; Casani *et al.* 2005).

Several reviews of high pressure membrane integrity monitoring techniques have been reported with a focus on existing, widely accepted methods (DeCarolis *et al.* 2006b; Kumar *et al.* 2007; Antony *et al.* 2012). In order to fully realize the rejection capabilities of high pressure systems, new, robust techniques that can be implemented in real-time and online are required.

This chapter presents a review of existing integrity tests and focuses on emerging techniques that have the potential to demonstrate the online rejection capabilities of high pressure membrane systems. Some existing patented methods are also presented followed by a discussion of current methods and potential methods that show promise for future development.

2.2 The Target - Poliovirus

Human bodies are under constant attack by any number of infectious microorganisms in the same way that medieval castles were laid under siege by armies of old. Humans survive many of these attacks by developing immunity that promotes biochemical and cellular defence mechanisms to counter

pathogenic organisms (Hill 2006). Humans can avoid harmful microorganisms by maintaining a strong immune system, instituting good personal hygiene and good nutrition. Systems for drinking water treatment, sewage treatment, medical services, vaccination and epidemiological intervention complement wise ecological practices to limit the occurrences of disease epidemics.

Unfortunately, human, animal and environmental reservoirs still harbor many infectious organisms that cause diseases such as diphtheria, cholera, typhoid fever and tuberculosis. Global travel and interconnection has seen the rise in the transmission of deadly organisms such as Ebola that has been widely reported by international media since 2013. These deadly threats still plague much of the world and could re-emerge if public health protection is compromised.

Conventional treatment incorporating membrane filtration plus disinfection practices has been the most successful means of preventing the spread of pathogens in a society. Eliminating water borne pathogens by providing effective water treatment purification shifts the primary mode of disease transmission to person-to-person contact. However, if treatment facilities are compromised then serious consequences for public health arise. Hill (2006) observes that monitoring for all bacterial, viral and protozoan species that cause water borne diseases would be extremely expensive and a drain on operational resources so for this reason, a certain target species must be identified and monitored. Bacterial and protozoan pathogens are largely eliminated by unit operations employed upstream of high pressure membranes but not necessarily for virus. The performance of advanced water treatment operations that incorporate high pressure membranes is critical to the effective control of virus.

Monitoring for viruses is challenging and requires specialist skills and apparatus and is undertaken offline in a laboratory with results available sometime after the samples were taken. This is not conducive to timely monitoring of membrane integrity and somewhat akin to locking the gate after the horse has bolted. Consequently, the challenge is to select a target virus that a non-microbial surrogate can mimic in terms of size and shape. Viruses are classified into families, and then genera, based on many criteria, including physical and biological properties. The *Picornaviridae* (Pico meaning small) are the smallest of the RNA viruses (Adu 2005) and the *picornaviruses* are divided into four groups (American Water Works Association 1999); poliovirus (3 types), coxsackievirus (30 types), echovirus (34 types), enteroviruses (68 to 71 types).

Poliovirus, a human enterovirus, is the smallest member of a family of viruses called the *Picornaviridae* with a shell (capsid) between 25-30 nm in diameter (American Water Works Association 1999; Adu 2005). The poliovirus causes poliomyelitis, or polio, an infectious disease that remains prevalent in Afghanistan and Pakistan and can result in paralysis that is often permanent. Figure 2.2 shows a rendered image of a poliovirus that is housed in a capsid made of protein, with a cross-section exposing the viral RNA. The poliovirus capsid contains a single molecule of ribonucleic acid, or RNA, which is the primary information used to replicate new particles. When the virus infects a cell, the RNA genome enters the cell and programs it to generate new virus particles. These particles are then released from the cell and go on to infect new cells. Antibiotics are ineffective against viral infections but immunizations careful hygiene and effective water and sewage treatment can prevent viral infections. To date, there is no known cure for the disease (Adu 2005).

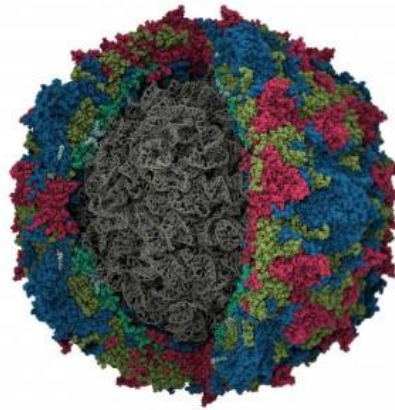


Figure 2.2: An image of the poliovirus capsid and RNA from Racaniello (2004).

An important characteristic of enteroviruses is their resistance to high and low pH and relative stability over a pH range of 3-5 for up to 3 hours (American Water Works Association 1999). Alcohol at 70 vol%, 1% quaternary ammonium compounds and other laboratory disinfectants are not effective against enteroviruses which are reported to be insensitive to detergents that otherwise destroy lipid containing viruses (American Water Works Association 1999). In theory, high pressure RO and some NF membranes should exclude virus size particles. This research will therefore adopt the poliovirus as the target virus to model a non-microbial surrogate that can challenge high pressure membrane systems. The surrogate must be detected at very low concentrations to meet the target of at least 4 log₁₀ removal.

2.3 The “Ideal” Integrity Test

In order to evaluate individual integrity monitoring systems, it is important to define the characteristics of an “ideal” system. In general, an ideal system is one that can accurately measure the ability of a system to reject pathogens in a

reasonable time so that the risk of these pathogens entering the product water is minimised or eliminated. It should also meet economic requirements so that the additional cost of treating water by the system is not excessive. Table 2.1 presents a summary of the key criteria that any potential monitoring system should be measured against.

Table 2.1: Criteria for ideal integrity monitoring systems or devices.

Criteria	Requirement(s)
Technique Considerations	
Test type	<ul style="list-style-type: none"> • Test should be online and provide integrity performance (LRV) results in real-time. • Detection in permeate from membrane elements, individual pressure vessels or membrane array of complete membrane train. • System shutdown unnecessary, normal operations continue during integrity surveillance.
Sensitivity	<ul style="list-style-type: none"> • High sensitivity at low challenge species concentration.
Selectivity	<ul style="list-style-type: none"> • Challenge species should be representative of the smallest virus rather than chemical compounds, and not be subject to changes in detection resulting from variations in environmental or chemical conditions such as NOM, Salinity, pH and temperature.
Output	<ul style="list-style-type: none"> • Test should deliver minimum LRV of 4 log₁₀ sensitivity.
Financial considerations	
Capital cost	<ul style="list-style-type: none"> • In the same order or less of capital cost as existing online real-time systems such as TOC instrumentation.
Installation Integration	<ul style="list-style-type: none"> • The ability to be fully integrated into existing systems as well as new systems seamlessly (greenfield and brownfield applications).
Operation	<ul style="list-style-type: none"> • Should require minimal training for operators.
Running costs	<ul style="list-style-type: none"> • Operation should not add more than \$0.02 per kL of treated water or around 1-1.5% of the tariff charged to consumers on a continuous basis and depending on the frequency and duration at much lower levels.

2.4 Direct Integrity Monitoring

Direct monitoring techniques are used to measure the integrity of single membrane elements or for very small RO systems. These tests are pressure

based and are used to detect defects such as pinholes in membrane sheets and glue-line failures. Vacuum decay and pressure decay tests are the most common direct monitoring techniques applied to NF and RO membranes (Crozes *et al.* 2002; U.S. Environmental Protection Agency 2005; ASTM 2008; ASTM 2010). The capital costs for instrumentation to measure vacuum or pressure decay is relatively low. In addition, the techniques are not able to detect holes the size that can permit the passage of virus sized particles except at very high pressures that could potentially result in damage to membrane elements.

Electrical conductivity (EC) is generally used as an indicator of membrane integrity; however, the sensitivity of such measurements can be grossly distorted through an array. Temperature, feed concentration, pressure, position along an array and fouling have an effect on permeate EC. Slight fluctuations in permeate EC can hide compromised membranes.

The closest instantaneous monitoring uses total organic carbon (TOC) measuring devices but these are prone to drift. Moreover, TOC is not representative of virus nanoparticles as it is a measure of soluble compounds in water that are smaller and because of their chemical structure can be more flexible so the compounds may pass through membranes where larger virus nanoparticles would be rejected. As a consequence, TOC monitoring will generally provide a more conservative LRV because the soluble compounds can be transported across the membrane into the permeate where virus nanoparticles would otherwise be rejected. The sensitivity of TOC is limited because of the low feed concentrations of around 60 mg/L and the resolution of the instruments at around 150 $\mu\text{g/L}$ which can only provide an LRV of around 2.6 \log_{10} .

Dow Filmtec (Jons *et al.* 2005) developed a non-destructive membrane integrity test that passes a short pulse of a highly rejected challenge species (either MgSO_4 or Na_2SO_4). While this protocol appears promising, it does not provide continuous security against membrane breaches, however, it does present a potentially useful tool to characterise the failure mode and location in the array. Similarly, Veolia Water has developed an integrity test using sulphate as a surrogate described by (Cote *et al.* 2001; Cote *et al.* 2004). Sulphate is generally present in most water that requires treatment, however, the concentration can vary considerably. The measurement of sulphate can be achieved *ex-situ* and reported quickly but this test does not provide real-time information on the integrity of the membrane system and can become difficult where multiple trains operate in parallel.

2.4.1 Vacuum Decay Testing

In a vacuum decay test (VDT), the permeate tube of a membrane element is sealed and a vacuum is applied to the tube. A schematic representation of VDT equipment is provided in Figure 2.3. The basic procedure in accordance with ASTM D3923 (ASTM 2008) and ASTM D6908 (ASTM 2010) involves soaking the membrane element for a period of time in RO permeate water (usually overnight), draining the membrane module for a defined period of time (usually an hour) and sealing one end of the permeate tube using a leak tight cap. As shown in the schematic, Figure 2.3, the system can be integrated with a digital flow meter and computer to record the VDT data and generate the decay curve.

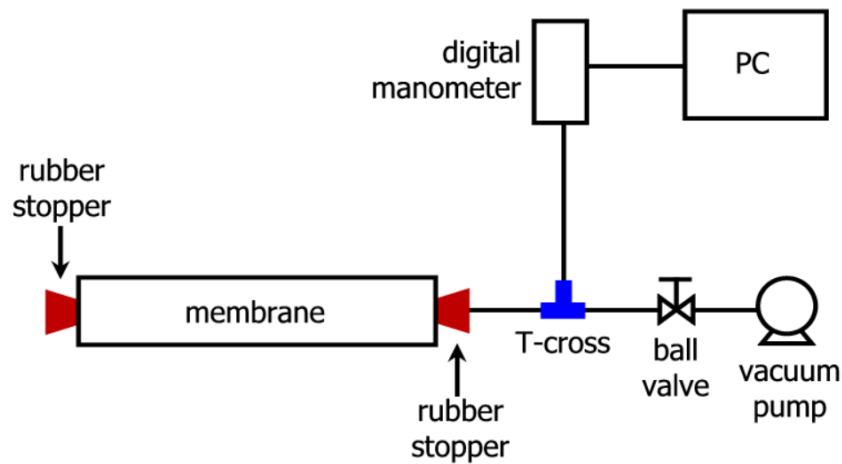
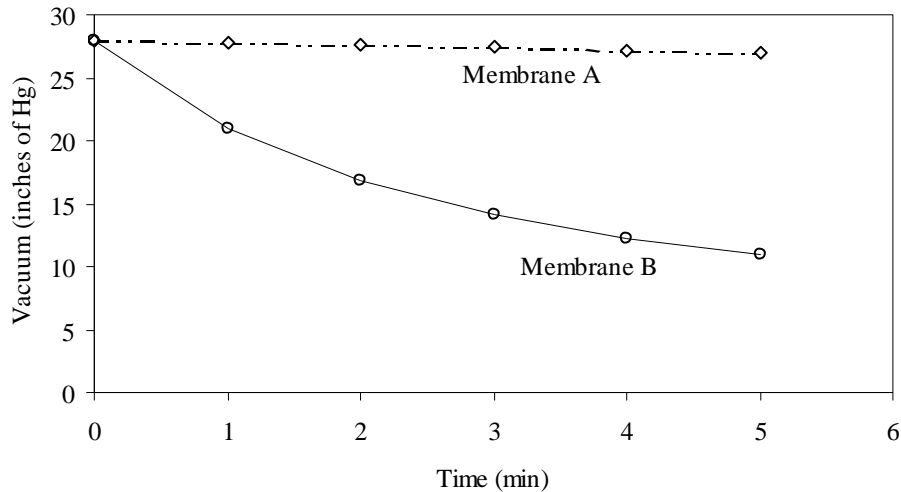


Figure 2.3: Schematic illustration of VDT apparatus.

The rate of decay of the applied vacuum pressure is monitored over a set period of time. For RO elements, a decay rate of $>10 \text{ kPa min}^{-1}$ represents a significant membrane defect and this test is typically performed on elements by the manufacturer prior to sale (Adham *et al.* 1998a; Kruithof *et al.* 2001; ASTM 2008). This method can be applied to a single element or a complete pressure vessel containing several elements for small scale RO systems (Eriksson and Mueller 2003). Figure 2.4 shows typical VDT results from two different commercially available RO membranes with one intact and one compromised. The vacuum pressure of the intact membrane shows only a slight decline whereas the compromised element shows a rapid decline indicative of a gross defect.



**Figure 2.4: VDT results from two different RO membranes.
from: (DeCarolis *et al.* 2006b).**

The VDT method is applicable only for the detection of mechanically damaged membrane elements or damaged O-rings but will not detect a chemical impairment that creates much smaller inconsistencies in the membrane. Therefore, this method is generally only useful as a screening procedure to detect significant defects in an RO system. However, some reports suggest that correlate well with the virus and TOC rejection by RO membranes and it is therefore a potentially useful integrity screening procedure for RO membrane elements (Adham *et al.* 1998a). Since the test is applied directly to membrane elements, the test cannot be performed when filtration is taking place (Casani *et al.* 2005) and this does not enable real-time membrane integrity monitoring in the strictest sense, but could allow frequent monitoring to identify slow degradation of system integrity.

2.4.2 Pressure Decay Testing

In a pressure decay test (PDT), the feed and concentrate ends of a membrane element are sealed and compressed air is introduced. In this case, the permeate side remains open and the pressure decay is measured over time. This test is particularly useful for measuring the integrity of low pressure hollow fiber MF and UF membranes (U.S. Environmental Protection Agency 2005; ASTM 2010; Pearce *et al.* 2012) and although the PDT is not common for NF and RO membranes, one study conducted PDTs on an entire stage of RO vessels for a small scale RO application (Wilbert and Linton 2000). The membranes were drained and then the permeate side was pressurised to 600 kPa (87 psi) and pressure decay monitored over a 10-minute period. The study concluded that this method was sensitive in detecting breaches but was not practical for full-scale systems because the elements must be drained prior to the test. In practice, the main aim of the PDT for RO in most cases is to determine an LRV for relatively large protozoa and this only requires low pressures. Moreover, this technique, that has similarities to the VDT, has the potential to induce telescoping in spiral wound elements.

2.5 Indirect Integrity Monitoring

Indirect monitoring techniques measure one or more parameters in the permeate and when compared to the feed water, a determination of the permeate quality can be reported. Some types of indirect monitoring techniques can be performed online but the instrumentation usually lacks the sensitivity required to accurately evaluate permeate quality.

2.5.1 Challenge Testing

In a challenge test, a surrogate species is introduced into the feed water at a known concentration in order to evaluate the amount of the surrogate that can pass into the permeate. The removal efficiency is reported as a log reduction value (LRV) that is calculated according to the following formula:

$$\text{LRV} = \log_{10} (C_f / C_p) \quad (2.1)$$

where C_f is the feed concentration of challenge species, and C_p is the amount detected in the permeate (Bennett 2008).

Although LRVs are widely reported and relate to the potential removal efficiency of pathogens including viruses for RO, the determination of LRVs is limited by the feed concentration of the surrogate and the detection limits of the surrogate in the permeate. Figure 2.5(a) shows a theoretical example of one limitation with a plot of calculated LRV as a function of a variable feed concentration at a fixed minimum permeate concentration. In Figure 2.5(b), the LRV is calculated based on a fixed feed concentration and variable permeate concentration. For a challenge test, a constant feed concentration would be more appropriate so at a nominal 1 mg/L feed concentration, the concentration in the permeate would need to be significantly low in order to achieve a reasonable LRV as shown in Figure 2.5(b). It is also clear that the lower the concentration in the permeate, the greater the increase in LRV indicating that low detection limits are critical for surrogate species. Conversely, increasing the feed concentration at constant permeate concentration has little effect on the calculated LRV over the range presented in Figure 2.5(a). Nevertheless, the aim of a challenge test is to report a removal efficiency based on the feed concentration of the surrogate so it is also

important to be consistent with dosing of surrogates for a given system to enable direct comparisons of LRVs over time.

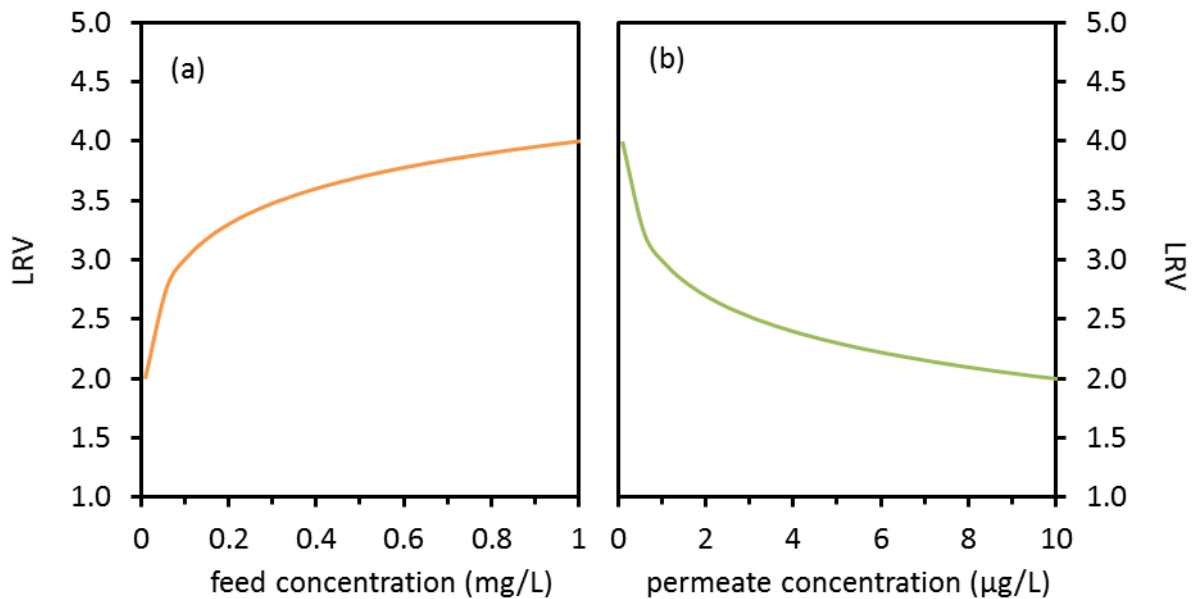


Figure 2.5: Calculated LRVs as a function of feed/permeate concentration. (a) variable feed concentration with constant permeate concentration (0.01 µg/L) and (b) constant feed concentration (1 mg/L) with variable permeate concentration.

The principle of LRV applies to any integrity monitoring technique that has the capacity to enumerate the feed and permeate concentrations of the surrogate and is adopted as the industry standard for integrity verification.

2.5.2 Particle Monitoring

A typical particle monitor measures changes in light transmittance through a fixed volume of permeate as a result of particles blocking the light source. The minimum particle size these monitors can detect is *ca.* 0.5 µm, which is considerably larger than any particle that could breach an NF or RO system. As such, particle monitors are generally used in MF and UF systems rather than NF

and RO systems. In addition, air bubbles can significantly interfere with the signal output resulting in erroneous results.

Online particle monitoring for RO is generally not recommended due to the high removal of particles by MF prior to RO treatment (Adham *et al.* 1998a). However, not all RO treatment processes utilize MF/UF pre-treatments so in general, the resolution for these particle monitoring systems is dependent on the type of pretreatment. In addition, particles large enough to be detected in particle counters may be present in RO permeates in events such as O-ring or permeate interconnector damage that are considered as gross integrity failures.

2.5.3 Turbidity Monitoring

The principal of turbidity monitoring is similar to that of particle monitoring whereby the passage of light through a sample is measured and related to the concentration of suspended particles. Typical nephelometric sensors also suffer from similar disadvantages including low sensitivity and interference. Laser turbidimetry, however, can reportedly measure much lower turbidity values (Banerjee *et al.* 2001; Naismith 2005) but this is limited to particles larger than *ca.* 1 μm in diameter that is in the order of thirty fold larger than the smallest pathogens of concern at between 25-30 nm.

2.5.4 Sulphate Monitoring

Sulphate monitoring can potentially be implemented online and can reportedly provide high resolution, provided the feed concentration is consistent and sufficiently high. Measurement is performed by ion chromatography and a resolution of 3 \log_{10} removal has been reported with a feed sulphate

concentration of 140 mg/L and a detected permeate sulphate concentration of 0.1 mg/L (Kruithof *et al.* 2001). However, online systems are relatively expensive to install and maintain with capital costs exceeding \$200,000.

As a soluble chemical species, sulphate is much smaller than the smallest pathogens such as viruses so this technique only offers a conservative evaluation of membrane integrity. Moreover, the mechanism of transport of sulphate through a membrane would be expected to differ significantly than that of a solid virus particle. In addition, biological species entrained in biofoulants on the membrane surface can utilise the oxygen under anoxic conditions so the measured sulphate concentration in the feed can be reduced thereby altering the log removal value. Scaling forming compounds such as BaSO_4 and CaSO_4 can also alter the measured permeate sulphate concentration as well as adversely affecting membrane performance and prematurely trigger the need for a clean-in-place (CIP) procedure to restore performance. These issues do represent a limitation to the efficacy of this technique.

2.5.5 Conductivity Monitoring

Conductivity testing can be implemented online or *via* intermittent probing with the latter providing higher sensitivity than the online technique (Adham *et al.* 1998a). This is useful when the feed water contains a relatively high concentration of salt that is efficiently rejected by RO (DeCarolis *et al.* 2006b). An example of conductivity monitoring plot for two different RO systems installed with cellulose acetate and thin film composite membranes is provided in Figure 2.6. When damage occurred to the O-ring installed in the RO system, permeate conductivity spiked to detect the leak.

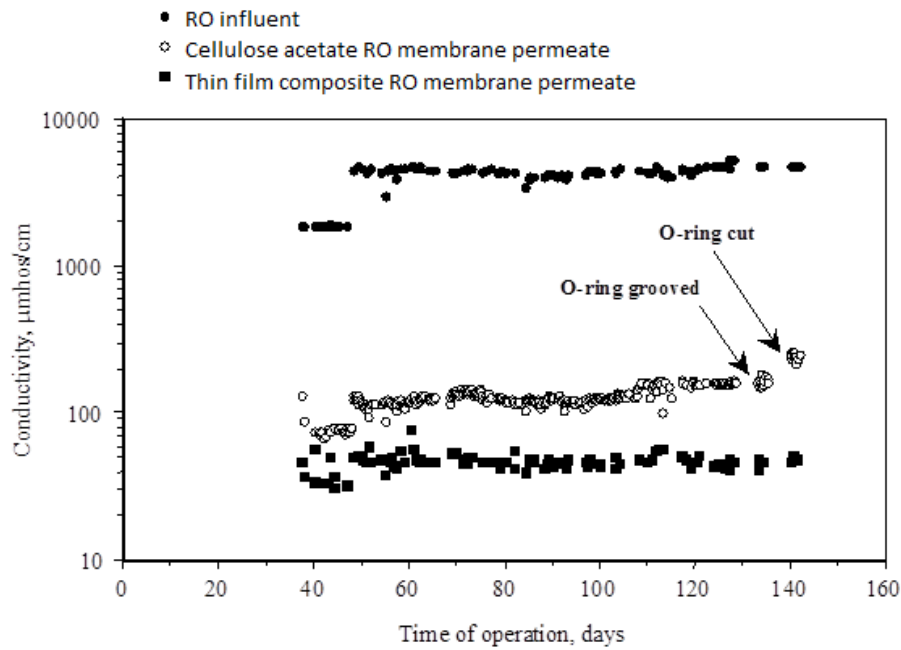


Figure 2.6: Example of conductivity monitoring for RO systems from Montgomery Watson (1997).

Due to its ease of implementation, conductivity monitoring is a common method for detection of integrity breach at the full-scale for NF and RO systems. However, the resolution of this method is low and will provide only up to 2 \log_{10} removal when feed EC is around 20,000 $\mu\text{S}/\text{cm}$ and permeate EC is 200 $\mu\text{S}/\text{cm}$. Electrical conductivity readings are subject to fluctuations as a result of temperature, ionic species in the feed as well as membrane fouling. Ionic speciation can have a significant impact on electrical conductivity with predominantly monovalent species having a higher EC/TDS ratio whereas a greater proportion of divalent ions in the feed will reduce the EC/TDS ratio. This can be significant in industrial applications that have a high degree of variation in discharged wastewater characteristics and have the potential to cloud the log removal calculation in specific circumstances.

2.5.6 Total Organic Carbon Monitoring

Total organic carbon (TOC) monitoring involves the oxidation of carbon and the detection of carbon dioxide generated during the process. The measurement of TOC is reported to be more sensitive than conductivity testing and particle counting (Adham *et al.* 1998a). A major limitation of this test and most other indirect techniques is the sensitivity of the instrumentation. A high sensitivity instrument is ideal to measure the parameter in the permeate where the concentration would be expected to be low at around 150 µg/L as witnessed at Orica's GTP. It is unlikely, however, that the same instrument could reliably measure the same parameter in the feed where the concentration would be significantly higher at around 50 mg/L typical of feed water at Orica's GTP.

The need for two complex and expensive instruments limit the use of this technique to large treatment plants that produce large volumes of treated water for direct or indirect potable use applications. Additionally, changes in organic and inorganic carbon dioxide (CO₂) composition within the feed, in temperature and fouling conditions may result in higher or lower than anticipated organic rejections resulting in inaccurate integrity results. Currently, TOC detection is rated for similar log reduction values as conductivity with an LRV of 2.5 reported at Orica's GTP. Online total organic carbon (TOC) monitoring has been implemented online for continuous integrity monitoring of RO systems. Online TOC analyzers are currently installed at Orange County Water District's groundwater replenishment system to monitor TOC before and after the RO system. Two different systems are utilised to measure TOC in the RO feed (< 50 mg/L) and RO permeate (> 4 µg/L).

Online TOC monitoring at the full-scale has also been implemented at the NEWater plant in Singapore to monitor the integrity of an RO system installed for IPR applications. A Sievers 820 online TOC instrument with a detection limit of 150 µg/L is installed at this facility (Seah 2012) and also used in the Western Corridor indirect potable reuse scheme in Queensland, Australia. Changes in organic composition in the feed may lead to variations in TOC rejection as specific organic species may result in greater or reduced transport across the membrane system and such variations in organic feed composition may interfere with LRV detection.

2.5.7 Periodic Testing

Periodic monitoring methods include conductivity profiling, conductivity probing and UV-254 probing. Conductivity profiling involves sampling permeate from each pressure vessel and analysing the conductivity, allowing this method to detect a breach in a particular pressure vessel. Conductivity probing is widely used to determine the location of a leak within a pressure vessel and is usually combined with conductivity profiling (Hydranautics 2012). This method, therefore, helps determine whether the integrity breach is in the membrane element, end connectors or interconnectors (Montgomery Watson 1997). Probing for UV absorbance at the 254 nm wavelength has also been reported (Wilbert and Linton 2000) but the method is limited because it can only achieve low resolution which depends on the concentration of UV active species present in the RO feed water.

An illustration of a conductivity probing setup is presented in Figure 2.7 and Figure 2.8 shows an example of a spike in conductivity which clearly indicates breaches in membrane integrity.

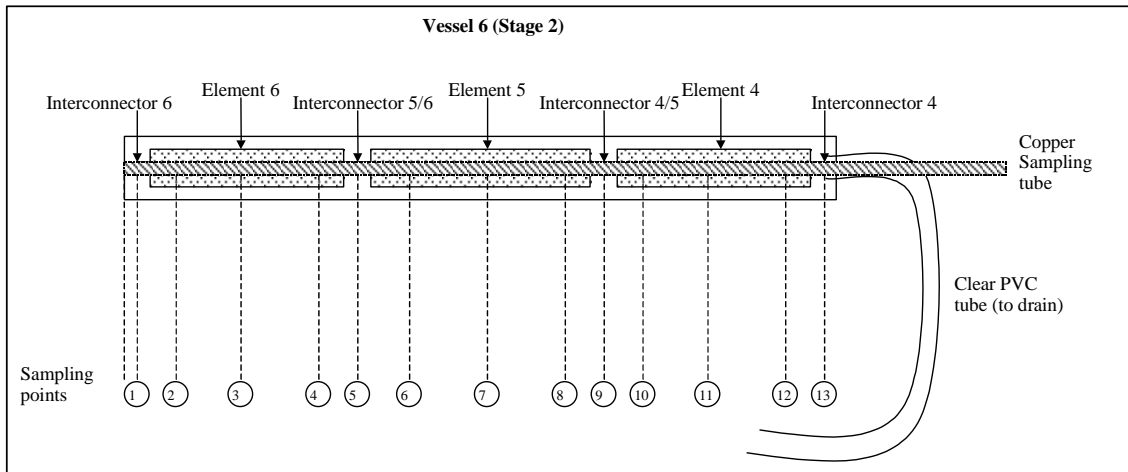


Figure 2.7: Schematic representation of conductivity probing setup from DeCarolis *et al.* (2005).

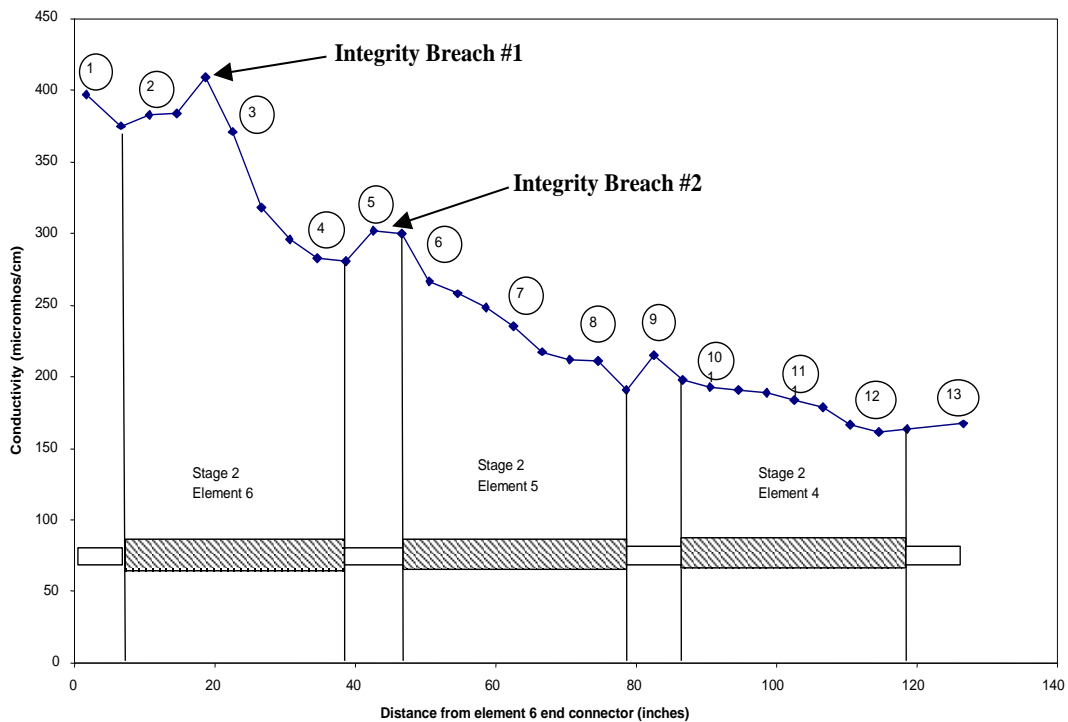


Figure 2.8: Conductivity probing of breached pressure vessel from: DeCarolis *et al.* (2005).

An example of the results obtained from conductivity probing of a suspected vessel at Orica's GTP is shown in Figure 2.9. In this case, the probing process in the suspected vessel identified one significant integrity breach. Notice that the

permeate EC average was approximately 550 $\mu\text{S}/\text{cm}$ whereas membrane A2 permeate EC was in excess of 15,000 $\mu\text{S}/\text{cm}$ so the membrane integrity breach was heavily masked by the flow from the other five membranes producing permeate. The difference between the average permeate EC and the compromised membrane permeate EC represents less than $1.5 \log_{10}$.

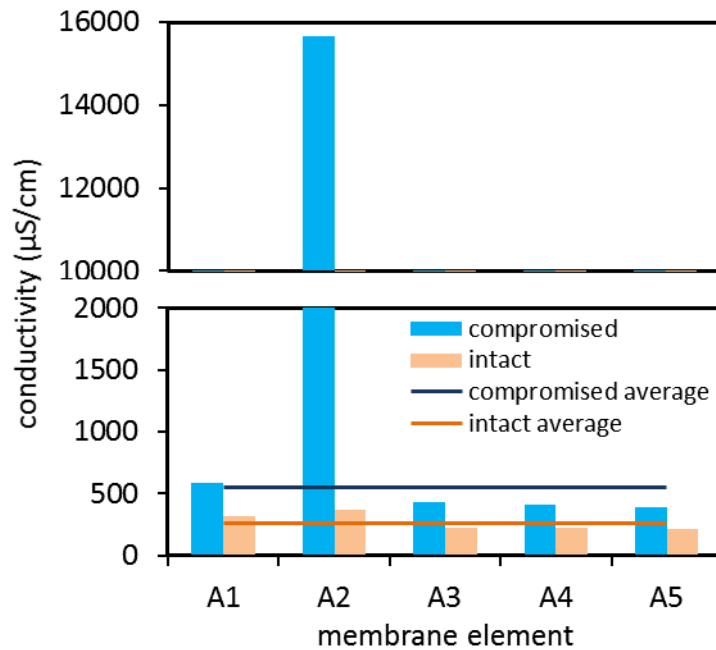


Figure 2.9: Permeate EC profile from a fourth stage RO.

2.5.8 Dye Testing

Chemical tracers have been used widely to study flow patterns in a range of water and soil systems (Harden *et al.* 2003; Binet *et al.* 2007). These include the use of fluorescent dyes such as Fluorescein (Ford and Thornton 1983; Gitis *et al.* 2002; Harden *et al.* 2003; Chua *et al.* 2007) and Rhodamine WT (RWT) (Stanbro and Pyrch 1979; Harden *et al.* 2003; Binet *et al.* 2007; Chua *et al.* 2007) and synthetic food dyes such as Brilliant Blue FCF (Flury and Fluehler 1995; Reinken *et al.* 1996).

The fluorescent dyes are particularly useful as water tracers due to their high sensitivity of detection and selectivity when contained in systems with other fluorescent compounds. Detection limits for these compounds are in the region of 100 ng/L levels so only small amounts are needed (Chua *et al.* 2007). Rhodamine WT is a non-toxic fluorescent chemical that was specifically developed as a water tracing dye (Smart and Laidlaw 1977; Sutton *et al.* 2001). As such, it is reported to be stable under a range of saline conditions (Stanbro and Pynch 1979; Magal *et al.* 2008) and has shown potential for use in RO integrity monitoring (Kitis *et al.* 2003b) with a minimum detection limit of approximately 10 ng/L (Ford and Thornton 1983). Instrumentation for measuring fluorescent tracers, including online commercial probes for measuring RWT, are readily available (YSI Environmental 2001; Aqualab 2004).

Integrity monitoring using RWT has been widely reported for RO systems in order to assess virus removal or to determine LRVs (Kitis *et al.* 2003a; Kitis *et al.* 2003b; Lozier *et al.* 2003; U.S. Environmental Protection Agency 2005; DeCarolis *et al.* 2006b; ASTM 2010; AWRCoE 2011; Lozier *et al.* 2011; Lozier *et al.* 2013; Ostarcevic *et al.* 2013; Victorian Government Department of Health 2013). In addition to its high sensitivity, RWT was also reported to be stable under a range of environmental conditions and not to be readily adsorbed onto membrane surfaces.

However, the fluorescence can be affected by the presence of chlorinated oxidizing agents, UV light and temperature. Under full scale and pilot testing using RWT, LRVs of $>4 \log_{10}$ have been achieved for several RO membranes (Kitis *et al.* 2003a; Lozier *et al.* 2013; Ostarcevic *et al.* 2013). As a soluble chemical,

however, the correlation between RWT and solid particles such as viruses and other pathogens is limited, with RWT providing a conservative estimate of pathogen LRV. Table 2.2 presents a summary of several RWT field or laboratory tests and LRVs obtained. In most cases, high LRVs can be achieved with low concentrations of RWT in the feed.

Table 2.2: Summary of reported RWT integrity tests.

Feed concentration (type*)	LRV	Reference(s)
0.1-1 mg/L (C)	3.5-5.3	(Kitis <i>et al.</i> 2003a)
1-2 mg/L (C)	3.9	(Kitis <i>et al.</i> 2003b)
1 mg/L (C)	2.7-3	(Lozier <i>et al.</i> 2003)
0.1-1 mg/L (C)	2-5	(Lozier <i>et al.</i> 2013)
0.1 mg/L (C)	2.6	(Lozier <i>et al.</i> 2011)
5-10 mg/L (P)	>4	(Ostarcevic <i>et al.</i> 2013)

*type: C = continuous, P = pulse

2.5.9 Microbial Surrogates

Microbial surrogates include the MS2 bacteriophage that is adopted as a substitute for pathogenic viruses (Victorian Government Department of Health 2013). It is often used in membrane integrity testing due to its similar shape, size and composition to some common enteric viruses (Jacangelo *et al.* 1991; Mi *et al.* 2004). Standard methods or protocols for performing challenge tests using MS2 seeding have been developed and the results of pilot and full scale tests are widely reported (Adham *et al.* 1998b; Colvin *et al.* 2000; Acker *et al.* 2001; California Department of Public Health 2001; Lozier *et al.* 2003; Mi *et al.* 2004; U.S. Environmental Protection Agency 2005; DeCarolis *et al.* 2006a; DeCarolis

et al. 2006b; Jacangelo *et al.* 2006; MWH 2007; Victorian Government Department of Health 2013). In one example, an LRV > 5 was reported for the removal of MS2 by intact RO membranes (Mi *et al.* 2004).

Unfortunately this technique is inherently difficult to implement in full scale plants due to high costs, sampling preparation and preservation, and the potential for false positive results (Gitis *et al.* 2002). Moreover, there are some potential health risks associated with using live bacteriophage particularly at the relatively high concentrations required for challenge tests. The use of this testing protocol to determine the integrity of an operational high pressure membrane system is limited by this risk and implementing this testing procedure online is not likely. In addition, enumerating the MS2 bacteriophage must be done in a laboratory and this time consuming assessment does not provide for a real-time integrity assessment of the operating membrane plant.

2.5.10 Non-microbial Surrogates

The use of non-microbial surrogates removes some of the risk involved in performing challenge tests with high concentrations of bacteriophage. Other than fluorescent dyes, non-microbial surrogates include fluorescent latex micro- and nano-spheres (Acker *et al.* 2001; Kitis *et al.* 2003a; Kitis *et al.* 2003b; Mi *et al.* 2004; Gitis *et al.* 2006; Pontius *et al.* 2009; Ostarcevic *et al.* 2013), gold nanoparticles (Gitis *et al.* 2006) and magnetic nanoparticles (Deluhery and Rajagopalan 2008; Guo *et al.* 2010), and other readily detectable particles (Choi *et al.* 2011). These particles offer the potential for real-time and online monitoring which is one of the key criteria for NF/RO integrity testing established for this research.

Most nanoparticle challenge tests do not consider the effects of surface chemistry and other factors that may influence rejection. For example, some nanoparticles have been reported to aggregate and foul the surface of membranes (Lohwacharin and Takizawa 2009) and that can improve the rejection of similar sized particles resulting in higher LRVs than clean membranes thereby providing an overestimate of system integrity. Other disadvantages include the costs associated with the production of fluorescent nanoparticles on a large scale. Although fluorescence detection instruments are widely available and relatively inexpensive, fluorescent nanoparticles can be very expensive and large quantities would be required for full scale operations.

Fluorescence can also be quenched in the presence of salt, organic species, oxidants and several other chemicals and under certain environmental conditions. In addition, depending on how the fluorescent markers are attached to the latex particles, they can leach from the surface into the surrounding carrier solution. This can lead to detection of the dye marker in the permeate which would otherwise reject the intact particle, thus biasing the LRV determination.

Magnetic nanoparticles can potentially be recovered and reused, but the instrumentation to detect these particles would add considerable cost to existing and new plants. Magnetic resonance relaxometers used to detect magnetic nanoparticle are commercially available as bench top relaxometers, however, the relaxometer and MR scanner are impractical due to their high cost that results principally from the large magnets employed and lack of miniaturised electronic components (Koh and Josephson 2009).

Silver nanoparticles have recently shown some promise for integrity monitoring with particles of 62 ± 10 nm used to challenge used RO membrane elements (Lawler *et al.* 2013). In these tests, the feed concentration was > 8 mg/L and the maximum LRV obtained was $2.57 \log_{10}$ although higher LRVs for UF and MF membranes have been reported for similar particles (Antony *et al.* 2012). In addition, the detection technique used was inductively coupled plasma with optical emission spectrometer that restricts this method to offline analysis in a laboratory like environment.

2.5.11 Spiked Integrity Monitoring

A relatively new technique, the spiked integrity monitoring (SIM) test is performed intermittently and online by dosing or injecting a challenge species into the feed (Kruithof *et al.* 2001; van Hoof *et al.* 2003). In these cases, powdered activated carbon (PAC) was used as the challenge species that was detected using particle counters and relatively high LRVs achieved depending on the dose of the PAC added to the feed. Although this technique is applicable to MF/UF membranes, it could be applied to NF and RO systems providing the PAC is sufficiently small and monitoring systems are available to detect small particles. However, the potential for sub-micron PAC particles to agglomerate with biofoulants can result in artificially high LRVs and premature fouling coupled with increased biological activity in the large surface area to volume PAC particles.

2.5.12 Pulse Integrity Test

The pulse integrity test (PIT) is similar in principal to the SIM and involves the addition of a short pulse of a highly rejected chemical species such as magnesium or sodium sulphate (Jons *et al.* 2005). The sulphate is monitored in

the permeate over time then compared to known profiles representing intact and compromised membranes. Defects such as holes and glue-line leaks present distinct sulphate profiles which can also be attributed to different locations in a membrane module.

This technique has the potential to be used online and in real-time providing the test is calibrated for each system although this would be complicated, time consuming and expensive for large installations. There is also a potential to develop this technique further using other tracer species such as RWT which could increase the detection limits and also enable a concurrent LRV determination. However, as previously discussed, the limitations of using sulphate as a surrogate include contributing to biological fouling and chemical scaling. Both of these conditions would reduce the sulphate available to migrate across a membrane and would artificially improve the apparent LRV. Unlike a challenge test, the membrane is only subjected to the RWT for a very short period minimizing the contact and potential absorption on the membrane surface. The estimated LRV using this technique was *ca.* $3.7 \log_{10}$.

2.5.13 TRASAR® Testing

The TRASAR® system is based on the addition of fluorescent chemical with antiscalant compounds in order to monitor and control antiscalant dosing in RO systems and to prevent overdosing (Zeiber *et al.* 2003). Monitoring the fluorescent marker that is part of the antiscalant chemical can be used as a potential integrity monitoring system. Fluorescence is measured in the permeate with LRVs up to $6 \log_{10}$ when the chemical is added in a spiked dose and $2 \log_{10}$

when added with antiscalant (DeCarolis *et al.* 2006a; DeCarolis *et al.* 2006b; MWH 2007).

In principal, the system is similar to that of the dye test except that in the case of the TRASAR® system, the fluorescent compound is a larger molecule than typical fluorescent dyes with a molecular weight *ca.* 610 Daltons. It would therefore be expected that the sensitivity of the TRASAR® would be lower than a dye such as RWT so much higher concentrations would be needed to achieve an LRV of 6 log₁₀. In addition, the use of the TRASAR® fluorescent chemical compound would detect integrity breaches from chemicals of concern such as endocrine disruptors that are smaller than virus particles, however, this is a departure from the main focus of this research.

2.6 Integrated and Multi-Parameter Monitoring Systems

A range of other techniques for monitoring the condition of low and high pressure systems have been reported. Some of these techniques offer the potential for real-time monitoring while others are more qualitative and require integration with other instruments. Online hybrid systems can offer multiple detectors in a single unit that can increase sensitivity of these units and reduce the need for separate instrumentation.

2.6.1 Small Sensor Cell Membrane Testing

A micro sieve sensor membrane is placed in the permeate side of the crossflow stream of a high pressure system. A change in the TMP of the sensor membrane is detected as an integrity breach but it can take more than one hour to detect even a very small breach. In addition, the system is sensitive to the flux so to

overcome this, a second sensor membrane can be added (Fane 2009). This technique has shown promise at both the bench- and pilot-scale but a limitation using this technique is the long delay before an integrity breach is detected.

2.6.2 Binary Gas Integrity Testing

The binary gas integrity test (BGIT) measures the diffusion of a select pair of gases injected into the feed of a low pressure membrane system. For a membrane with an integrity breach, the low permeating gas is detected in the permeate using mass flowmeters and the composition determined using infrared spectroscopy (Giglia and Krishnan 2008). This technique is reported to be highly sensitive and has been well correlated to virus removal (Giglia and Krishnan 2011). However, the sensitivity can be limited by the minimum detectable excess flow and a range of intrinsic membrane factors can influence the measured gas diffusion rate. In this case, normalization to a baseline measurement would be necessary to compare membrane performance over time. In addition, the need for multiple gases and detectors limits the applicability and practicality of this technique. There may be some potential to apply this technique to high pressure membranes at the small scale but the complexity associated with larger systems would generally preclude its adoption.

2.6.3 ZAPS Liquid Station

The Zero Angle Photo-Spectrometry (ZAPS) Liquid Station offers real-time water quality monitoring based on an entirely optical system utilizing three simultaneous techniques to measure a wide range of water quality parameters (Optimos Solutions 2012; ZAPS Technologies Inc. 2013b). It uses absorption, fluorescence and reflectance measurement techniques with a single sensor which eliminates

the differential drift of multi-sensor devices. In addition, it uses no reagents, and is self-cleaning and self-calibrating. It is typically used to monitor source water, drinking water treatment and distribution systems, wastewater treatment and re-use and industrial water systems (ZAPS Technologies Inc. 2012b; ZAPS Technologies Inc. 2012a; ZAPS Technologies Inc. 2013a). The parameters it measures include TOC, UV254 transmission, specific UV absorbance, nitrate + nitrite, turbidity, BOD and COD. The detection ranges of the TOC and BOD alone can enable LRVs of ca. 5.7 and 6.5 log₁₀ respectively.

In addition to the monitoring of standard indicator compounds present in the water sample, the system is capable of detecting *E. coli* by proxy. Since enteric pathogens cannot occur without the presence of enteric bacteria, testing for these bacteria can be used to monitor pathogen risk. The ZAPS system detects tryptophan that is a highly fluorescent amino acid that bacteria and other living microorganisms utilize to manufacture proteins. The *E. coli* bacterium maintain high concentrations of tryptophan as part of their cellular structure so this chemical can, therefore, be used as a biomarker to detect their presence. However, tryptophan is a common amino acid in many proteins and is not unique to *E. coli* and that may limit its sensitivity for detecting this species.

2.7 Pathogen Detection Systems

The ability to detect and quantify potentially hazardous pathogens in food and water is increasingly important to prevent and minimize the proliferation of infectious diseases (Ivnitski *et al.* 1999). The development of biosensors has grown rapidly over the past few decades with a range of devices available commercially and as prototypes (Pejcic *et al.* 2006; Irudayaraj 2009; Mukundan

et al. 2009). Some of these show promise in terms of developing membrane integrity monitoring techniques where the removal of viruses and other pathogens is critical.

2.7.1 BioSentry Device

The BioSentry device is a commercially available instrument that can detect chemical and biological contamination in water and report detected problems continuously in real-time with online capabilities. The device measures unique bio-optical signals of particles and compares them to those in its library to identify microbial contaminants such as *E. coli*, *Giardia* and *Cryptosporidium* (Adams 2009). In addition to microbial species, the device is reported to detect chemical contamination in drinking water so it has the potential to be adapted to monitor membrane integrity.

The system uses multiple sensors to measure a range of quality indicators and also uses a multi-angle light scattering detector at 660 nm to determine the size, shape, and internal structure of detected particles. However, the current configurations of the system limit size analysis to particles greater than 400 nm (JMar 2011) and that is an order of magnitude larger than the required resolution to be able to detect virus with an average size between 25-30 nm.

2.7.2 Real-time Polymerase Chain Reaction Monitoring

The real-time polymerase chain reaction (RT-PCR) technique is based on the detection of part of the viral genome (Langlet *et al.* 2007). Although the technique is relatively fast, it requires specialised sampling, testing and analysis and is therefore an expensive test that at present must be performed offline in a

laboratory environment. In addition, the technique cannot differentiate between infectious and non-infectious viruses which can complicate the results (Shirasaki *et al.* 2009).

2.7.3 Evanescent Wave Fiber Optic Sensors

Evanescent wave fiber optic sensors (EWFOS) use a laser spectrofluorometer to detect a laser derived evanescent wave that is excited over a sample (Lee and Thompson 1996; Lim 2003; Taitt *et al.* 2005; Byrne *et al.* 2009). These sensors can be highly customised to detect a range of pathogens and can be integrated into existing systems enabling the potential for online testing using flow-through systems. Although these EWFOS systems are currently susceptible to interference due to complex background matrices, it is expected that future biosensors could be increasingly sensitive measuring concentrations as low as 1 CFU/mL (Taitt *et al.* 2005) but this may not be sensitive enough to measure low permeate concentrations to provide a high LRV.

2.7.4 Surface Generated Acoustic Wave Biosensors

In a surface generated acoustic wave (SGAW) biosensor, metal electrodes mechanically generate acoustic waves through a substrate such as a liquid medium (Bisoffi *et al.* 2008). Biochemical interactions with target pathogens result in changes in the acoustic wave that are detected and then analysed with output signals related to the type and concentration of pathogen in the medium. The SGAW biosensors offer rapid, real-time, label-free analyses which are claimed to be cost effective and easy to use although they are not currently available commercially and some require long incubation times (Rocha-Gaso *et al.* 2009).

At present, reports on these systems are limited so they do not address potential issues such as diffusion and detection of pathogens in large volumes of water.

2.7.5 RAPTOR Fiber Optic Biosensors

The RAPTOR fiber optic biosensor is a type of EWFOs that monitors complex formation by evanescently exciting surface-bound tracer antibody fluorophores with a diode laser (Anderson *et al.* 2000; Byrne *et al.* 2009). The assay is achieved in less than 10 minutes in a fully automated, portable unit with few moving parts and long lasting probes. This system has been successfully demonstrated in food safety applications (Nanduri *et al.* 2006) and for the detection of pathogens in irrigation and recreational waters (Kramer and Lim 2004; Leskinen and Lim 2008). A major limitation of the system is the need for replacement of the fiber probes and fluorescent reagents as soon as a positive is obtained, although up to four antibody probes can be used to detect multiple pathogens (Anderson *et al.* 2000).

2.7.6 Block II Chemical Biological Mass Spectrometer

The Block II chemical biological mass spectrometer (CBMS) is an integrated system that can identify chemical and biological contaminants in a single unit (Griest *et al.* 2000). The US military developed the CBMS, that is similar to the RAPTOR biosensor system, primarily for the detection of threats and as such, the instrument is portable and robust. The CBMS system can only use a single detection mode at any time but the instrument has the ability to rapidly switch between detectors. This detection system has potential as a membrane integrity device but it is not commercially available.

2.7.7 Miniaturised Portable Biosensors

This technique uses a miniaturised gold electrode biosensor to detect pathogens by immobilization of antibodies onto the bio-functionalised electrode. An electrochemical technique based on impedance spectroscopy, the test can take several hours to complete and is currently only being developed for clinical purposes (Diouani *et al.* 2008). At present the device has been developed to detect different strains of the avian influenza virus but it has the potential for further development to detect other similar viruses, however, the time to develop data and the technical capacity to operate and maintain the instrumentation limits its application in the field for membrane integrity surveillance.

2.7.8 Microarray Biosensors

A microarray biosensor uses an automated concentration system to detect pathogens in water using a range of detectors including fluorescence (Byungchul *et al.* 2009) and other optical techniques (Weller 2005). Systems can be configured for online integration and although offering rapid analyses, these tests generate minor quantities of waste products (U.S. Environmental Protection Agency 2009). Moreover, the detection limits of typical bacteria are relatively high in the order to 10^5 CFU/mL for *E. coli* so it is unlikely that high LRVs could be achieved with these sensors.

2.7.9 Surface Plasmon Resonance Biosensors

Surface plasmon resonance (SPR) biosensors offer qualitative and quantitative label-free detection and analysis of biomacromolecules including proteins and nucleic acids in real-time (Homola *et al.* 1999; Wei *et al.* 2007; Bedford *et al.*

2012; Li *et al.* 2012). There is a wide range of configurations for various applications but the general principal of SPR biosensors is based on the change in refractive index of a metallic surface irradiated with a light source. Light is reflected at an angle defined by the type and amount of target bacteria in the solution that are bound to the metallic surface that is measured and quantified. Although most configurations are capable of detecting large molecules, some sandwich assays and competitive inhibition assays can detect much smaller molecules and the presence of gold nanoparticles can also enhance SPR signals (Li *et al.* 2012). Utilizing this technique in the field for membrane system integrity surveillance may be challenging because of the environmental exposure of the instrumentation.

2.7.10 Quantum Dot Based DNA Nanosensors

These ultrasensitive nanosensors use quantum dots (QDs) linked to DNA probes to capture and concentrate DNA from specific targets. The detection is based on fluorescence resonance energy transfer (FRET) to detect DNA at low concentrations which is capable of generating a distinct, highly detectable FRET signal (Zhang *et al.* 2005). Single QD-based sensors have also been developed to detect multiple virus strains in a single assay (Zhang and Hu 2010). Although typically used for clinical tests, there is a potential for other applications such as direct integrity monitoring for pathogen transport through membrane systems. The system requires specialised personnel to operate the bench scale systems and it is a relatively expensive technique that limits the potential application in membrane integrity surveillance.

2.7.11 Laser Scanning Cytometry

Online laser scanning cytometry (LSC) can be used to detect and enumerate microspheres in feed and permeate samples (Ladner *et al.* 2007). The LSC technique is based on fluorescence using a fixed laser light source but on a fixed membrane sample rather than in a flowing solution such as a permeate sample. At present the technique is only applicable to micron sized particles using a bench-scale prototype instrument, although there is a strong potential to develop more sensitive, portable instruments providing the costs can also be reduced.

2.7.12 Microfluidic Biochip Systems

Microfluidic systems for detecting pathogens cover a range of miniaturised devices utilizing techniques to measure DNA, protein and pathogen cells in integrated biochip devices (Mairhofer *et al.* 2009). Microfluidic biochips can utilize the detection systems of a range of techniques including RT-PCR for DNA analysis, protein/enzyme sensing, and cell-based assays to identify and quantify different cellular systems. In general, these systems offer high surface to volume ratios in microchannels which increases the probability of pathogen interaction and cell capture at the sensor surfaces allowing for the rapid identification of small amounts of pathogens (Anderson *et al.* 2000). A wide range of commercial examples of these systems are available that can target different pathogens such as viruses and bacteria (Mairhofer *et al.* 2009). Rapid developments in technologies such as these could ultimately lead to developing these systems for membrane integrity monitoring (Anderson *et al.* 2000), however, there have not been any recent developments that further the prospects for this technique for membrane integrity surveillance.

2.8 Emerging Techniques

Developments in nanotechnologies over the past few decades have required new techniques for the detection of synthetic nano-sized particles in a range of media (Sanvicens *et al.* 2009; Herrmann *et al.* 2012; Carr and Wright 2013). Most viruses and many bacteria fall within the nanometer size range so techniques used to detect nanoparticles in water are readily applicable to NF and RO integrity monitoring, particularly where high sensitivity at low concentrations are available. The ability to detect single virus particles in a solution is perhaps the ultimate challenge for a membrane integrity test and there are several recent attempts to achieve this goal.

2.8.1 NanoSight Particle Tracking

The NanoSight nanoparticle tracking analysis (NTA) system was first commercialised in 2004 and covers a range of biological and biochemical applications (Carr and Wright 2013). Not unlike conventional zetasizer instruments, the NTA system can measure the particle size and zeta potential of nanoparticle suspensions. In addition to these analyses, the NTA system can measure fluorescence and the concentration of particles in solution in the size range 10-2000 nm diameter (NanoSight 2013). A report of the application of NTA technologies was recently published detailing a wide selection of examples of the versatile system in use, including uses in virology and vaccines, nanoparticle systems, and drug delivery (Carr and Wright 2013). The potential for scaling the system to a robust, portable, online instrument is not clear and this may limit its use to offline assays only.

2.8.2 Online Chemical Oxygen Demand

AquaDiagnostic Pty Ltd produces an online system to measure chemical oxygen demand (COD) of water samples (AquaDiagnostic 2013). Results can be obtained in less than 5 min using a robust, portable instrument that can perform a direct measurement of absolute COD that avoids the need for calibration. The minimum detection limit is reported to be 0.2 mg/L with a working COD range up to 350 mg/L, but some consumables and reagents are required. Table 2.3 shows results of a test performed using the COD analyser on the first and second pass RO permeates from a water recycling plant in Victoria, Australia. The COD results clearly show the sensitivity of the technique to measure low levels of organics and the test was also able to demonstrate a significant difference between the first and second pass RO membranes. Although the COD of the RO feed was not measured, the RO feed had a TDS of 3,160 mg/L so the 2nd pass permeate had an apparent LRV of 3.1.

Table 2.3: Example COD results of 1st and 2nd stage RO permeates.

RO Permeate	TDS (mg/L)	COD (ppm)
1 st pass	48.2	1.57
2 nd pass	2.4	0.27

The challenge for the online COD technique is to differentiate between chemical compounds and biological material that both exert a chemical oxygen demand. The data provided by the COD instrumentation is similar to that provided by the more expensive TOC instrument and has similar limitations based on the vagaries of feed concentration and the interferences and inhibitions arising from heavy metal contamination and chloride ion concentrations.

2.8.3 Whispering Gallery Microlasers

Whispering gallery mode (WGM) microlasers are a type of evanescent wave sensor that detects discrete changes in the resonance frequency of a WGM excited in a microspherical cavity. The resonance shift is detected in response to the presence of bound single virus particle such as the influenza virus (Vollmer *et al.* 2008). The WGM concept is based on the observation that sound waves could travel around a concave surface first discovered in the late 1800's in the whispering gallery of St Paul's Cathedral (Quinten 2011). The relatively recent development of WGM microresonator systems based on this acoustic phenomenon offer label-free detection of single viral pathogens but is currently only available as bench-scale systems (Vollmer 2010; Zhu *et al.* 2010; He *et al.* 2011). In addition, only very small volumes can be measured so this may limit its applications to low throughput applications.

2.8.4 Fluorescence Emission Excitation Matrices

Typical fluorescence emission excitation matrix (EEM) spectroscopy scans present emission fluorescence signals as a function of incremental changes in excitation wavelengths (Johnson *et al.* 1977). The result is a three dimensional, or contour, plot which highlights areas of high fluorescence intensity (Senga and Minami 1991). In water and wastewater samples, these areas are related to dissolved organic matter (DOM) in water samples with specific regions attributed to distinct components including proteins and organic acids. Fluorescence EEMs are widely used to monitor water quality (Yan *et al.* 2000; Baker 2002b; Stedmon *et al.* 2003; Carstea *et al.* 2010; Hambly *et al.* 2010a), to track effluent flows (Baker 2001; Baker 2002a), and to monitor recycled water schemes (Bierozza *et*

al. 2010; Hambly *et al.* 2010a; Hambly *et al.* 2010b; Galinha *et al.* 2011). In most cases, qualitative data is obtained but in some cases, semi-quantitative data can be obtained and changes in organic species can be monitored (Singh *et al.* 2009). Figure 2.10 shows examples of EEMs from the RO feed and first stage RO permeate from a water recycling plant in Victoria, Australia. The RO feed clearly shows regions of fluorescent organics (Figure 2.10a)) that are not present in the first stage RO permeate.

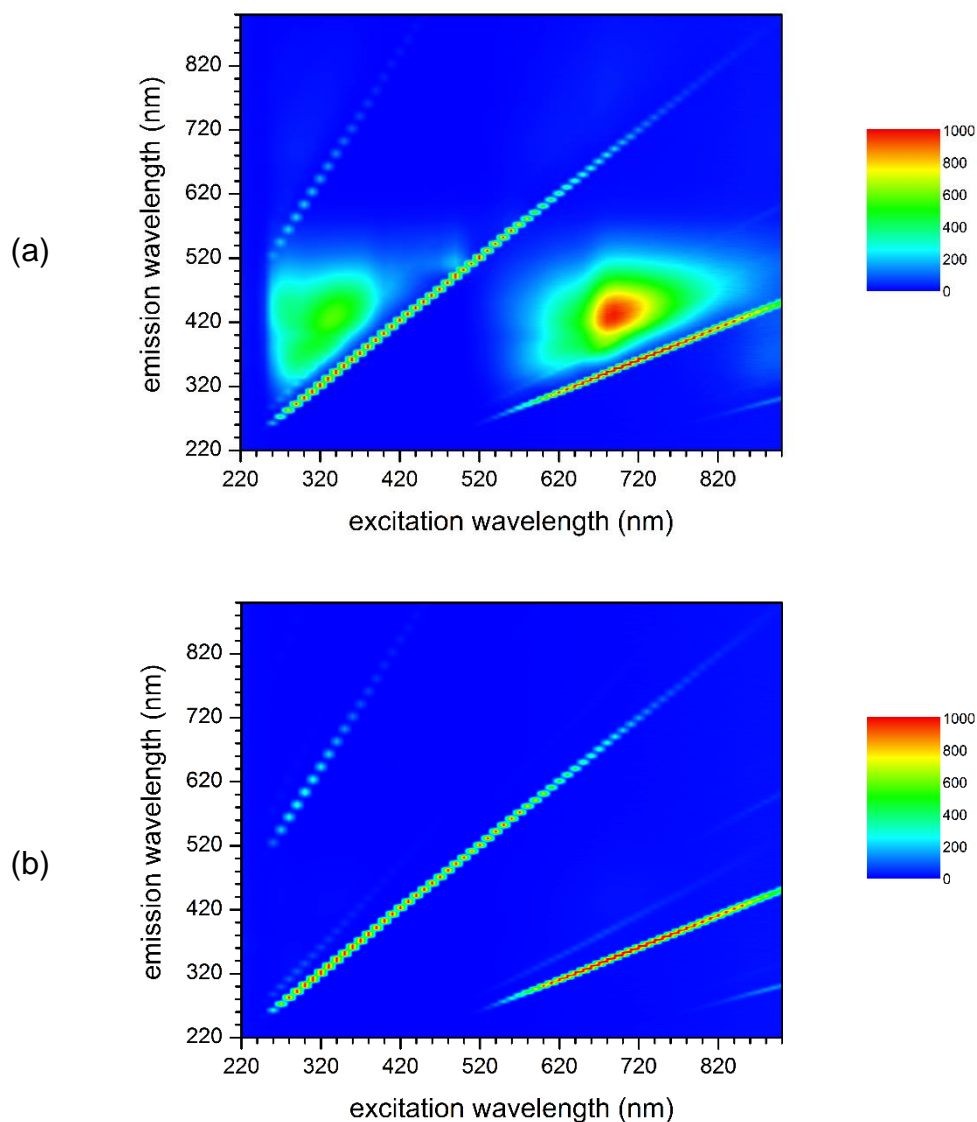


**Figure 2.10: Examples of EEMs from RO feed and permeate
(a) feed and (b) 1st pass permeate.**

Some reports have claimed the use of fluorescence EEMs to characterize RO permeates from multiple pass systems (Singh *et al.* 2012). In this report, qualitative and qualitative analyses of EEMs could distinguish between the different stages with a general trend towards lower organic fluorescence across the stages. Recently, a direct evaluation of the use of fluorescence EEMs for RO integrity monitoring compared the technique to conductivity testing (Pype *et al.* 2013). The results outlined a procedure for analysing the EEMs and the results suggest that the fluorescence technique is more sensitive than conductivity testing with DOM rejections of >99.9% obtained or better than 3 log₁₀ removal.

Quantifying the capacity to reject DOM can be used to infer the integrity of a membrane system and will generally understate the case as low molecular weight DOM can pass through a high pressure membrane where virus nanoparticles will be rejected leading to a more conservative LRV for the system being tested. The ability to identify the log removal potential of a membrane system using EEM is suitable where DOM is the principle measure, however, where nanoparticles such as virus are the primary concern, then this technique provides an inferred, qualitative surveillance capacity.

2.8.5 Quantum Dots

Many types of quantum dots (QDs) are reportedly highly detectable with strong fluorescence at low concentrations (Knappenberger *et al.* 2007; Borisov *et al.* 2008; Ni 2008; Zhang *et al.* 2010; Zhang and Liu 2010; Schneider *et al.* 2011). Typical QDs are formed using cadmium or zinc with the latter preferred due to its lower toxicity to humans and the environment (Geszke *et al.* 2011). Due to their high sensitivity and their ease of synthesis, QDs could potentially be used for

challenge tests providing the size of the particles could be extended beyond the relatively small sub-10 nm range to virus sized particles in the order of 20 nm (Pandey *et al.* 2006).

More recently, a new class of QD has emerged based on carbon. Nano-diamonds or carbon QDs are reported to be biocompatible, highly fluorescent, easy to synthesize and can be formed in a range of sizes (Mochalin and Gogotsi 2009; Wee *et al.* 2009; Hu *et al.* 2010; Bourlinos *et al.* 2011; Boudou *et al.* 2013; Havlik *et al.* 2013; Tan *et al.* 2013). These materials are now finding applications in the medical field as tracers and biomarkers (Liu *et al.* 2012; Liang *et al.* 2013) and due to their apparent compatibility with biological systems, they may offer a new type of safe, highly sensitive membrane integrity challenge test. The use of nano-diamonds to detect the presence of brain tumours in humans has been reported by researchers at Sydney University (Boulet 2015) where targeted drug delivery methods to destroy tumour growths are being developed. The technique is still primarily focused on human therapies but has potential to monitor membrane integrity as the nano-diamonds are reported to be relatively inexpensive although this report was on the basis of medical treatments so the relativity may be heavily biased and may be very expensive in terms of water industry.

2.9 Patented Integrity Monitoring Techniques

There are many patented techniques for integrity monitoring, although most are related to the integrity of porous hollow fiber MF/UF membranes. Of the patents relating to NF/RO membranes, the techniques vary from pulsed integrity test (Jons *et al.* 2010) to the detection of a pressurised gas (Jons 2011). None of the

current techniques satisfies the thesis objectives to develop a real-time high pressure membrane integrity monitoring technique.

2.10 Discussion – Potential Techniques for Further Development

Table 2.4 presents a summary of current and emerging techniques for NF/RO membrane integrity monitoring. The advantages and limitations are presented with a brief description of the test and the general application of the test to membrane systems. It is evident from the data presented in this Chapter that there are numerous techniques that are already available to be fully explored as options for online integrity monitoring and others that could be further developed. However, the limitations reported and the complexity of some of the techniques reduces the opportunities considerably. The membrane integrity techniques presented in Table 2.4 are colour coded with red signifying techniques not considered suitable to meet the objectives of this research. Techniques shaded in green are considered to have some potential and are assessed to determine whether they meet the objectives of this research.

Table 2.4: Summary of current and emerging integrity monitoring methods.

Monitoring Technique	Membrane Applications	Mode	Description	Scale	Advantages/Limitations	References
Existing Techniques – Direct Monitoring						
Vacuum Decay Testing	NF and RO membranes	Offline	Element soaked with RO permeate water overnight, drained then capped, vacuum applied, decay monitored over 1 min, fail at >10 kPa/min decay	Post-manufacturing, bench- and pilot-scale	Applies only to individual elements and not to the entire system	(Adham <i>et al.</i> 1998a; California Department of Public Health 2001; Lozier <i>et al.</i> 2003; ASTM 2010)
Pressure Decay Testing	MF, UF, NF, and RO membranes	Offline	One side of the membrane pressurised, pressure loss over time monitored	Bench- and pilot-scale, can be used for entire stage of NF and RO systems	Not practical for full-scale elements due to drainage requirement; pressurizing permeate side can cause damage to NF/RO membrane; therefore, not widely used for these systems	(Adham <i>et al.</i> 1995; Wilbert and Linton 2000; California Department of Public Health 2001; ASTM 2010)
Existing Techniques – Indirect Monitoring						
Particle Monitoring	MF and UF membranes	Online	Particle concentration measured in feed and permeate	Pilot-scale	Good for low-pressure membranes but not for NF/RO as particle size is too large; resolution dependent on particle concentration in feed water	(Wilbert and Linton 2000)
Turbidity Monitoring	MF and UF membranes	Online	Similar to particle, monitoring, concentration measured in feed and permeate	Full- and pilot-scale	Minimum particle size is 1 µm, low resolution	(Banerjee <i>et al.</i> 2001)

Monitoring Technique	Membrane Applications	Mode	Description	Scale	Advantages/Limitations	References
Sulphate Monitoring	NF and RO membranes	Offline	Sulphate concentrations measured in feed and permeate	Full-scale; can be used for entire stage of NF and RO systems	Expensive to monitor continuously using ICP	(DeCarolis <i>et al.</i> 2006b)
Conductivity Monitoring	NF and RO membranes	Online	Conductivity of feed and permeate monitored	Bench, pilot, full-scale; can be used for entire stage of NF and RO systems	Low resolution; removal limited to 2 log ₁₀ for water reuse applications, probing more effective than online monitoring	(Montgomery Watson 1997)
TOC Monitoring	NF and RO membranes	Online	TOC concentrations measured in feed and permeate	Full-scale; can be used for entire stage of NF and RO systems	Used in several installations but equipment to detect very low levels are expensive	(Montgomery Watson 1997; DeCarolis <i>et al.</i> 2006b)
Periodic Testing	NF and RO elements, trains	Online	Can involve multiple tests including conductivity probing and UV-254	Full-scale of NF and RO systems	Offers multiple, periodic testing, can locate defects but is complex to implement in full scale application	(Montgomery Watson 1997)
Challenge Tests						
Dye Testing	NF and RO membranes	Online	Log removal of dye measured by calibrated absorbance or fluorescence at optimum wavelength	Pilot- and full-scale	Can provide up to 4 log ₁₀ resolution; fouling can be an issue for some dyes but not Rhodamine WT	(Wilbert and Linton 2000; DeCarolis <i>et al.</i> 2006b)
Biological Surrogates (e.g. MS-2 Bacteriophage, <i>E. coli</i>)	MF, UF, NF, and RO membranes	Offline	High concentrations surrogate introduced into feed and concentration measured in permeate	Pilot- and full-scale	Seeding required since MF/UF pretreatment will remove most surrogates; can be expensive	(California Department of Public Health 2001)

Monitoring Technique	Membrane Applications	Mode	Description	Scale	Advantages/Limitations	References
Fluorescent Microspheres	MF and UF membranes	Offline	Microsphere concentration in feed and permeate measured by fluorescence	Pilot- and full-scale	Up to 4 log ₁₀ removal reported but expensive due to cost of particles	(DeCarolis <i>et al.</i> 2006b)
Spiked Integrity Monitoring	MF and UF membranes	Online	PAC particles injected in feed side and particle concentration measured in permeate	Full-scale	Applicable only for micron size particles	(van Hoof <i>et al.</i> 2003)
Pulse Integrity Test	NF and RO	Online	Measures a pulse of highly rejected species (i.e. sulphate)	Pilot scale	Can locate defects if calibrated	(Jons <i>et al.</i> 2005)
TRASAR®	NF and RO membranes	Online	Fluorescent molecules injected with antiscalant. Fluorescence measured in permeate using trace leak detection	Full-scale; can be used for entire stage of NF and RO systems	Up to 6 log ₁₀ removal reported with non-continuous spikes; 2 log ₁₀ when used with antiscalant	(DeCarolis <i>et al.</i> 2006b)
Integrated and Multi-Parameter Monitoring Systems						
Small sensor cell with collection membrane	MF and UF membranes	Online	Microsieve sensor membrane placed in permeate side stream; change in TMP of sensor membrane detects breach	Bench- and pilot-scale	Can take > 60 minutes to detect very small breach	(Fane 2009)
Binary Gas Integrity Test	MF and UF membranes	Online	Diffusivity of low permeating gas detected in permeate using mass flowmeters and composition with FTIR	Bench-scale	Complex to implement in larger membrane systems. Gas permeability may be an issue as would the cost of inert gases required.	(Giglia and Krishnan 2008)

Monitoring Technique	Membrane Applications	Mode	Description	Scale	Advantages/Limitations	References
ZAPS Liquid Station	General water quality monitoring device; could be applicable for MF, UF, NF and RO	Online	Measures multiple optical parameters simultaneously	Full-scale	Can potentially report high LRVs for TOC and BOD. Already being used in a limited way but presents challenge to quantify system LRV as it uses tryptophan, a common amino acid in many proteins not unique to E. coli and that may limit its sensitivity	(ZAPS Technologies Inc. 2013b)
Pathogen Detection Systems						
BioSentry Device	General water quality monitoring device; could be applicable for MF, UF, NF, and RO	Offline	Multi-angle light scattering at 660 nm used to determine particle size, shape, and internal structure	Bench-scale	Valid only for particles greater than 0.4 micron	(JMar 2011)
Real-Time Polymerase Chain Reaction (RT-PCR)	Water quality monitoring specifically for viruses	Offline	Feed and permeate collected and virus detected using various assays and a sequence of centrifugation, filtration, and enumeration techniques	Bench-scale	Requires specialised personnel, sample preparation, and long time periods for results; expensive	(Shirasaki <i>et al.</i> 2009)
Evanescence Wave Fiber Optic Sensor	Detection of pathogens	Online	Laser derived evanescent wave is excited over sample and fluorescence measured using laser spectrofluorometer	Bench-scale	Long detection time (several hours)	(Lee and Thompson 1996; Lim 2003; Byrne <i>et al.</i> 2009)

Monitoring Technique	Membrane Applications	Mode	Description	Scale	Advantages/Limitations	References
RAPTOR Fiber Optic Biosensor	Detection of pathogens	Online	Monitors complex formation by evanescently exciting surface-bound fluorophores with a diode laser	Bench-scale	Portable, results in less than 10 minutes	(Anderson <i>et al.</i> 2000)
Miniaturised portable biosensor	Detection of pathogens	Online	Electrochemical technique (impedance spectroscopy) used to detect virus by immobilization of antibodies onto biofunctionalised gold electrode	Bench-scale	Long detection time (several hours)	(Diouani <i>et al.</i> 2008)
Microarray Biosensor Instrument	Detection of pathogens	Online	Automated Concentration System (ACS) uses advance array biosensor to detect pathogens in water	Bench-scale	Laboratory scale.	(U.S. Environmental Protection Agency 2009)
Surface Plasmon Resonance Biosensors	Detection of pathogens	Online	Illumination of a metallic surface by visible or near-infrared radiation from a monochromatic light source <i>via</i> a hemispherical prism; electromagnetic waves are generated and detected	Bench-scale	Not currently available as a commercial technique for field applications.	(Wei <i>et al.</i> 2007)
Quantum Dot Based DNA Nanosensors	Detection of pathogens	-	Ultrasensitive nanosensor based on fluorescence resonance (FRET) for detecting DNA	Bench-scale	Requires specialised personnel; expensive	(Zhang <i>et al.</i> 2005)
Laser- Scanning Cytometry (LSC)	Detection of pathogens	Online	LSC used to detect microspheres in feed and permeate samples	Bench-scale	Only applicable for micron sized particles	(Ladner <i>et al.</i> 2007)

2.11 Towards a New Membrane Integrity Monitoring Technique

The techniques identified in the review of the literature presented in this Chapter were distilled down fluorescent chemical compounds and tagged nanoparticles. In the proceeding chapters, a selection of dyes, fluorescent chemicals and fluorescently tagged nanospheres will be assessed to determine whether any of these materials can be used as reliable surrogates and can provide the level of detection required to meet the objectives of this research. Techniques based on light scattering of particles, which are relatively unexplored in the literature but which present a potentially new and innovative detection method, will also be explored.

This research will develop a robust non-microbial surrogate representative of the polio virus, the smallest enterovirus used as the target to challenge membrane integrity. In isolation, this would not meet the objectives of this research that requires the development of an integrated membrane integrity technique and that demands a detection system that has the sensitivity to provide an LRV performance up to and potentially beyond $4 \log_{10}$. Accordingly, light scattering was used to detect and enumerate a non-microbial surrogate.

Chapter 3

Screening Food Grade Dyes and Fluorescent Compounds

3.1 Preamble

In the quest to identify suitable non-microbial surrogates for membrane integrity testing, it is essential that any surrogates meet the minimum requirements of a challenge species as outlined in Table 2.1. Inherent to these minimum requirements is stability across a range of conditions that may represent varying feed water chemistries and environmental parameters. In this Chapter a range of food grade and fluorescent tracer dyes were tested under various conditions to identify the influence on fluorescence by those conditions.

3.2 Introduction

Chemical tracers are widely used to study flow patterns in a range of water and soil systems (Harden *et al.* 2003). Synthetic food dyes are a popular choice for tracing water flow patterns due to their high visibility and detection and importantly, low toxicity to the environment (Flury and Fluehler 1995; Reinken *et al.* 1996). Hydrological tracers are typically sourced from the class of triarylmethane dyes and this class includes dyes that are mostly red, violet, blue, or green in colour (Mon *et al.* 2006). An ideal dye to trace the movement of water should move conservatively with minimal interaction with the solid phase and without decaying during the time period of the tracer test (Mon *et al.* 2006). Brilliant Blue FCF and other similar dyes are used successfully because they are

relatively inert and are not toxic to the environment (Flury and Fluehler 1994; Flury and Fluehler 1995; Reinken *et al.* 1996; Ketelsen and Meyer-Windel 1999; Schwartz *et al.* 1999; Germán-Heins and Flury 2000; Kasteel *et al.* 2002; Nobles *et al.* 2004; Mon *et al.* 2006; Amoozegar *et al.* 2008; Morris *et al.* 2008; Nobles *et al.* 2010).

In addition to the range of food dyes used as tracers, several fluorescent dyes are often used to study flow patterns in water and soil systems with compounds such as fluorescein (FL) (Ford and Thornton 1983; Gitis *et al.* 2002; Harden *et al.* 2003; Chua *et al.* 2007) and Rhodamine WT (RWT) (Smart and Laidlaw 1977; Stanbro and Pyrch 1979; Shiau *et al.* 1993; Laenen and Bencala 2001; Sutton *et al.* 2001; Harden *et al.* 2003; Binet *et al.* 2007; Chua *et al.* 2007) commonly used for this purpose. The fluorescent dyes are particularly useful due to their high sensitivity and selectivity (Harden *et al.* 2003; Binet *et al.* 2007; Chua *et al.* 2007). The use of RWT as a potential surrogate for use in RO integrity monitoring has been widely reported (Kitis *et al.* 2003a; Kitis *et al.* 2003b; Zornes *et al.* 2010; Lozier *et al.* 2011; Lozier *et al.* 2013) with detection limits as low as 0.01 ppb (Ford and Thornton 1983). Moreover, the use of RWT for high pressure integrity testing is specified in both ASTM D6908 (2010) and the US EPA Membrane Filtration Guidance Manual (U.S. Environmental Protection Agency 2005).

As potential surrogates for membrane integrity monitoring, any tracer dye should be stable over a wide range of physicochemical feed water parameters. Temperature, for example, is a parameter that can vary significantly with different feed waters and can potentially affect the sensitivity and detection of tracer dyes. Fluorescent dyes in general are sensitive to changes in temperature with high

temperatures resulting in lower fluorescence intensities (Smart and Laidlaw 1977). Salt is known to quench the fluorescence of some compounds (Verity and Bigger 1996) so any tracer dye must either be resistant to this effect or be subjected to adequate calibration over an expected salt concentration range. The effect of UV light on the absorbance of the tracer dyes is also important in terms of storage and preservation to avoid degradation.

This chapter identifies a range of food and fluorescent dyes that could potentially be used as tracer compounds for membrane integrity monitoring. The dyes are screened for their overall detectability and sensitivity when subjected to a range of water conditions including various temperatures, pH values, salt content and the presence of potentially interfering compounds.

3.3 Fluorescence

Fluorescence is the process where the introduction of energy by physical (absorption of light), mechanical (friction), or chemical mechanisms on receptive molecules creates electronically excited states that then emit light. Fluorescence is the property of some atoms and molecules to absorb light at a particular wavelength and to subsequently emit light of longer wavelength after a brief interval, termed the fluorescence lifetime.

The fluorescence process is governed by three important events, absorption, excitation and emission. Light energy is absorbed by a susceptible molecule and excites the energy levels within the molecule. The result of the excitation is the desire to stabilize the energy state that results in the emission of a longer wavelength photon and the return of the molecule to the ground state. Figure 3.1 illustrates the process of fluorescence where light in the UV visible range between

400 nm and 750 nm is incident on susceptible molecules and is absorbed resulting in the emission of fluorescence with a longer wavelength than the incident light. Figure 3.2 illustrates the variety of responses resulting from the interaction of light incident on a molecule or particle.

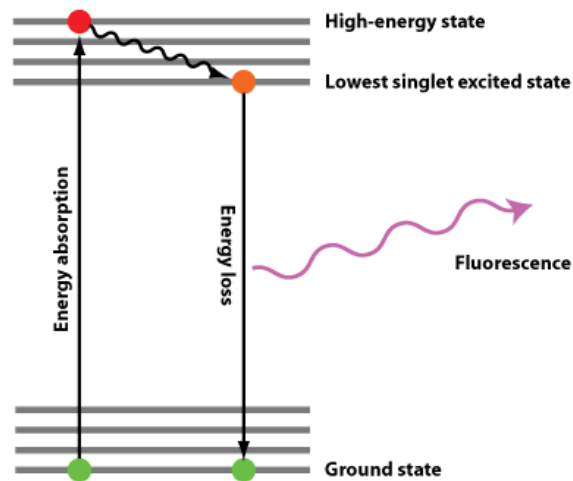


Figure 3.1: Energy interaction with a molecule creating fluorescence from (Osterhus 2013).

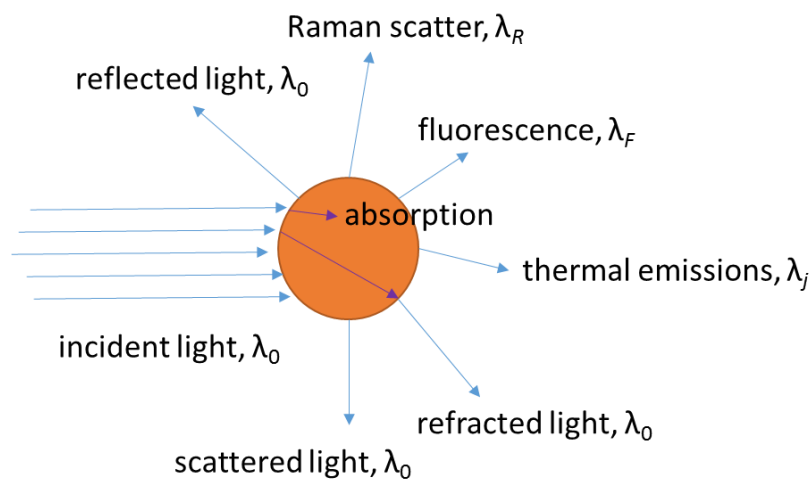


Figure 3.2: Interaction of light with a molecule or particle adapted from (Seinfeld and Pandis 2012).

British scientist Sir George G. Stokes first described fluorescence in 1852 and named the phenomenon after the blue-white fluorescent mineral fluorite (fluorspar) (Stokes 1852). Stokes also discovered the wavelength shift of fluorescence to longer values in emission spectra that bears his name.

3.4 Screening Methods

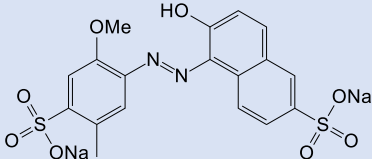
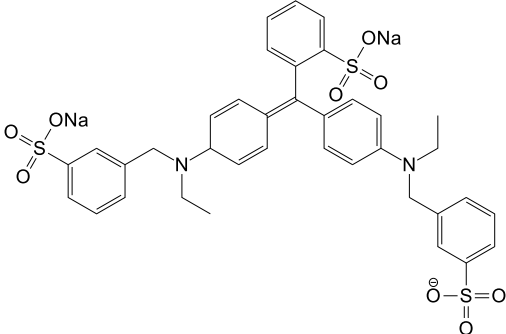
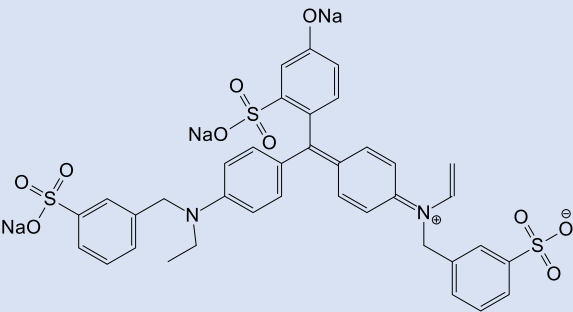
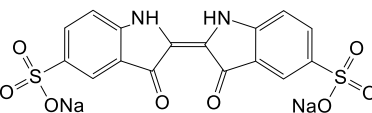
3.4.1 Potential Surrogates

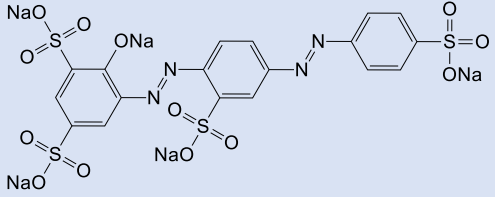
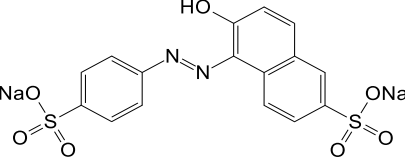
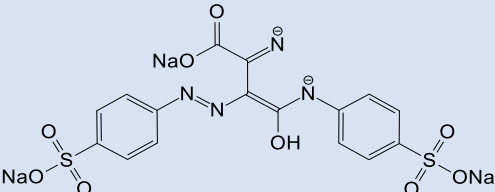
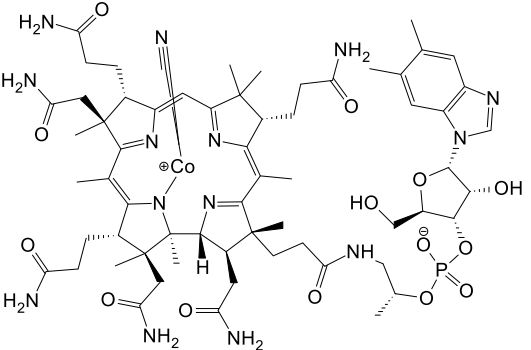
A series of compounds including food-grade and fluorescent dyes were selected in accordance with the initial screening criteria and their structures and properties are listed in Table 3.1.

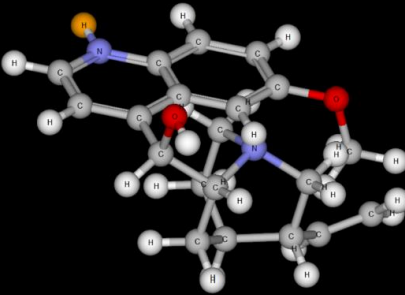
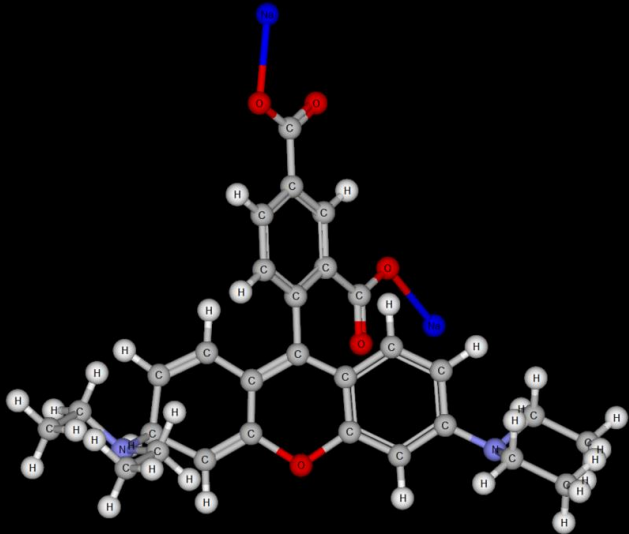
3.4.2 Surrogate Detection Limit and Calibration

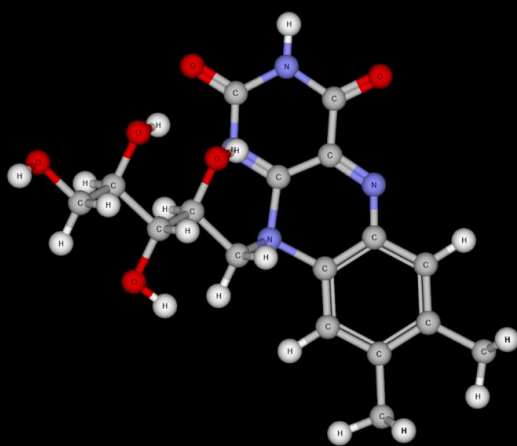
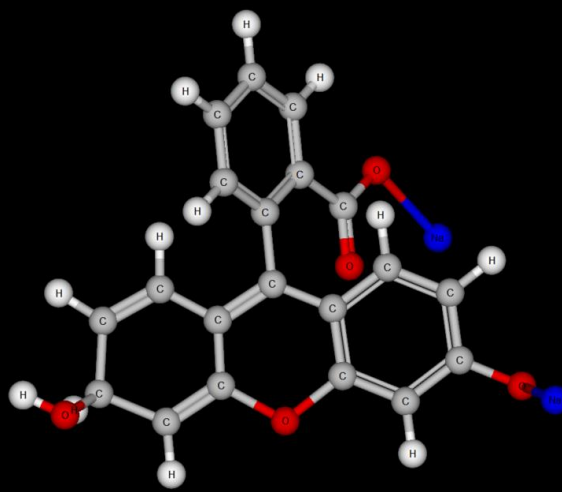
Stock solutions of the dyes were prepared at natural pH using deionized (MilliQ) water. The minimum detection limits and sensitivities were determined by either UV spectroscopy (Shimadzu UV/vis spectrophotometer, Model UV-1800) or fluorescence spectroscopy (Shimadzu spectrofluorometer, Model RF-5301) and calibration curves were prepared from low to high concentrations for each dye accordingly at 25°C and pH 7.

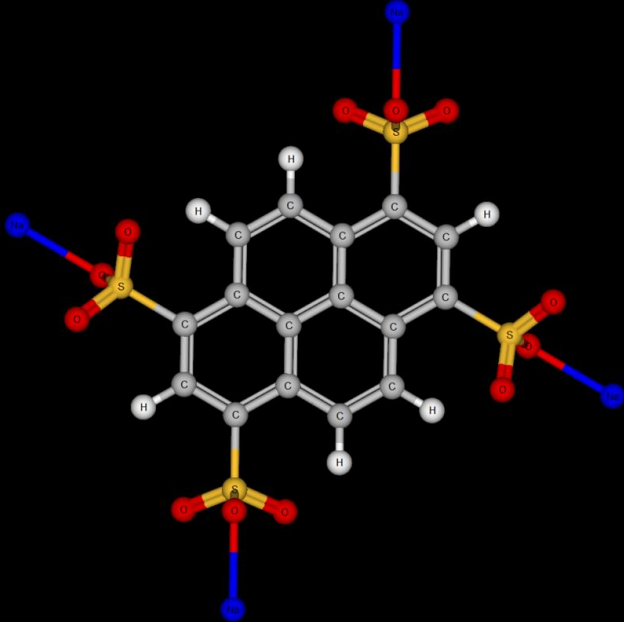
Table 3.1: Properties of food and fluorescent dyes selected for screening

Dye	Formula and MW	Structure	Properties
Allura red	$C_{18}H_{14}N_2Na_2O_8S_2$ 496 g/mol		<ul style="list-style-type: none"> • λ_{max} 504 nm • \$508/kg • red food dye
Brilliant Blue	$C_{37}H_{35}N_2Na_2O_9S_3$ 793 g/mol		<ul style="list-style-type: none"> • λ_{max} 625 nm • \$3,182/kg • food colourant, water tracer dye • also known as Brilliant Blue FCF, Food Blue #2
Fast green	$C_{37}H_{31}N_2Na_2O_{10}S_3$ 828 g/mol		<ul style="list-style-type: none"> • λ_{max} 427-622 nm • \$6,424/kg • food dye
Indigotine	$C_{16}H_8N_2Na_2O_8S_2$ 466 g/mol		<ul style="list-style-type: none"> • λ_{max} 602 nm • \$1,474/kg • food dye and pH indicator

Dye	Formula and MW	Structure	Properties
Ponceau S	$C_{18}H_9N_4Na_5O_{13}S_4$ 732 g/mol		<ul style="list-style-type: none"> • λ_{max} 520 nm • \$1,632/kg • food-grade dye, used for protein staining
Sunset yellow	$C_{16}H_{10}N_2Na_2O_7S_2$ 452 g/mol		<ul style="list-style-type: none"> • λ_{max} 482 nm • \$1,734/kg • food colouring dye
Tartrazine	$C_{16}H_9N_4Na_3O_9S_2$ 534 g/mol		<ul style="list-style-type: none"> • λ_{max} 425nm • \$275/kg • food colouring dye
Vitamin B12 (RB)	$C_{63}H_{88}CoN_{14}O_{14}P$ 1355 g/mol		<ul style="list-style-type: none"> • λ_{max} 361 nm • \$1,355/kg • heat stable slowly loses activity when exposed to light, oxygen and acid • also known as cyanocobalamins

Dye	Formula and MW	Structure	Properties
Quinine (QN)	$C_{20}H_{24}N_2O_2$ 324 g/mol		<ul style="list-style-type: none"> • $\lambda_{ex}/\lambda_{em}$ 331/383 nm • \$18,768/kg • common pharmaceutical chemical • max. dimensions (Å): 9.7113 9.1211 8.0024
Rhodamine WT (RWT)	$C_{29}H_{30}N_2Na_2O_5$ 532 g/mol		<ul style="list-style-type: none"> • $\lambda_{ex}/\lambda_{em}$ 566/582 nm • \$105/kg • synthetic red to pink dye with brilliant fluorescent qualities • used as a water tracing dye, can stain organic materials • also known as Acid Red #388 • CAS # 37299-86-8 • max. dimensions (Å): 14.9676 13.4641 11.9723

Dye	Formula and MW	Structure	Properties
Riboflavin (RF)	$C_{17}H_{20}N_4O_6$ 376 g/mol		<ul style="list-style-type: none"> • $\lambda_{ex}/\lambda_{em}$ 365/550 nm • \$1,210/kg • poorly water soluble • decomposes in light • also known as Vitamin B2 • max. dimensions (Å): 13.2986 13.1015 11.9068
Uranine (UR)	$C_{20}H_{12}Na_2O_5$ 378 g/mol		<ul style="list-style-type: none"> • $\lambda_{ex}/\lambda_{em}$ 480/510 nm • \$244/kg • Also known as Acid yellow #73, Fluorescein sodium salt • max. dimensions (Å): 11.0268 10.4798 10.2407

Dye	Formula and MW	Structure	Properties
1,3,6,8-pyrene- tetrasulfonic acid tetrasodium salt (PyTS)	$C_{16}H_6Na_4O_{12}S_4$ 610 g/mol		<ul style="list-style-type: none"> • $\lambda_{ex}/\lambda_{em}$ 360/380 nm • \$109/gram • also known as TRASAR® (Sabnis 2015) • Currently only available as a proprietary antiscalant system • CAS #59572-10-0 • max. dimensions (Å): <ul style="list-style-type: none"> • 14.4199 • 10.6294 • 10.5210

3.4.3 Effect of Temperature

Changes in the UV absorbance or fluorescence intensity of the selected surrogates were measured over the range 10-30°C at 5°C increments at constant pH (7) and no added salt. The same sample was heated by immersing a beaker containing the surrogate into a water bath or ice bath. For measurements above ambient room temperature, samples were heated 2-5°C higher than the target and for measurements below room temperature, samples were cooled 1-3°C lower to allow for cooling/heating in the measurement period respectively. Once the desired temperature was reached, the sample was immediately transferred to the appropriate cuvette and the absorbance or fluorescence reading taken. For consistency, samples were normalised to the measurement taken at 10°C.

3.4.4 Effect of Sample pH

The effect of pH on selected surrogates was measured over the pH range 5.5-7.5 at increments of 0.5 and at constant temperature (25°C) and no added salt. In this case, the pH was adjusted by adding small volumes of 0.1 M HCl or NaOH and the measurements were normalised by comparing the absorbance or fluorescence to a sample that was diluted with the same volume of water at the natural pH of each solution.

3.4.5 Effect of UV Light Exposure

Samples were exposed to a UV light source (UVA) for up to 24 h to determine the effect of exposure. The absorbance or fluorescence of the solutions were measured before treatment and after 1, 3, 6, 12 and 24 h of UV exposure. The data were normalised to the measurements taken before exposure.

3.4.6 Effect of Water Chemistry

Other potential interfering compounds, such as salts, organic compounds and oxidants, were tested alone or in combination with the dyes and these are listed in Table 3.2. In each case, samples were compared to solutions diluted with the same volume of MilliQ water as the test solution.

Table 3.2: Interfering agents used for surrogate screening

Compound	Concentration/ppm
Sodium chloride, NaCl	500-16000
Calcium chloride, CaCl ₂	500-6000
Acetic acid	10-50
Residual chlorine	0-3
Chloramine	0-1
Hydrogen peroxide	5
Polysaccharide (dextran, neutral polymer)	10
Protein (bovine serum, anionic polymer)	10
Polysaccharide (sodium alginate, anionic polymer)	10
Polyethyleneimine (cationic polymer)	12

3.4.7 Bench-scale Continuous Dose Dye Testing

Subsequent to the screening process, two fluorescent dyes were selected for further testing. The fluorescent dyes that provided high sensitivity and that were widely used in the water industry were used in a bench scale challenge test to compare between continuous and pulsed application of the dye. In both cases, the bench scale test rig was comprised of a Sterlitech CF042 stainless steel cross flow cell with an active membrane surface area of 42 cm². Permeate samples were collected and tested for the presence of the dyes using a Perkin Elmer LS50

spectrofluorometer. A flow-through cell was constructed and used to continuously monitor the fluorescence of the permeate for some samples. Dow Filmtec BW30 membranes were used in all experiments.

Figure 3.3 shows the schematic representation of the continuous dose membrane filtration cell. An initial dye concentration of 1 mg/L in the feed was used with the concentrate recycled. The low recovery rate of 40% combined with the small loss of fluorescent dye in the permeate had a small influence on the applied concentration over the duration of the test, and this was considered to be negligible. This feed concentration was determined using 10 ng/L as the limit of detection in order to capture up to 5- \log_{10} LRV resolution if possible.

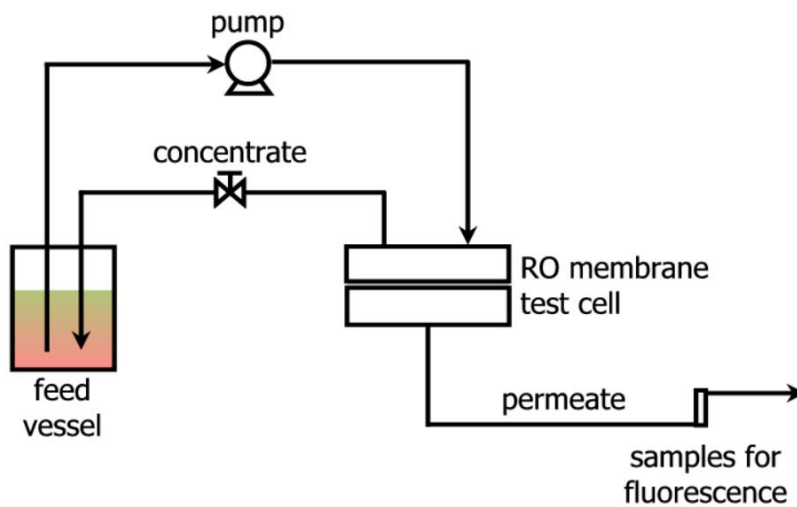


Figure 3.3: Schematic diagram of continuous dose dye challenge test.

3.4.8 Bench-scale Pulsed Dose Dye Testing

A schematic of the pulsed dose setup is shown in Figure 3.4. In this test, concentrations of 1-10 mg/L were used with various volumes dosed via a 3-way

switching valve in order to introduce a fixed volume of dye over a known period of time. During the pulsed dose, the concentrate was collected separately to avoid dye from entering the main feed vessel and it was switched back following the removal of the dye from the system.

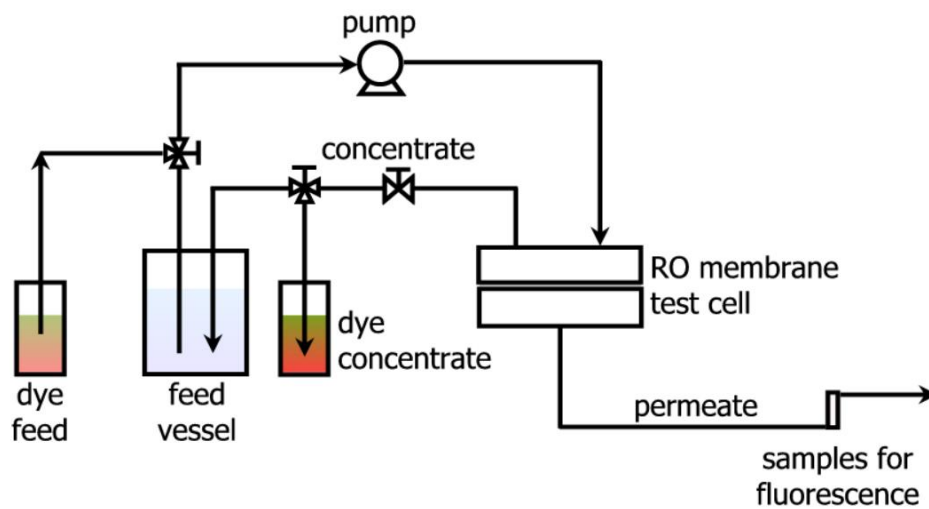


Figure 3.4: Schematic diagram of pulsed dye challenge test.

Several membrane defects were simulated on sections of flat sheet membrane samples. These included an O-ring defect that was simulated by cutting the O-ring and removing a 1 mm section of the material to provide a pathway for contaminants to enter the permeate directly from the feed side of the membrane. Scratching the surface of the membrane sheet with a 0.8 mm hypodermic needle simulated mechanical damage of the membrane. Puncturing the membrane with the same hypodermic needle simulated a pinhole integrity breach. A glue-line leak was simulated by removing the inner O-ring and a further membrane sample was oxidised by exposure to 1000 mg/L of hypochlorite for 1 h.

3.4.9 Dye Absorbance

In addition, experiments to measure the potential absorbance of fluorescent dyes on a membrane surface were performed. Visual data of any stained membrane material was recorded, however, quantifying the mass of dye absorbed by the membrane was not possible with the bench scale equipment. A stained membrane indicated that some of the rejection was the result of absorbance rather than direct rejection.

3.5 Results and Discussion

Initial screening tests were performed to determine the optimum measurement UV wavelengths or fluorescence emission/excitation wavelength pairs on the various potential surrogates to identify one or more compounds that have the potential for use to measure membrane integrity. Continuous and pulsed challenge tests were conducted using two fluorescent dyes selected based on the performance during the screening tests.

3.5.1 Food Dye Screening

For the selected food dyes, the optimum wavelengths measured by UV-vis spectrophotometry are presented in Figure 3.5.

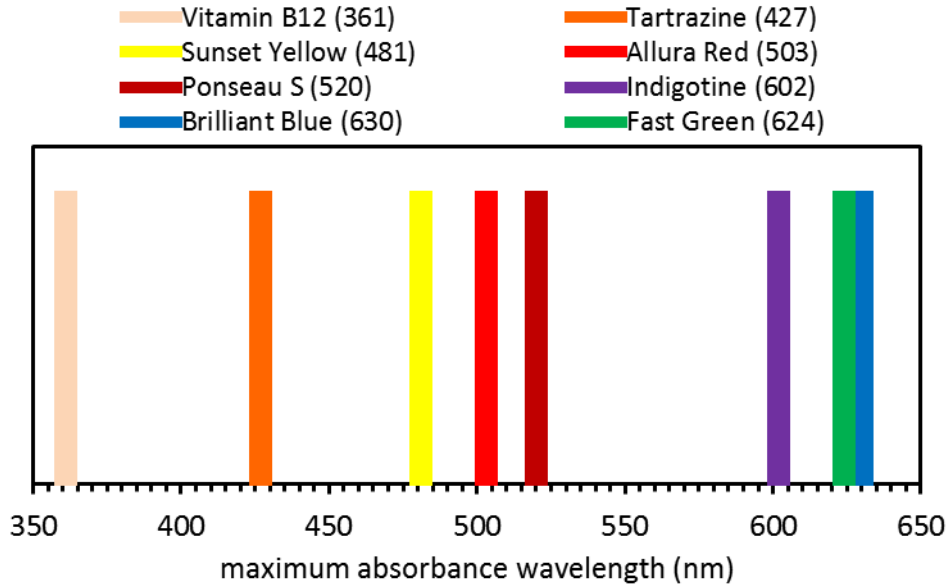


Figure 3.5: Optimal wavelengths for selected food grade dyes.

The corresponding calibration curves for these dyes is shown in Figure 3.6 and it is clear that the blue/green dyes are more sensitive than the red/yellow dyes which is a function of the wavelength of their measurement. Based on this observed higher sensitivity of the blue/green dyes, only Brilliant Blue (BB) and Fast Green (FG) dyes were selected for further assessment. Figure 3.7 indicates that FG is slightly more sensitive than the BB dye but the absorbance is significantly reduced for samples in the mg/L range. This suggests that a dose in excess of 100 mg/L would be required to provide an LRV of $2 \log_{10}$.

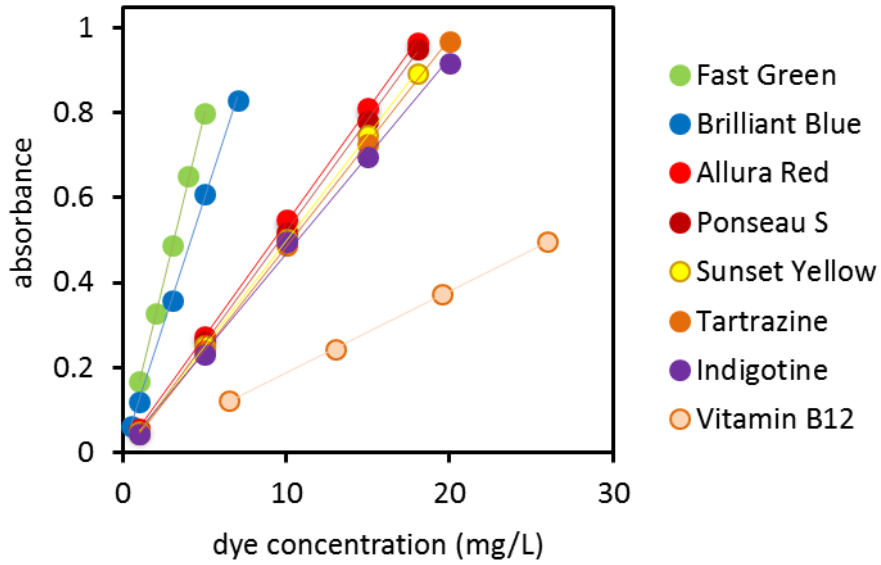


Figure 3.6: Calibration curves for selected food grade dyes.

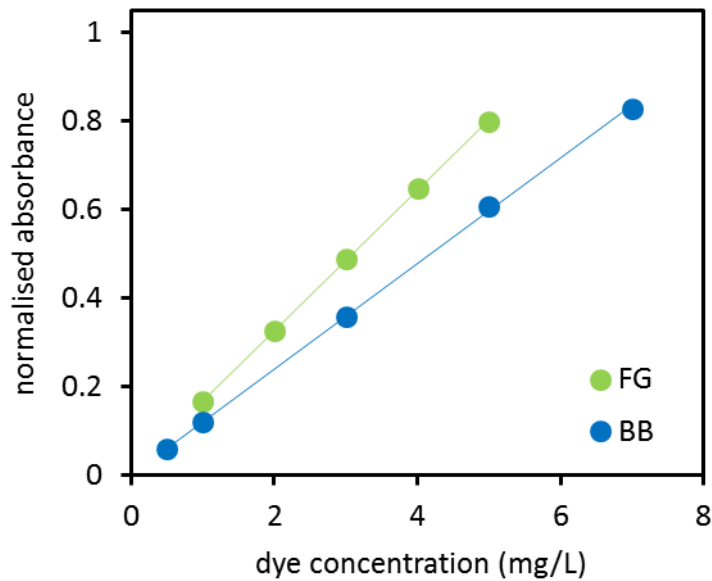


Figure 3.7: Calibration curve of FG and BB dyes.

As shown in Figure 3.8, BB is more stable than FG across a pH range between 5.5 and 7.5 that is the typical range for RO feed water. Fast Green can be effective below pH 6.5 but is less stable as the pH increased up to pH 7.5. The

stability of FG at elevated pH conditions introduces a confounding effect if this dye was used as a surrogate in an integrity test, as pH conditions can change across a membrane depending on the water chemistry. The effect of dissolved gases such as carbon dioxide can result in either an elevation or decrease in permeate pH based on feed water pH and temperature that would lead to lower LRVs than would otherwise be the case.

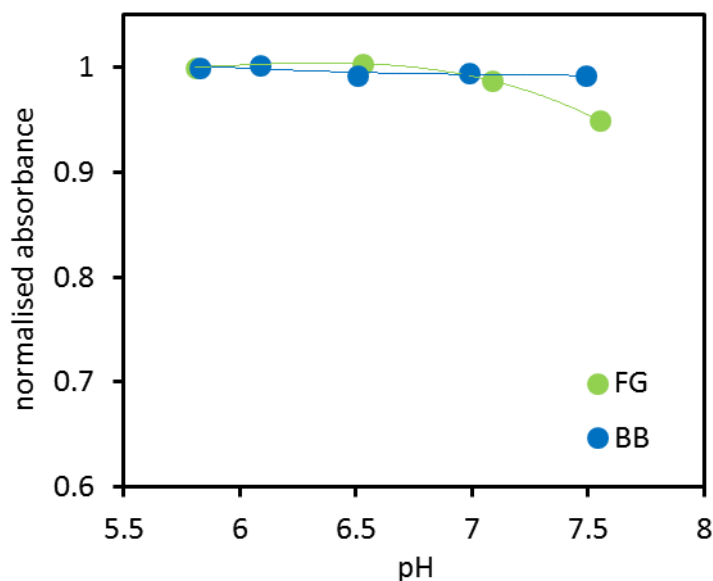


Figure 3.8: Effect of pH on FG and BB dyes.

As illustrated in Figure 3.9, BB and FG are relatively stable across a range of temperatures. Temperature variations are expected in many water reuse schemes as a result of diurnal and seasonal influences and using FG as a surrogate based on a standard calibration has the potential to marginally over state membrane integrity although the impact is small. Varying temperature conditions does impact both dyes with an observed reduction in detection by around 5%. Although BB is a marginally better surrogate dye under varying temperature conditions, the low sensitivity of both dyes limits their application.

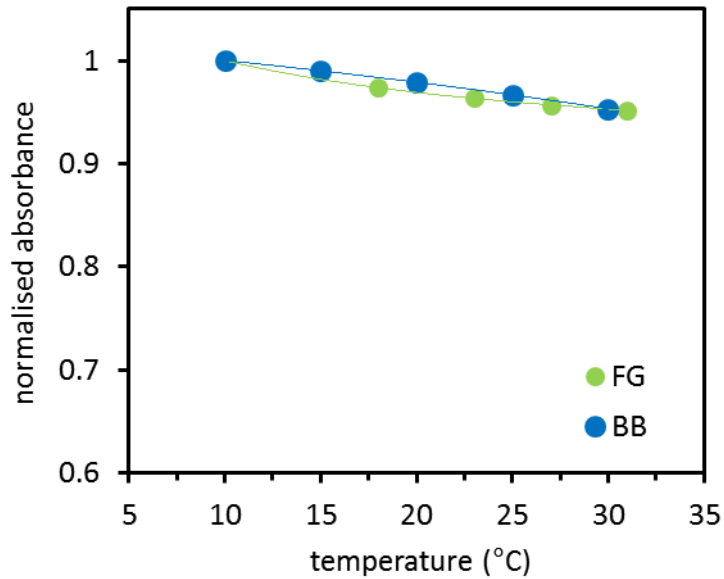


Figure 3.9: Effect of temperature on FG and BB dyes.

Exposure to UV light has a marked impact on both BB and FG with a non-linear response from FG but a major reduction in absorbance for BB as shown in Figure 3.10. The detection of the latter is reduced by around 25% after 24 hours of UV exposure while FG has deteriorated by around 15% in a non-linear fashion. Developing a calibration curve for potential UV exposure for both dyes severely limits and challenges their applicability as membrane integrity surrogates.

Figure 3.11 shows that BB is stable when exposed to chloramine but its detection is reduced by around 5% by the addition of residual chlorine as sodium hypochlorite at a dose rate of 1 mg/L. Chloramine moderately affects FG with a 6% reduction in detection but this is reduced by 10% when exposed to 1 mg/L of chlorine. The application of BB appears viable where disinfection in the form of chloramination is adopted otherwise both dyes are challenged where chlorine residuals are evident. It is common to dose chloramine into NF and RO feed water to reduce differential pressure increases as a result of biological fouling.

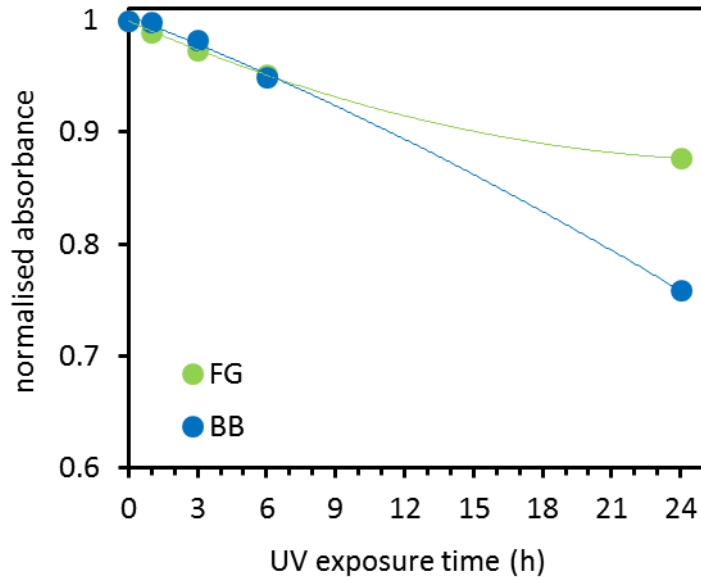


Figure 3.10: Effect of UV exposure on FG and BB dyes.

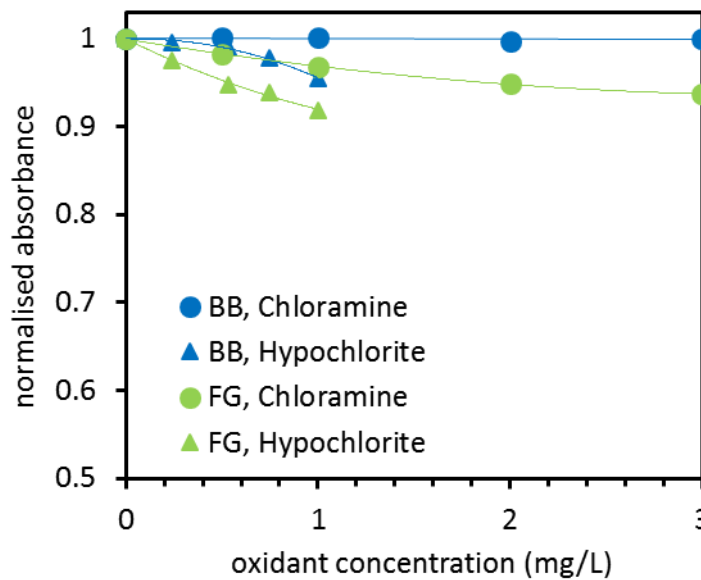


Figure 3.11: Effect of oxidants on FG and BB dyes.

The summary of responses shown in Figure 3.12 suggest that BB is less challenged by the range of additional environmental exposures compared to FG. It is clear from these results that the food grade dyes in general did not meet the requirements of the established selection criteria matrix (see Table 2.1). On this basis, it is evident that the selected food grade dyes are not suitable surrogate

candidates for membrane integrity monitoring. This is primarily due to the nature of the detection method that has a much higher minimum threshold concentration for detection than required.

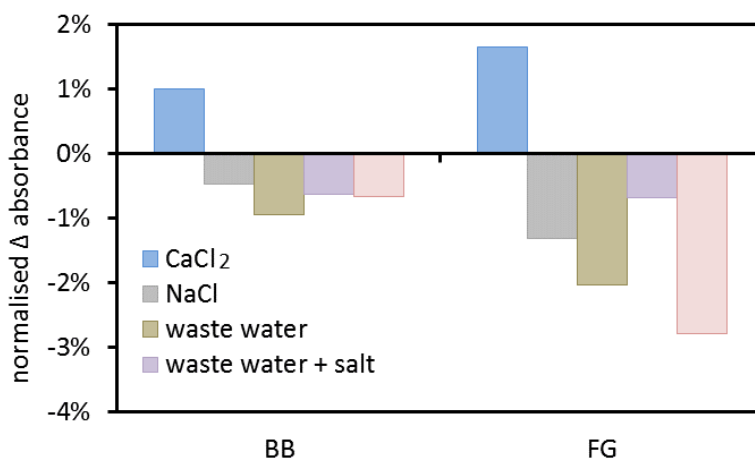


Figure 3.12: Effect of environmental conditions on FG and BB dyes.

3.5.2 Fluorescent Dye Screening

The use of RWT as a potential surrogate for membrane integrity testing has shown some promise in comparison with microbial and particle dyes surrogates (Kitis *et al.* 2003b). Recently, the use of UR has also been reported with the development of a pulsed marker membrane integrity monitoring system which demonstrates LRVs of greater than 4-logs (Frenkel and Cohen 2014; Surawanvijit *et al.* 2015). In this study, RWT and UR compounds were partially screened for temperature and pH effects (Frenkel and Cohen 2014).

The calibration curves of the fluorescent dyes are shown in Figure 3.13. Under the conditions tested, the (Vitamin B12) RB and (Quinine) QN chemicals showed relatively poor sensitivity with high concentrations required to elicit a strong fluorescence response (Figure 3.13 (a)). Of the other dyes tested, the PyTS dye

shows the highest sensitivity followed by RWT then UR (Figure 3.13 (b)) and in all cases, detection in the $\mu\text{g/L}$ range was possible using the Shimadzu RF-501 instrumentation. Calibration would need to be repeated for new fluorescence detectors. These results are in contrast to those reported by Frenkel and Cohen (2014) with UR showing higher sensitivity than RWT.

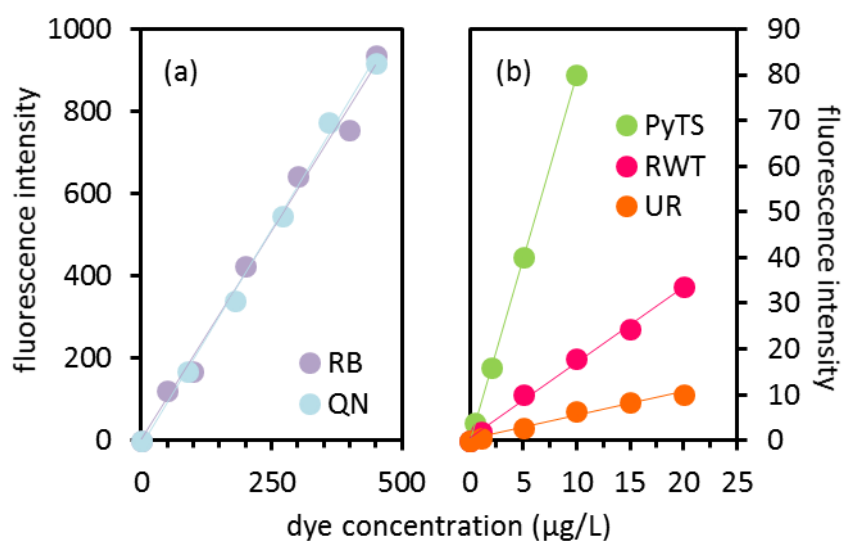


Figure 3.13: Calibration curves of fluorescent dyes.

The effective detection limits for the fluorescent dyes appear to be greater than 5 $\mu\text{g/L}$ for UR, around 2 $\mu\text{g/L}$ for RWT and $<1 \mu\text{g/L}$ for PyTS. On this basis it appears that PyTS provides a better sensitivity at moderate fluorescence levels compared to RWT and UR. Given that QN and RB offered considerably weaker fluorescence of the five dyes tested, these were excluded from further screening.

The fluorescence intensity of the dyes was then tested over a temperature range 10-30°C with the results normalised to 10°C. Figure 3.14 shows the effect of this temperature increase for the dyes and in each case, the intensity decreases with increasing temperature. This effect is similar for PyTS and UR with decreases of up to 18% and 21% in fluorescence intensity respectively. The effect on RWT is

more significant with a decrease of 37% over the tested temperature range. However, since the observed trend in intensity is linear, this effect can be addressed by preparing multiple calibration curves at various temperatures. This may be considered onerous in an operating environment and may limit the application of these dyes under operation conditions, however, this could be compensated by a software programme to provide updated calibration based on temperature feedback.

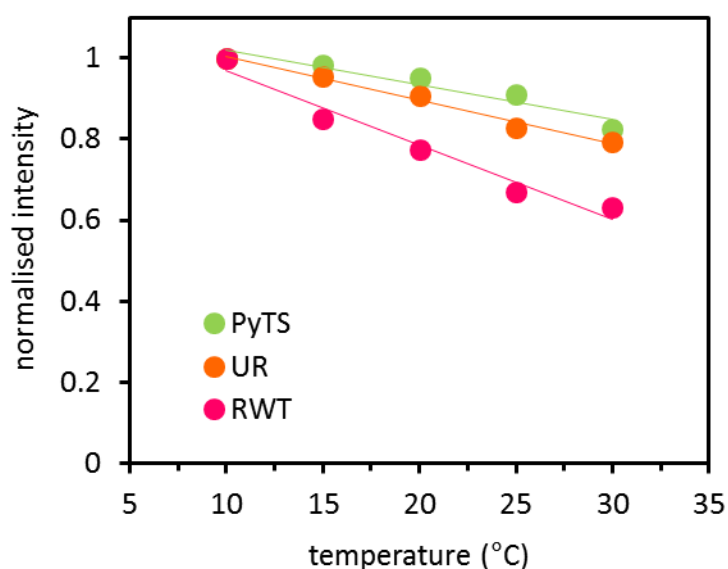


Figure 3.14: Effect of temperature on dye fluorescence.

The normalised fluorescence intensity of the dyes as a function of pH was measured and the results are shown in Figure 3.15. No change was observed for PyTS and RWT over the pH range tested but a significant change was observed for UR. In this case, a substantial increase in fluorescence intensity occurred over the pH range 5-7.5, equivalent to an increase of 235%. Again, this effect is linear so additional calibrations can be used to account for this effect. The stability of RWT with pH was also reported by Frenkel and Cohen (2014), however, they

also reported relative stability for UR with pH. In their study, high concentrations of the dyes were tested that could be considered outside the range of quantitative fluorescence with concentration at 2.5 mg/L, very close to the expected feed concentration, and potentially in the range where self-quenching could occur (Jones and Rahman 1994).

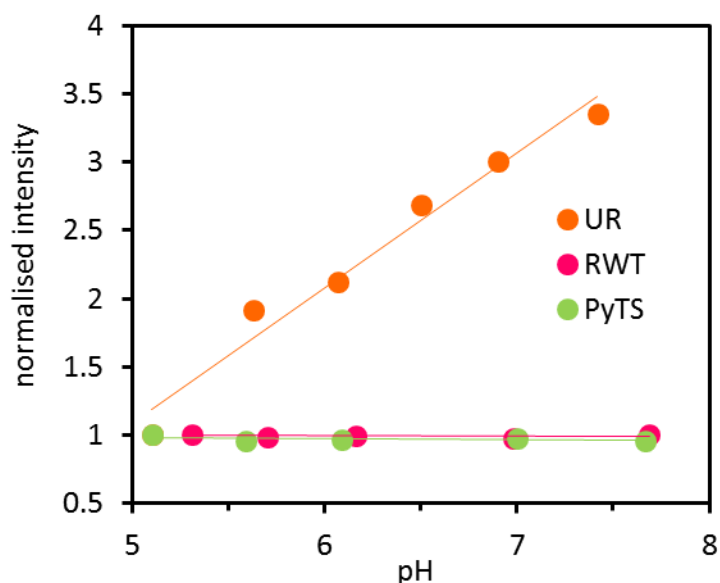


Figure 3.15: Effect of pH on dye fluorescence.

Measuring pH in permeate with low salinity presents challenges and requires frequent calibration of the secondary parameter to ensure that the primary parameter, fluorescence, this may be considered onerous in an operating environment and may limit the application of UR under operational conditions. Uranine alone in aqueous solution occurs in cationic, neutral, anionic and dianionic forms making its absorption and fluorescence properties strongly pH dependent (Song *et al.* 2000; Gholivand *et al.* 2008). It, therefore, exhibits intense fluorescence in alkaline solutions (Pirillo *et al.* 2008) and this drops very sharply at pH values below 5.5 (Turner Designs Solutions 1998).

The normalised fluorescence intensity of the dyes in the presence of salts at different concentrations is shown in Figure 3.16 and Figure 3.17 for NaCl and CaCl₂ respectively. In the case of NaCl, Figure 3.16, the effect on PyTS and RWT is negligible but a significant increase in fluorescence intensity is observed with increasing salt concentration for UR. This trend is similar to the change in pH for UR but in this case, a lower increase in 43% is observed over the salt concentration range. In the case of both pH and NaCl changes, the concentration of sodium is increasing which may be responsible for the observed changes as UR as sodium and oxygen are on terminal branched ends of the compound as illustrated in Table 3.1. In the presence of increasing CaCl₂ concentrations (Figure 3.17), there is no significant change in the normalized fluorescence for RWT or PyTS with only a slight increase in that of UR (<10%) and this may be attributed to the structure of the compound as previously discussed.

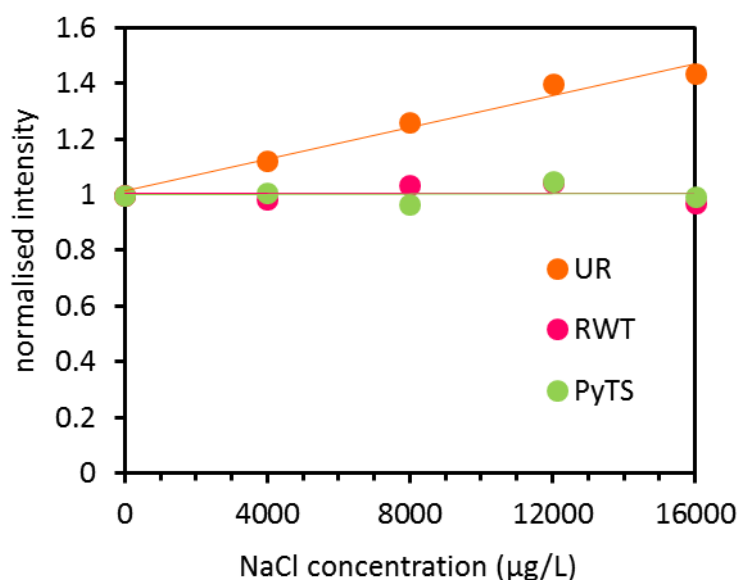


Figure 3.16: Effect of NaCl on dye fluorescence.

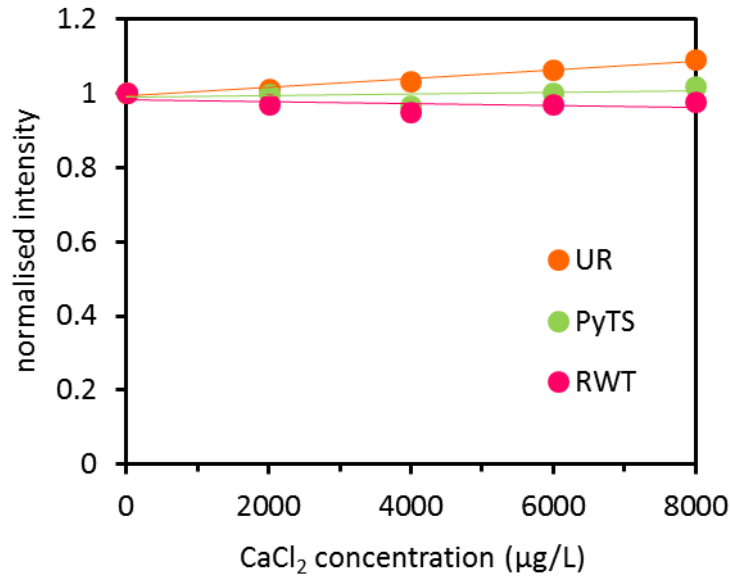


Figure 3.17: Effect of CaCl₂ on dye fluorescence.

Figure 3.18 shows the effect of residual chlorine on the fluorescence intensities of the dyes respectively. The presence of residual chlorine significantly decreases the normalised fluorescence for PyTS and RWT, however, the fluorescence intensity for UR increases by up to 20% in a non-linear manner and again, the addition of sodium ions may be responsible for this increase. The presence of free chlorine in the feed water may therefore be indicated by a sharp decrease in RWT intensity or an increase in UR intensity. This may trigger further investigation to ensure free chlorine does not come into contact with the polyamine membrane layer and cause oxidative damage (Sandin *et al.* 2013). It appears that the presence of residual chlorine would limit the use of these fluorescent dyes as effective surrogates.

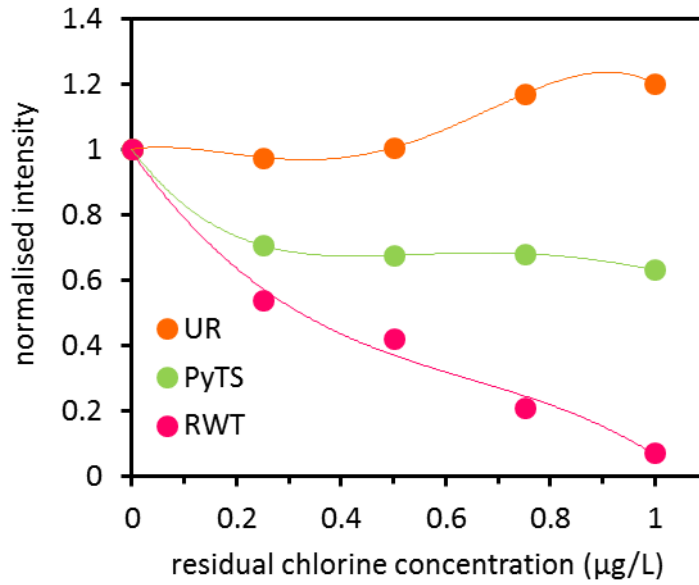


Figure 3.18: Effect of residual chlorine on dye fluorescence.

In the case of chloramine shown in Figure 3.19, both PyTS and RWT show no significant change in normalised fluorescence intensity with increasing concentration but UR increases by >100%. Although it would not be expected that free chlorine would be present in the feed water, it is reasonable to expect the presence of chloramine so the use of UR may provide a higher log reduction due to the elevated bias under moderate chloramine residuals.

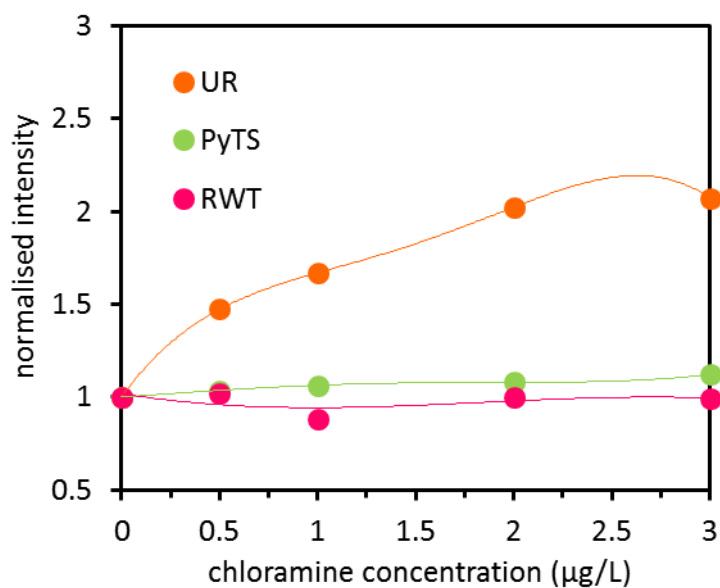


Figure 3.19: Effect of chloramine on dye fluorescence.

The effect of UV light exposure on normalised fluorescence intensity is shown in Figure 3.20. Over the time period tested, the intensity of RWT and PyTS decreased with the decrease more significant for PyTS (30% in 9 h) but for UR, a slight increase was observed (<10%). Although RWT remains relatively stable for at least 6 hours of UV exposure, the fluorescence diminishes by around 20%. In the case of PyTS, the emission/excitation wavelengths are closer to that of the UVA light source so this may impact on the fluorescence intensity. It is typical for fluorescent dyes to be packed and shipped in amber or opaque bottles so to minimize the exposure to UV light so this is a challenge for their use under operational conditions.

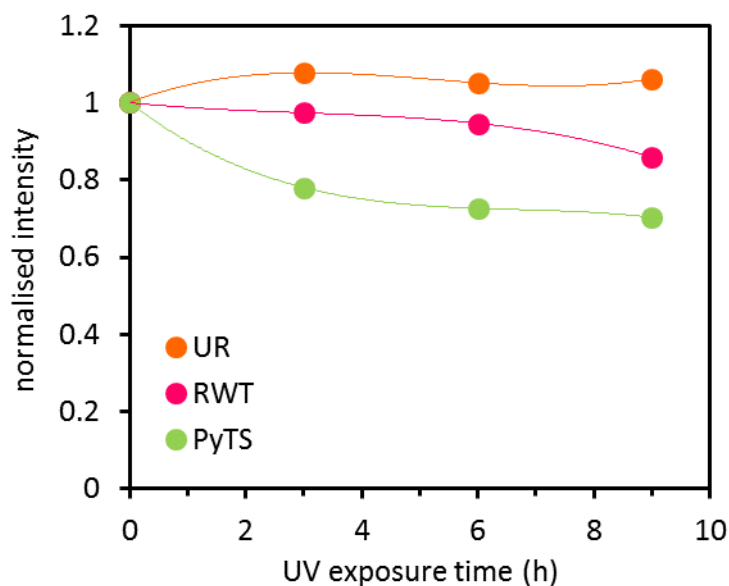


Figure 3.20: Effect of UV exposure on dye fluorescence.

It is clear that for any membrane challenge test, the surrogate species is introduced into feed water then detected in the resulting permeate. Depending on the feed water composition, there may be other fluorescent compounds or quenching species including those screened in this work. A sample of RO feed water was obtained from a local plant producing tertiary treated water using activated sludge processes and UF with each dye separately spiked into samples and compared to a similarly spiked sample into the RO permeate from the same plant. Figure 3.21 shows the normalised fluorescence intensities of these samples and in each case the fluorescence increases in the RO feed water compared to the permeate. For RWT and PyTS, the increases were 10% and 25% respectively but for UR, a substantial increase of 220% was observed. This may suggest some interaction between UR and the organic matter and or the sodium concentration present in the RO feed water, but since the organics and sodium species will be rejected by the membrane process, it is not clear whether

the increased fluorescence intensity will be reflected in the permeate. The control for each sample was a permeate sample collected at the same time from the treatment facility.

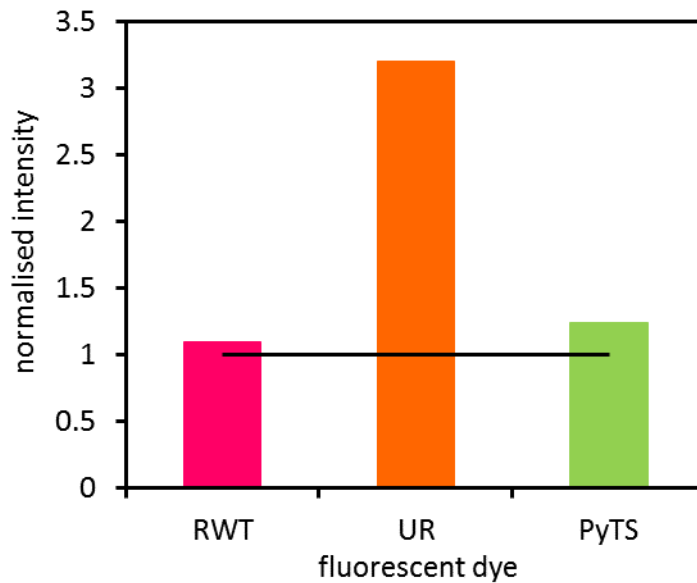


Figure 3.21: Change in fluorescence of dyes in RO feedwater.

Table 3.3 shows a summary of the screening results for each of the fluorescent dyes and provides a qualitative assessment of the observed effect with each screening variable. In some cases, a significant effect was observed that challenges the stability of the proposed chemical surrogate. It is possible to account for these effects but the key issue is the stability of the surrogate across a variety of water chemistries expected in feed water. The ability to calibrate for certain conditions is only useful where the feed water chemistry remains constant and this is not generally the case. An example in point is that the change in temperature and pH may be easily accounted for by preparing multiple calibrations and/or by online measurements, however fluctuations during the testing procedure may invalidate the integrity results.

Of the dyes, UR is the least stable fluorescent compound where the fluorescence intensity invariably increases under many of the test conditions. Both PyTS and RWT are relatively stable with PyTS marginally more stable but potentially problematic to obtain and use for integrity testing.

Table 3.3: Summary of screening results.

Screening variable	RWT	UR	PyTS
Availability	Excellent/no effect	Excellent/no effect	Average/moderate effect
Sensitivity	Excellent/no effect	Good/minimal effect	Excellent/no effect
Temperature	Poor/significant effect	Average/moderate effect	Average/moderate effect
pH	Good/minimal effect	Average/moderate effect	Good/minimal effect
NaCl	Excellent/no effect	Average/moderate effect	Excellent/no effect
CaCl ₂	Excellent/no effect	Average/moderate effect	Excellent/no effect
Residual chlorine	Poor/significant effect	Poor/significant effect	Poor/significant effect
Chloramine	Good/minimal effect	Poor/significant effect	Good/minimal effect
UV light	Good/minimal effect	Good/minimal effect	Average/moderate effect
RO feed water	Average/moderate effect	Poor/significant effect	Average/moderate effect

Key

Excellent/no effect	Excellent/no effect
Good/minimal effect	Good/minimal effect
Average/moderate effect	Average/moderate effect
Poor/significant effect	Poor/significant effect

3.6 Bench-scale Challenge Test Results

The screening process detailed previously and summarized in Table 3.3 above indicated that PyTS offered the greatest stability and sensitivity of the three dyes tested. However, RWT and UR were selected for further challenge testing because PyTS is a component of a proprietary antiscalant formulation and was commercially unavailable. Even though PyTS has been assigned a specific CAS number (CAS #59572-10-0) it is not readily available as a concentrated

compound but rather in a diluted form as part of an antiscalant product. A local supplier provided a cost of \$109/gram but even with a significant discount of 50% this represents a cost of \$54,500/kg, or \$54.50/kL of treated water, clearly beyond the ability of any service provider to implement. The dilution and integration with an antiscalant formulation may significantly reduce the sensitivity of PyTS fluorescent dye. The concentrated PyTS fluorescent dye that was available was used in the continuous and pulsed challenge tests.

3.6.1 Continuous Dosing Challenge Test

Under continuous dosing of 1 mg/L of each of the selected fluorescent dye solutions, RWT and UR, through an intact membrane, high LRVs were obtained as shown in Table 3.4. The rejection values determined for RWT and UR show that UR offered a slightly lower LRV due to the reduced sensitivity of this dye at low concentrations as was evident during the initial screening tests reported previously. The rejection value for PyTS is considerably higher and this confirms that the dye has greater sensitivity at low concentrations but is not available as the concentrated solution that was used during the continuous and pulsed challenge tests. The LRVs for the three fluorescent compounds are reported in Table 3.4 and indicate that PyTS provided a better indicator of membrane impairment than RWT followed by UR.

Table 3.4: Average LRV for continuous dosing of fluorescent dyes

Dye	Average LRV
RWT	4.19 ± 0.13
UR	3.96 ± 0.10
PyTS	4.59 ± 0.18

These data indicate that the fluorescent dyes achieved a threshold LRV greater than $4 \log_{10}$ for PyTS and RWT whereas UR fell just short of the sensitivity benchmark.

3.6.2 Pulsed Dosing Challenge Tests

The pulsed dose challenge tests required optimising the pulse involved, assessing the concentration of the dye, the volume used for the pulse, and the length of time taken to observe the output fluorescence. It was important to collect an adequate number of data points to capture the peak fluorescence as the pulsed dose passed through any imperfections in the membrane. This would be particularly important in the case of a compromised membrane element where the permeate flux may be high.

A flow-through cell connected to the fluorescence spectrophotometer was ideal as it continuously monitored the fluorescence wavelengths corresponding to a particular dye. A plastic fluorescence cuvette was modified for these experiments to enable the flow of permeate through the cell from the bottom and out the top with the instrument set to capture data points at 1 s intervals. Initially, 1 mg/L solutions were tested but this dose did not offer the level of sensitivity in the pulse to enable a representative LRV determination so it was clear that a longer pulsed dose would be required. A higher pulsed dose rate of 10 mg/L was selected with pulses between 10 s to 1 min used representing volumes of 200 mL to 1.2 L, respectively, through the system. The total volume processed using the pulsed dose challenge test represented 0.5-3 swept volumes of the 2.5-inch membrane. The observed data suggested that duration of the pulse performed better at 3 swept volumes but this metric must be determined for each membrane array. The

monitoring duration should be extended until no further fluorescent dye was evident in the permeate and that varied depending on the fluorescent dye used with RWT taking longer than other dyes.

Figure 3.22 shows a typical trace of fluorescence in the permeate versus time for RWT dosed for 10 s at 10 mg/L. In this case, a peak was observed after 5 s and the fluorescence signal returned to the baseline value of zero confirming that all the residual soluble RWT remaining had been removed from the system. Based on the peak fluorescence value, the LRV for this test was 4.6 log₁₀, a higher result than that reported for the continuously dosed value of 4.19 log₁₀.

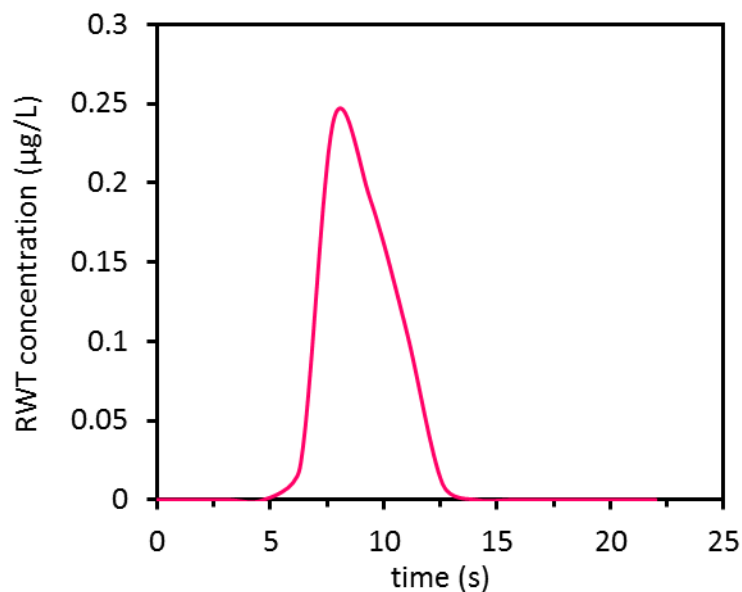


Figure 3.22: Concentration of RWT with time for 10 mg/L pulsed dose.

In Figure 3.23, a similar plot of concentration in the permeate versus time for UR using a 30 s pulsed dose is presented. In this case, the peak value of 0.9 µg/L in the pulse corresponded to an LRV of 4.04 log₁₀ that is slightly higher than that obtained from the continuous dosing at 1 mg/L of 3.96 log₁₀.

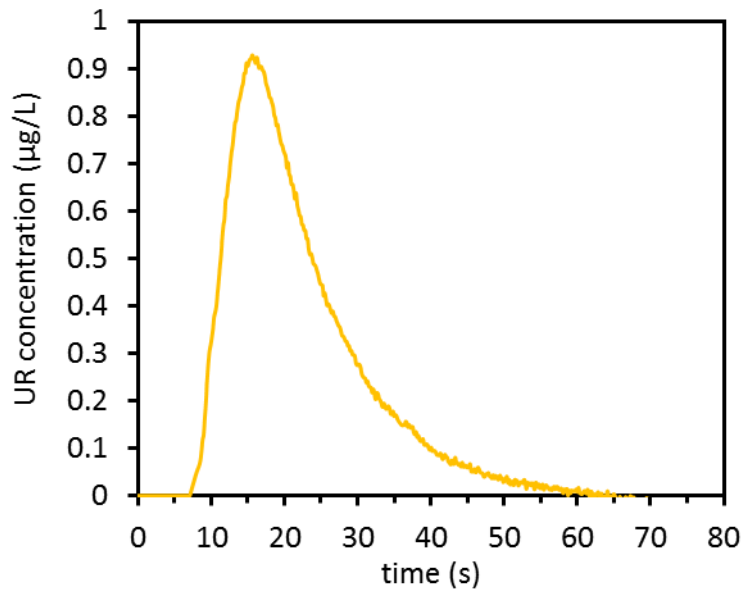


Figure 3.23: Concentration of UR with time for 10 mg/L pulsed dose.

Figure 3.24 shows the concentration in the permeate versus time plot for the pulsed dose of PyTS at 10 mg/L for 60 s. The peak value of 0.12 µg/L in this pulse corresponded to an LRV of 4.92 log₁₀ that is also higher than the value of 4.59 log₁₀ obtained by continuous dosing the UR at 1 mg/L. For each of the pulsed dose curves, a sharp increase in concentration is observed in the seconds after the pulse is introduced followed by a peak and a more gradual decline in the concentration until no further dye is present in the permeate.

These curves show a similar profile that may be indicative of a typical profile for an intact membrane, the decay length over time increased for the longer pulsed doses. The profile for the RWT test presented a slightly different shape, however, and this may be due to the shorter pulse time resulting in fewer data points. It is important to consider the duration of the pulsed dose relative to the overall time taken to pass the membrane to ensure the membrane was fully covered by the dye throughout the cycle. A continuous challenge test at full scale may require at

least three swept volumes of the membrane array to stabilise the system followed by up to six swept volumes to ensure a stable permeate concentration was achieved to determine the rejection capacity of the high pressure membrane system. The pulsed dose challenge test duration required between two and three swept volumes applied for a well-defined peak to be developed.

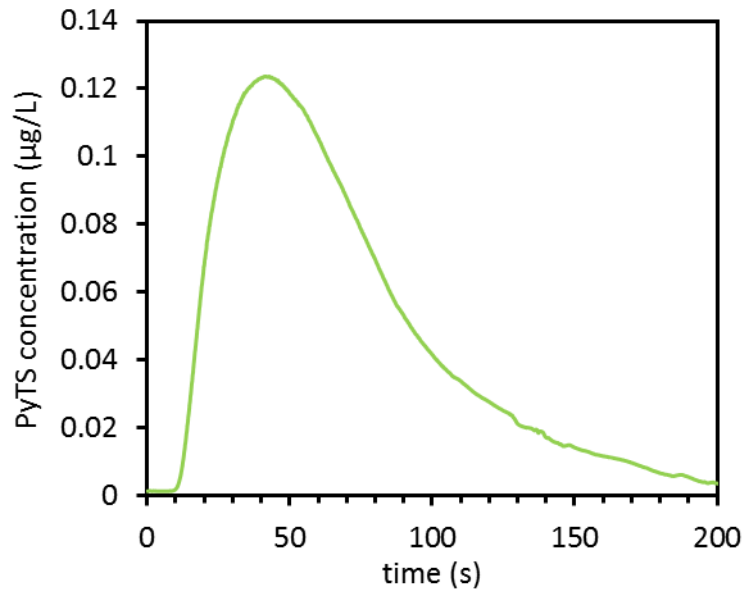


Figure 3.24: Concentration of PyTS with time for 10 mg/L pulsed dose.

A comparison of the LRV results obtained for the continuous and pulsed application of the three fluorescent dyes is shown in Figure 3.25. The data indicates that the pulsed dose challenge test invariably produced higher rejection values but required ten times the concentration of fluorescent dye. While the concentration of fluorescent dye applied was ten times the concentration applied for the continuous test the total mass differential depended on the duration of the continuous test compared to the duration of the applied pulse. The comparison between the dosed integrity tests showed that the pulsed dose required

approximately three times more fluorescent dye than the continuous dose, an unexpected result but certainly noteworthy.

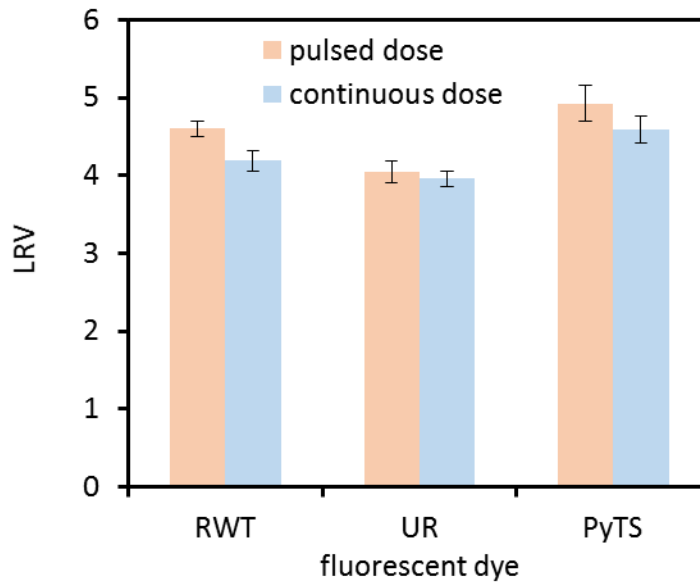


Figure 3.25: Comparison of pulsed and continuous dose LRVs.

The information provided by the pulsed dose challenge tests indicated that this type of membrane challenge might be more efficient and representative than the implementation of a continuous challenge test that may continue for longer and have lower sensitivity.

3.6.3 Pulsed Dosing on Applied Defects

The time/concentration traces of RWT, PyTS and UR for the pulsed dose tests are shown in Figure 3.26 (a), (b) and (c) respectively. Each fluorescent dye appeared to show unique characteristics that have the potential identify a particular membrane defect or breach in small-scale experiments. No fluorescence signal was observed for any of the dyes used with the intact membrane under the test conditions, therefore, limiting the calculated LRV to a

nominal value of $5 \log_{10}$ based on the feed concentration of 10 mg/L at a resolution of 0.1 $\mu\text{g/L}$. The concept used to limit the LRV to the feed concentration is the same adopted for the MS2 bacteriophage determination of LRV when no PFU are enumerated in a permeate sample so the denominator of one unit is used because less than unity as a detection limit does not translate to a calculated LRV (Victorian Government Department of Health 2013).

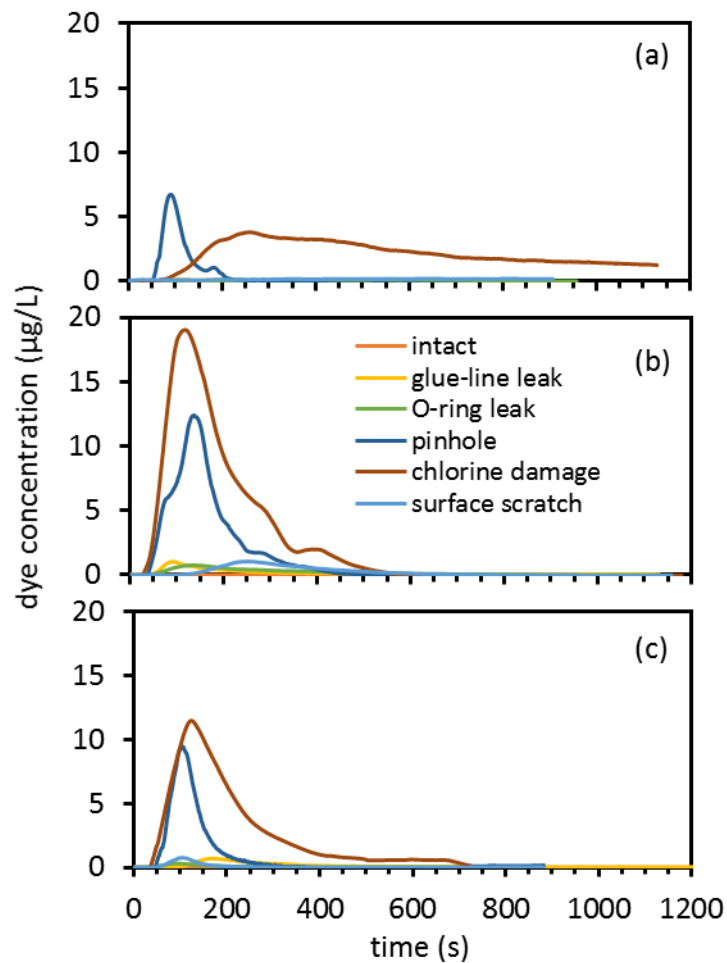


Figure 3.26: Pulse dose curves for (a) RWT, (b) UR, and (c) PyTS.

The LRVs determined for each of the defects are summarised in Table 3.5 with high values between $4 \log_{10}$ and $5 \log_{10}$ for O-ring, glue line failure and surface scratch defects and lower values were recorded between $2.7 \log_{10}$ and $3.4 \log_{10}$

for the pinhole and chlorine damaged membranes. Relatively high LRVs were obtained for the glue-line leak but in this case, the defect was difficult to simulate in the small scale apparatus and a true glue-line leak would clearly result in much lower LRVs (Jons *et al.* 2005). The corresponding flux values measured for each dye and defect are shown in Table 3.6.

Table 3.5: LRVs calculated from pulse dose tests.

	Intact	Glue-line leak	O-Ring	Pinhole	Chlorine	Surface scratch
RWT	5.0	5.0	5.3	3.2	3.4	5.2
UR	5.0	4.0	4.2	2.9	2.7	4.0
PyTS	5.0	4.2	4.5	3.0	3.0	4.2

Table 3.6: Specific flux values for pulse dose tests.

	Intact	Glue-line leak	O-Ring	Pinhole	Chlorine	Surface scratch
RWT	5.66	6.72	5.68	8.32	5.09	5.89
UR	5.92	6.78	5.71	7.34	4.65	5.56
PyTS	5.57	6.91	6.52	8.07	4.73	5.15

Units: (kg/m²/h/bar)

Performance of the fluorescent dyes reported under the conditions of the tests indicated that UR was detected at a greater concentration across the majority of impaired conditions followed by PyTS and then RWT. The rejection potential was also closely related to the physical size of the compounds previously reported in Table 3.1 that also records the three-dimensional structure for each of the fluorescent dyes. The physical size developed by computer simulated models indicated that the size of the molecules from largest to smallest was RWT > PyTS

> UR as shown in Table 3.7. The physical size reflected the rejection and sensitivity observed during the pulsed dose challenge tests at a pilot scale.

Table 3.7: Average dimensions of fluorescent dyes.

Fluorescent Dye	Size in nm
RWT	1.5 x 1.35 x 1.2
UR	1.1 x 1.1 x 1
PyTS	1.4 x 1.1 x 1.1

Further evaluation of the dye performance in terms of rejection showed that the rejection from highest to lowest was RWT (532 g/mol) > PyTS (610 g/mol) > Ur (378 g/mol) that corresponded closely to the molecular weight of each of the fluorescent dyes previously reported in Table 3.1. The MW coupled with the larger, more complex structure of RWT made it more likely to be rejected more than PyTS as shown by the data in Table 3.7 above.

3.6.4 Dye Adsorption

Using continuous dosing challenge tests, dyes may be expected to adsorb on the membrane surface and could potentially lead to blockages similar to a foulant layer. Experiments using 1 mg/L RWT were performed in order to quantify the amount of dye adsorbed on a membrane surface after several hours of continuous dosing. Under a constant pressure of 15 bar, the permeate was recirculated back into the feed solution which was temperature controlled using a chiller. Samples of the feed solution were taken at 15 minute intervals for 3 hours and quantified following dilution.

Figure 3.27 presents a photograph of the membrane after 3 hours' recirculation in 1 mg/L RWT against a new reference membrane. There was evidence of pink staining on the membrane that was substantial around the edges where the inner O-ring was in contact with the membrane.



Figure 3.27: Photograph of (a) stained and (b) new reference membrane.

Figure 3.28 shows the concentration of the undiluted feed solution as a function of time. There was no significant change in the RWT concentration after 3 hours suggesting that the staining occurred with minimal RWT. There may also be a high level of error associated with the measurement that involved a substantial dilution of the feed solution to obtain a reasonable fluorescence result. Under a pulsed integrity test, minimal dye adsorption would be evident due to the reduced contact of the dye with the membrane even though higher concentrations were used.

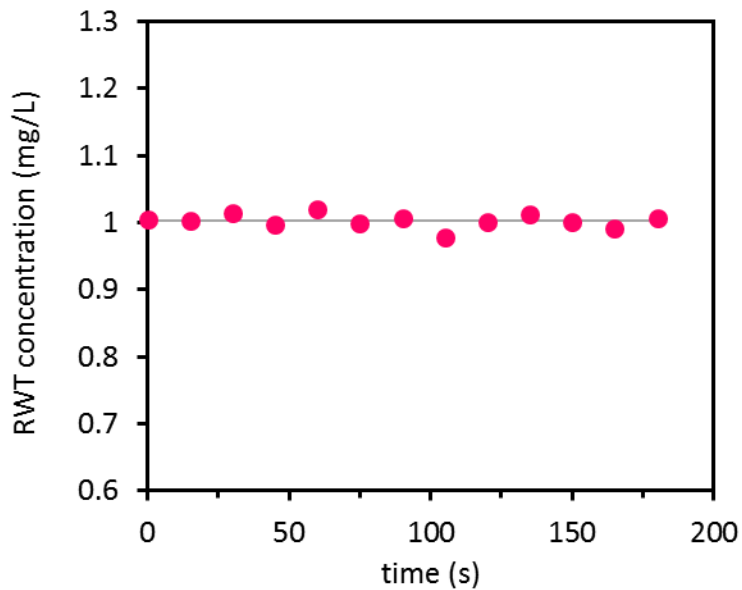


Figure 3.28: Concentration of RWT over 3 hours continuous dosing.

Continuous dosing of a fluorescent dye for prolonged periods to complete a membrane integrity test challenges the criteria of cost and also increases the likelihood that loss through adsorption may occur. Fluorescent dyes that adsorb onto, and within, the membrane material may bias the results of a challenge test and call into question the veracity of the results obtained because the concentration of the dye in the permeate was reduced. Consequently, the concentration of the feed solution was less than that applied and that has some significance for the calculated LRV where the numerator was less than expected.

One alternative is the use of a pulsed dose challenge test where a known volume of a dye solution is introduced over a short period with the permeate monitored for the presence of the dye. This offers advantages including the ability to apply a higher pulsed dose concentration that can improve sensitivity and also provide the possibility to provide a diagnostic tool that defines the type of defect in a system. The potential to develop a hydraulic modelling tool to identify the location

of defects in large membrane arrays would provide a considerable benefit to operators.

Overall, the results of these experiments show that the LRVs obtained for an intact system are higher than those obtained via continuous dosing with a 10-fold increase in feed concentration for the pulsed system over a short duration. Adsorption experiments with RWT showed visible staining of the membrane under continuous dosing after 3 h although this was not reliably defined.

The disadvantage associated with the use of RWT or any other soluble chemical surrogate is that they do not satisfy the selection criteria (see Table 2.1). In particular, a surrogate for the smallest virus would require a larger particle rather than a soluble chemical compound that is at least twenty fold smaller than the target virus. The value of these compounds could be in the screening for chemicals of concern such as endocrine disruptors, however their specific limitations must be accounted for when results are assessed. Given that the cost of the surrogate should not add more than \$0.02/kL of water treated, these surrogates would fail the application cost criteria.

3.7 Conclusions

The results clearly demonstrate that the food grade dyes are not suitable surrogate candidates for membrane integrity monitoring. The UV detection method used to quantify the dyes has a much higher minimum threshold concentration for detection than fluorescence, thereby limiting their use as surrogate compounds. Table 3.3 highlights the view that none of the three fluorescent compounds offer a completely stable platform that can be used as a surrogate across a wide range of operating and environmental conditions to

monitor membrane integrity. The implications of the screening tests performed on the fluorescent dyes brings into question what is actually being measured in the permeate. Increased temperature affected RWT by significantly reducing fluorescence and while temperature fluctuations are seasonal the comparison of LRV across seasons without any compensation for the applied dose may alter the perception of performance related to the sensitivity of the dye and the limit of detection. In effect, a higher dose rate would be required to compensate for the higher detection limit as a consequence of lower fluorescence.

Greater emphasis is required to determine whether the environmental or chemical conditions have any significance for LRV determination but there does not appear to be sufficient attention to these conditions on the reliable interpretation of results. These screening tests to determine the effect of each environmental/process parameter were completed separately, but the implication of a variety of conditions occurring simultaneously was not developed and may result in different performance outcomes.

The sensitivity of PyTS and RWT was clearly in the desired range that would afford the opportunity to determine at least a 4 log₁₀ removal efficiency. However, the stability of these compounds represents a challenge to consistently report the membrane integrity across a number of chemical and environmental conditions. Of the dyes tested, UR represents the least attractive fluorescent compound as it was unstable across several screening variables while RWT and PyTS were susceptible to some instabilities and reduced fluorescence under some conditions. This may lead to a poorer integrity response that would potentially

affect decisions made on the basis of the results obtained from the surveillance program.

While RWT is used as the default fluorescent dye to determine the integrity of high pressure membranes, there are a number of issues that relate to the stability and repeatability of membrane integrity testing and reporting identified by the screening tests. The stability of these fluorescent compounds across temporal and chemical characteristics of the carrier fluid used to perform the tests is shown to be poor under certain circumstances. The instability of these fluorescent compounds does not provide adequate assurance to quantify the integrity of high pressure membranes.

The search for an alternative surrogate using fluorescent polymer nanoparticles is the subject of the next chapter. Using nanoparticles can be more effective as a viable non-microbial surrogate rather than a chemical compound that is much smaller than the target virus. Some fluorescent chemicals can demonstrate greater stability when encapsulated or otherwise entrapped in a polymer matrix. Chapter 4 presents the results of the analysis of a range of fluorescently tagged nanoparticles in order to determine whether they are able to provide a stable surrogate that could be used to accurately and precisely measure the rejection capacity of high pressure membranes.

Chapter 4

Fluorescent Polystyrene Nanoparticles

4.1 Preamble

Fluorescent dyes such as RWT are capable of providing an indication of membrane integrity, however, they provide more conservative membrane integrity responses because they are typically twenty times smaller than the smallest virus. Fluorescent dyes are able to exploit transport mechanisms into permeate that nano-sized particles are unable to by virtue of their size. Consequently, the use of fluorescent chemicals provides a more conservative LRV for high pressure membranes because dye is able to pass through membranes that may have imperfections that would not otherwise allow transport of virus into the permeate. Therefore, the measured LRVs with dyes are more sensitive to membrane imperfections than an LRV determined for virus.

The search to identify suitable non-microbial surrogates for membrane integrity testing that represent virus sized particles leads to the assessment of nano-sized particles. In the same manner as the fluorescent dyes, it is essential that any surrogates meet the minimum requirements of a challenge species as outlined in Table 2.1. In this chapter, selected fluorescently tagged nanospheres were subjected to a range of chemical and environmental conditions that may represent varying feed water characteristics to determine their stability and sensitivity.

4.2 Introduction

The concept of adopting nanospheres to detect membrane integrity breaches is an extension to the fluorescent chemicals and depending on the diameter of the particles, these may serve as a better surrogate for virus. Nanoparticles with a similar diameter to that of poliovirus at around 30 nm have a similar physical form and would undergo similar modes of transport across and through impaired high pressure membrane processes. This chapter examines whether fluorescently tagged particles of a similar size to the target virus can be used to determine the nanoparticle rejection performance, and therefore membrane system integrity. The attenuation of fluorescence intensity is critical in the development of a sensitive and particle selective membrane integrity monitoring technique.

Chemical compounds that were examined in Chapter 3 have a different transport mechanism through high pressure membranes that are based on size exclusion characteristics of the membrane rather than only from a breach in the integrity of the membrane itself. Consequently, nanoparticles are seen as a more viable method of detecting the ability of a high pressure membrane to reject virus particles (Gitis *et al.* 2006). As previously reported in Chapter 3, NF membranes would not readily reject chemical compounds with typical MWCO values between 1,000 and 2,000 Da, whereas tight NF and RO membranes with MWCO below 500 Da would have a better virus rejection rate. Similarly, aged membranes that have been oxidised will exhibit a poorer rejection of fluorescent chemical compounds indicating a low LRV but the membrane's capacity to reject virus may be unaffected leading to a higher LRV (Jacangelo *et al.* 2015), This discrepancy in rejection performance can adversely affect membrane integrity that may lead

to early replacement of membranes unnecessarily or report reduced effectiveness of the membrane system tested.

The use of nanoparticles has been adopted in a wide range of applications that include pharmaceutical, medical imaging and cosmetics such as sunscreen lotions (Salata 2004), and can be readily purchased from a range of companies (e.g. Sigma-Aldrich, EPRUI nanoparticles and microspheres Pty Ltd, Applied Nanotech etc.). Nanoparticles are generally defined as particles that range between 1-100 nm across the largest dimension of the material and this closely mirrors the size range of enteric viruses that are targeted by membrane integrity surveillance programs. Gitis *et al.* (2006) and Lozier *et al.* (2003) report that the size and surface charge characteristics of some fluorescently tagged PS nanoparticles are similar to enteric viruses. Consequently, fluorescently tagged nanoparticles have been identified as potential surrogates for enteric viruses used in membrane integrity surveillance programs (Gitis *et al.* 2006).

Polystyrene (PS) or latex microspheres can be obtained in a range of uniform sizes and with various surface characteristics (Pontius *et al.* 2009). Fluorescent microspheres can be prepared with a variety of dyes including RWT allowing them to be enumerated using fluorescence detectors (Pontius *et al.* 2009). Moreover, the fluorescent dye allows them to be detected against background particles in relatively low concentrations (Becker *et al.* 1999). To maximize the fluorescence signal the surface should be smooth and without noticeable defects (Liao *et al.* 2004) since variations in surface area can cause apparent changes in sensitivity and can contribute to false positive and negative results. Gold nanoparticles (Gitis *et al.* 2006; Borisov *et al.* 2008) and magnetic particles

(Deluhery and Rajagopalan 2008; Yang *et al.* 2010) have attracted considerable interest due to the high sensitivity of these particles and the wide availability of particle counters but are expensive to use as part of a regular membrane integrity monitoring program.

Polystyrene microspheres are negatively charge-stabilised colloidal particles that vary significantly with respect to charge and hydrophobicity depending on the manufacturing processes (Sigma-Aldrich Pty. Ltd. 2011). The particles can be prepared with a variety of functional groups on the outer surface and carboxylated microspheres, for example, have –COOH functional groups conjugated to their surfaces. These are generally produced by the polymerization of the monomer styrene *via* spontaneous coalescent bead formation and are provided as suspensions of polymer particles and water, with small amounts of surfactant and other salts (Sigma-Aldrich Pty. Ltd. 2011). In addition, they can be further functionalised by the addition of fluorescent tags on their surface. Microspheres that include fluorescent tags have found uses in biomedicine (Fluorescent Microsphere Center 1999; Farquar and Leif 2009) as well as in process monitoring (Kaplan *et al.* 1999; Lozier *et al.* 2003; Bohrerova *et al.* 2005; Bielefeldt *et al.* 2010) and other tracer studies (Kaplan *et al.* 1999; Hammer *et al.* 2001; Gitis *et al.* 2002; Juck *et al.* 2005).

Polystyrene microspheres have been used as tracers due to their size, uniformity and surface characteristics (Pontius *et al.* 2009). Becker *et al.* (1999) reported the use of fluorescently dyed PS microspheres as colloid tracers and discussed the use of the microspheres in terms of their perfect spherical shape, size, availability, resistance to biodegradation, stability at temperatures up to 100°C

and various physical properties such as the specific gravity of 1.06 that favours an aqueous suspension. Becker *et al.* (1999) further explained the ability of microspheres to be impregnated with fluorescent dyes which allows them to be detected against background particles. However, fluorescent microspheres have been found to be a poor phage surrogate in MF and UF studies (Pontius *et al.* 2009) and in addition, they are expensive and the fluorescent tag has a relatively short lifetime (Kitis *et al.* 2003a; Kitis *et al.* 2003b; Lozier *et al.* 2003).

Gold nanoparticles have been cited by a number of researchers as tracers in biological systems and Gitis *et al.* (2006) demonstrated their use as non-microbial surrogates for UF integrity testing. A log removal of approximately 4.5 was achieved using an initial dose of 5.2 mg/L using the gold nanoparticles to challenge uncompromised cellulose ester and cellulose acetate ultrafiltration membranes with a MWCO of 10 kDa and 20 kDa, respectively (Gitis *et al.* 2006).

Lozier *et al.* (2003) reported that the passage of viruses can be favourably compared to the decrease in LRV provided by PS microspheres migrating through compromised membranes with micron-sized membrane holes. A membrane integrity test was performed using a solution containing 24 nm PS microspheres dosed into an RO test unit which provided an LRV greater than 4 for uncompromised RO membranes and an LRV of around 2 for a compromised membrane with a 300-500 μm pinhole. These researchers demonstrated that the use of PS microspheres can provide similar LRV results when compared with MS2 as the virus surrogate (Lozier *et al.* 2003).

Research into inorganic nanoparticles in sunscreens (Cross *et al.* 2007) and in wastewater (O'Malley 2015) has investigated the potential toxicity of

nanoparticles that are available as non-microbial surrogates for membrane integrity surveillance. Colvin (2003) and Dreher (2004) have reported on the environmental and toxicological assessment of manufactured nanoparticles and raised some concerns regarding their potential toxicity. Until recently, the major drawbacks to the adoption of fluorescently tagged nanoparticles as potential surrogates for the quantification of membrane integrity in high pressure membranes has been the limited commercial availability and relatively high cost. Nevertheless, Behrens *et al.* (2001) reports that fluorescently tagged PS nanoparticles and other tracers such as gold nanoparticles have been used to characterise movements in surface and groundwater systems because they are considered to be non-toxic and highly stable in water systems.

Recent improvements in quality control throughout the manufacture of fluorescently tagged nanoparticles may provide a useful alternative to the current range of membrane integrity monitoring methods. It is important to carefully consider the commercial availability at a reasonable cost, toxicity and membrane fouling potential of nanoparticles if they are to be successfully applied to membrane integrity testing for high pressure membranes. In order to identify the suitability of selected PS fluorescent particles as surrogates for membrane integrity monitoring, this chapter aims to screen a range of commercially available fluorescent nano- and micro-spheres in accordance with the methods described in Chapter 3.

4.3 Materials and Methods

Experiments were performed using several types of fluorescent spheres in various sizes purchased from Sigma-Aldrich Pty. Ltd. (2011) and Polysciences

Inc. (2009) as shown in Table 4.1. The spheres were supplied as 2.5% aqueous solutions and were stored in the refrigerator (<4°C) to deter microbial growth in accordance with the manufacturer's instructions.

Table 4.1: Characteristics of nano/microspheres studied.

	Code	Size (µm)	Details
Sigma particles			
LB0780	FB	0.05	<ul style="list-style-type: none"> • amine modified • $\lambda_{ex}/\lambda_{em}$: 360/420 nm • fluorescent blue
L5155	FY	0.03	<ul style="list-style-type: none"> • carboxylate modified • $\lambda_{ex}/\lambda_{em}$: 470/505 nm • fluorescent yellow/green
L9777	FR	0.50	<ul style="list-style-type: none"> • sulphate modified • $\lambda_{ex}/\lambda_{em}$: 575/610 nm • fluorescent red
L9904	FO	0.10	<ul style="list-style-type: none"> • amine modified • $\lambda_{ex}/\lambda_{em}$: 520/540 nm • fluorescent orange
Polysciences particles			
Carboxylic YG	YG	0.05	<ul style="list-style-type: none"> • 3.64×10^{14} particles/mL • $\lambda_{ex}/\lambda_{em}$: 441/486 nm • fluorescent tag: Uranine
Carboxylic BB	BB	0.05	<ul style="list-style-type: none"> • 3.64×10^{14} particles/mL • $\lambda_{ex}/\lambda_{em}$: 360/407 nm • fluorescent tag: Coumarin
Polychromatic Red	PR	0.50	<ul style="list-style-type: none"> • 3.64×10^{11} particles/mL • Vivid orange under UV • Bright red under 475-490 nm filter • Yellow under 545-610 nm filter • fluorescent tag: Phycoerythrin

Figure 4.1 shows an SEM image of the larger Polysciences PR microspheres and it is clear that the spheres are relatively uniform in size with an average 0.44 µm diameter. Similar to the fluorescent compounds screened in the previous chapter,

the fluorescent microspheres must have a high sensitivity at low concentrations and must be stable over a range of environmental conditions. These conditions include variations in pH, temperature, salinity and the presence of other chemicals that may increase or decrease their fluorescent intensity as illustrated by the previous work reported in Chapter 3.

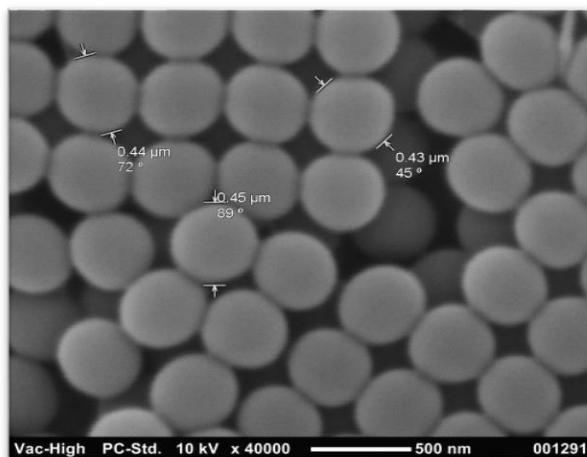


Figure 4.1: SEM image of PR microspheres.

Solutions of the various microspheres were prepared initially for calibration and then known concentrations of microspheres were prepared from the stock solution supplied using deionised water. The fluorescence intensities were measured using a Shimadzu RF501 spectrofluorometer in accordance with the screening methods used for the fluorescent dyes presented in Chapter 3 in order to determine the fluorescence responses under various chemical and environmental exposure.

4.4 Results and Discussion

4.4.1 Calibration and Screening

Figure 4.2 shows the linear calibration curves of the Sigma particles but it is clear from this data that the sensitivity of the particles is relatively low in the mg/L range rather than $\mu\text{g/L}$ range of typical fluorescent compounds. The particles from this manufacturer were therefore excluded from further testing.

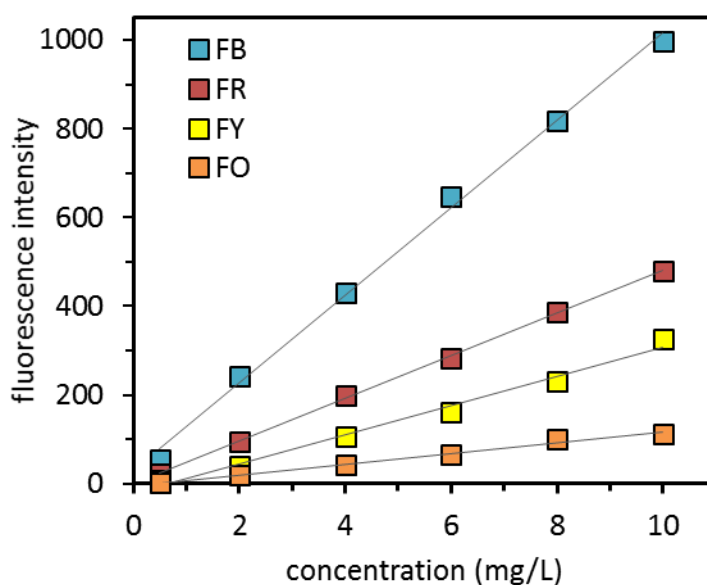


Figure 4.2: Calibration curves of Sigma nanoparticles.

The calibration curves of the three Polysciences fluorescent nanoparticles are shown in Figure 4.3 with the concentration plotted on a log scale to better discriminate between the respective sensitivities. The smaller sized particles were significantly more sensitive than the larger particles, with the microsphere PR having an order of magnitude lower sensitivity than the BB and YG nanoparticles across the range of measured intensities. The fluorescently tagged 50 nm nanoparticles have a higher fluorescence potential when compared

against the larger 500 nm PR microspheres because the greater exposed surface area for an equal mass provides more sites for fluorescent tags. The surface area to volume ratio for 50 nm nanoparticles is an order of magnitude greater than that provided by microspheres with a diameter of 500 nm, therefore, this represents a greater opportunity to support more fluorescent tags on the nanoparticles. The calibration curves illustrated in Figure 4.3 indicate that PR is around ten times less sensitive than either of the other fluorescently tagged nanoparticles.

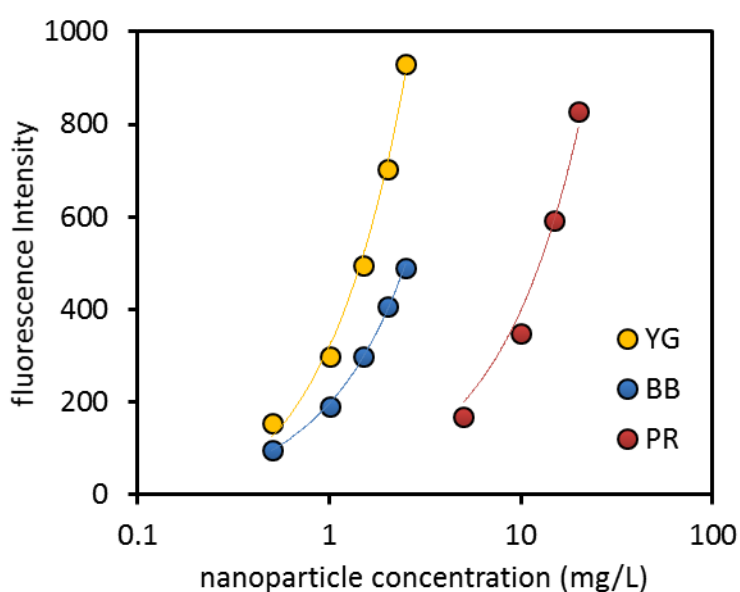


Figure 4.3: Calibration curves of Polysciences nanoparticles.

As shown in Table 4.1, the YG nanoparticles are tagged with Uranine dye and this enables a comparison between the particles and the previously screened UR chemical (see Chapter 3). The fluorescence calibration curves of UR and YG, with the concentration expressed on a log scale to better differentiate sensitivity, is illustrated in Figure 4.4 and it is evident that for a similar fluorescence intensity, the mass of YG particles required to achieve the same intensity value as UR would be around two orders of magnitude. This would mean that at least one

hundred times the applied dose rate would be required to achieve a similar intensity response from the fluorescently tagged nanoparticles.

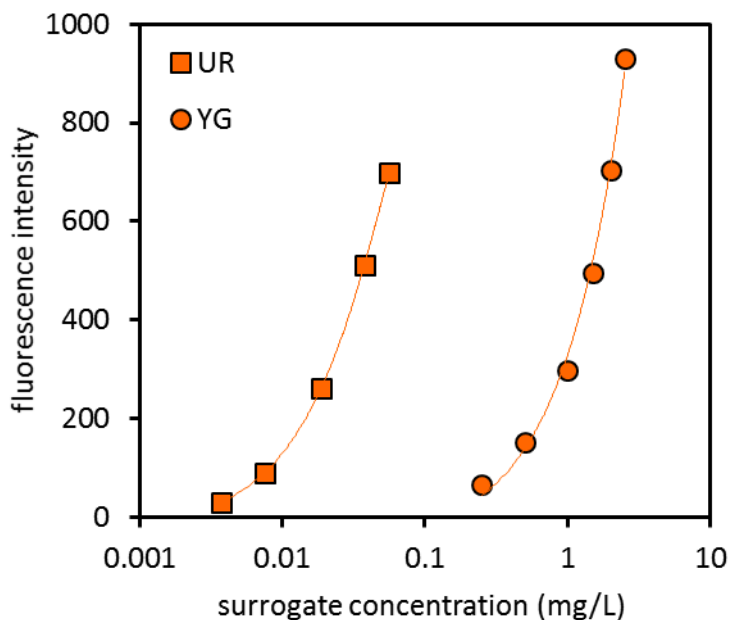


Figure 4.4: Calibration curves of UR dye and YG nanoparticles.

It is clear that the sensitivity of the fluorescently dyed nanoparticles is significantly lower than that of the soluble fluorescent chemicals and this attenuation in fluorescence is the result of the relative mass of fluorescent dye used to coat the PS nanoparticle and the fluorescent dye as a soluble compound. In addition, the PS polymer will attenuate the exposure of other fluorescently coated particles due to shielding, and therefore the passage of the excitation light will be affected thereby further reducing the signal intensity.

Figure 4.5 shows the effect of varying the pH from acidic to alkaline conditions. Invitrogen (2004) state that carboxylate-modified microspheres should be used at a pH greater than 5, otherwise the charge groups on these particles may be neutralised, leading to agglomeration. The results show that at relatively low pH,

the YG and BB are quite stable but as the pH increased, the fluorescence intensity slightly increased. As illustrated by the data reported in Chapter 3, the fluorescence properties of UR are strongly pH dependent (Song *et al.* 2000; Gholivand *et al.* 2008). Although UR exhibits intense fluorescence in alkaline solutions (Pirillo *et al.* 2008), this drops very sharply at pH values below 5.5 (Turner Designs Solutions 1998) as shown previously. The fluorescence intensity of the PR, the larger 500 nm micro-spheres, remained relatively stable over the tested pH range.

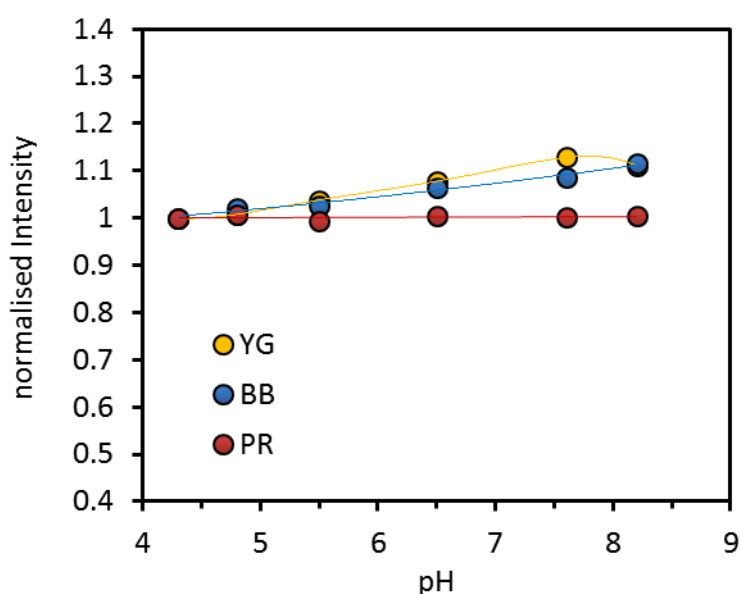


Figure 4.5: Effect of pH on nanoparticle fluorescence.

The charge of the nanoparticles was analysed by measuring the zeta potential over a range of pH values to further investigate the effect of pH. This was performed in order to identify any conditions of pH where the particles may be inclined to adsorb onto a membrane surface and/or agglomerate into larger particles. In Figure 4.6 the change in zeta potential with pH is shown which confirms that the particles are all negatively charged over the pH range 2-12.

Although the YG particles are close to neutrally charged at around pH 2, the strong negative charge on the particles suggests good separation in aqueous suspension at pH values >2. The surface charge of carboxylate modified microspheres ranges between 0.1 and 2 milliequivalents/g and was stable in relatively high concentrations of electrolytes (up to 1 M univalent salt). However, they will adsorb proteins and other biomolecules, although much less strongly than hydrophobic microspheres. It is also easier to further reduce nonspecific binding by the introduction of additives such as BSA or dextrans (Molecular Probes Inc. 2004). This has the potential to alter the fluorescence response given that BSA and some dextrans can fluoresce.

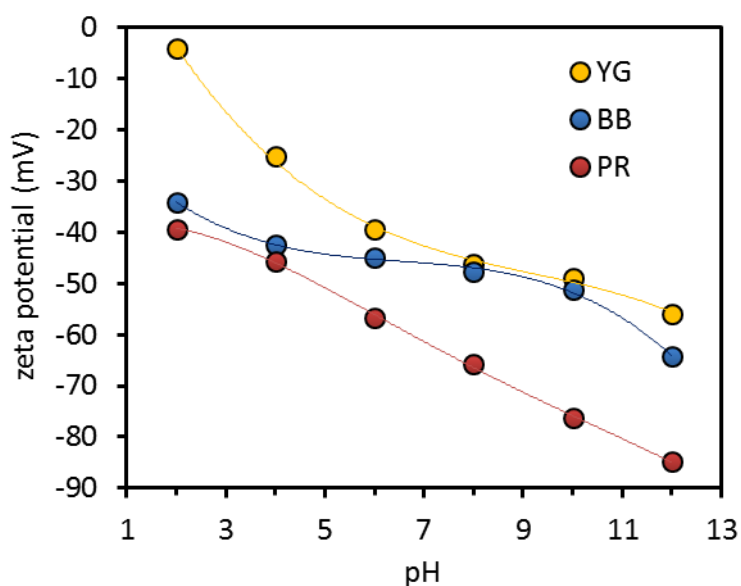


Figure 4.6: Effect of pH on nanoparticle surface charge.

Figure 4.7 shows the variation of fluorescence intensities with temperature for the nanoparticles. The results suggest that the fluorescence of the YG nanoparticles decreased slightly with increasing temperature, while the other two remained relatively stable. A similar observation was reported for UR and the other dyes in

the previous chapter, and would facilitate the need for calibrations at various temperatures.

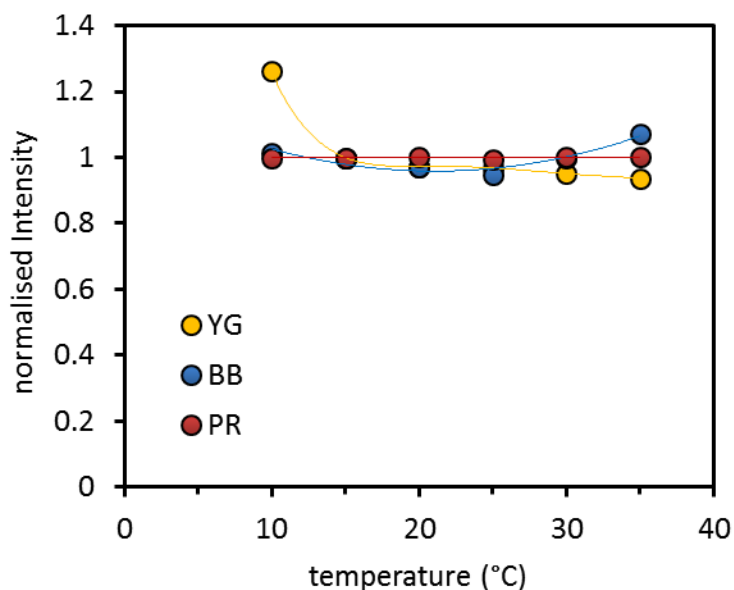


Figure 4.7: Effect of temperature on nanoparticle fluorescence.

Figure 4.8 shows the effect of sodium chloride concentrations up to 16,000 mg/L and CaCl_2 concentrations up to 6,000 mg/L on the fluorescence intensities of the nanoparticle solutions. The results show that in both cases PR and YG are relatively unaffected by the presence of either salt over the concentration range. Conversely, both salts have a dramatic impact on the BB particles with a 3-fold increase in the fluorescence in the presence of NaCl and an even greater increase of nearly 20-fold in the presence of CaCl_2 . The active fluorescent compound in the BB nanoparticles, Coumarin, is derived primarily from plant sources and is readily conjugated to form different compounds with variable fluorescence properties (Jones and Rahman 1994).

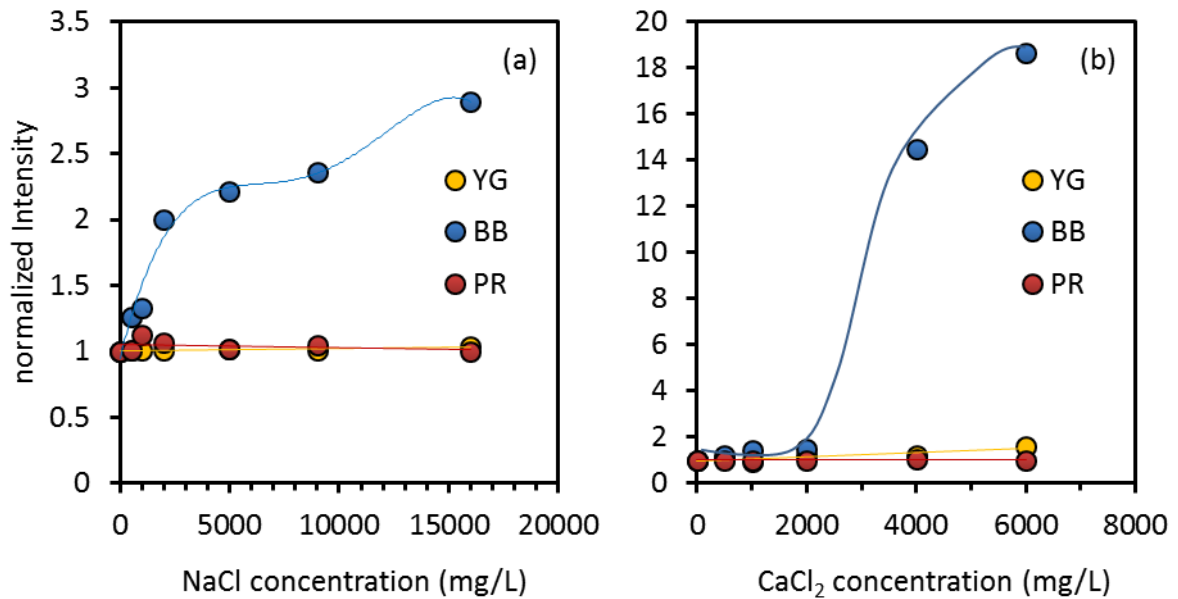


Figure 4.8: Effect of salts on nanoparticle fluorescence in the presence of (a) NaCl and (b) CaCl₂.

Uranine is a highly fluorescent xanthene dye molecule (Szabelski *et al.* 2010), and like many fluorescent chemicals and dyes, it can be highly sensitive to UV light (Turner Designs Solutions 1998). Figure 4.9 shows that the intensity of all three fluorescent nanoparticles significantly decreased with increasing UV exposure times. In this case, BB was the most severely affected with around 50% of its fluorescence dissipated over the first hour. The PR particles were the most stable but were completely ineffective after 6 h whereas the YG particles maintained around 30% of their original fluorescence after the 6 h test. These results suggest that the particles must be used cautiously and stored appropriately in amber bottles or in a dark place at all times but do have a finite shelf life.

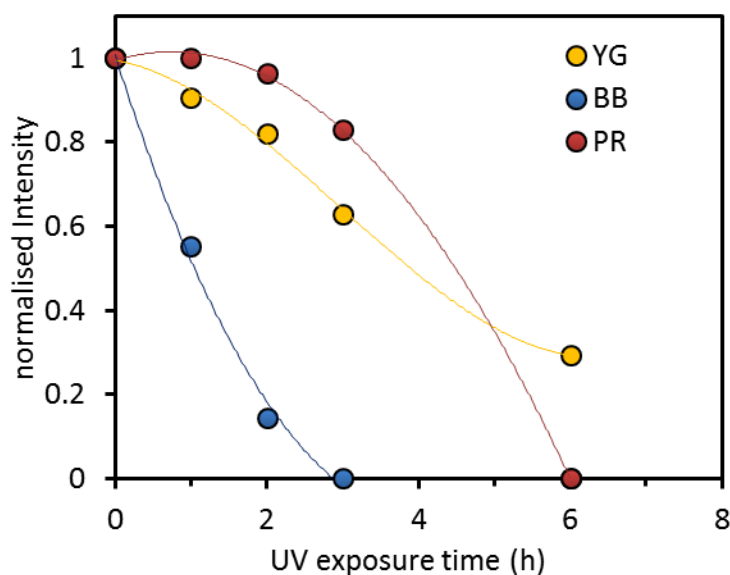


Figure 4.9: Effect of UV exposure on fluorescence intensities.

In addition to the screening tests presented, the nanoparticles were further exposed to a range of other chemicals identified in Chapter 3. These included acetic acid, a common surrogate for NOM, ionic species that can result in a change of the overall charge of the water, and disinfectants. Figure 4.10 shows the effect that 10-50 mg/L of acetic acid has on the emission intensity of the fluorescently tagged particles. It is clear from the data that YG was not affected by the presence of acetic acid whereas the fluorescence intensity increased marginally for BB and decreased marginally for PR. Practically, all three of the tagged particles exposed to acetic acid performed well and were not significantly affected by the presence of acetic acid.

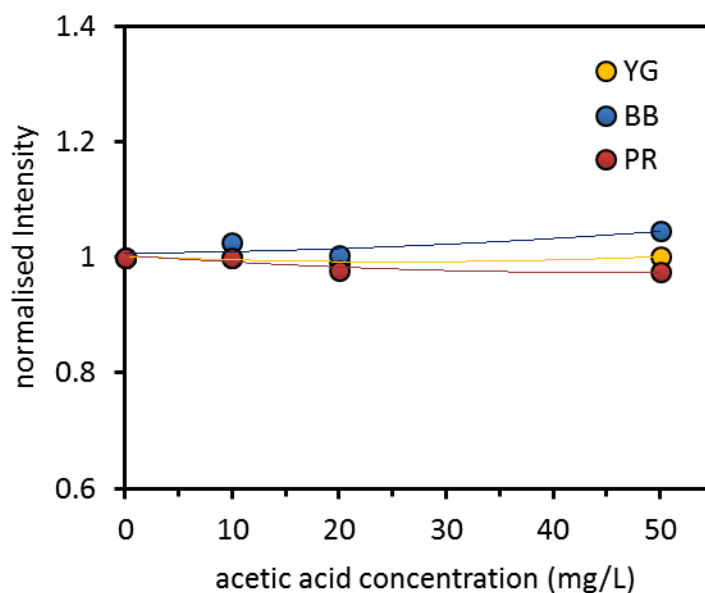


Figure 4.10: Effect of acetic acid exposure on fluorescence intensities.

The fluorescently tagged particles were subjected to a number of other compounds that were considered surrogates for NOM such as BSA as a protein surrogate, polyethyleneimine (PEI), dextran and sodium alginate. In addition to these organic surrogates, the tagged particles were exposed to oxidising compounds such as residual chlorine, chloramine and peroxide. These organic and oxidising compounds were chosen to reflect the likely feed water characteristics that the tagged particles would be exposed to, and to assess the impact that they have on fluorescent intensity. Figure 4.11 indicates that PR was the most stable across the range of organic and oxidising compounds with only slight effects from exposure to chloramine and PEI. While this performance against these compounds indicates a positive outcome, it is outweighed when the sensitivity and size comparison of PR eliminates it as a potential non-microbial surrogate. The most variable performance from exposure to the NOM and oxidising agents was the UR coated nanoparticle, YG. Exposure to PEI

significantly increased the fluorescence intensity by around 265% and in a range of 10% – 20% for all other challenge compounds with the exception of around 15% reduction in intensity when exposed to chloramine. These data clearly indicate that YG does not perform well under individual interfering compounds and is not considered stable enough when other characteristics are included in the assessment such as exposure to UV and varying pH conditions.

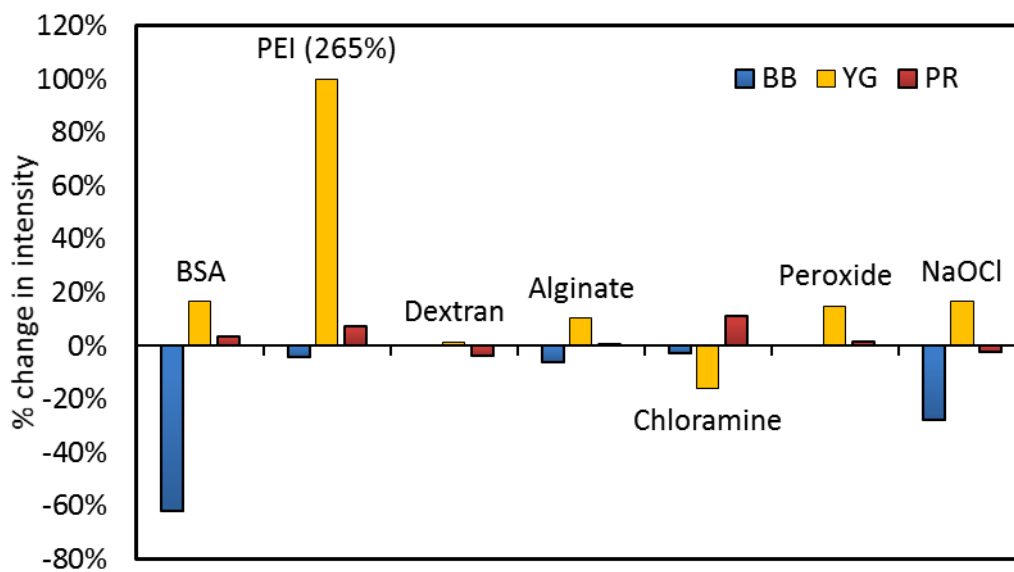


Figure 4.11: Effect of interfering agents on fluorescence intensities.

4.4.2 Toxicity and Costs

Since the mid-seventies nanoparticles have been progressively used in many industrial and medical applications with increased regularity. Polymeric nanoparticles are used extensively in medical therapy where they may allow more effective targeting of drugs at the cellular and subcellular level, as well as polymer imaging and diagnostics (Cupaioli *et al.* 2014). Polymeric nanoparticles have been used in food and drug preparations for direct consumption and many are

accepted in the food and medicine sectors as non-toxic. Other non-microbial surrogates based on metals are the subject of further toxicity including quantum dots based on Cd (Fan *et al.* 2011) and other nanoparticles based on Ti (Dreher 2004; Cross *et al.* 2007). The fluorescent nanoparticles screened in this study are claimed to be non-hazardous and non-toxic (Polysciences Inc. 2009).

Perhaps the most prohibitive aspect limiting the use of fluorescently tagged nanoparticles is that they are very expensive in comparison to the fluorescent dye costs presented in Table 3.1 from the previous chapter. The indicative cost to introduce fluorescent nanoparticles as a non-microbial surrogate as part of a membrane integrity monitoring program would equal or exceed the cost of water provided by the operator. The prices for one kg of fluorescently tagged nanoparticles would add, at a minimum, a cost of \$1.50/kL of treated water. The cost of fluorescently tagged nanoparticles alone is sufficient to eliminate them from further assessment, however, their low sensitivity adds to their lack of suitability.

4.4.3 Screening Summary

Table 4.2 presents a summary of the effects of the screening variables on the fluorescence intensity of the nanoparticles. Screening the YG particles, with a UR coating, under the test conditions was similar to that of the fluorescent dye UR as reported in Chapter 3. The challenge with the UR coated nanoparticle is that the sensitivity is two orders of magnitude lower than the fluorescent dye. The UR coated particles are one of the more common fluorescent probes with a very high molar absorptivity in the visible region, large fluorescence quantum yield, and high photo stability (Gholivand *et al.* 2008). Overall, the PR nanoparticles appear

to be the most stable under all of the conditions tested although these are clearly too large to be considered a viable NF/RO membrane virus surrogate as they are an order of magnitude greater than the target virus size.

Table 4.2: Summary of screening results.

Screening variable	YG	BB	PR
Sensitivity	Red	Red	Red
Size	Blue	Blue	Red
NaCl	Blue	Red	Blue
CaCl ₂	Blue	Red	Blue
pH	Red	Red	Red
Temperature	Yellow	Green	Blue
UV light	Red	Red	Red
Residual chlorine	Green	Green	Green
Chloramine	Green	Green	Green
Acetic Acid	Blue	Green	Green
NOM Surrogates	Red	Red	Yellow
Toxicity	Grey	Grey	Grey
Cost	Red	Red	Red

Key

Excellent/no effect	Blue
Good/minimal effect	Green
Average/moderate effect	Yellow
Poor/significant effect	Red
Unknown	Grey

The use of these fluorescent nanoparticles can now be eliminated as a potential non-microbial surrogate on the basis of the measured performance across a range of environmental and chemical conditions.

4.5 Conclusions

Sensitivity remains the key challenge that must be overcome before fluorescently tagged nanoparticles can be adopted as part of an integrated membrane integrity

monitoring and surveillance system. Sensitivity of fluorescently tagged nanoparticles is at least two orders of magnitude lower than that demonstrated using fluorescent dye compounds and therefore does not offer a plausible replacement that can be used as a non-microbial surrogate.

The conditions against which the fluorescently tagged nanoparticles were subjected included variations in pH, temperature, salinity and the presence of other chemicals. It is clear that the fluorescent microspheres tested did not have a high sensitivity at low concentrations and were not stable over a range of environmental conditions. The performance of the proposed surrogates showed that a variety of conditions had a significant effect on the measured intensity and the only stable commercially available product, PR, but it was far too large to be considered as a viable, virus like, surrogate. While PR was stable, its sensitivity in the order of 10 mg/L was far too high to be considered viable, as it would require at least 10,000 mg/L to provide a 4 log₁₀ removal capacity.

Table 4.2 compares the performance of the fluorescently tagged nano-and microspheres against acceptable benchmarks required so that they could be used as a non-microbial surrogates in membrane integrity surveillance program. It is clear that none of the tested particles could be used as non-microbial surrogates as they all performed poorly against more than one of the several screening challenges. The performance of the fluorescently tagged particles failed the primary test of sensitivity so their applicability in membrane integrity surveillance was curtailed. The fluorescent dyes, assessed in Chapter 3, provided much better sensitivity but were too small at around 1.5 nm, or more than an order of

magnitude smaller, to properly replicate virus particles and therefore provided a more conservative membrane integrity measurement.

The concept of using nanosized particles, as a surrogate for enteric virus, remains valid but the use of commercially available fluorescently tagged nanoparticles that were tested has been shown to be unsuitable due to the sensitivity limitations and the dose required to show 4 log₁₀ removal capacity. Therefore, the objective identified in Section 4.2 remains, that is, to find a nanoparticle that must have a high sensitivity at low concentrations and must be stable over a range of environmental conditions.

Chapter 5 Synthesis of PMMA Nanoparticles

5.1 Preamble

Commercially available fluorescent nanoparticles were selected and screened as potential surrogates for integrity monitoring in the previous chapter. There are clearly several limitations associated with using fluorescently tagged nanoparticles with the cost of implementing these at full scale, sensitivity and stability presenting significant challenges. The synthesis of a wide range of polymeric nanoparticles can be achieved readily in most laboratories and fluorescent tags can be introduced by further chemical treatment. In this chapter, poly(methyl methacrylate) (PMMA) nanoparticles were synthesised and characterised to develop an inexpensive, highly detectable, virus like, non-microbial surrogate for membrane integrity monitoring.

5.2 Introduction

The standard definition of a nanoparticle is one that has two or more dimensions in the order of 1 to 100 nm (ASTM 2006; ISO 2008). Other definitions of nanoparticles include particles that have a diameter that is less than 1,000 nm in size (Kreuter 2000), however, when the nanoparticles are used to mimic the size of enteric viruses the more suitable standard definition of less than 100 nm may be successfully argued. Based on the definition of a nanoparticle it is clear that some of the nanoparticles screened in the previous chapter do not meet the definition of nanoparticles and are rather more accurately defined as microparticles.

Nanoparticles are present in the environment and natural sources include volcanic eruptions and forest fires. Other sources include pollution from the exhaust of burning processes in car motors or industry. Nanoparticles are also synthesised for a range of uses including pharmaceuticals such as drug delivery and many scientific and industrial applications. Examples of nanoparticle use include zinc oxide nanoparticles in coatings to reduce UV exposure, iron nanoparticles used to treat ground water pollutants, and fluorescent nanoparticles used for imaging in biomedicine.

Nanoparticle surfaces can be customised with various types of functionalities by incorporating desired functional monomers to the polymerization recipe. Among the physical interactions, electrostatic attraction is common because the nano-solid matrix is usually charged and the surface has a high affinity to an oppositely charged dye. An example of this selectivity is where negatively charged silica particles can embed a positively charged dye to form fluorescent silica nanoparticles (Wang *et al.* 2011b).

5.2.1 Poly(methyl methacrylate) (PMMA)

Poly(methyl methacrylate) is known commonly as acrylic and is widely used as a glass substitute and in a wide range of applications. A typically transparent thermoplastic, PMMA is routinely produced by emulsion polymerization with the use of free radical initiators. Although the methyl methacrylate (MMA) monomer used in production of PMMA is toxic, the polymer is non-toxic and has good compatibility with biological systems (Bernardy *et al.* 2010). The structure of MMA and the resulting PMMA polymer are shown in Figure 5.1 with the C=C bond the site of polymerization.



Figure 5.1: Structures of (a) MMA and (b) PMMA.

5.2.2 Synthesis of PMMA

Poly(methyl methacrylate) nanoparticles can be synthesised into a wide range of sizes with various properties as illustrated by the different methods identified in Table 5.1. Varying polymerization conditions such as temperature, monomer concentration, and adding other components such as surfactants or solvents can significantly alter the size and properties of the resulting PMMA nanoparticles. The monomer methyl methacrylate (MMA) is used and this is typically produced with a small amount of inhibitor to prevent self-polymerization. Table 5.1 also shows that there are techniques to purify the monomer but in some cases PMMA is used without treatment.

The synthesis of PMMA nanoparticles is usually performed in water and may be aided with additives such as surfactants and co-solvents. The MMA monomer is slightly water soluble so nucleation occurs mainly in the water phase (He *et al.* 2003a). In a typical surfactant emulsion process, the initiator decomposes into free radicals in the water phase and first attacks the monomer to form radicals that grow in the water phase before precipitating. These precipitates, which are surrounded by surfactant, then become polymer precursors or seeds. Radicals in the precipitated polymer will continue to grow by accepting monomers from the water phase until termination occurs. Small particles are formed if a critical amount of surfactant is available to aid the generation of other seed particles and/or to cover the newly formed surfaces (He *et al.* 2003a).

Table 5.1: Methods to produce PMMA micro- and nano-particles.

Monomer treatment	Initiator	Temperature (°C)	Additives	Particle Size (nm)	Comments	Ref.
Nitrogen distillation	2,2'-Azobis[2-(2-imidazolin-2-yl)propane)]dihydrochloride	60	PEG copolymer	135-285		(Chen <i>et al.</i> 2000)
Nitrogen distillation	Potassium persulphate	70			300 rpm stirring rate	(Lee <i>et al.</i> 2000)
Distillation	Azo-bis-isobutyronitrile	80			>25 reaction time	(Huang and Brittain 2001)
Nitrogen distillation	Azo-bis-isobutyronitrile	80	Fluorescent tags	>300	2 h reaction time	(Bosma <i>et al.</i> 2002)
Rectification	Potassium persulphate	70-90	Sodium dodecyl sulphate	17-33	3-5 h	(Dan <i>et al.</i> 2002)
Nitrogen distillation	Azo-bis-isobutyronitrile		Fluorescent tags	<600	Synthesizes fluorescent monomer	(Jardine and Bartlett 2002)
As received	Ammonium persulphate	75-85	Sodium dodecyl sulphate	<20	Differential micro-emulsion polymerization	(He <i>et al.</i> 2003a)
Purified	Ammonium persulphate		Transition metal catalysts	<100	400 rpm	(Sahoo and Mohapatra 2003)
Reduced pressure distillation	Potassium persulphate	70	Acetone	45-215	Microwave irradiation polymerization, 200 rpm	(Bao and Zhang 2004)
Nitrogen distillation	Azo-bis-isobutyronitrile	80	Fluorescent tag	150-1000	Cross-linked particles	(Dullens <i>et al.</i> 2004)
Reduced pressure distillation	Potassium persulphate	70	Sodium dodecyl sulphate	17-27	Modified micro-emulsion	(Jiang <i>et al.</i> 2004)

Monomer treatment	Initiator	Temperature (°C)	Additives	Particle Size (nm)	Comments	Ref.
Inhibitor removal column	Azo-bis-isobutyronitrile	60-80	Sodium dodecyl sulphate	49.5-118.8	Mini-emulsion with RAFT agent	(Shim <i>et al.</i> 2004)
As received	Azo-bis-isobutyronitrile	70 / 4-48 h			Cauliflower-like particles	(Wang <i>et al.</i> 2004)
As received	Potassium persulphate	90	toluene	100-400	Argon atmosphere	(D'Amato <i>et al.</i> 2006)
Alkaline wash, purified & dried	Ammonium persulphate	60	Silica seed particles	120-330	Raspberry-like particles	(Min <i>et al.</i> 2006)
Reduced pressure nitrogen distillation	Potassium persulphate	65	Rhodamine 6G	190-960	<i>p</i> -styrene sulfonate for stabilization	(Nagao <i>et al.</i> 2006)
Reduced pressure distillation	Azo-bis-isobutyronitrile	70	Sodium lauryl sulphate	60-180	atom transfer radical polymerization	(Pan and Yi 2006)
Inhibitor removal column	Potassium persulphate	70-80	2-vinyl-4,4'-dimethylazlactone	various	Polymerisable surfactant	(Stanek <i>et al.</i> 2006)
Vacuum distillation	Potassium persulphate	Reflux temperature		255-301	Self-assembly of photoionic crystals	(Gu <i>et al.</i> 2007)
As received		60-95	Rare earth complexes		Fluorescent particles	(Guanming <i>et al.</i> 2007)
As received	Azo-bis-isobutyronitrile	70	Sodium dodecyl sulphate	20	Nitrogen purge	(Norakankorn <i>et al.</i> 2007)
Reduced pressure distillation	Redox system	40-60		165-223		(Chiu and Don 2008)
Alkaline wash, purified & dried	Ammonium persulphate	85	Sodium dodecyl sulphate	220	PMMA shell, alumina core	(Liu <i>et al.</i> 2008)
Inhibitor removal column	<i>t</i> -butyl hydroperoxide	80 / 3h			Composite particles for rubber coating	(Sunintaboon <i>et al.</i> 2009)
As received	Potassium persulphate	70	Sodium stearate		Nitrogen purge, 700-750 rpm	(Arora <i>et al.</i> 2010)

Monomer treatment	Initiator	Temperature (°C)	Additives	Particle Size (nm)	Comments	Ref.
As received	Ammonium persulphate	75	Acetone	32-75	3 h reaction time, sealed vessel	(Camli <i>et al.</i> 2010a)
As received	Ammonium persulphate	75	Acetone, ethylene glycol methacrylate	<100	3 h reaction time, cross-linked particles	(Camli <i>et al.</i> 2010b)
Gas phase	Ammonium persulphate	75	Sodium dodecyl sulphate	18.4	Nitrogen purge, 400 rpm	(Chen <i>et al.</i> 2010b)
Vacuum distillation	Potassium persulphate	60 /210 min	Sodium dodecyl sulphate	75-80	Tunable fluorescent dyes	(Chen <i>et al.</i> 2010a)
As received	Ammonium persulphate	75	Sodium dodecyl benzene sulfonate	10 (shell thickness)	Magnetic hollow spheres	(Wang <i>et al.</i> 2010)
Alkaline wash, distillation	Benzoyl peroxide	80	Sodium dodecyl sulphate		Silica core (20 nm), nitrogen purge	(Zheng <i>et al.</i> 2010)
Reduced pressure distillation	Azo-bis-isobutyronitrile	70 / 12 h	Polyacrylic acid	>3 µm	Methanol co-solvent	(Chen <i>et al.</i> 2011)
Alkaline wash, distillation	Potassium diperiodatocuprate (III)	25-45	Chitosan graft	54-350	Nitrogen purge	(Liu <i>et al.</i> 2011)
As received	Potassium persulphate (-ve), azo-bis-isobutylamine hydrochloride (+ve)	70	Fluorescent tags		Fluorescein, Rhodamine 6G &B	(Wang <i>et al.</i> 2011b)
As received	Potassium persulphate (-ve), azo-bis-isobutylamine hydrochloride (+ve)	70	Luminescent tags		Ru(bpy) ₃ Cl ₂ , nitrogen purge	(Wang <i>et al.</i> 2011a)

5.2.3 Free Radical Polymerization

Free radical polymerization is a technique by which a polymer forms by the successive addition of free radical building blocks. Free radicals can be formed *via* a number of different mechanisms that usually involve separate initiator molecules. The initiating free radical adds monomer units and thereby grows the polymer chain. Initiation involves two main steps:

- Radicals are created from the initiating molecules, then
- Radicals are transferred from the initiator molecules to the monomer units' present forming the polymer chain.

Radical formation by thermal decomposition occurs when the initiator is heated until a bond is homolytically cleaved, producing two radicals. Polymerization is the process of increasing the polymer chain length, or propagating. After the radical initiator is formed, it attacks a monomer such as styrene, also known as ethenylbenzene, shown in Figure 5.2 *via* molecular bonds. The ethene monomer, for example, holds one electron pair securely between the two carbons in a sigma bond with another more loosely held in a π bond. The free radical uses one electron from the π bond to form a more stable bond with the carbon atom. The other electron returns to the second carbon atom, turning the whole molecule into another radical thus beginning the polymer chain.

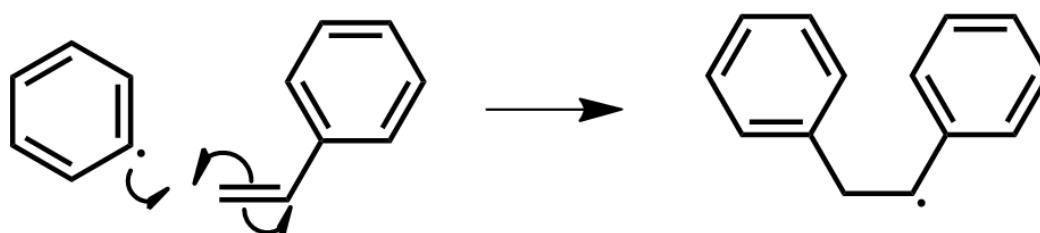


Figure 5.2: Radical initiator attack on a monomer to start a polymer chain.

Once a chain has been initiated, the chain propagates until the monomer has depleted *via* living polymerization or until termination occurs. In the case of living polymerization, propagation can continue if more monomer is added to the reaction. If longer chains are desired, the initiator concentration should be kept low; otherwise, many shorter chains will result. Chain termination can occur by the following:

- Chain termination – the combination of two active polymer chain ends, i.e. poly(vinyl chloride) (PVC), which couple together to form one long chain (Figure 5.3):

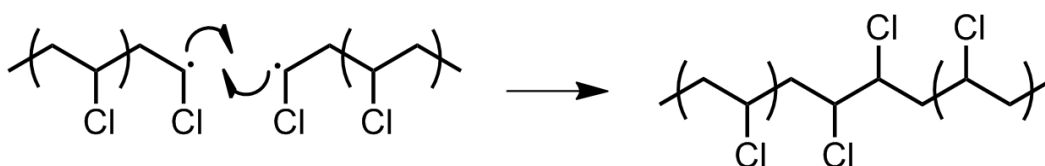


Figure 5.3: Termination by the combination of two polymers.

- Radical disproportionation - occurs when a hydrogen atom from one chain end is moved to another, producing one polymer with a terminal unsaturated group and another with a terminal saturated group illustrated in Figure 5.4.

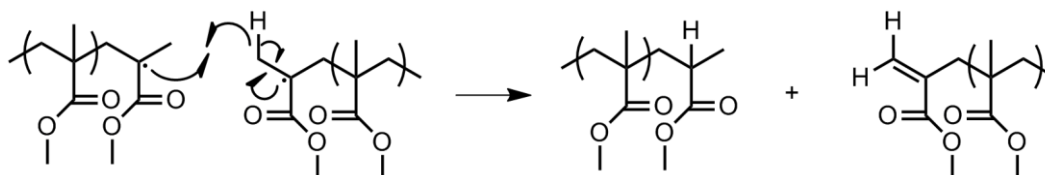


Figure 5.4: Termination by disproportionation of PMMA.

- Radical termination occurs by combination of an active chain end with an initiator radical as illustrated by Figure 5.5.

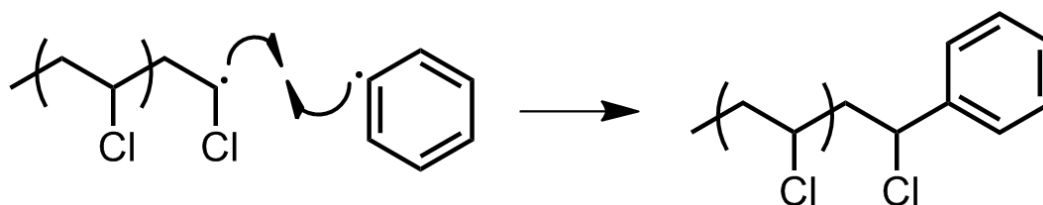


Figure 5.5: Termination of PVC by reaction with radical initiator.

In emulsion polymerization, the polymer blocks prefer to adopt the lowest energy level that is in the form of a sphere. Bulk polymerization can also be used to create other forms and shapes, typically with the use of moulds. In this synthesis, the spherical form is the desired shape as it closely mimics the shape of the target virus and therefore represents a better surrogate form.

5.2.4 Surfactant Aided Emulsion

Surfactants have a very valuable property because they decrease the surface tension between the boundaries of two phases, and surfactants can therefore form oriented, stabilizing films. A surfactant is comprised of a hydrophilic head that is usually charged and a hydrophobic tail that is not charged. The hydrophilic heads prefer to be in the aqueous phase, while the hydrophobic tails prefer to be in the oily phase of a mixed solution. Figure 5.6 shows how surfactant molecules stabilize oil droplets and prevent them from coalescing, thus making the emulsion much more dispersed (ACT Government 2007). Moreover, anionic surfactant results in emulsion droplets with an overall negative charge. In the case of PMMA synthesis, the monomer is the oily phase that is dispersed in water.

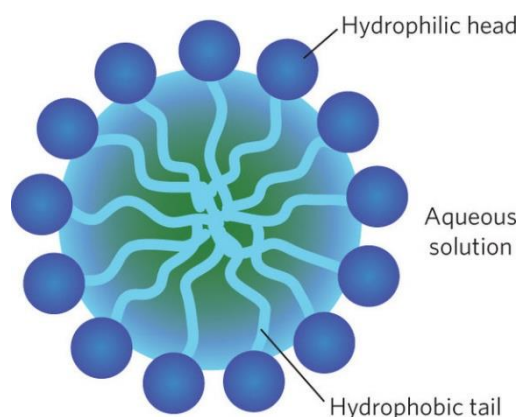


Figure 5.6: Schematic representation of a stabilised surfactant emulsion.

5.3 Aims

The aim of this phase of work was to produce a nanoparticle of similar size as the smallest enteric virus, poliovirus at around 30 nm, and use this as a non-microbial surrogate. Establishing a consistent and reliable pathway to synthesise polymeric nanoparticles by optimizing the synthesis pathway conditions to obtain PMMA nanoparticles of known, monodisperse particle sizes and uniform spherical morphology. The specific aims were to investigate the following manufacturing variables on nanoparticle size PMMA particles:

- The effect of processing variables (temperature, time, stirring speed)
- The effect of monomer concentration
- The effect of additives (surfactant, acetone co-solvent), and
- The effect of tagging with fluorescent dyes (RWT, Quinine)

Additionally, the detection of low concentrations of nanoparticles using fluorescence spectroscopy was also investigated. It was considered that the ability to optimise fabrication and detection conditions should result in an inexpensive but very effective non-microbial surrogate.

5.4 Materials and Methods

5.4.1 Materials

All materials were purchased from Sigma-Aldrich (Sydney, Australia). The monomer, methyl methacrylate monomer, was used as received without further purification. The initiators, ammonium persulphate (APS) and 2,2'-azobis(2-methylpropionamide) dihydrochloride (azobis), the surfactant sodium dodecyl sulphate (SDS), and co-solvent acetone were used as received. De-ionised water (MilliQ water, $\Omega > 18$ MOhm) was used throughout all experiments.

5.4.2 Preparation of PMMA Nanoparticles

The polymerization process was conducted in single or multiple neck round bottom flasks fitted with a water-cooled glass condenser (Nowbray Glass) to prevent evaporation. A series of flasks of different sizes were used including 25, 50, 100 and 500 mL capacity flasks (Jena Glass, Germany and Nowbray Glass). During the process, the flask was immersed in a water bath that was heated using a stirrer-hotplate (IKA-RCT basic safety control) with magnetic stirrer. All compounds were introduced through a neck of the flask that was hermetically closed with stoppers. A range of egg/oval shaped, Teflon coated, magnetic stirrers were used to optimize the emulsion in the flask and these were purchased from Pro-Sci-Tech, Sydney Australia.

In most experiments, polymerization was performed under nitrogen atmosphere where the nitrogen entered through a long needle and exited through a short needle passing through a septum in the top of a condenser then to a bubbler to monitor flow. Aluminium foil was used to cover the water bath to help minimize

temperature fluctuations. The top of the condenser was hermetically sealed using paraffin and after every run the flasks were cleaned with deionised water. Figure 5.7 (a) shows a photograph of a typical experimental setup and a schematic representation is given in Figure 5.7 (b).

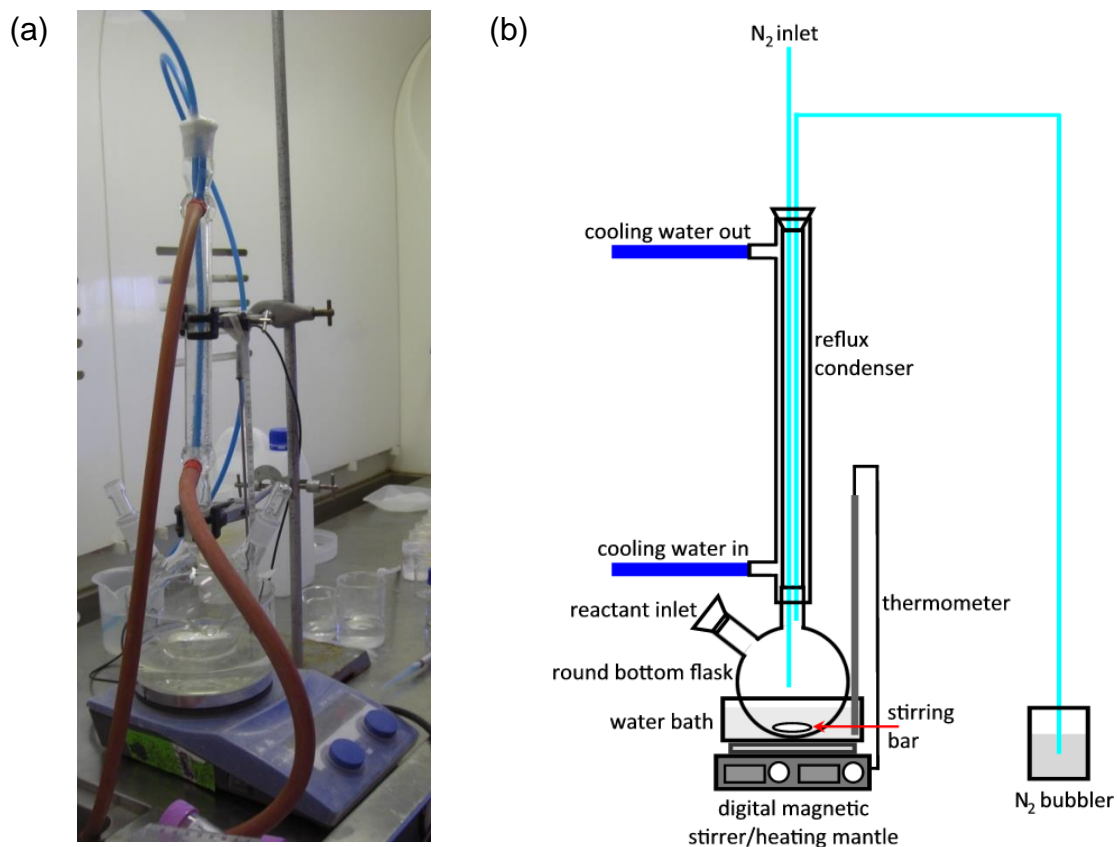


**Figure 5.7: PMMA polymerization apparatus
(a) photograph and (b) and schematic.**

A typical PMMA nanoparticle synthesis reaction was performed according to the following polymerization procedure.

- Deionised water was added to a 25 mL single neck round bottom flask and heated in a temperature controlled water bath under stirring and a slow flow of nitrogen until it reached the temperature of 70°C.
- The surfactant was introduced to the water under rapid stirring and after 1 min, the monomer (MMA) was added.

- When the emulsion reached 70°C again and the conditions were stable, the initiator was introduced.
- A milky white suspension was observed as the polymerization proceeded and after 2 hours, the condenser was removed, stirring was stopped and the PMMA dispersion was stored in a sealed tube.

The effects of monomer, initiators, acetone and surfactant on the particles were studied in accordance with the conditions detailed in Appendix A. A total of 104 experiments were performed in order to fully assess and optimise the synthesis conditions.

5.4.3 PMMA Characterization

The nanoparticles were examined for their average size, charge, surface, polymer functional groups and fluorescence behaviours. The size was determined from images of the nanoparticles obtained using a JOEL NeoScope (JCM-5000) scanning electron microscope. A drop of the PMMA suspension was placed on an aluminium sample holder, dried and coated with up to 6 nm of gold using a NeoCoater (MP19020NCTR) coater prior to obtaining the SEM images. In some cases, the suspensions were diluted prior to mounting on the sample holder. The images were acquired at magnifications up to 40,000x under high vacuum and using an accelerating voltage of 10 kV.

The resolution of the SEM used during this work was not adequate to present a stable image when the particles were too small (sub 100 nm) so dynamic light scattering measurements were performed using a Zetasizer Nano ZS (Malvern Instruments). The particle charge was also measured using the Zetasizer. All samples for the Zetasizer and the zeta potential were prepared by diluting the particle dispersion in deionised water by a ratio of up to 1:1000.

Fluorescence measurements were performed using a Shimadzu spectrophotometer (RF-5301). Samples for fluorescence were serially diluted up to concentrations of parts per billion and samples were measured in plastic or quartz cuvettes to obtain EEMs. Acquisition of the EEM data was obtained by scanning the range of emission (y) wavelengths at constant, incremental excitation (x) wavelengths. Data were recorded for each series of excitation wavelengths and the resulting fluorescence and scattering intensity (z) indicated as a particular colour on the 2D plot across a range of 200 nm and 900 nm wavelengths. The intensity scale shown in conjunction with each EEM plot represents the enumeration of photons detected by the sensor in counts per second (cps) and the intensity is normalised to show the relative difference across the excitation and emission spectra as an image.

The functional groups of some of the particles were measured with an FTIR spectrophotometer (Shimadzu IRAffinity-1). Dried nanoparticles were mounted on an ATR crystal prior to measuring the FTIR spectrum. All measurements were conducted at room temperature.

5.5 Results and Discussion

Poly(methyl methacrylate) nanoparticles with different average diameters were synthesised using emulsion polymerization. The operating conditions used to obtain all 104 samples and the mean diameters of selected samples are presented in Appendix A.

5.5.1 General PMMA Synthesis

The first PMMA samples were prepared according to a published standard procedure (CTG Marine Systems 2002). Figure 5.8 shows an SEM image of a typical example of PMMA produced in the first series of experiments. The SEM picture shows particles of different sizes and a bigger piece that appears to be fused. It is clear from this image that most of the nanoparticles are spherically shaped. The presence of the larger fused piece and a strong odour of MMA monomer after the reaction was terminated were evidence of an incomplete polymerization process. Any remaining monomer is able to continue the free radical emulsion polymerization, even at lower temperatures, resulting in larger particles (Peng *et al.* 2012). The processing time was extended to complete the polymerization process to overcome the incomplete synthesis reaction.

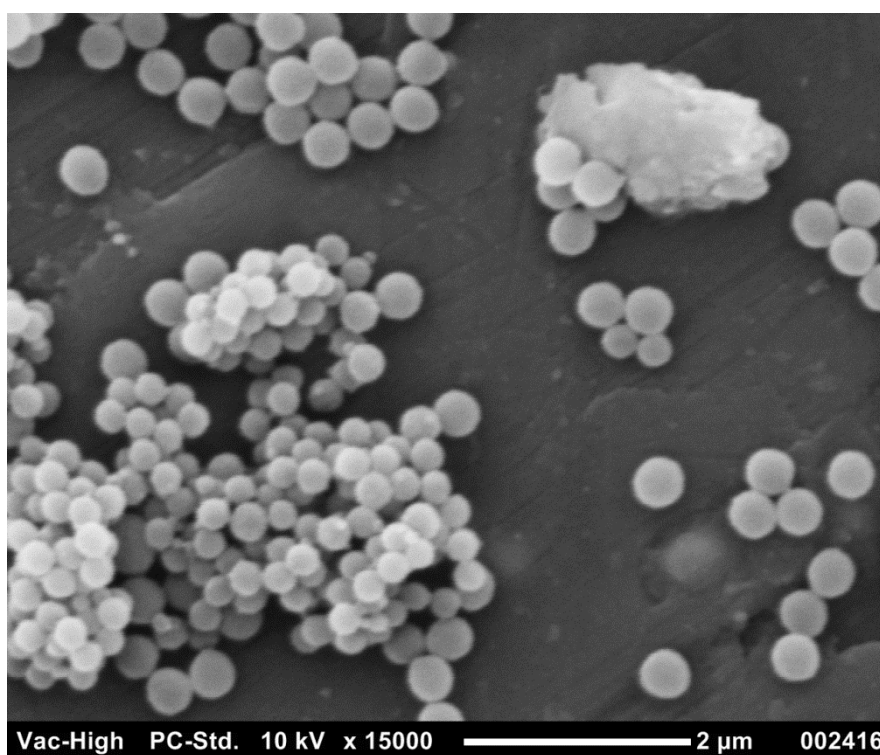


Figure 5.8: SEM image of typical PMMA sample.

5.5.2 Effect Polymerization Time

Figure 5.9 to Figure 5.12 show SEM images of samples synthesised using four different reaction times at a temperature of 70°C, 16 vol% MMA, 1,200 rpm stirring speed, and either APS or azobis initiators. These figures show that the particle sizes are relatively constant and after a running time of 3 h (Figure 5.12) there was no detectable monomer odour suggesting the polymerization was complete. For the samples with shorter run times (Figure 5.9 and Figure 5.10), there was clearly monomer present that can result in continued polymerization. The sample reacted for 120 min (Figure 5.11) contained only a trace of monomer odour. The use of different initiators and concentrations also resulted in slight variations in the particles size; however, this was not the focus of this set of experiments but rather to verify the polymerisation time.

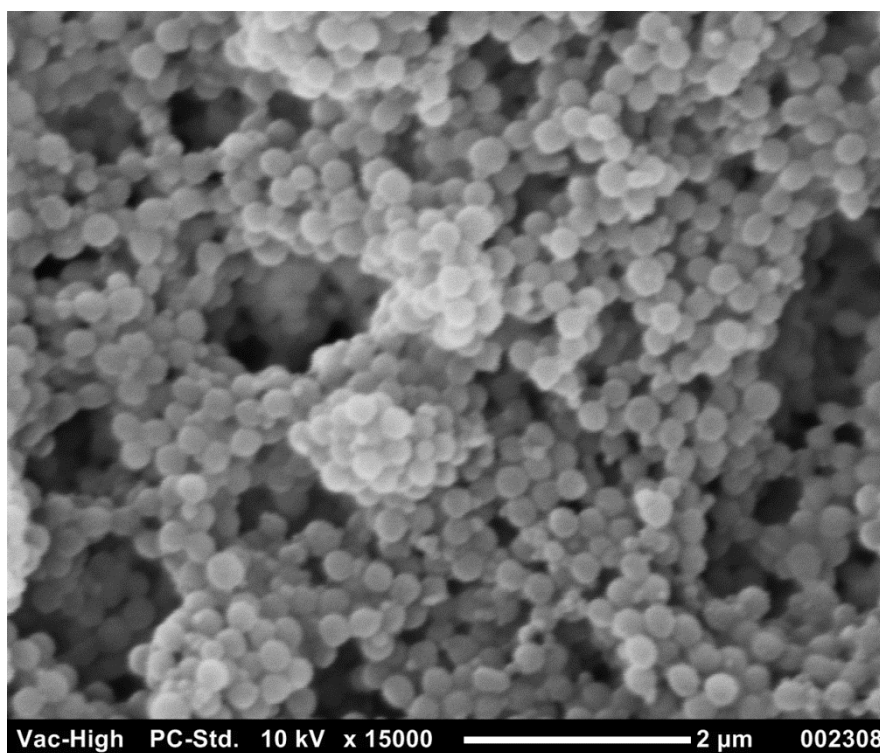


Figure 5.9: SEM image of sample polymerised for 40 min using 3 vol% azobis initiator.

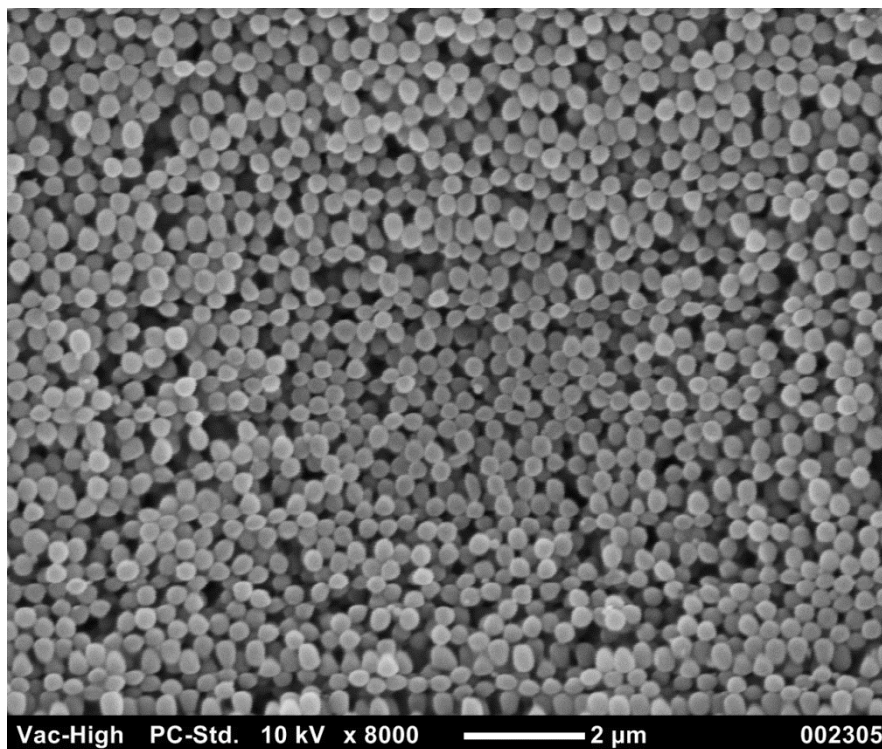


Figure 5.10: SEM image of sample polymerised for 90 min using 1.5 vol% azobis initiator.

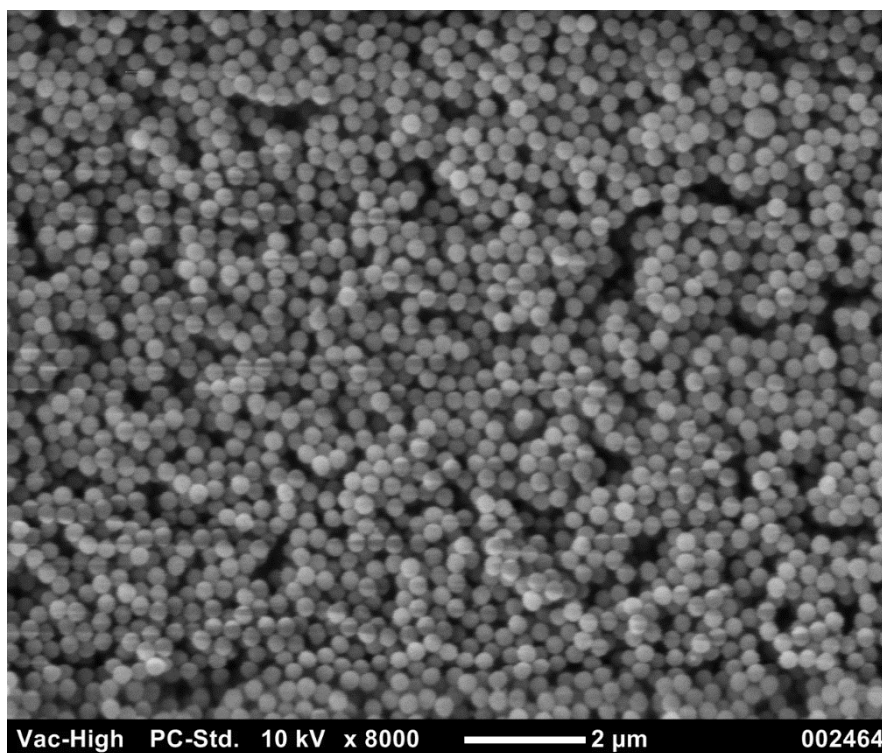


Figure 5.11: SEM image of sample polymerised for 120 min using 1.5 vol% APS initiator.

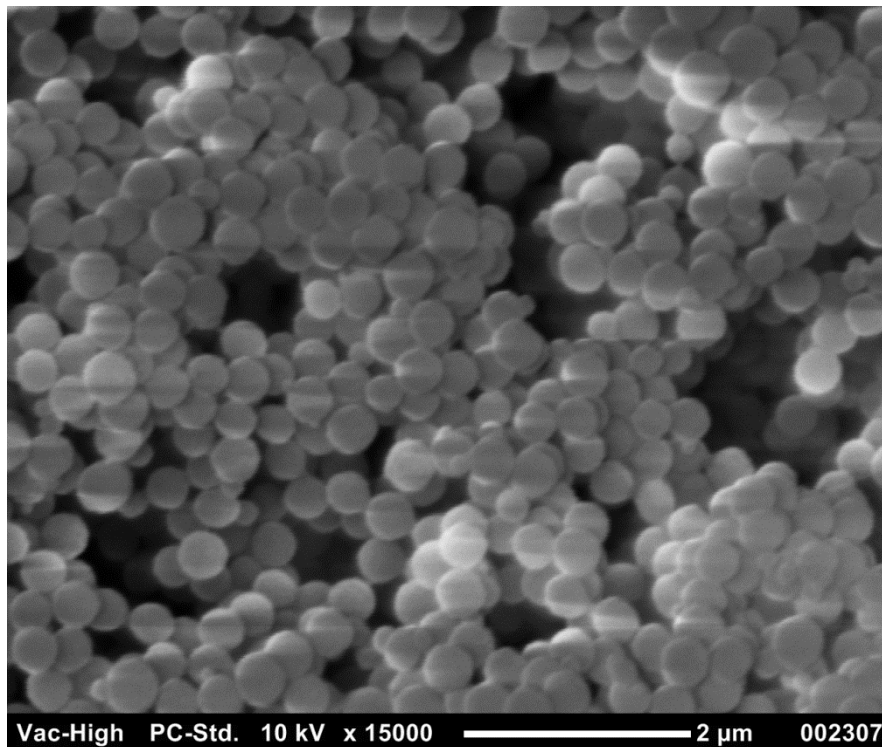


Figure 5.12: SEM image of sample polymerised for 180 min using 3 vol% azobis initiator.

A runtime of 120 min was further selected with a reduction in monomer concentration to 3 vol% in order to ensure the process was completed in a timely manner, that the monomer was consumed before the process ends, and to decrease the particle size. Some researchers recommend reaction times in excess of 24 h (Huang and Brittain 2001) but this would clearly add undue expense to the PMMA synthesis, particularly if the monomer is consumed within a few hours. Figure 5.13 shows an SEM image of PMMA produced using 3 vol% MMA at a temperature of 70°C, 1,200 rpm stirring speed, and 1.5 vol% APS initiator confirming that this adjustment was successful. The illustration also indicates that the PMMA produced using a run-time of 120 minutes were monodisperse and had a relatively uniform diameter between 140 and 180 nm

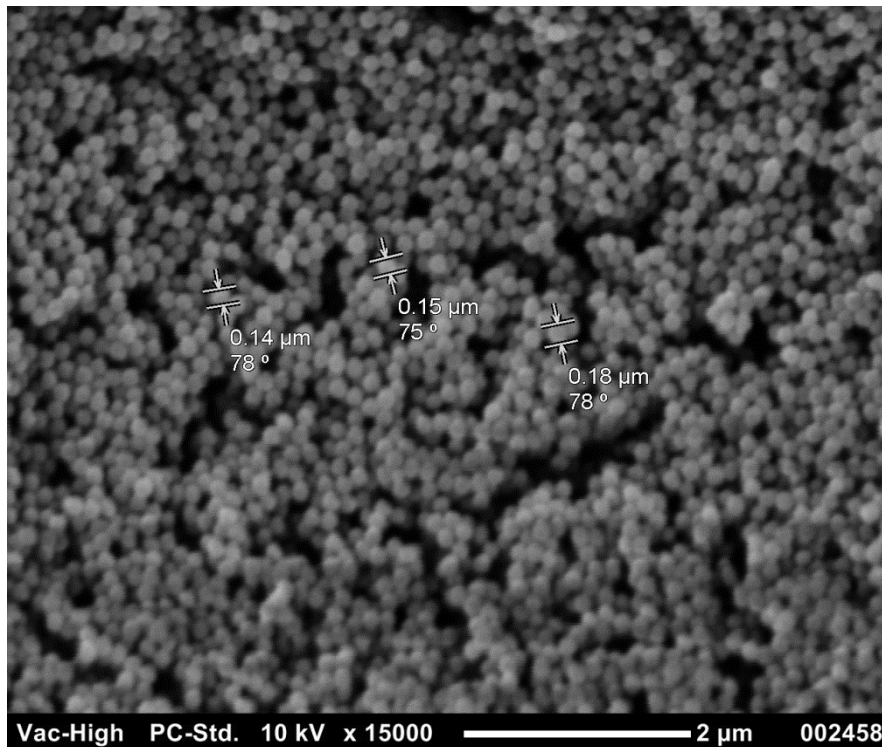


Figure 5.13: SEM image of PMMA polymerised for 120 min using 3 vol% MMA, 70°C, 1,200 rpm stirring speed, and 1.5 vol% APS.

5.5.3 Effect of Processing Temperature

The literature reported in Table 5.1 show a range of temperatures can be used to polymerize PMMA nanoparticles. Temperature is a critical process variable that promotes the reactivity of the heat activated initiators. The effect of temperature on the polymerization process was therefore explored and Figure 5.14 to Figure 5.16 show SEM images of samples polymerised at temperatures of 60, 80 and 70°C respectively using 16 vol% MMA, 3 vol% azobis and 1,200 rpm stirring speed.

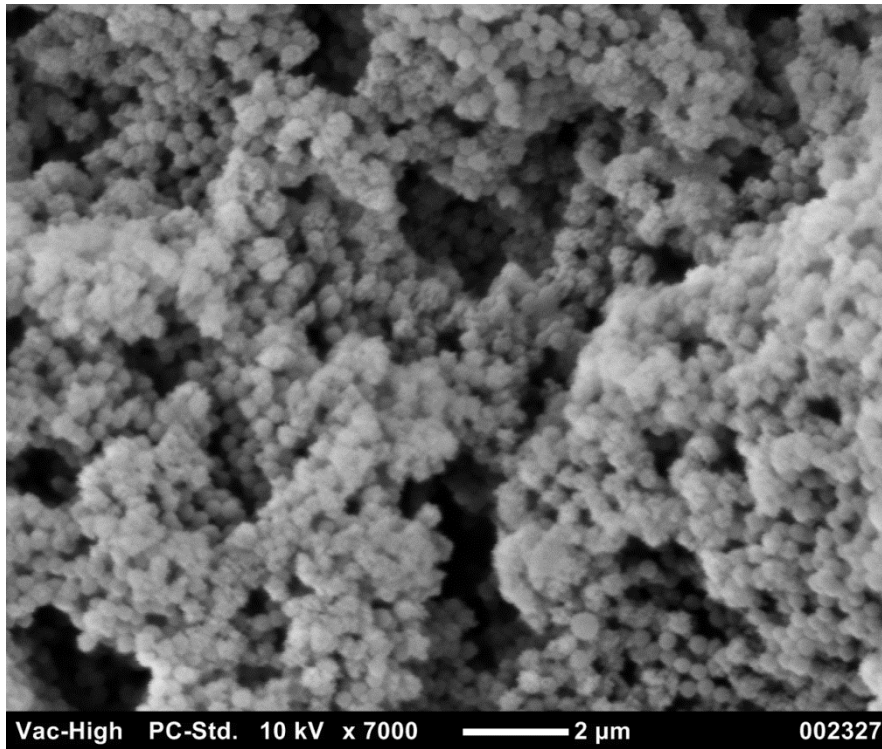


Figure 5.14: SEM image of PMMA polymerised at 60°C.

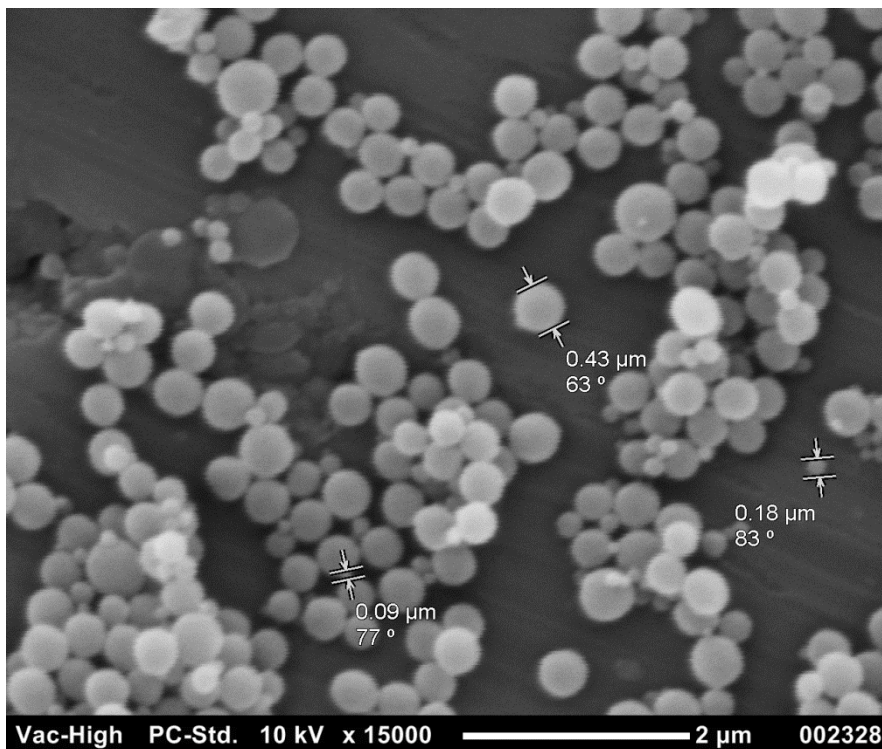


Figure 5.15: SEM image of PMMA polymerised at 80°C.

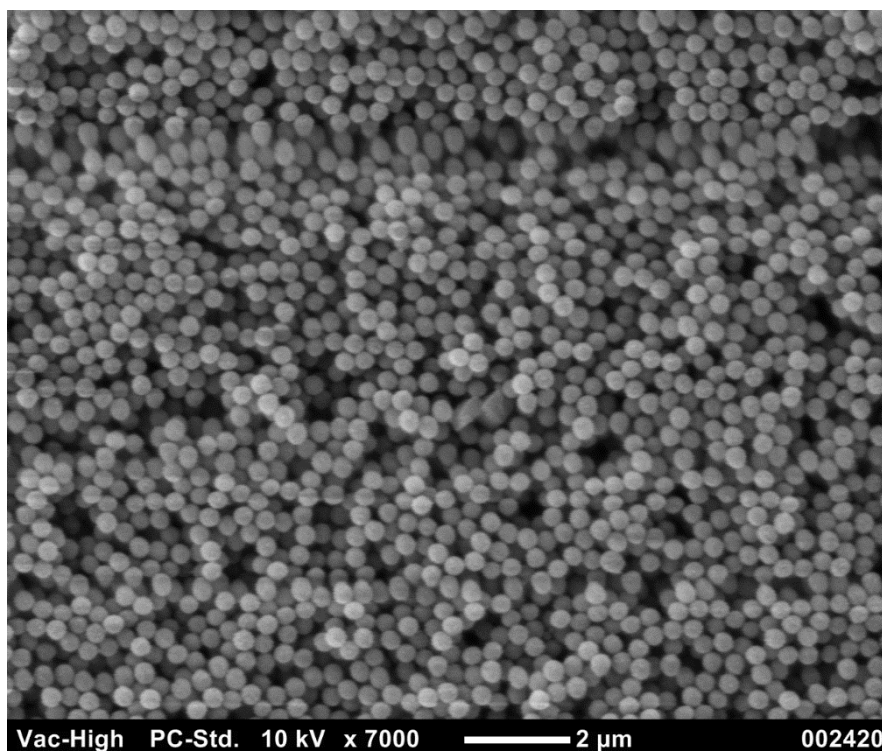


Figure 5.16: SEM image of PMMA polymerised at 70°C.

Figure 5.14 demonstrates that the temperature of 60°C is not high enough for complete polymerization of PMMA. A strong monomer odour was present in this sample and the SEM picture also shows highly fused particles. Figure 5.15 was prepared at a temperature of 80°C and the resulting spheres are varying sizes with many larger particles that could be the result of a very fast reaction or the presence of excess monomer in the vapour phase causing larger particles to form when the monomer condenses.

Figure 5.16 illustrates that 70°C is the most appropriate temperature for this PMMA emulsion polymerization process using the selected initiator. The spheres are relatively mono-dispersed in size and there is no fusion as in the case of the lower temperature. A temperature of 70°C is the ideal reaction temperature for this system and is clearly the common temperature used in the literature as

shown in Table 5.1. This is primarily a function of the decomposition and subsequent activity of the heat activated initiators.

5.5.4 Effect of Flask Volume and Stirring

The synthesis of uniform, mono-disperse particles requires stable conditions to guarantee steady dispersion in the emulsion. The vortex formed under stirring is therefore important to obtain well dispersed uniform monomer droplets that can be discretely polymerised into nanoparticles. For that reason, the selection of the right sized stirrer and stirring speed to impart sufficient energy intensity to achieve a homogenous emulsion, and vessel for the total volume is important. In the case of a small stirrer, the energy yield is low and the particle polymerization will be poor due inadequate monomer dispersion. The speed of stirring is limited to the equipment used with 1,200 to 1,500 rpm the typical range of maximum speeds for most laboratory stirrers. These dimensional criteria are important considerations for large scale production of appropriately sized PMMA nanoparticles.

Figure 5.17 illustrates a very uniform particle size and shape prepared in a 100 mL flask with a 20 mm oval shaped magnetic stirrer at 1,500 rpm. In this case, uniform particles were produced suggesting the stirrer enabled a stable emulsion to be formed prior to the polymerization. The flask size is also important but only with respect to the total volume of the solvent/solute required. The vessel volume to stirrer diameter/length ratio that provides the mixing energy intensity is therefore critical to obtain the optimum emulsion and ensure a consistent PMMA nanoparticle size and shape is produced.

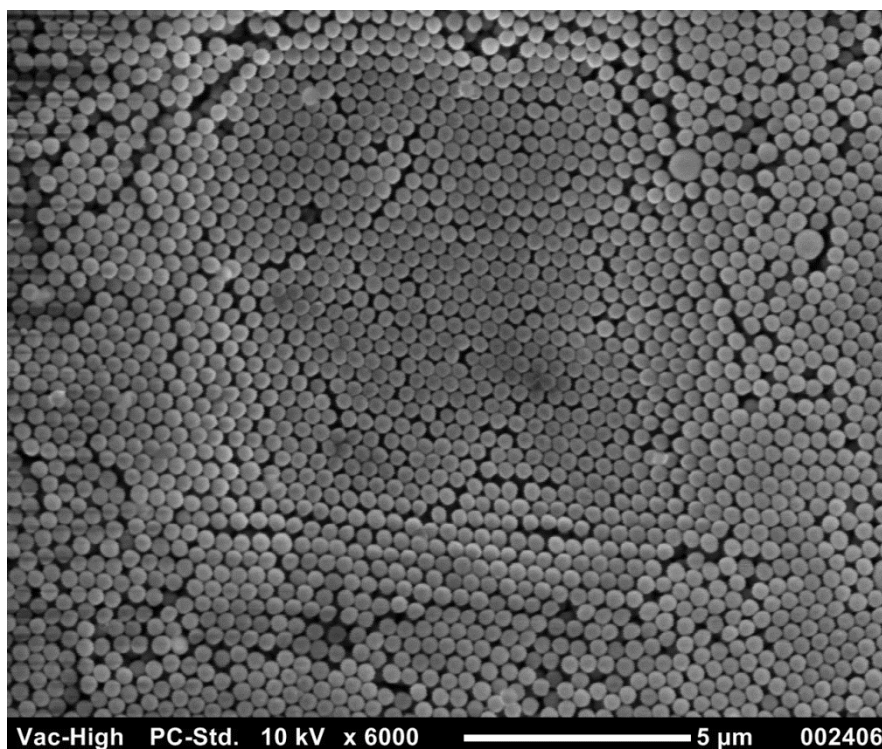


Figure 5.17: SEM image of PMMA polymerised in a 100 mL flask using 6 vol% MMA and 1.5 vol% APS.

5.5.5 Effect of Initiator

The polymerization of PMMA can be altered or enhanced by the use of additives including surfactants and co-solvents such as acetone as well as different types of initiators (see Table 5.1). The effect of various monomer concentrations, the use of surfactants and co-solvents, and the types and concentrations of initiators and on the resulting PMMA particle size was investigated.

Initial experiments were conducted using azobis, a common azo compound free radical initiator. The results from initial experiments suggested this chemical had partially decomposed after prolonged storage and attempts to purchase a new product were unsuccessful. The lack of azobis supplies was the direct result of shipping restrictions due to potential dangers during transport. It is evident from

the recent trends in the literature (Table 5.1) that the more common initiators are the persulphates, ammonium persulphate (APS) or potassium persulphate (KPS), so APS was adopted as the initiator because it was more readily available.

5.5.6 Effect of Monomer Concentration

Under polymerization conditions optimised from earlier experiments (temperature 70°C, stirring speed 1,200 rpm, reaction time 120 min), the effect of monomer concentration on average particle diameter was investigated. There is a general tendency towards increased particle diameter as the monomer concentration increased as illustrated by Figure 5.18. This can be explained by the absorption of residual monomer molecules by the primary nucleating particles which were formed at the initial stages of polymerization (Camli *et al.* 2010a).

The reduction of the monomer concentration also accelerates the polymerization process that is terminated when no further monomer remains in solution. The size of the particles is not significantly different for concentrations up to and including 10% monomer. There appears to be a critical concentration around 10% where a rapid increase in particle size occurs. Nonetheless, the minimum particle size is close to 200 nm, which is still much larger than the target poliovirus previously identified and therefore not suitable as a non-microbial surrogate. Adjustments to the method were required to synthesize smaller PMMA particles to be used as a surrogate for the target virus. Adjustments to the synthesis of PMMA to produce smaller particles were explored and are discussed in following sections.

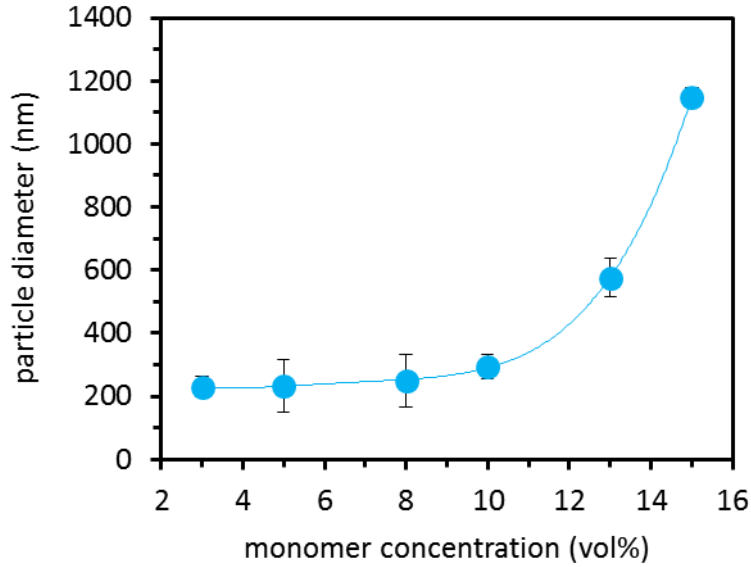


Figure 5.18: Effect of monomer concentration on particle size.

Figure 5.19 shows the effect of PMMA particle surface charge as a function of monomer concentration. In general, the charge is relatively constant at *ca.* -40 mV, with a general trend towards a relatively stable surface charge across the range of monomer addition. The results show that the particles are all highly negatively charged and this would be expected from the structure of PMMA, as illustrated by Figure 5.1 earlier. This is an important feature as the ability to dope the PMMA with a fluorescent dye depends on the capacity to produce a negatively charged nanoparticle. Given the high surface area, this would facilitate the addition or bonding of fluorescent tags similar to the fluorescently tagged latex nanoparticles assessed and presented in Chapter 4.

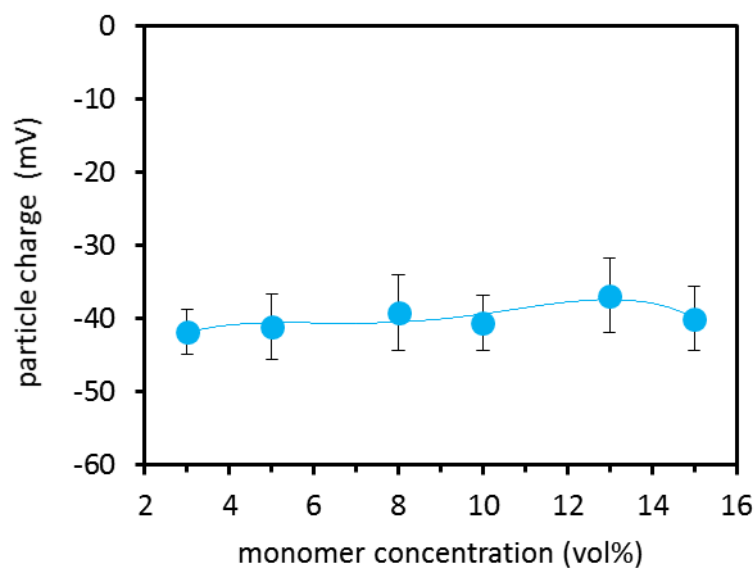


Figure 5.19: Effect of monomer concentration on particle charge.

5.5.7 Effect of Surfactant

The synthesis of smaller particles, especially in the sub 100 nm range, generally requires the addition of surfactants to form smaller micelles during polymerization (Jhaveri and Carter 2007) and the amount of surfactant present has a strong influence on particle size (He *et al.* 2003a).

As expected, the addition of surfactant resulted in the formation of smaller particles as shown in Figure 5.20. A series of samples were prepared with constant volume of surfactant (0.03 mL) and a decreasing concentration of monomer from 10% to 1% by volume. All other conditions were kept constant as previously optimised (70°C, 1,200 rpm stirring speed, 120 min reaction time) and Figure 5.21 shows the resulting reduction in particle size with respect to the surfactant concentration measured by the Zetasizer. The smallest particle size obtained was *ca.* 16 nm with a surfactant concentration of 16.67% relative to the monomer.

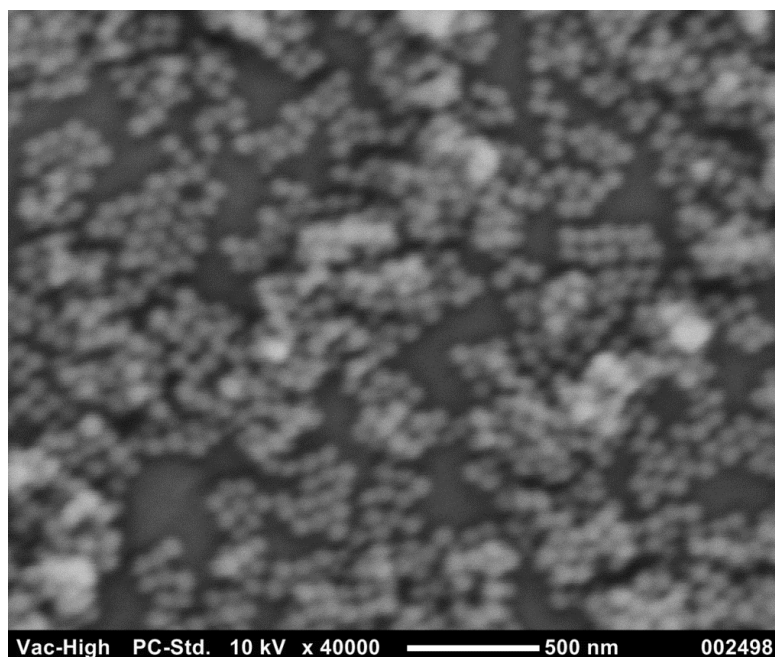


Figure 5.20: SEM image of particles formed in the presence of surfactant.

The results are in accordance with the literature which suggests that particle size decreases with increasing concentration of surfactant (He *et al.* 2003a). Consequently, adjusting the mode of synthesis can determine the size of the PMMA nanoparticles, a critical factor when the size of the target virus and the ability to dope the surface with fluorescent tags to improve response intensity are considered. At 6 vol% surfactant, the nanoparticles produced had sizes between 25 nm and 40 nm and this compares favourably with the target virus size for polio of around 30 nm (Schijven and Hassanizadeh 2000). The synthesised nanoparticle size and shape were, therefore, considered as a good non-microbial surrogate for a small virus such as polio.

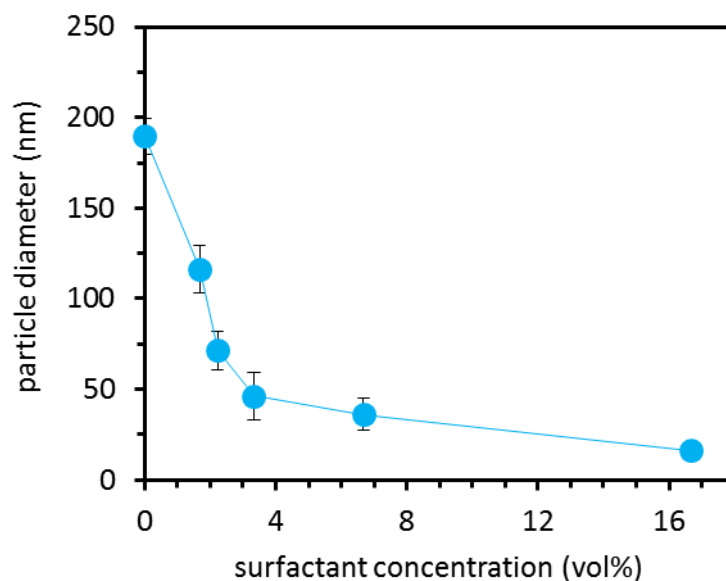


Figure 5.21: Effect of surfactant concentration on particle size.

Figure 5.22 illustrates the PMMA surface charge as a function of surfactant concentration and this shows that the charge became more negative with increasing surfactant concentration. The negative charge of the PMMA significantly reduced the potential for the nanoparticles to clump or stick together or be adsorbed by the negatively charged membrane. Although the introduction of a surfactant into the solution to promote the synthesis of smaller particles affected the surface charge, the resulting zeta potentials were in the range -37 to -50 mV. So it is clear that the addition of a surfactant did not have an adverse effect on the surface charge of the PMMA nanoparticle.

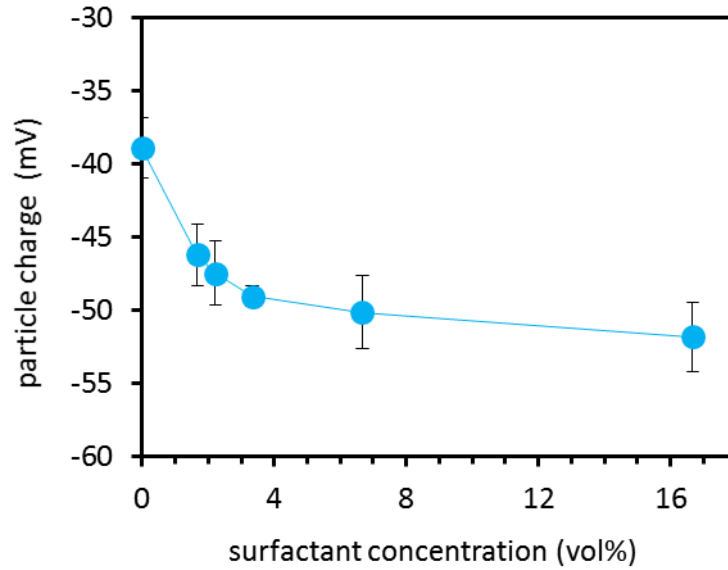


Figure 5.22: Effect of surfactant concentration on particle charge.

5.5.8 Effect of Acetone Co-solvent

Acetone is a water-miscible co-solvent that can increase the solubility of the MMA monomer in the continuous phase. This can increase the number of nucleating seeds in the final solution, resulting in a reduced particle size of less than 100 nm without the use of surfactants (An *et al.* 2006). The addition of acetone is reported to be able to also facilitate particle stabilization due to the exponential reduction in solution surface tension (Narkis 1979). There are two intrinsic factors that determine the resulting value for particle diameter; namely,

- The influence of solution dielectric constant, and
- The solubility of the monomer (Rao and Geckeler 2011).

The addition of acetone up to 20% can exponentially decrease the dielectric constant of an acetone-water mixture resulting in unstable primary nucleating particles in the continuous phase, and subsequently larger particles are produced. Above 20% acetone, further decreases in the solution dielectric

constant are minimal, and thus the increase in monomer solubility dominates resulting smaller particle size (Camli *et al.* 2010a; Camli *et al.* 2010b).

Samples were prepared with different acetone concentrations to investigate this phenomenon but all other variables were kept constant as previously optimised. Figure 5.23 illustrates this change in diameter as a result of varying the acetone content where the particle diameter increased slightly over the concentration 2.5 to 5-vol% and after that the particle diameter remained relatively constant. In contrast to similar studies, under the conditions of the experiments in this work, no significant reduction in size was obtained in the presence of acetone. Moreover, high acetone concentrations of 30 vol% and higher resulted in highly heterogeneous particle sizes which may be due to the solubility of PMMA in acetone (Miller-Chou and Koenig 2003). This result completely contradicted the literature and the research objective of adding acetone to the solution so the continued use of a co-solvent such as acetone could not be supported.

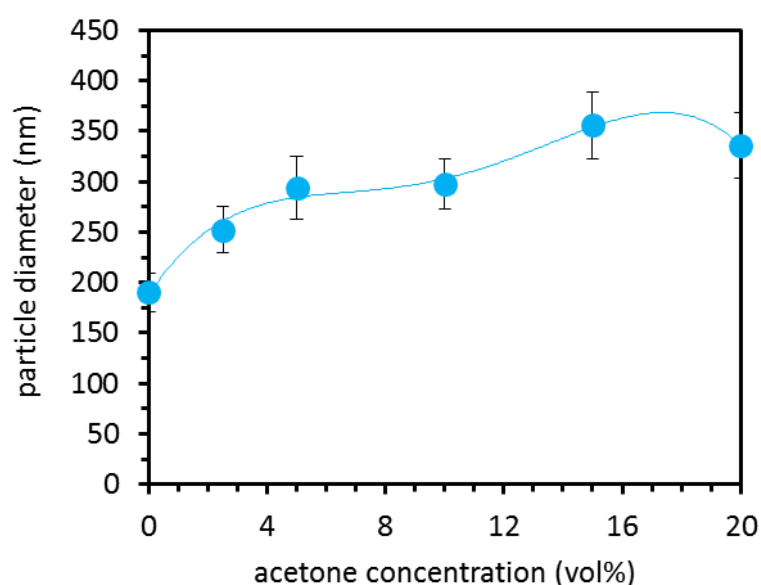


Figure 5.23: Effect of acetone concentration on particle size.

The SEM image of a sample prepared using 10% acetone is shown in Figure 5.24 and it is clear that the particles are very similar in shape and size and have self-assembled into layers upon drying indicating a high level of uniformity but are approximately 250 nm in diameter. Figure 5.25 shows the SEM image of a sample prepared using 40% acetone that demonstrates that high acetone content can lead to highly poly-disperse particles with visible surface cracking. The residual acetone in the reaction vessel following polymerization could partially dissolve the PMMA and/or attack the nanoparticles resulting in cracking. This illustration is further evidence that the use of a co-solvent adversely affects the objective of producing small nanoparticles and can lead to fused particles that offer no value to membrane integrity monitoring.

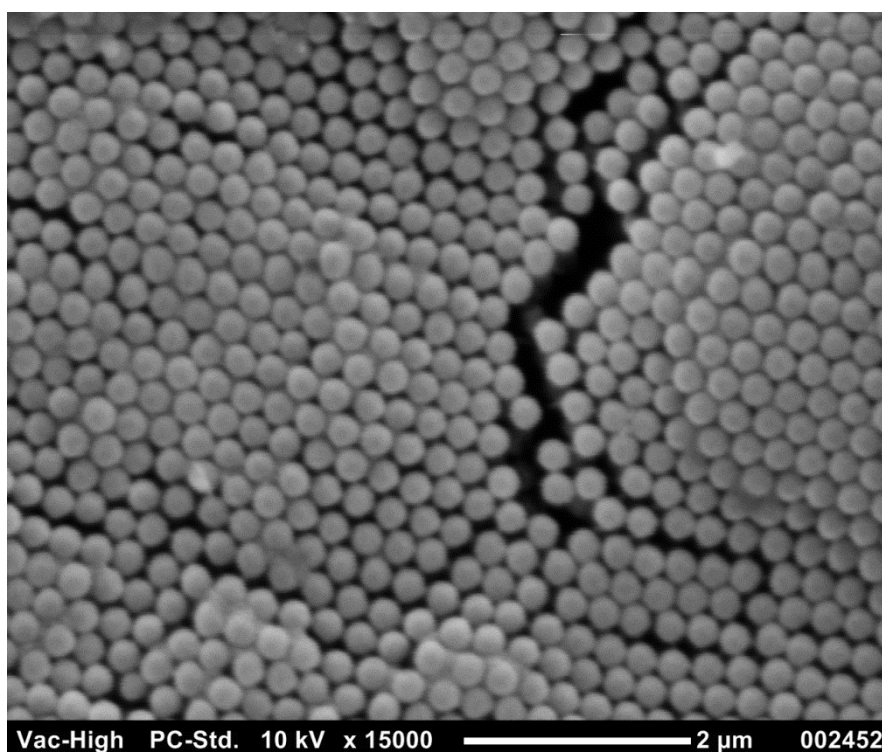


Figure 5.24: SEM image of PMMA formed using 10% acetone using 6wt% MMA, 1.5 vol% APS, 1,200 rpm at 70°C.

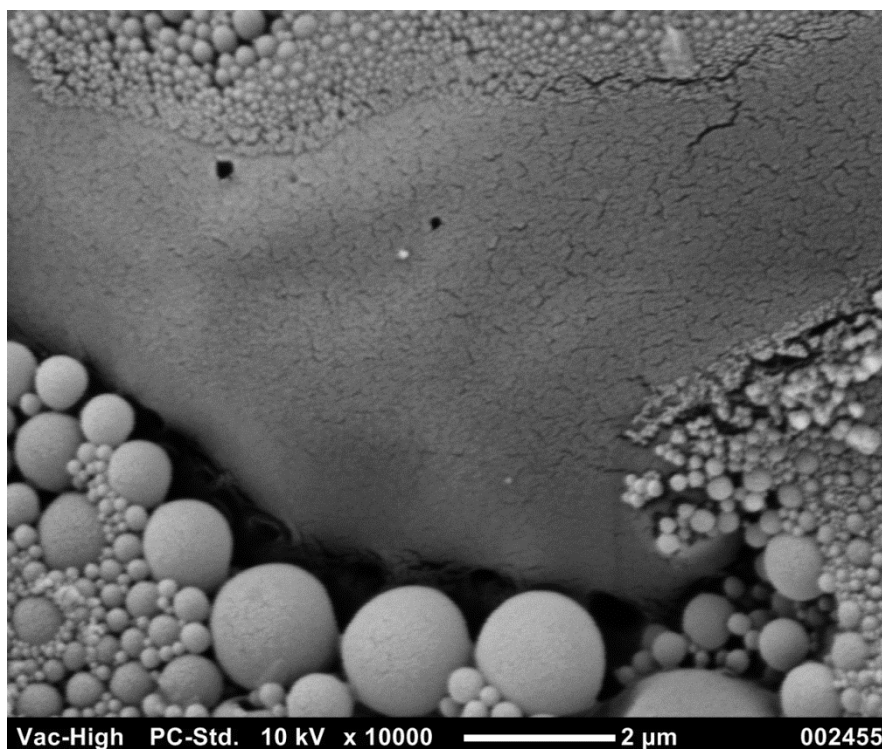


Figure 5.25: SEM image of PMMA formed using 40% acetone using 6wt% MMA, 1.5 vol% APS, 1,200 rpm at 70°C.

Figure 5.26 shows the charge on the PMMA particle surface with increasing acetone concentration. This plot shows that the charge is relatively constant in a negative range between -30 and -40 mV suggesting the presence of acetone co-solvent has little effect on the surface characteristics of the PMMA nanoparticles. This suggests that the cracking of the PMMA particles in acetone (Figure 5.25) is a physical rather than a chemical change in the material. The further use of a co-solvent to synthesis PMMA nanoparticles was no longer warranted and the method developed specifically excludes acetone as an ingredient.

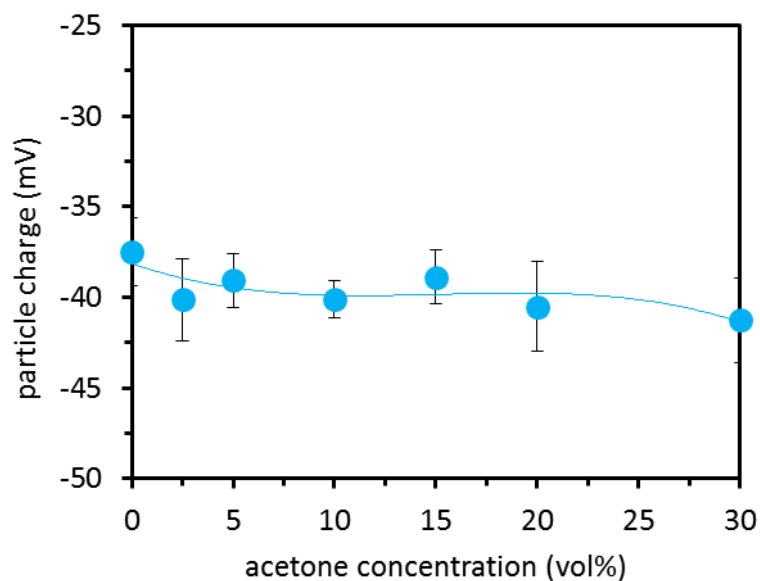


Figure 5.26: Effect of acetone concentration on particle charge.

5.5.9 Effect of Nitrogen Purge

The synthesis of PMMA nanoparticles is typically performed under nitrogen atmosphere to prevent oxidation of the particles during their formation. However, this would add considerable expense to the production of PMMA particularly if produced at a much larger scale. Figure 5.27 shows the FTIR spectra of samples produced under identical conditions with one sample polymerised under nitrogen and the other polymerised without nitrogen. The spectra are typical of PMMA with characteristic peaks observed at $1,730\text{ cm}^{-1}$ due to the carbonyl stretching vibrations of the C=O ester groups in PMMA (Feng and Li 2006; Liu *et al.* 2008; Wang *et al.* 2010), aliphatic C–H stretch at $2,950\text{ cm}^{-1}$ (Liu *et al.* 2008), $1,388\text{--}1,443$ due to methyl bending vibrations (Wang *et al.* 2010) and $1,149\text{ cm}^{-1}$ due to stretching vibrations of C–O–C (Wang *et al.* 2010).

It is evident that there are no significant differences in the spectra suggesting that the absence of a nitrogen atmosphere during the reaction had no adverse effects

on the resulting PMMA structure. The carbonyl peak at $1,730\text{ cm}^{-1}$ in particular has not increased or shifted in the sample where nitrogen was not used, suggesting that no additional oxidation has occurred. This observation is important for the synthesis as it suggests that the nitrogen purge can be omitted from the reaction thus reducing the overall production costs without any adverse impact on the synthesis of PMMA nanoparticles.

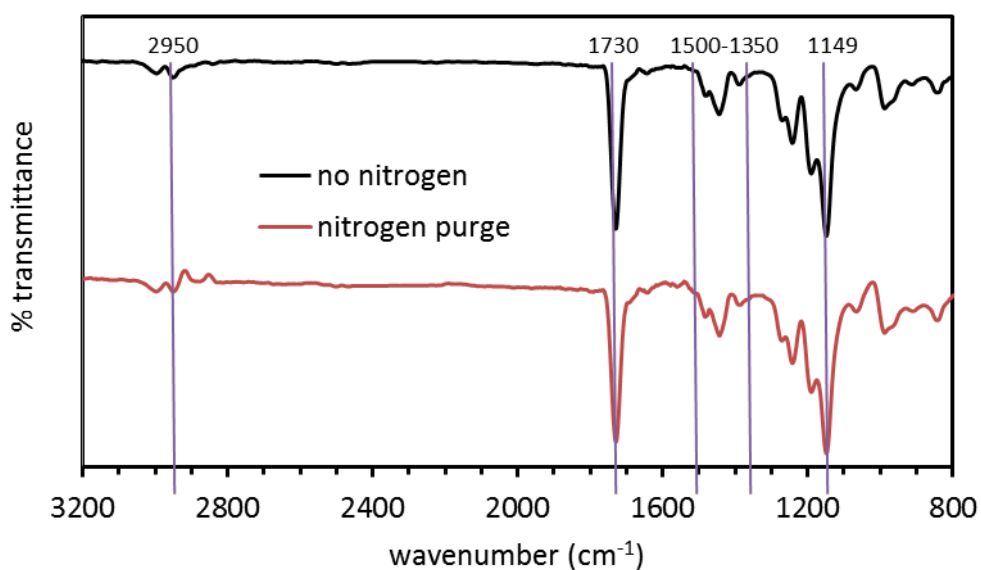


Figure 5.27: FTIR spectra of samples formed with and without nitrogen.

5.5.10 Addition of Fluorescent Dyes

In order to use nanoparticles as surrogates to quantify membrane integrity, highly detectable particles are required at low concentrations by methods such as fluorescence. Samples were therefore prepared by polymerization of MMA in the presence of the fluorescent dyes Quinine and RWT. Figure 5.28 shows the SEM image of a sample polymerised in the presence of Quinine and it is evident that in some places the particles appear to be fused or bonded together. The surface

is also displaying classic distortion due to charging as a result of poor conductivity of the PMMA material (iitkgp.vlab.co.in 2013).

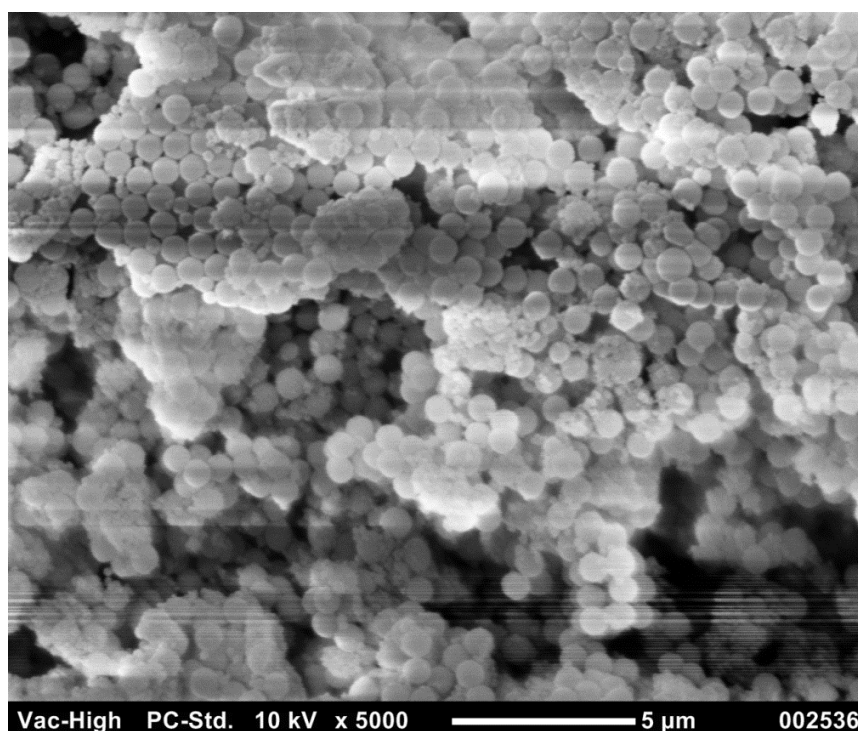


Figure 5.28: SEM image of PMMA polymerised with Quinine using 3wt% MMA, 1.5 vol% APS, 1,200 rpm at 70°C.

In contrast, Figure 5.29 shows an SEM image of a sample of PMMA polymerised in the presence of Quinine in earlier experiments using azobis initiator and a higher monomer concentration. In this case, the spheres have a rough appearance with a seemingly smaller spheres incorporated into a larger bulk sphere. This may represent a uniform distribution of quinine in the structure with particles that are fairly uniform in size and shape.

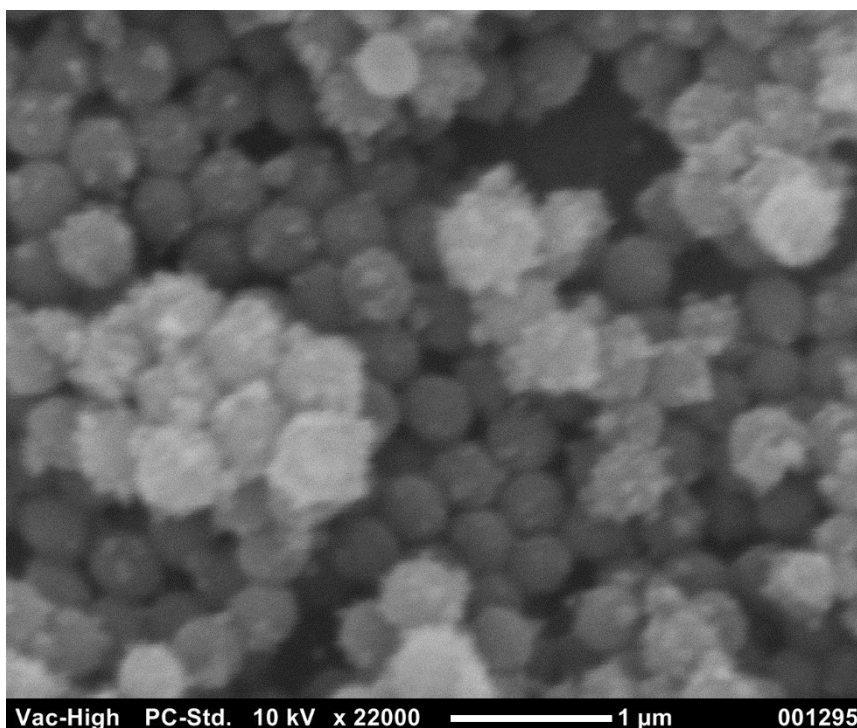


Figure 5.29: SEM image of PMMA successfully polymerised with Quinine using 6wt% MMA, 3 vol% azobis, 1,200 rpm at 70°C.

Figure 5.30 shows the SEM image of PMMA synthesised in the presence of RWT that shows a range of diameters between 100 and 650 nm. Further experiments in the presence of fluorescent compounds were unsuccessful and attempts to repeat the co-polymerization with Quinine (Figure 5.29) were ineffective. The resulting fluorescence of the particles was diminished as shown in Figure 5.31. The data shows that at an equivalent concentration in solution, the fluorescence of Quinine is more than 3.3 times that of the Quinine/PMMA spheres. This is consistent with the results shown earlier in Chapter 4 where the fluorescence of UR is significantly higher than that of the UR coated PS spheres.

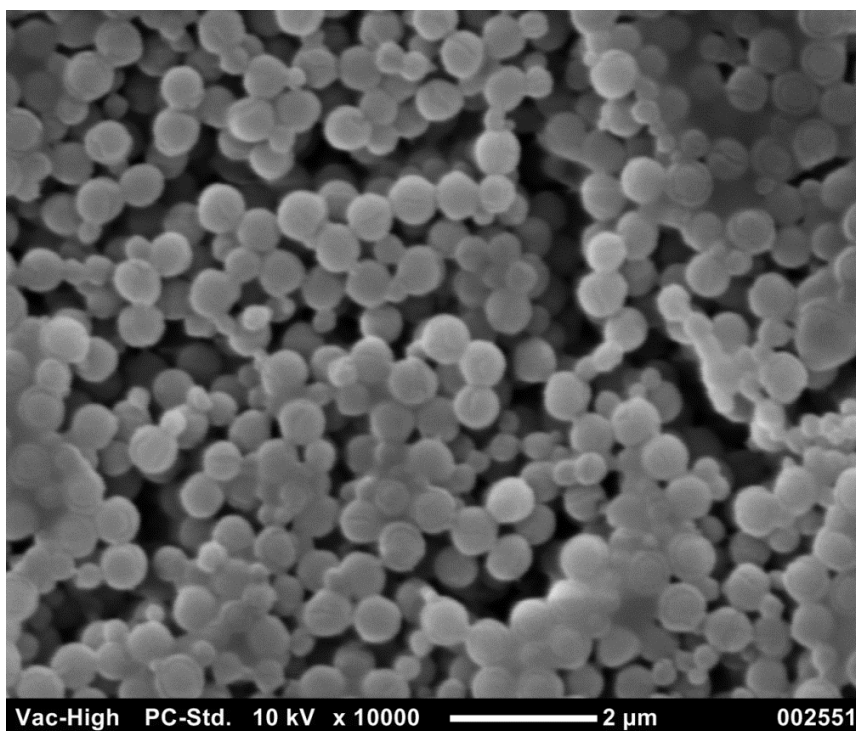


Figure 5.30: SEM image of PMMA polymerised with RWT using 3wt% MMA, 1.5 vol% APS, 1,200 rpm at 70°C.

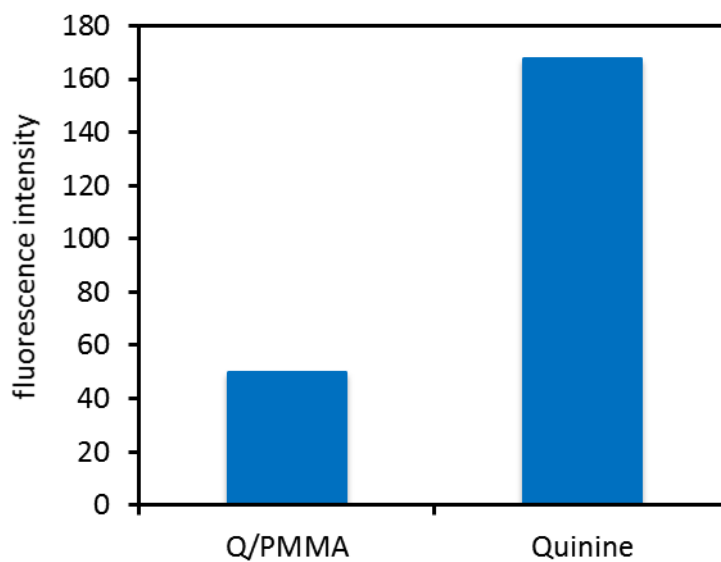


Figure 5.31: Fluorescence of Quinine and Quinine/PMMA copolymer.

5.5.11 Light scattering of PMMA

The primary particle sizing of the nanoparticles was conducted by dynamic light scattering using a Zetasizer. In some cases, the Zetasizer reported sample fluorescence in relation to the data quality. In response to the apparent fluorescence, some of the PMMA nanoparticles were prepared for fluorescence measurements to determine whether the samples were naturally fluorescent. Emission excitation matrix (EEM) data (Andersen and Bro 2003; Bahram *et al.* 2006) were obtained and prepared as contour plots and Figure 5.32 shows an EEM plot of one PMMA sample. This data shows clearly that there is evidence of Raman and Rayleigh scattering (Zepp *et al.* 2004; Ben *et al.* 2011) but no true fluorescence. However, it may be possible to use the observed scattering quantitatively (Lindner *et al.* 2001; He *et al.* 2003b) and this will be further discussed in the next chapter.

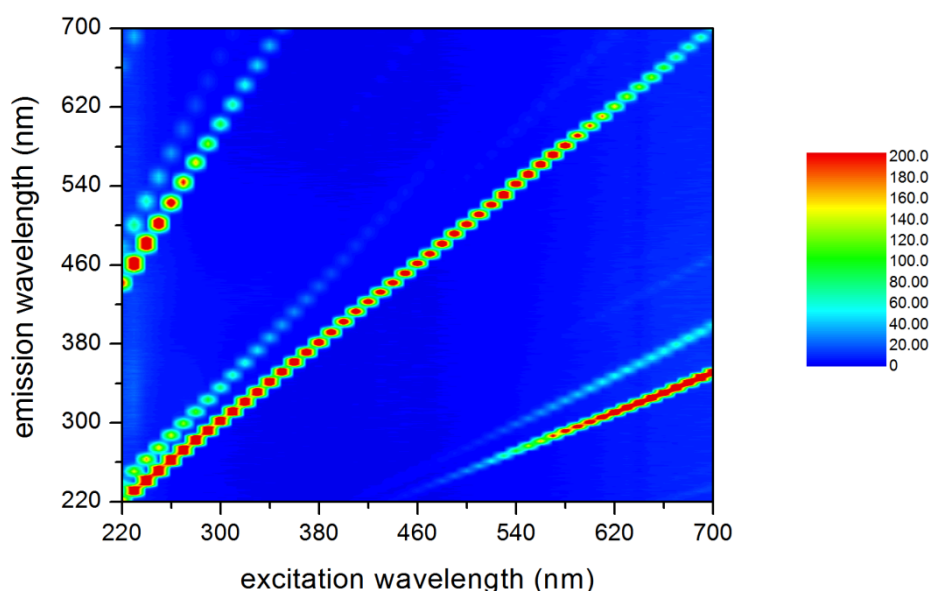


Figure 5.32: EEM contour plot of 27 nm PMMA sample.

Figure 5.33 shows the EEM contour plot of a PMMA sample produced in the presence of surfactant. This sample also shows the various scattering lines but also a strong independent fluorescence in the excitation and emission regions 220-240 nm and 330-390 nm respectively. This fluorescence may be due to the presence of surfactant residual with some organic surfactants known to fluoresce quite significantly (Gholivand *et al.* 2008).

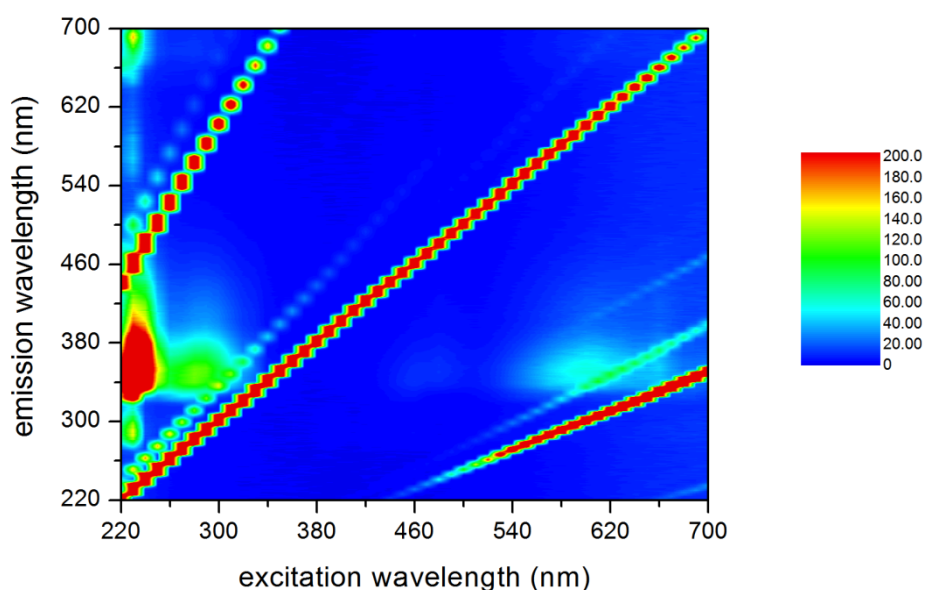


Figure 5.33: EEM contour plot of 16 nm PMMA sample with surfactant.

Monitoring the fluorescence by EEMs may offer a useful monitoring tool by detecting the presence of organic compounds (Henderson *et al.* 2009; Singh *et al.* 2009; Singh *et al.* 2012; Pype *et al.* 2013). Rather than monitoring membrane integrity at frequent intervals across the production cycle, the fluorescence of organic material could be used as an indicator of compromised membrane integrity and therefore be used as a trigger to initiate a membrane integrity test. This feature is explored in more detail in the next chapter.

5.6 Conclusions

Poly(methyl methacrylate) nanospheres of a wide range of sizes were synthesised using a free radical emulsion polymerization process. The synthesis was successful in more than 95% of attempts as evidenced by the formation of stable nanoparticle suspensions. The particle diameter was influenced by a range of different factors including reaction time, temperature, monomer concentration, additives and mixing intensity.

The preparation of uniform sized particles was made possible by improving the monomer/water emulsion with more consistent stirring and smaller flasks. Some nanoparticles prepared in the presence of surfactant were <100 nm and with increasing surfactant concentration, PMMA particle diameter less than 20 nm was obtained. Small particles in this order of magnitude are ideal for use as non-microbial surrogates for membrane integrity testing. Based on these results, it seems possible to tailor the size of a required particle by adjusting the surfactant concentration combined with the modifications developed during the production of PMMA.

The addition of acetone as an additive or co-solvent was not successful in that low acetone concentrations did not reduce the particle size. Furthermore, at high concentrations that may be required to obtain <100 nm particles, cracks and pores on the surface of the spheres as well as polydisperse particles and fusion of particles to form an ill-defined amalgam were found in the SEM images. The use of acetone as a co-solvent should, therefore, be avoided where particle sizes of less than 100 nm are required.

Structural analysis of two identical samples prepared in the presence and absence of nitrogen purge showed that there was no effect on the functional groups of PMMA when nitrogen was not used. Although a nitrogen or argon purge is widely used in the literature, it may not be necessary and would indeed reduce the cost of production of large PMMA quantities.

The presence of residual surfactant, which is also a foaming agent, is not ideal as it may adversely affect the attachment of fluorescent tags and it also may fluoresce and cause interference. In this regard, a washing process for the nanoparticles could be used to clean the particles and remove this residue. However, separating the particles using a centrifuge was not successful, except where relatively large particles were synthesised. The very small particles would not settle, even at high rotation speed. Membrane separation may provide an alternative to clean and concentrate the nanoparticles if required to prepare for the attachment of fluorescent tags. Attempts to attach fluorescent tags to the PMMA nanoparticles failed as the particle size increased to similar proportions to the commercially available PR microspheres evaluated in Chapter 4.

Conducting a variety of experiments to optimise the production of PMMA and consistently produce 30 nm nanoparticles that are the same size as the target virus and even smaller particles was reliably achieved. As stated previously, particle size synthesis was sensitive to a number of fabrication conditions and adjustments were required to establish reliable nanoparticle production. The methods described in the literature (see Table 5.1) did not produce PMMA with the desired particle size and the modifications to the synthesis of PMMA provided

by this work can be used to consistently produce a reliable non-microbial surrogate.

Finally, the PMMA nanospheres were observed to have some interesting optical properties, although light scattering was responsible for most of the observed fluorescence reported by the Zetasizer. The potential to use this light scattering is further explored in the next chapter as it suggests that the particles may be detectable and quantifiable without adding fluorescent dyes thereby greatly simplifying the production process.

Chapter 6

Rayleigh Scattering as a Membrane Integrity

Monitoring Tool

We all *know* what light is; but it is not easy to *tell* what it is.

Samuel Johnson, from Vol. 3 of Boswell's Life (Loudon 1983)

6.1 Preamble

During the development and refinement of PMMA nanoparticle synthesis it became evident that light scattering was recorded in the fluorescence EEMs obtained during routine analysis. The Rayleigh light scattering phenomenon was sensitive to low concentrations of nanoparticles and this was considered to be a better method of detection compared to fluorescence. The ability to consistently produce PMMA nanoparticles the same size or smaller than the target virus coupled with the potential to quantify nanoparticles via light scattering made the quest to further develop a more sensitive fluorescently tagged PMMA nanoparticle, and the associated production costs, less relevant to this research.

Consequently, the light scattering effect was examined further to determine whether the untagged PMMA nanoparticle could be quantitatively detected and used to enumerate the LRV of a membrane system. The move use light scattering to detect nanoparticle surrogates to quantify membrane integrity is a novel approach as previous research has focused on the use of fluorescence to detect surrogates. Light scattering of surrogates is an altogether new phenomenon in membrane integrity research.

6.2 Introduction

The aim of this research was to identify a suitable non-microbial virus surrogate and develop a protocol to test for the surrogate in permeate samples as part of a challenge test, and to establish this as a real-time, online technique. For a successful challenge test, it is critical to employ a sensitive, accurate monitoring process and fluorescence was established early on as one such technique.

Initial experiments using fluorescent dyes were able to show that these have very high resolution limits at low concentrations and high LRVs were demonstrated. However, there were some limitations with the use of these chemical compounds such as size and stability under varying environmental and chemical conditions. Fluorescent nanoparticles were considered a better representation of virus particles than soluble dyes because they were similar in size, but they unfortunately lacked the sensitivity of the fluorescent dyes.

In both cases the cost to use the dyes and fluorescently tagged nanoparticles resulted in them being prohibitive for full-scale testing with perhaps one exception, namely the fluorescent tracer dye RWT. It has been shown that RWT can adsorb onto membranes and that has implications on LRV enumeration as this feature may artificially enhance LRV results. RWT is currently used to test the membrane integrity of full scale plants but costs three times more than the criteria established as an objective for this research at \$0.02/kL of treated water (refer to Table 3.1 in Chapter 3). In addition, the size of RWT is not a suitable analogue for virus particles as it is more than twenty times smaller than poliovirus, the target virus adopted for this research.

Attempts to produce fluorescent nanoparticles that were more sensitive than commercially available products to reduce costs commenced with the facile synthesis of PMMA nanospheres that was achieved using basic chemicals and equipment. However, the ability to introduce fluorescence onto very small nanoparticles by surface treatment did not achieve the required detection sensitivity to allow economic use of fluorescent nanoparticle. Further, the light scattering phenomenon used to quantify the PMMA nanoparticles made the work on coating the PMMA with a fluorescent dye less relevant to the direction of this research.

Fortunately, the PMMA nanospheres synthesised during this work demonstrated some remarkable optical properties that are unique to small particles, and was selected for further detailed evaluation. Numerous authors have reported intense light scattering responses with a recent example provided by Tang *et al.* (2015) that ascribed the phenomenon as resonant Rayleigh scattering (RRS). However, the light scattering phenomenon observed in this work has been shown to be the result of elastic Rayleigh scattering rather than RRS. Rayleigh scattering was further investigated in this Chapter as a potential quantitative technique that could be integrated as part of a challenge test to effectively determine membrane integrity in real-time.

The phenomenon of light scattering is reported with an overview of the physics of light that describes Rayleigh scattering (RS). Samuel Johnson was right to pen the words, “**we all know what light is; but it is not easy to tell what it is**” (Loudon 1983).

6.2.1 Light Scattering

Light scattering is the interaction between light (electromagnetic wave) and the atomic structures of the scattering object (quantum physics), in this case a PMMA particle. There are several known types of light scattering effects including Rayleigh, Raman, Tyndall, Brillouin and Mie light scattering as illustrated below in Figure 6.1.

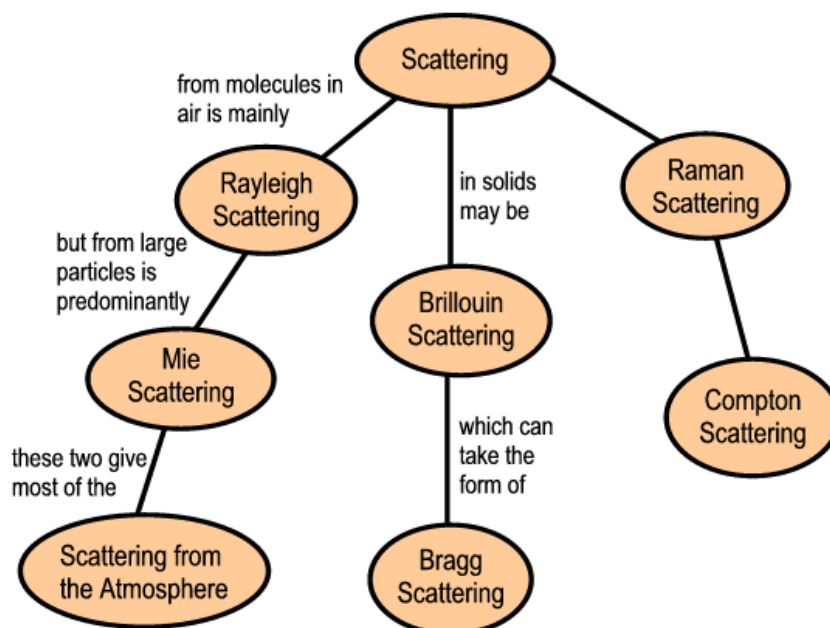


Figure 6.1: Typical light scattering phenomena from (Nave 2016).

Light scattered by molecules in the atmosphere and by extension very small particles in gaseous and aqueous solutions where the scattered light wavelength remains the same as the incident light wavelength is termed as elastic scattering, and is recognised as Rayleigh scattering. Rayleigh scattering is a function of the particle size that the incident light encounters.

Particles with a dimension that are one-tenth the wavelength of the incident light source are responsible for the phenomenon of Rayleigh scattering (Nave 2016). The intensity of the scattered light is directly proportional to the inverse of the fourth power as represented in Figure 6.2. Rayleigh scattering is considered to be elastic as the scattered light energy and the incident light energy have not changed. Scattering where the scattered light energy has either a higher or lower energy is called Raman scattering.

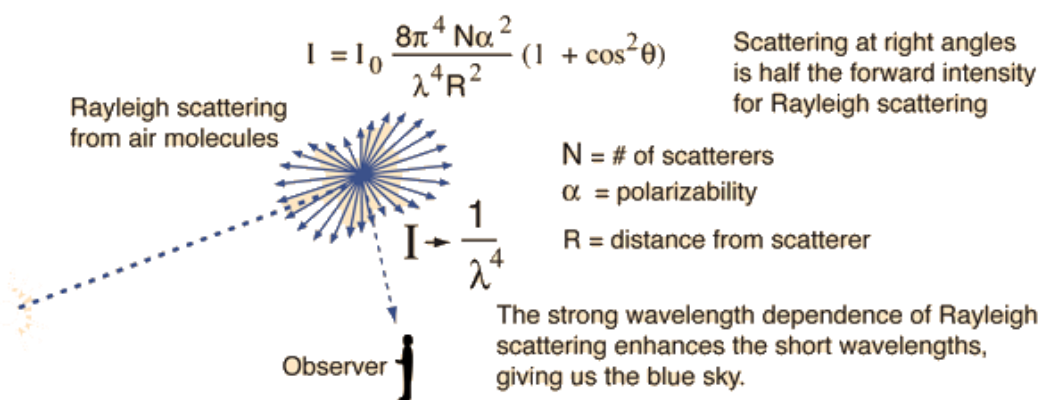


Figure 6.2: Rayleigh scattering phenomenon from (Nave 2016).

Mie scattering defines the scattering effect for particles that are around one third of the incident light wavelength or larger. Mie scattering is not strongly wavelength dependent and Mie scattering intensity for large particles is proportional to the square of the particle diameter. Mie scattering occurs when light interacts with a particle with a diameter of similar size to the incident wavelength such as water droplets, aerosols, or other particles in the atmosphere. In that case, there is no relationship between scattering strength and wavelength, which is why clouds look white and the sky also seems whitish when polluted. Figure 6.3 shows a

comparison between Mie and Rayleigh scattering as a function of particle size (Nave 2016).

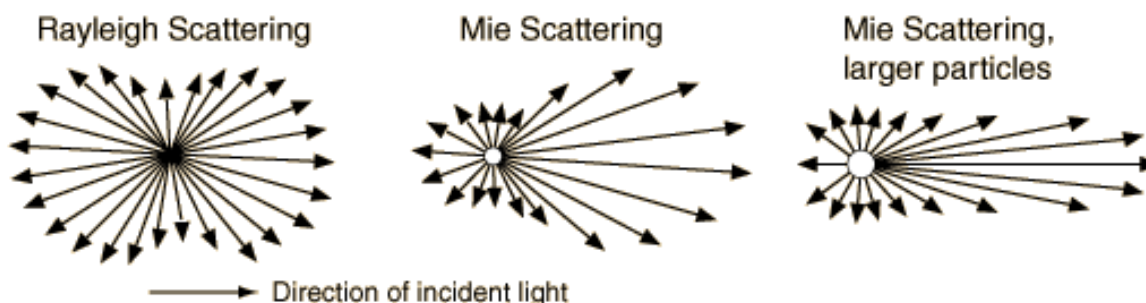


Figure 6.3: A comparison between Rayleigh and Mie scattering from (Nave 2016).

Practical examples of Mie scattering include the production of the white glare around the sun when a lot of particulate material is present in the air and the white light from mist and fog. Light scattering is a complex field of science and this work will only focus on Rayleigh scattering and describe the implications of particle size as it relates to the synthesised PMMA nanoparticles.

6.2.2 Rayleigh Scattering

As a glass substitute, PMMA has some interesting optical properties and latex solutions of PMMA nanoparticles have the ability to scatter light. When light penetrates gaseous and liquid materials that contain molecules and/or nanoparticles it scatters according to the phenomenon first reported by Lord Rayleigh during the nineteenth century (Strutt 1871). The size of the particles has a very strong effect on the scattered light intensity, and light scatters in all directions and is expressed by equation 6.1.

$$I_0 \propto d^3 \tag{6.1}$$

Where,

I_0 is the RS light intensity and d is the diameter of the particle in suspension.

Lord Rayleigh also determined that the intensity of scattered light is inversely proportional to the fourth power of the wavelength of light as expressed by equation 6.2:

$$I_0 = \frac{1}{\lambda^4} \quad 6.2$$

Where,

I_0 is the RS light intensity and λ is the wavelength of the incident light.

This equation illustrates that the shorter wavelengths of violet and blue in visible white light have a stronger potential to scatter than the longer wavelengths toward the red end of the visible spectrum. This type of scattering is, therefore, responsible for the blue colour of the sky during the day and the red, orange and yellow colours during sunrise and sunset.

6.2.3 Blue Light Scattering

The application of RS in the broader context of what is experienced every day can place the objective of this research into context, that is, RS is a measurable phenomenon. The visible light spectrum includes a number of components and each component has its own wavelength and corresponding energy. Figure 6.4 illustrates the visible light spectrum and the component light frequencies that represent the colours violet, blue, green, yellow, orange and red. Their respective wavelengths range from around 400 nm to 700 nm, so blue light with the shortest wavelength has greater energy than red light with a longer wavelength. As a

result, the sky looks blue to the observer because blue light is scattered far more than red light as it has more energy than red light. The human eye cannot see violet light, so its scattering cannot be seen even though it has a shorter wavelength and would scatter more than blue light.

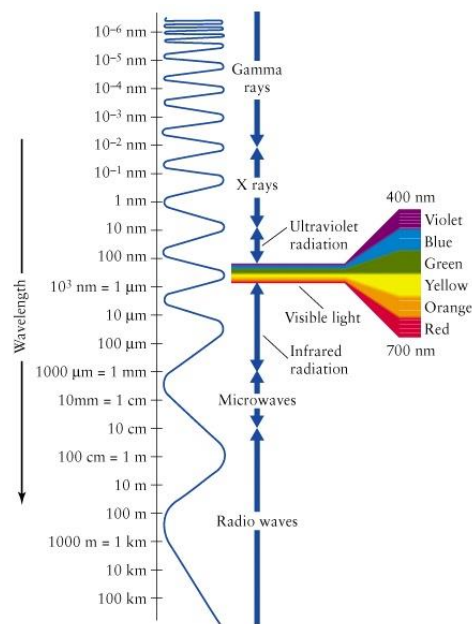


**Figure 6.4: Visible light spectrum wavelengths
from (Freedman *et al.* 2014)**

Light travels further through the atmosphere at dawn and dusk and an observer can see red, orange and yellow light because they have a longer wavelength that scatters less than blue light. Red light has a frequency of around 700 nm whereas blue light has a frequency of 400 nm. Therefore, blue light scatters with an intensity around 9.4 times more than red light.

6.2.4 Resonant Rayleigh Scattering, or is it?

A number of researchers have ascribed RRS as the phenomenon used to establish the concentration of a variety of molecular and particulate materials. As

an analytical method, light scattering reported as RRS is a relatively new technique that has been used to determine trace amounts of various chemicals including vitamins (Liu *et al.* 2006; Wang *et al.* 2007; Ma *et al.* 2009b), metals (Long *et al.* 2004), dyes (He *et al.* 2005; Peng *et al.* 2010), polysaccharides (Zhou *et al.* 2011), enzymes (Cai *et al.* 2011a; Cai *et al.* 2011b), polymers (Liang *et al.* 2011), explosives (Tu *et al.* 2008), and various pharmaceuticals (Luo *et al.* 2001; Liu *et al.* 2007; Ma *et al.* 2009a; Cui *et al.* 2011; Dong *et al.* 2012; Song *et al.* 2012). In most cases a particle or chemical agent is observed in the presence of another agent that when combined with the former either increased or decreased the RRS intensity. The light scattering phenomenon ascribed as RRS is generally linear with concentration with relatively low detection limits reported, typically ng/L or pg/L. The key issue is whether the light scattering phenomenon attributed as RRS correctly defines the scattering phenomenon observed in this research.

In addition to the phenomenon attributed as RRS, two concurrent scattering phenomena are often observed at double and half of the incident light wavelength, and researchers have attributed these secondary spectral lines as frequency doubling scattering (FDS) and second order scattering (SOS). The FDS and SOS spectral lines are real and can be explained by quantum physics, however, whether they are a function of the oscillation electrons in the molecule or nanoparticle, or whether they are a function of the interaction of the monochromator grating and the incident light is explored in the Methods section of this Chapter.

Researchers have used the combination of RRS with the secondary spectral FDS and SOS lines to develop new analytical techniques for a wide range of

applications. Three distinct scattering spectra and three less intense scattering spectra are clearly observed in the EEM contour plot of a dilute PMMA sample of ca. 70 nm particles presented in Figure 6.5. The three less intense scattering lines are the result of Raman scattering while the other three more intense lines are the subject of further examination as stated previously.

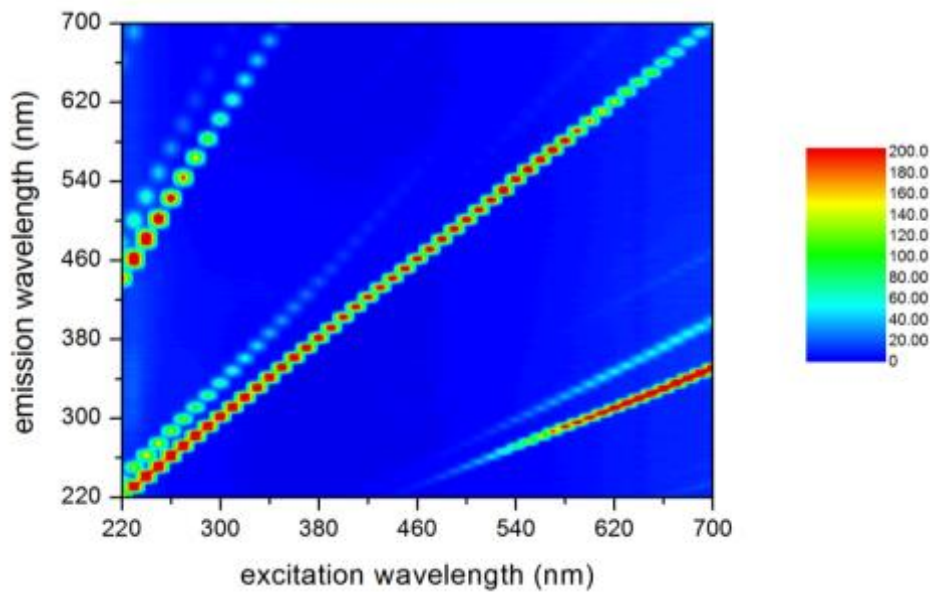


Figure 6.5: EEM contour plot of dilute PMMA sample.

Coupled with standard EEMs that can be used qualitatively to demonstrate membrane integrity (Singh *et al.* 2009; Murphy *et al.* 2011; Singh *et al.* 2012), a technique based on light scattering and EEMs can potentially provide both qualitative and quantitative data. Moreover, a challenge test using light scattering has the potential for development into an online, real-time high pressure integrity monitoring system that can truly demonstrate the capabilities of NF and RO membranes for virus rejection.

Sene *et al.* (2009) reported using the secondary spectral lines resulting from light scattering to quantitatively measure nanoparticles in solution. These authors demonstrated a quantitative nephelometric technique to measure 17 nm fullerene particles in water with reference to light scattering in general terms rather than specific reference to RRS. The authors developed a technique that used optical absorbance in the UV-vis range to quantify the particles of fullerene in solution by direct absorbance. In addition, the authors used nephelometry to detect nanoparticles in solution and referred to light scattering but focused on the second order spectral lines rather than the first order spectral line produced by Rayleigh scattering.

Sene *et al.* (2009) claim that with this technique, it is possible to quantify fullerene nanoparticles using a standard spectrofluorometer without optical filters. Moreover, the applied method used the secondary spectral lines was able to provide a minimum detection limit of 17 ppb, and they also suggest that the method is more than 20 times more sensitive than standard optical absorption. Although the work of Sene *et al.* (2009) was primarily focused on absorbance followed by light scattering using the second order spectral lines, the authors also recognised the value of light scattering and the implication for measuring nanoparticles directly using the RS phenomenon.

The interaction of light with nanoparticles is still a relatively new concept (Nobbmann and Morfesis 2009; Brar and Verma 2011; Zhu *et al.* 2011; Becker 2012) and there are several light scattering theories based on the ratio of the size of the particle relative to the wavelength of the incident light, λ . As reported previously, Mie scattering relates to particles that are relatively large with a

diameter $\geq \lambda/3$, whereas RS dominates for much smaller particles with a diameter $\leq \lambda/10$. The interaction of the PMMA nanoparticles used as a non-microbial surrogate for target virus at around 30 nm with incident light at greater than 400 nm conveniently meets the criteria for RS.

The results of this study illustrate an excitation and emission wavelength that are equal, not diminished or amplified, as would otherwise be the case if the phenomenon were RRS. It is not evident that the phenomenon reported in literature was actually RRS or that the secondary spectral lines were the interaction of light energy with the electrons of the material illuminated or just an artefact of the grating and the wavelength.

Luin *et al.* (2004) discriminates between RS and RRS by referring to the energy levels between the two phenomena. Rayleigh scattering is the elastic scattering of light where the energy and therefore the wavelength remains unchanged by the scattering process with no loss of energy is experienced as defined by the energy/wavelength relationship defined by equation 6.3:

$$\mathbf{E (eV)} = \frac{h.c}{\lambda} = \frac{1.24}{\lambda} \quad 6.3$$

Where,

E is the energy (eV), h is Planck's constant (6.626×10^{34} Joule.s), and c is the speed of light (2.998×10^8 m/s).

The RRS response depends on the excitation of the atomic structure of molecules or nanoparticles, where the incident light energy (wavelength) can excite vibrational modes in the structure of molecules or nanoparticles thereby

producing scattered light with either a diminished or amplified wavelength depending on the wavelength of the additional scattered light emitted by the electron state. The scattered light energy will be reduced, or amplified, by the amount of the vibrational transitional energies in the molecules.

Consequently, a spectral analysis can identify satellite spectral lines below the RS peak at the incident wavelength. It is also possible to observe scattered light at wavelengths lower than the incident light wavelength if there is significant excitation of the vibrational states of the scattering particles as the vibrational energy is added to the incident light wavelength. There is little evidence presented in the available literature to suggest that the scattered light behaves in anything other than elastic scattering as the wavelength of the incident light appeared to be the same as the scattered light. Similarly, there is little evidence reported in the available literature to confirm that the secondary spectral satellite lines are the result of anything other than artefacts of the monochromator interacting with the light source rather than true FDS or SOS resulting from scattering.

6.3 Research Objectives

The objective of this stage of the research was to verify that light scattering was an effective way to quantify synthesised PMMA nanoparticles used as a non-microbial surrogate for polio, target virus. The optical response to synthesised PMMA nanoparticles was explored using light scattering and its potential for use as a highly sensitive integrity test was assessed using Australia's first DPR facility destined for the Davis station in the Antarctic for the Australian Antarctic Division.

Further, this chapter presents information on commercially available instruments that have the potential to form part of an integrated membrane integrity monitoring system. The likely cost implications to apply light scattering and synthesised PMMA nanoparticles to assess membrane integrity performance is presented to compare against the initial cost benchmark of \$0.02/kL of treated water.

6.4 Materials and Methods

Light scattering as a potentially effective way to quantify the presence of the synthesised PMMA nanoparticles used as a non-microbial surrogate for a target virus required suitable medium that could be doped with specifically sized PMMA. Treated wastewater was considered a realistic medium that could be doped with PMMA and then analysed using the Rayleigh scattering phenomenon. The experiments were all developed to determine whether light scattering could be used to quantify nanoparticles in the permeate of high pressure membranes, more specifically through brackish water reverse osmosis membranes.

6.4.1 Synthesis of PMMA

Samples of PMMA were synthesised according to the method previously described in Chapter 5 with a range of sizes from 90 to 300 nm synthesised without the use of surfactant. The concentration of monomer was less than 2 vol% in order to obtain additional nanoparticles smaller than 90 nm. The objective was to synthesize PMMA particles that were of the same order of diameter as the target poliovirus so that they could be enumerated using the light scattering phenomenon. Previously, PMMA nanoparticles were synthesised with a diameter of 30 nm and the modified procedure described in Chapter 5 was used to create

more PMMA nanoparticles at 30 nm using a surfactant to verify that light scattering was a reliable measurement tool.

6.4.2 Wastewater Sampling

Treated wastewater samples were obtained from City West Water's Altona Treatment Plant (ATP, Victoria, Australia), with samples of RO feed, 1st stage and 2nd stage RO permeates used for EEM testing in accordance with the method described in Chapter 5. At the time of sampling, the RO plant had been operating intermittently due to challenges with the ultrafiltration pre-treatment units.

Additional samples were sourced from the Western Treatment Plant in Werribee (WTP, Victoria, Australia) and from the Melton Recycled Water Plant (RWP, Victoria, Australia) as examples of unfiltered and MF Class A treated water respectively. The water samples were all subjected to EEM testing prior to bench-scale filtration through a BW30 membrane using the system described previously (in Chapter 4). The brackish water RO membrane was operated at a recovery of 40% and a sample of permeate was spiked with a low concentration of 30 nm PMMA prior to a challenge test using 1 mg/L PMMA into the feed.

6.4.3 Measurement of Rayleigh Scattering

The RS intensity of PMMA nanoparticles was measured using a Shimadzu RF-501 spectrofluorometer. Samples of varying concentrations were prepared by diluting the stock solution(s). A 1 cm quartz cell containing a 3 mL sample of solution was inserted into the spectrofluorometer. A xenon lamp light source was passed through the sample at a given excitation wavelength and the emitted light was measured by the detector at the same wavelength.

6.4.4 Bench-Scale Challenge Testing

A bench scale test rig was comprised of a Sterlitech CF042 stainless steel cross flow cell with an active membrane surface area of 42 cm². Permeate samples were collected and tested for the presence of the dyes using a Perkin Elmer LS50 spectrofluorometer. Dow Filmtec BW30 membranes were used in all experiments using the system described previously (in Chapter 4).

6.4.5 Pilot-Scale Challenge Testing

A pilot scale 4 inch RO membrane filtration test was used to assess the rejection of 90 nm PMMA nanoparticles for a long-term demonstration of the RS technique. A BW30-4040 element was installed into the pilot rig (shown in Figure 6.6) to determine the PMMA nanoparticle rejection. De-chlorinated tap water, dosed with 1,650 mg/L NaCl and 4.2 mg/L 90 nm PMMA particles was used as feed solution. Filtration through the RO membrane was maintained at a feed velocity of 0.068 m/s and pressure 5.8 bar (single pass recovery ~ 10%). Approximately 120 samples were taken at hourly intervals with the system run semi-continuously for up to 3 months. The rejection of PMMA particles was determined by the RS method.

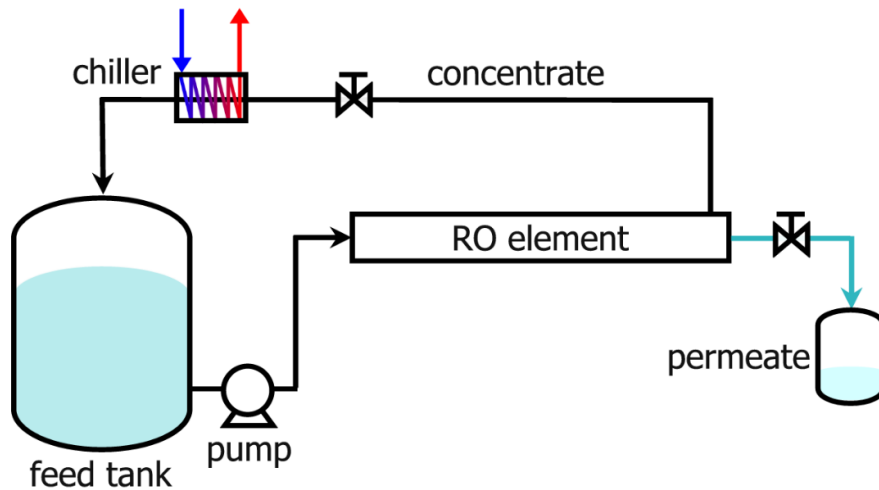


Figure 6.6: Schematic representation of pilot scale test rig.

6.4.6 Full-scale Challenge Testing

Integrating the individual components of the synthesised PMMA nanoparticles as a non-microbial surrogate for the target virus with a means to measure nanoparticles in permeate using light scattering is critical to developing a sensitive membrane integrity challenge test. The Australian Antarctic Division (AAD) commissioned Australia's first DPR treatment plant to be installed at the Davis Station in the Antarctic. Although the AAD DPR plant is small by comparison to international installations, it will nevertheless be used, after a proving period *in situ*, to provide safe drinking water by directly converting treated wastewater for residents of the Davis Station in the Antarctic.

The DPR plant configuration is shown in Figure 6.7 and the plant was supplied with biologically treated water from TasWater's Selfs Point biological nutrient removal plant during the testing and commissioning phase of the project. The Selfs Point plant uses UF membranes as a physical barrier to separate the biomass and the treated water. Membranes provided a more substantial and

reliable barrier against suspended solids and microbiological contaminants than secondary clarification would otherwise provide.

The biologically stabilised water is transferred to the DPR plant where the water is subjected to advanced treatment using ozone, MF, biological activated carbon (BAC) filtration, intermediate storage, cartridge filtration, RO, and two forms of disinfection using UV and chlorination. The treated water from this plant is considered suitable for DPR applications. The RO permeate had a light scattering signature, and it was recorded and subtracted as the background 'noise' from all scattered light intensities that ensured the intensity recorded was due to the nanoparticles without interference from background 'noise'.

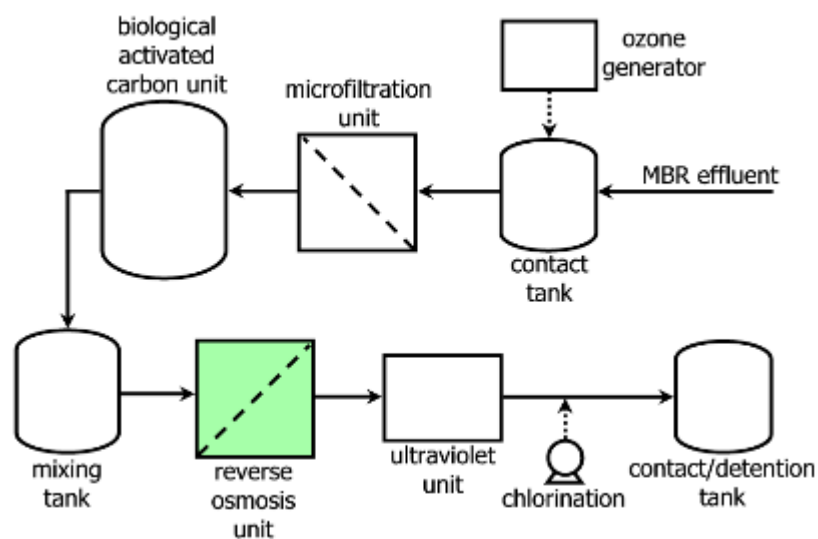


Figure 6.7: Schematic diagram of the AAD pilot plant in Hobart.

Figure 6.8 shows a schematic representation of the RO array that operated at 70% recovery. The system was comprised of 5 x 4" Dow Filmtec brackish water (BW30-4040) RO elements that were housed in separate pressure vessels. Sampling points were located on the feed and permeate side of each element as well as the mixed permeate, mixed concentrate and the BAC effluent that is the

source of the feed water to the RO membrane plant. The mixing tank was supplied with water from the BAC unit at 20 L/min. The water was pumped into the first RO element at 26 L/min with a permeate flow of 14 L/min, 6 L/min was discharged and 6 L/min concentrate recycled to the RO feed tank. Online conductivity was used to monitor permeate and concentrate from each element as well as the combined permeate from all of the RO membrane elements. In this configuration, the concentrate from element (n) is the feed for element (n+1). The fifth and last element was compromised by a scratch in the permeate tube.

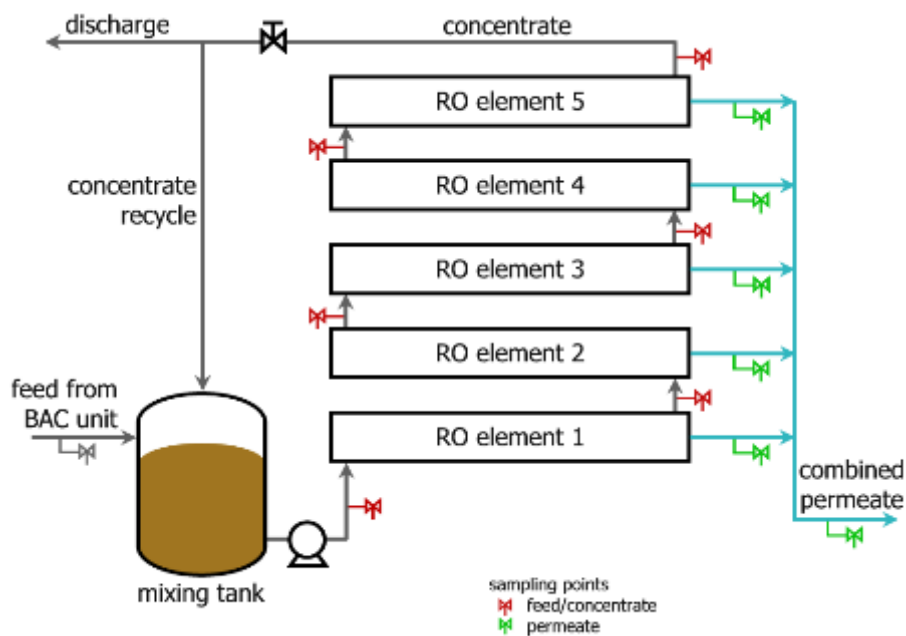


Figure 6.8: Schematic diagram of the RO array.

6.4.7 Challenge Tests

A series of challenge tests using the synthesised 30 nm PMMA nanoparticle surrogate, a mixed fluorescent dye incorporating RWT, UR and PyTS and MS2 bacteriophage were applied to the RO membrane system used as part of the DPR process. The MS2 bacteriophage, a living organism, was used as a

biological surrogate for enteric virus to challenge the rejection capacity of a membrane system. Bacteriophages are virus that infect bacteria that are added to the feed water of membrane systems to provide an indication of the LRV often mandated by regulatory agencies (Victorian Government Department of Health 2013).

These challenge tests provided data that allowed direct comparison between fluorescent dyes, MS2 bacteriophage, electrical conductivity and the RS membrane integrity monitoring technique developed through this research. The MS2 sample was supplied by South Australian Water Corporation and was provided as a frozen sample containing 1×10^{12} PFU/mL. Samples were shipped directly to the TasWater plant and stored frozen until the day of testing. The PMMA was synthesised in accordance with Section 6.4.1 and was stored in sample tubes along with the mixed dye solutions prior to shipping to the plant.

The plant was operated under normal conditions and stabilised until the test commenced. In each case, the challenge species was added to the 500 L mixing tank and the system operated to allow charging of the system before the test samples were taken. The synthesised PMMA nanoparticles were dosed at 2 mg/L, the mixed fluorescent dyes at 1 mg/L each and the MS2 bacteriophage was dosed at 1.5×10^6 PFU/mL. Conductivity was monitored to enable the LRV of the system to be determined concurrently with each challenge test.

A series of three paired permeate and feed sample was collected from each RO element in addition to a sample of mixed permeate and concentrate after 5, 10 and 15 minute intervals. The feed tank was drained and refilled following each test. All of the RO membrane elements were intact for the first series of PMMA

nanoparticle challenge tests. The fifth RO membrane element was damaged by gouging the permeate channel to induce a gross defect that would enable some of the challenge species to enter the permeate line after benchmarking the performance of the intact RO membrane elements. The damaged RO element remained during all subsequent nanoparticle, fluorescent dye and MS2 tests. Testing was conducted over two days in the order of the nanoparticle test, followed by the mixed dye test, and then the MS2 challenge test. The feed tank was emptied and the system flushed between tests. The samples collected during the various challenge tests were checked, packed and shipped back to the laboratory for testing.

6.4.8 Dye Analysis

The mixed dye samples tested by direct UV absorbance measurements for feed and concentrate samples and by fluorescence for the permeate samples using the same Shimadzu instrumentation described previously (see Chapters 3 and 4). For the UV dyes, calibration was performed using the mixed dye solution by scanning a series of standards over the range 900-200 nm. The peak absorbance for each dye was recorded and used to prepare the calibration within the range 0-1 mg/L. Similarly, fluorescence calibration was measured for each dye separately over the range of 0-4 µg/L at the wavelengths shown previously in Table 3.1. In each case, the calibration samples and test samples were tested in triplicate.

6.4.9 PMMA Analysis

The PMMA nanoparticles were enumerated by total organic carbon (TOC) analysis using a Shimadzu TOC-V instrument with ASI-V automatic sampler for

the feed and concentrate and by the RS method for the permeate samples. The TOC analysis was used to verify the concentration of PMMA nanoparticles because the spectrofluorometer did not have adequate detection range to measure RS of high particle concentrations. The detector was saturated by the scattered light intensity and would not have provided meaningful data.

6.4.10 MS2 Bacteriophage Enumeration

The MS2 bacteriophage samples were frozen after collection and transported back to the laboratory for immediate PFU enumeration. The following methods were used to prepare the various media, growth plates and host samples.

- Tryptone water (TW, Oxoid CM0087) was prepared using a 15 g/L ratio with MilliQ water for serial dilutions to enumerate MS2 bacteriophage. The solution was autoclaved at 121°C for 15 minutes. Sample dilutions were obtained by pipetting 9 mL of tryptone water into screw top sample vials into which 1 mL of sample was then pipetted into the first sample vial, making a 1/10 dilution. Then, 1 mL of the 1/10 dilution was added to the next sample vial, making a 1/100 dilution, and so on. Samples were diluted until it was expected that a sample would produce a countable plate for the stock MS2, the feed samples, and the compromised and mixed permeate samples.
- A sample of 1 mL of a previously grown *E. coli* (ATCC 700891) host solution of log growth phase in tryptone soya broth (TSB, OXOID CM0129) was added to 100 mL of freshly autoclaved and cooled TSB (30 g/L) in a sealed 500 mL Schott bottle. The bottle was then incubated in an orbital shaker at 37°C overnight.

- Tryptone agar (TA, Oxoid CM0131) was prepared by adding 40 g/L into RO water. The mixture was autoclaved for 15 minutes at 121°C. The solution was allowed to cool and then poured into 90 mm petri dishes and solidified and stored in the refrigerator until used.
- The soft agar layer was prepared by adding 7 g bacteriological agar (BA, Oxoid LP0011) and 30 g TSB into 1 L of RO water. The mixture was autoclaved for 15 minutes at 121°C and allowed to cool to below 44.5°C before 10% of the host *E. coli* was added.
- The serially diluted samples and the permeate samples were mixed with the soft agar host at a ratio of 1:5 mL and poured onto the previously prepared first agar layer petri dishes. Permeate samples were mixed at a ratio of 10:30 mL and poured across 4 petri dishes. The samples were incubated at 37°C for 16-24 h then removal and the MS2 colonies counted based on areas where the host had been consumed.

6.5 Results and Discussion

Prior to conducting the full-scale challenge tests, a series of bench and pilot scale experiments were performed to validate the RS technique and to further investigate the observed secondary spectral lines.

6.5.1 Secondary Spectral Lines

A dilute PMMA sample of *ca.* 70 nm particles was assessed for fluorescence by preparing EEM plots that show a two-dimensional representation of fluorescence intensity as a function of the fluorescence emission and excitation wavelengths. These EEM contour plots were used to demonstrate whether the spectral lines were the result of the incident light energy interacting with the atomic structure of

the material and, therefore, represent FDS and SOS or whether they were artefacts of the light source interaction with the grating in the monochromator and were secondary satellite spectra.

The sample of PMMA was analysed using the Shimadzu RF501 spectrofluorometer and the results are presented in Figure 6.9 clearly show the RS and the secondary spectral lines. In order to establish whether the secondary spectral lines were the product of the diffraction grating interaction with the incident light Lakowicz (2006) reported that a bandpass excitation filter could be used to remove unwanted wavelengths from the excitation beam. A bandpass excitation filter was inserted into the allocated slot in the spectrofluorometer and the same sample was measured again. Figure 6.10 clearly indicates that the secondary spectral lines were no longer present, and therefore confirmed that these spectral lines were artefacts rather than a phenomenon of light interacting with the atomic structure of the nanoparticles.

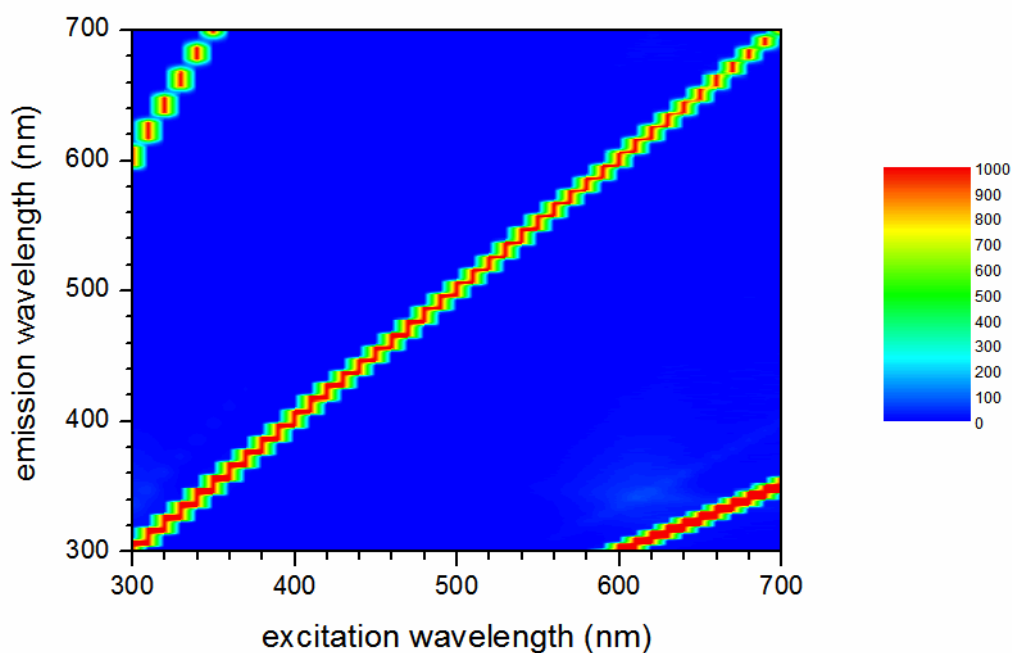


Figure 6.9: EEM matrix without the compensating filter showing the secondary spectral lines FDS and SOS.

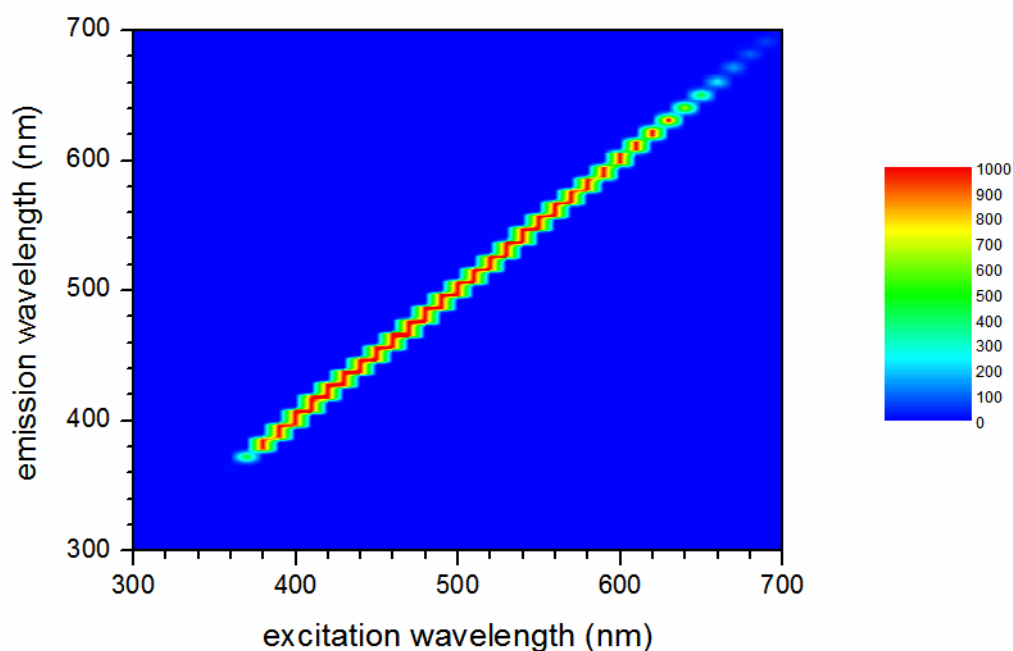


Figure 6.10: EEM matrix with the compensating filter showing only the Rayleigh scattering line.

Confirmation of the artefact spectral lines was conducted after all of the experiments were completed. The data reported in this work is based on the spectrofluorometer output without the benefit of the compensating filter. The secondary spectral lines were exactly half and double the emission data of the Rayleigh scattering spectra, respectively, but were clearly the result of the interaction between the light source and the grating used in the instrument.

Although the secondary spectral lines are artefacts, they represent the emission data of the scattered light at half and twice the wavelength of the excitation light source interacting with the diffraction grating of the monochromator. These light sources are incident on the sample of nanoparticles in the same way that the primary light source irradiated the sample. So the data that was reported still represents scattering but at half and double the wavelength of the incident light

and can be used, but the primary source of performance data is from the Rayleigh scattering data. It is clear that the spectral lines are artefacts but it forms part of the dataset collected and is referred to as part of the Rayleigh light scattering evaluation. While this work refers to the secondary spectral lines in the evaluation of the light scattering phenomenon the primary source of data relating to light scattering shall be the RS spectral line.

6.5.2 Analysis of Class A Water

In Australia, Class A water is the product of a wastewater treatment regime that physically, biologically, and chemically converts raw municipal wastewater into a product that is suitable for reuse in a variety of ways that, in Victoria, exclude direct and indirect consumption by humans. Class A water would certainly require further treatment for use as a direct or indirect substitute for potable water that includes desalination through reverse osmosis membranes as part of an advanced treatment regime that may also include coagulation and UF treatment. The production of Class A water removes most particles, some organics and dissolved materials as well bacterial contaminants but very small particulates, pathogens including some more resistant virus and dissolved salts remain. This is often not suitable for some reuse applications, particularly where salt may be an issue such as in industrial boilers or in some agricultural purposes. In order to determine the suitability of the RS technique to enumerate membrane integrity, samples were obtained from three wastewater treatment plants in Victoria.

City West Water, Altona

Water obtained from the ATP was subjected to fluorescence characterization and Figure 6.11 shows the EEM plot of the RO feed. There are two notable regions

of fluorescence with the lower region in the excitation/emission (Ex/Em) range 250-400nm/320-500nm representing the commonly reported regions of fluorescent dissolved organic matter (fDOM) (Matthews *et al.* 1996; Zepp *et al.* 2004; Peiris *et al.* 2010; Yu *et al.* 2011). The RS and secondary spectral lines are visible in this EEM. Typical EEMs used to identify organic species are usually confined to this region identified in Figure 6.11 and rarely extend beyond 600 nm, so the origin of fluorescence at the higher excitation wavelength is not usually reported. In addition, EEMs are plotted with the excitation wavelength in the y-axis and the emission wavelength in the x-axis. It seems more appropriate to plot the data as shown in this figure, since the emission and excitation wavelengths are the independent and dependent variables, respectively.

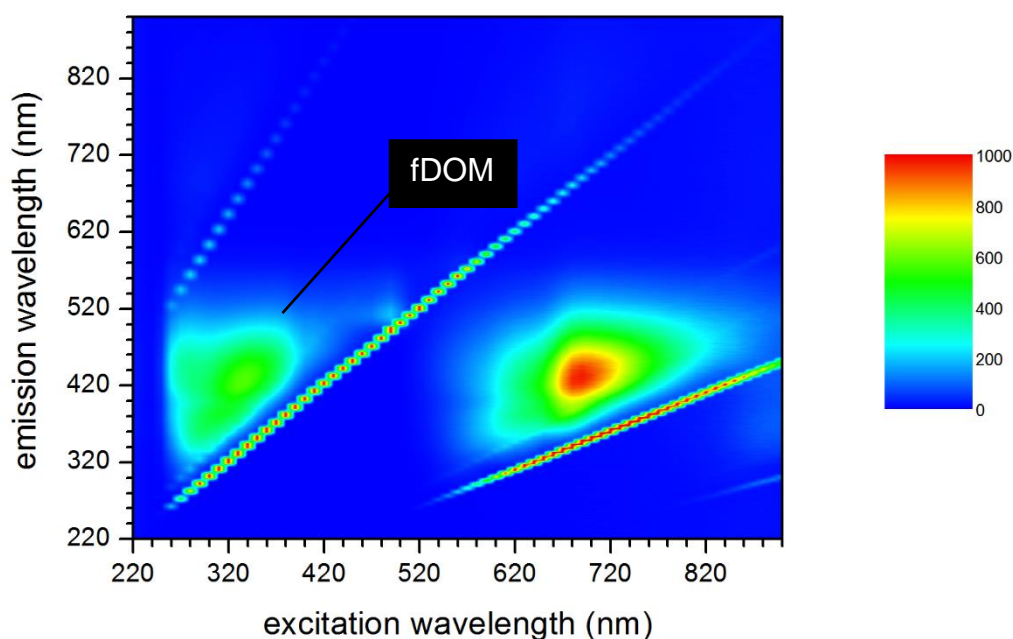


Figure 6.11: EEM plot of ATP RO feed.

Another common attribute of these types of plots is the tendency to remove the scattering lines and there are publications outlining methods to achieve their

removal (Rinnan and Andersen 2005; Larsson *et al.* 2007). It is often claimed that these lines are interferences that do not relate to water quality (Singh *et al.* 2009), but this study shows that it is primarily small particles in the water that are responsible for the observed scattering lines so they are directly related to water quality.

Figure 6.12 shows the EEM plot of the first pass RO permeate which is typically distributed for agricultural uses from this plant. The plot clearly shows that almost complete removal of fDOM is achieved during the first stage with only the scattering lines remaining. Interestingly, the EEM of the second stage RO shown in Figure 6.13 shows a significant increase in all the scattering intensities that may be a response to the presence of contaminants such as microbial growth as a result of the intermittent use of the RO system. This data (Figure 6.13) highlights the presence of some particulate fouling in the permeate by the increased RS intensity. This signature of background particulate material would interfere with the presence of any PMMA nanoparticles added during a membrane integrity challenge test, therefore, it is important to recognise the background noise before a challenge test is performed. The background noise recorded can be subtracted from any scattered light reported to normalize the intensity that was specifically related to the PMMA nanoparticles present in the permeate.

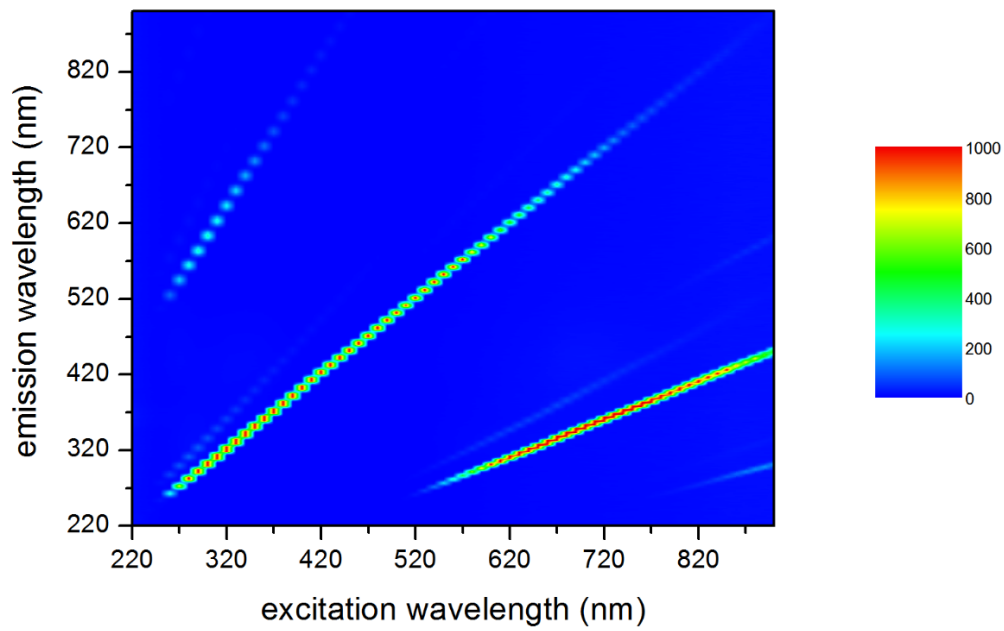


Figure 6.12: EEM plot of ATP 1st stage RO permeate.

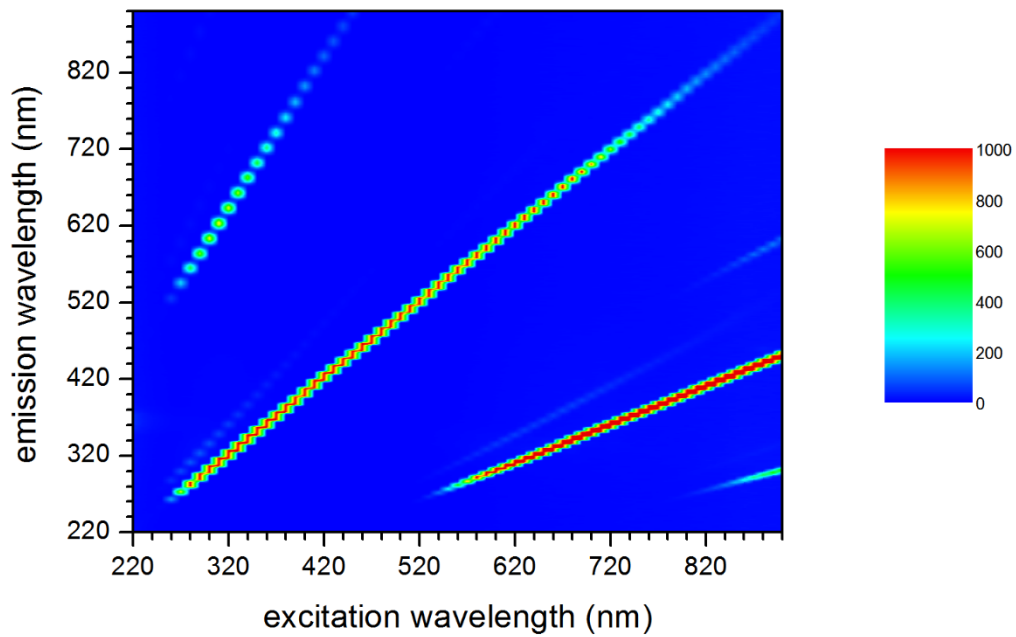


Figure 6.13: EEM plot of ATP 2nd stage RO permeate.

Melbourne Water, Werribee

Samples obtained from Melbourne Water's WTP were subjected to EEM assessment before and after specific treatment regimes in order to observe any changes in the RS and secondary spectral lines. The treatments included various types of coagulation, MF and ozone treatment. Only the raw water and a sample subjected to coagulation treatment were subjected to EEM analysis for the purposes of this study. In the case of the coagulation treatment, samples were dosed with 3 mg/L of polyaluminium chloride as Al^{3+} (Myat *et al.* 2013) and the EEMs recorded before and after treatment.

Figure 6.14 shows an EEM plot of the raw water that clearly demonstrates strong fluorescence in the fDOM region as well as intense RS and some evidence of the secondary spectral lines. In Figure 6.15, the EEM of the same water following coagulation treatment is shown. This figure shows that while the fDOM remained relatively unchanged, a significant reduction in the RS was observed, confirming that the scattering was due to the presence of particles that were removed by the coagulation and separation treatment.

The observed intensity profile of the RS line was greater and more distinct in Figure 6.14 than the line shown in Figure 6.15. The reduction in intensity can be attributed the removal of particulate material from the sample by the coagulation and separation treatment.

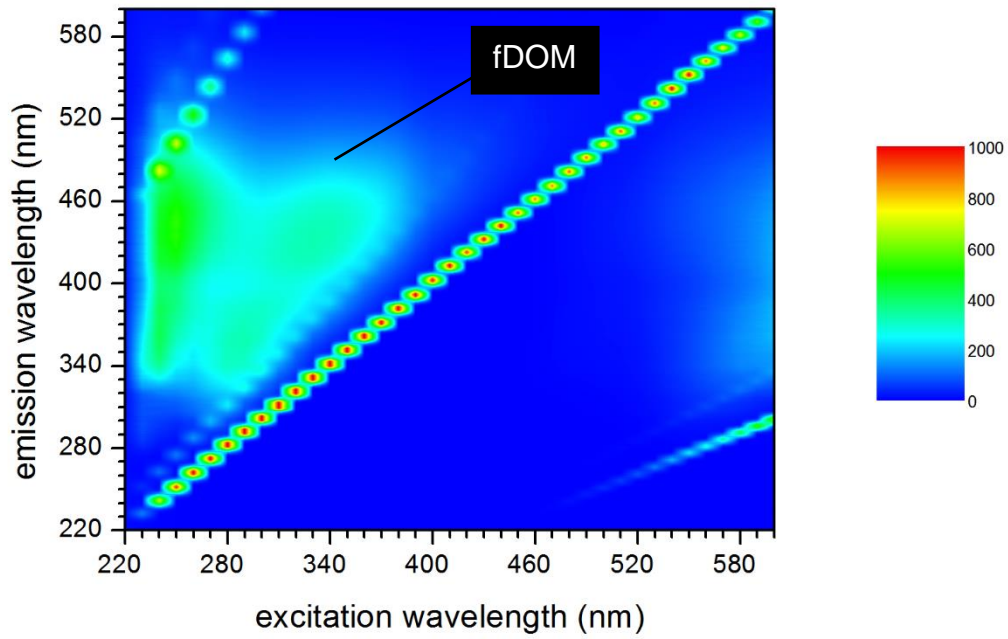


Figure 6.14: EEM of WTP raw water.

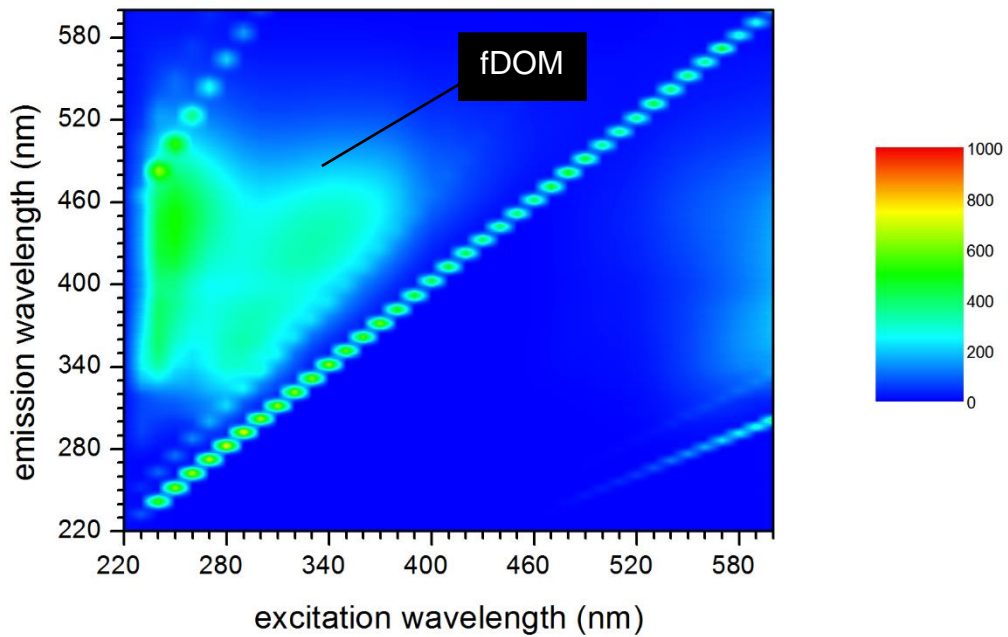


Figure 6.15: EEM of coagulation treated WTP water.

Western Water, Melton

Figure 6.16 shows an EEM contour plot of Class A water obtained from the RWP in Melton. The plot is very similar to that shown in Figure 6.11 with two notable regions of fluorescence with the lower fDOM region shifted to a slightly lower excitation wavelength range of 220-280 nm. The higher fluorescence region covers a very similar wavelength range as shown in Figure 6.11, but the origin may be the result of the interaction of light with the monochromator in a similar manner as the secondary spectral lines. While this fluorescent region was interesting it did not add to the objective of determining whether light scattering could be developed into a useful nanoparticle quantification measure. As such the fluorescence observed at the lower energy levels were not explored further.

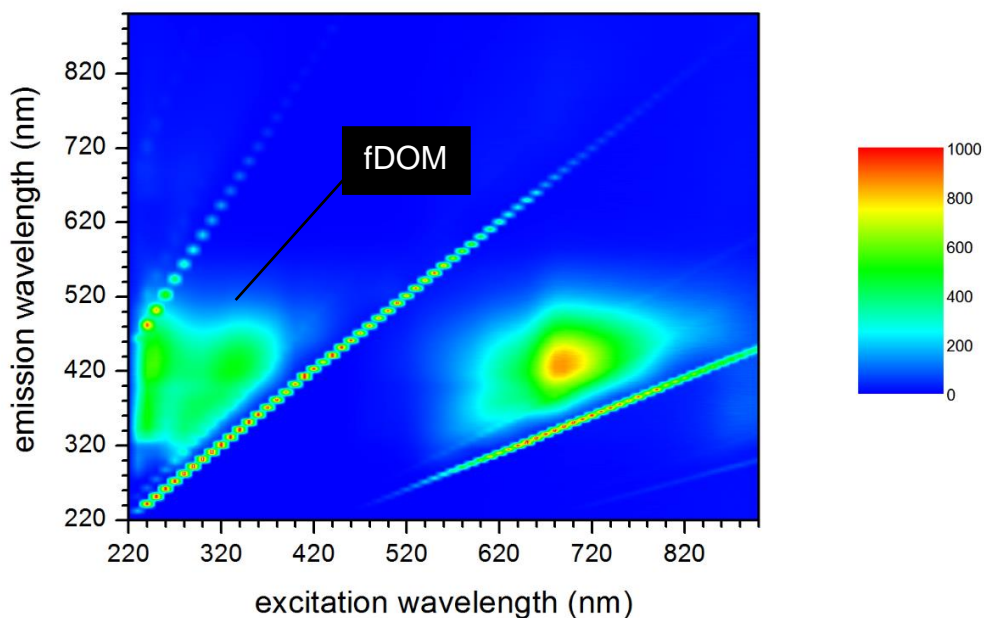


Figure 6.16: EEM plot of Melton's Class A water.

Figure 6.17 shows an EEM plot of the same Class A water produced at the RWP that has been treated by high pressure filtration through a BW30 membrane in a bench-scale setup to 40% permeate recovery. It is clear that the organic components were effectively removed as evidenced by the almost complete reduction in the fDOM region. In addition, a notable reduction in the intensity of the RS and the secondary spectral lines was observed.

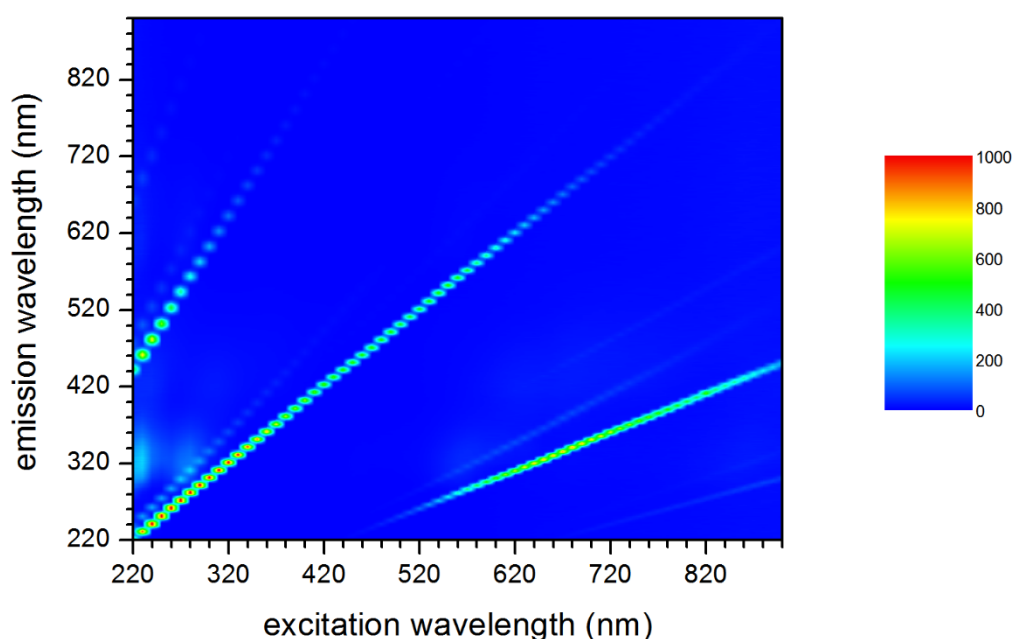


Figure 6.17: EEM plot of RO treated Class A water.

6.5.3 Scattered Light Response

The three wastewater samples used to evaluate light scattering performance in terms of being able to differentiate between the treated and untreated water samples based on the RS intensity. The light scattering technique demonstrated a reduction in RS intensity after the raw water was coagulated and this provided

a qualitative measure of the potential reduction in particulate material between the feed and the subsequent treated sample.

Treated water produced by the ATP exhibited a reduction in scattered light intensity between the feed water to the RO and permeate from the first stage RO. Interestingly, scattered light intensity increased across the second stage membranes where the intensity is higher than that shown for the feed to the second stage. Operators advised that the plant was challenged by the performance of the ultrafiltration unit operation and that the RO plant was operated intermittently. The increased intensity observed in the second stage permeate may be directly related to the intermittent operation of the RO plant that may have prompted the growth of biofilm that was disturbed when the plant was restarted. The observed increase in scattered light intensity suggested that further investigation of the performance of the RO plant was warranted, however, that was not possible as the operations team were focussed on different priorities during the sampling period.

Biologically treated wastewater from Melbourne Water's WTP was chemically treated with coagulant and samples were used to determine whether light scattering had the ability to discriminate between the two samples. The EEMs presented in Figure 6.14 and Figure 6.15 clearly demonstrate the different scattered light intensity between the untreated and the coagulated water sample. The scattered light intensity after coagulation has been reduced as a consequence of the applied treatment. It is interesting to note that the impact of coagulation on the fDOM was insignificant.

The Class A water produced by the Melton RWP facility that included MF and further treatment using RO in the laboratory exhibited a significant reduction in scattered light intensity and also a significant reduction in fDOM. The Rayleigh scattering spectra showed that some particles or colloids were still present in the permeate of the brackish water RO membrane used for this experiment. Light scattering has shown potential as a method of monitoring particles in water.

In Figure 6.18, the EEM plot of the permeate taken at 40% RO recovery and spiked with 1 $\mu\text{g/L}$ PMMA is presented. The plot is similar to that shown in Figure 6.17 but with considerably higher intensity signals for RS over a wide excitation wavelength range. The Class A water was then subjected to a challenge test of 1 mg/L of the same PMMA used in the spiked test. Using the secondary scattering Em/Ex pair of 710/355 nm, a calibration of PMMA was prepared and this is shown in Figure 6.19. In this case, the background scattering was corrected by normalising the data to the scattering of a water sample with no PMMA added. The response is clearly linear with a very high R^2 value and based on this data. The LRV of the challenged, uncompromised, membrane was determined to be 6.6 \log_{10} . It is interesting to note that Raman scattering is evident just above the Em/Ex range of 220-300/240-320 nm.

A limitation of the Shimadzu RF501 spectrofluorometer was that the instrument was not designed to measure the emission intensity at the same excitation wavelength. The instrument is primarily designed to analyse fluorescence rather than scattering although the secondary spectral intensities are readily measurable. Therefore, manually setting the excitation and emission wavelength at the same value to produce calibration curves for the RS line was required in

order to capture the RS intensities in response to the particles present in the samples.

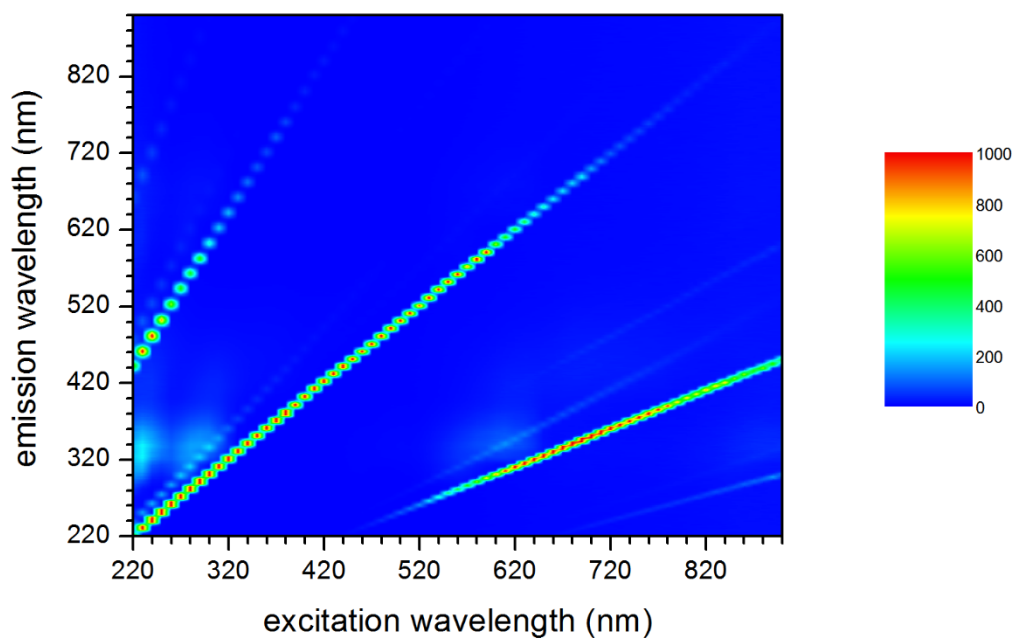


Figure 6.18 : EEM plot of permeate spiked with PMMA.

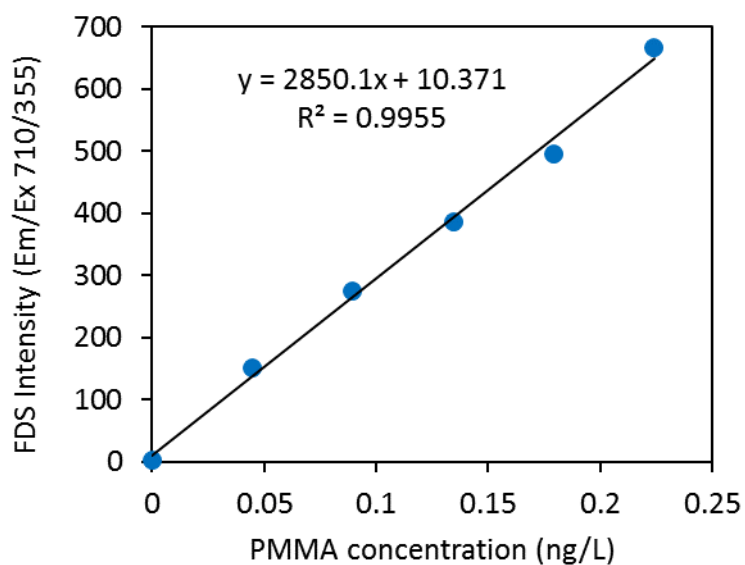


Figure 6.19: Calibration curve of 30 nm PMMA in MilliQ water.

The literature presented in Section 6.2.4 by a variety of researchers used the primary and secondary light scattering spectral lines to quantify nanoparticles and molecules in solution. These references were used to guide the direction of the current research using light scattering phenomenon. Consequently, this work reports RS and, in some cases, the secondary spectral lines to quantify the synthesised PMMA nanoparticles that can represent even the smallest virus particles.

It is important to reiterate that the secondary spectral lines are artefacts of the grating and light source interaction as confirmed in earlier data. The significance of secondary spectral lines is that it provides a reliable representation of the lower Em/Ex data that can also be used as a calibration tool even though they are an artefact of the interaction of the incident light and the diffraction grating that provides light at half and double the incident wavelength.

6.5.4 Bench-scale Detection of Applied Defects

Tests were performed using bench-scale BW30 flat sheet cell to determine whether the RS technique could detect an applied defect. One membrane was scratched on the surface and a hole was placed in another by piercing through with a syringe needle. Each of the membranes was subjected to a challenge test using 4 mg/L of relatively large PMMA particles (*ca.* 300 nm) that had been calibrated as shown in Figure 6.20. In this case, the RS pair at 700 nm was selected and it is clear that an excellent correlation exists between concentration and RS intensity confirming the application of this method for these larger particles although the sensitivity is considerably lower than the smaller particles shown previously. Again, the background scattering was corrected by

normalising the data to the scattering of a permeate sample with no PMMA added. The LRV results of the challenge test are shown in Table 6.1 and it is evident that the technique can clearly identify a membrane with a large defect such as a hole that was $> 0.5 \mu\text{m}$ in diameter. A scratched membrane surface may not be sufficiently damaged to allow a particle of this size to pass through to the permeate, however, even under the test conditions, the LRVs are high.

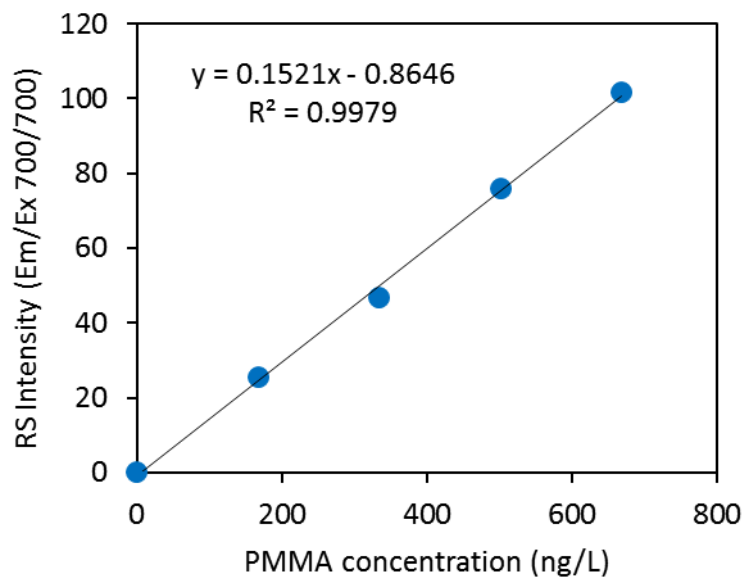


Figure 6.20: Calibration curve of 300 nm PMMA in MilliQ water.

Table 6.1: LRVs for RO membranes with defects.

Defect type	LRV
Membrane with no defect	4.28 ± 0.21
Scratched membrane	4.21 ± 0.09
Membrane with hole	3.71 ± 0.08

6.5.5 Pilot Testing

Challenging the membrane with 90 nm PMMA particles using the scattering technique tested the long-term integrity of a 4" BW30 membrane element but in this case, the secondary scattering spectral pair of excitation/emission wavelengths at 300/600 nm was selected. Permeate sampling was performed hourly but only up to six times per day so the testing was conducted over a long period of time rather than as a discrete test. Figure 6.21 shows the calibration using the secondary spectral pair and a good correlation exists as the artefact spectral line is a true reflection of the upper range of the RS line.

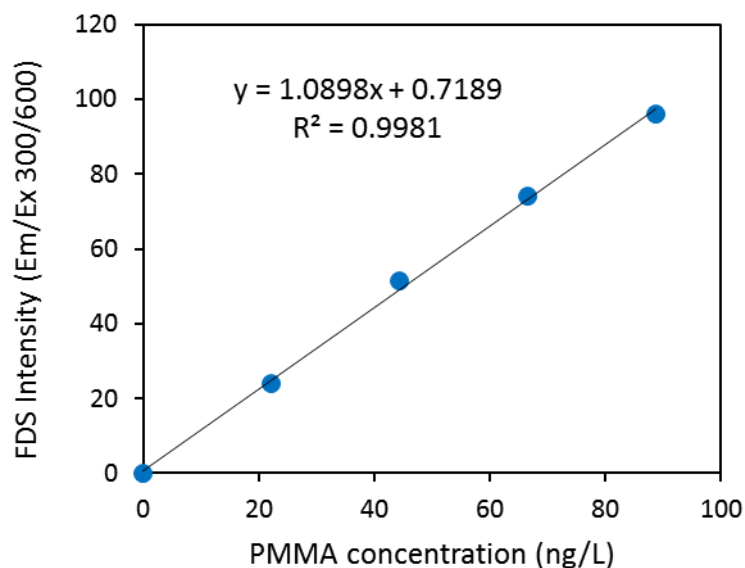


Figure 6.21: Calibration curve of 90 nm PMMA in MilliQ water.

Figure 6.22 shows the LRVs of the permeate over the testing period with little change in the LRV observed for an intact membrane as would normally be expected. The average LRV was *ca.* 5.05 ± 0.13 and that is much higher than the maximum of $2 \log_{10}$ that can be credited to a high pressure element under current conditions in the Australian water industry using conductivity (Victorian

Government Department of Health 2013). Moreover, a slight upward trend in LRV is apparent and this may be expected for a new membrane element as rejection improves following compaction during initial use. The test was conducted over 4 ½ days using the pilot scale rig with the feed temperature kept constant for the duration of the test. The low variability in LRV presented in Figure 6.22 illustrates the stability of the monitoring technique with minor deviations and the ability to recognise the effect of membrane conditioning provided by a rising trend in LRV.

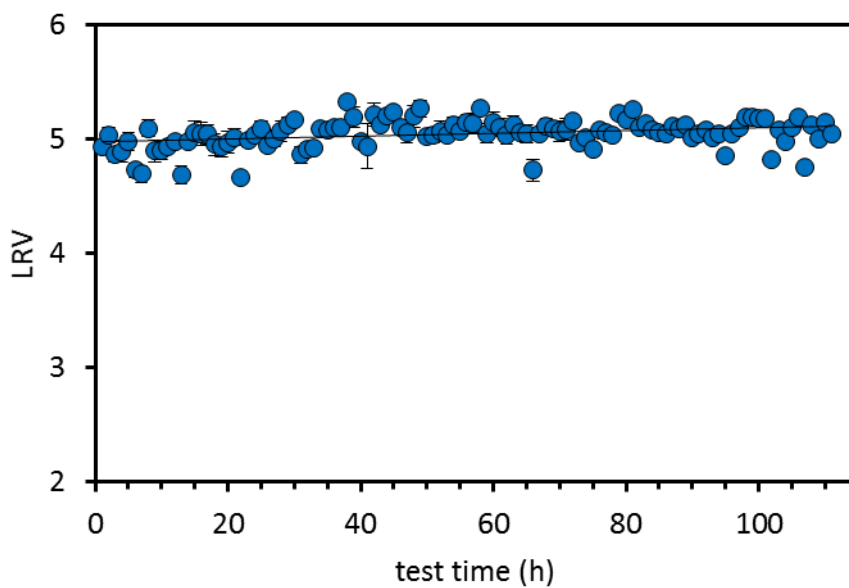


Figure 6.22: LRVs for 4" BW30 intact element.

This data supported the view that light scattering and more particularly, RS, had the potential to quantify nano-sized particles in permeate produced by high pressure membranes. The use of RS and the artefact secondary spectral lines can be translated to provide an unambiguous correlation to nanoparticle concentrations in permeate. Further evidence of this relationship is provided in the following section where the results of full-scale tests using Australia's first proposed DPR facility are reported.

6.5.6 Full-Scale Challenge Testing

Challenge tests were performed at the Australian Antarctic Division (AAD) wastewater recycling pilot plant located at the TasWater treatment facility in Hobart, Tasmania. While the facility was small it did represent Australia's first proposed direct potable reuse scheme, although in this case its main purpose will be to reduce environmental contamination in an ecologically sensitive environment at Davis Station in the Antarctic.

The full-scale testing was conducted on a five-element array and each pressure vessel contained one RO membrane element as shown in Figure 6.8. The system was operated at 70% recovery with feed/permeate sampling points and conductivity monitoring provided for each element. Testing was conducted over two days in the order of the nanoparticle test, the mixed dye test, and then the MS2 challenge test. The feed tank was emptied and the system flushed between tests. The average flux and permeate flows determined at the time of each challenge test are shown in Table 6.2.

Table 6.2: Average normalised flux values.

Challenge test	Permeate flow (L/min)	Flux (L/m²/h/bar)
PMMA	13.84 ± 0.13	2.88 ± 0.03
Mixed Dyes	13.95 ± 0.12	2.81 ± 0.04
MS2	13.43 ± 0.02	3.02 ± 0.01

6.5.7 Full-scale Nanoparticle Challenge Test

A PMMA nanoparticle challenge test was performed on the RO system with an initial 2 mg/L concentration of 30 nm nanoparticles in the RO feed tank. For the feed, concentrate, RO5 permeate and mixed permeate samples, the nanoparticles were quantified by TOC analysis. This form of analysis was used because the high concentration of nanoparticles saturated the spectrofluorometer detector as the instrument was not specifically fitted with high range light scattering detectors.

Rayleigh light scattering was used to quantify the untagged nanoparticles at very low concentrations for permeate samples taken from the intact RO membrane elements. Figure 6.23 shows the RS calibration curve for the 30 nm particles using the Em/Ex pair of 400/400 nm and a strong linear correlation was observed. In this case, the data is shown without background corrections to show the RS intensity of the RO permeate without PMMA. The geometric averages for LRV were determined across each membrane and are presented in Figure 6.24. An average LRV of $5.15 \pm 0.14 \log_{10}$ was obtained for the intact elements, with slight increases between the elements as a result of the increasing feed concentration. The compromised membrane and the mixed permeate samples reported less than 1 \log_{10} LRV in both cases.

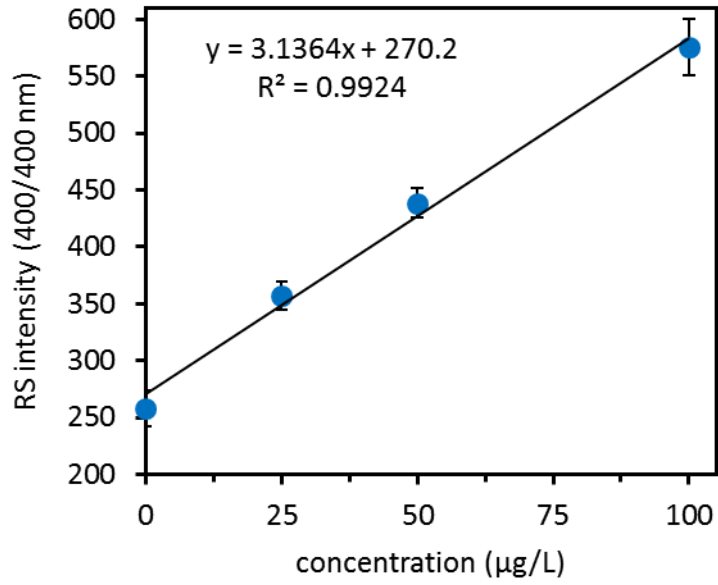


Figure 6.23: RS calibration curve for 30 nm PMMA.

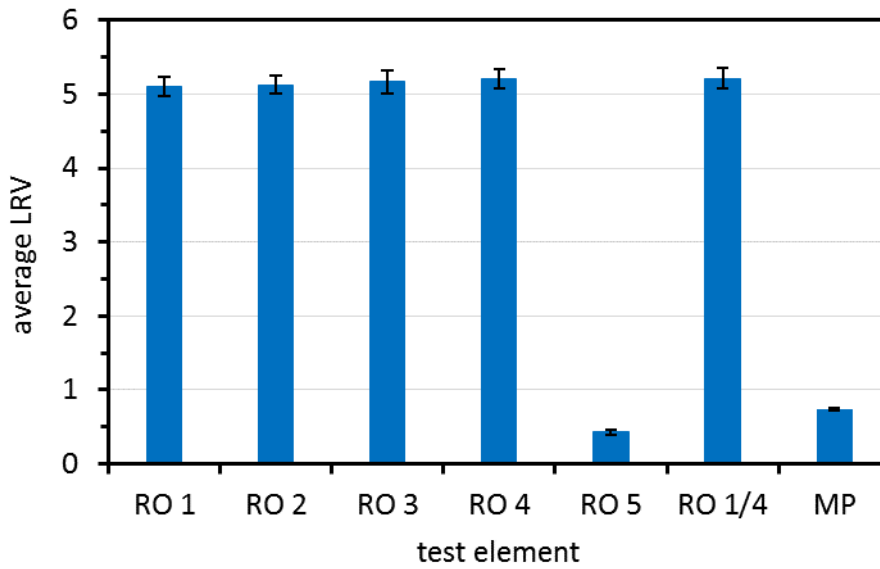


Figure 6.24: Geometric average LRVs for the nanoparticle challenge test.

6.5.8 Full-scale Mixed Tracer Dye Test

A mixed tracer dye test was used, as it was evident that the detection of the individual dyes was possible using both UV and fluorescence. However, there appears to have been a reduction in PyTS sensitivity compared to the individual screening tests reported in Chapter 3. The presence of the other fluorescent dyes, UR and RWT, may have partially quenched the PyTS fluorescence in the mixed solution. The calibration was still considered valid even though the fluorescence intensity was slightly diminished.

The concentration of the dye was determined by UV absorbance for the feed, concentrate and compromised membrane/mixed permeate samples. An example of a UV spectrum for the mixed dye solution is presented in Figure 6.25 and the calibration curves for the UV and fluorescence measurements are given in Figure 6.26 (a) and (b) respectively. It was important to establish whether the individual fluorescent dyes could be detected without interference from the other dyes used in the mixed solution. Figure 6.26 illustrated that detecting individual fluorescent dyes in a mixed solution was possible and their measurement by spectroscopy did not interfere with each other. At the same initial concentration, RWT showed the highest sensitivity followed by PyTS then UR, for both the UV and fluorescence measurements. In this study, the fluorescence measurements were performed with standard laboratory fluorescence detectors.

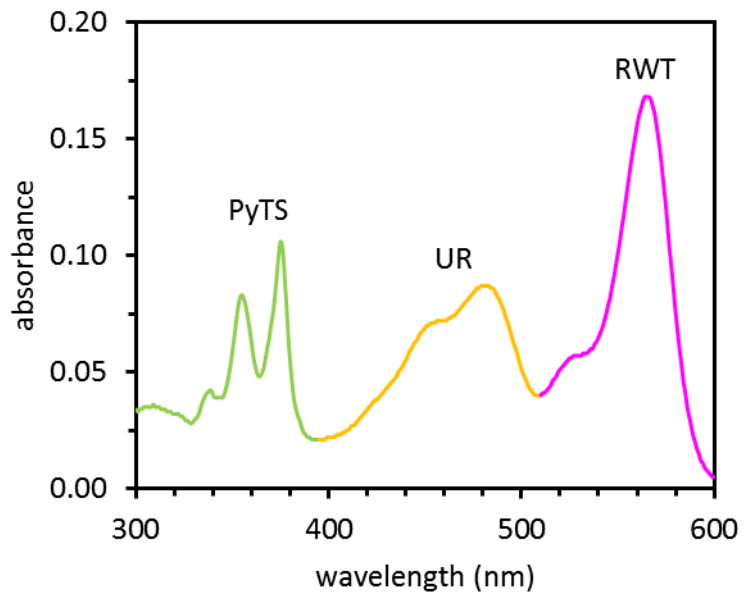


Figure 6.25: UV absorbance of mixed dye solution at 1 ppm each dye.

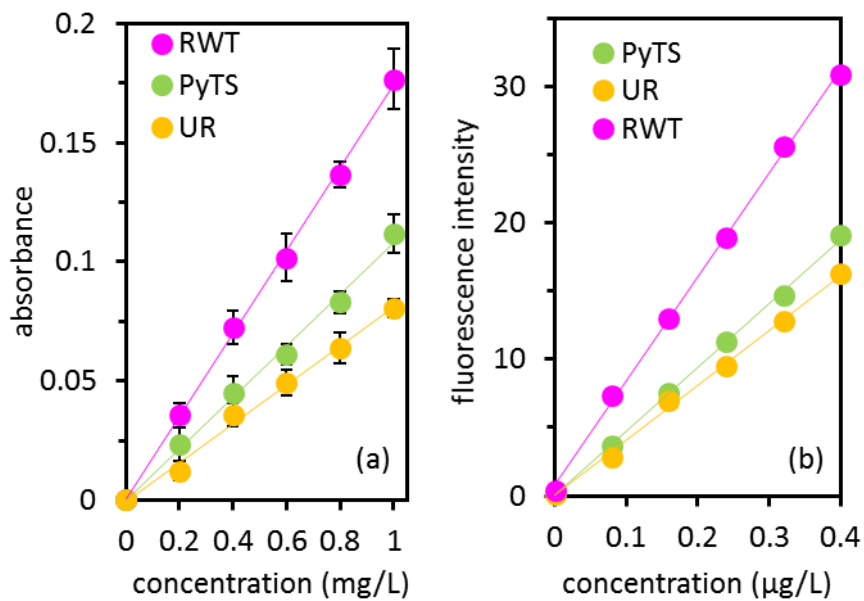


Figure 6.26: Calibration curves for fluorescent tracer dyes
(a) UV absorbance and (b) fluorescence intensity.

The geometrically averaged LRVs determined across each membrane for the three dyes are presented in Figure 6.27 with LRVs greater than $4 \log_{10}$ obtained for each dye for the intact membranes, and higher LRVs obtained for RWT (4.87 ± 0.38) than PyTS (4.23 ± 0.12) and UR (4.22 ± 0.10) at the same concentrations. Much lower LRVs were obtained for the compromised element and the mixed permeate as expected. The LRV across the feed to RO1 and the permeate from RO4 was also greater than $4 \log_{10}$ for each dye. The highest LRV result was reported using RWT with UR and PyTS displaying almost identical LRV responses. The RWT dye provided an LRV $0.5 \log_{10}$ more than either PyTS or UR RWT also reported greater variability.

Increasing LRV through the intact RO membrane arrays may be expected because the reject from the preceding membrane becomes the feed to the subsequent membrane. This phenomenon was exhibited by the nanoparticles (Figure 6.24) but the results for the dyes did not display such a trend in LRV across the first four membranes. The variation and lack of consistency suggests that the fluorescence response may have been affected by the increasing concentration of salinity or other chemical or environmental exposure highlighted during the screening tests reported previously in Chapter 3. Treated water delivered to a DPR facility would be subject to varying salinity, especially during wet weather events and under these conditions the variability of LRV results may be compromised unless auto calibration was a feature of dye challenge testing.

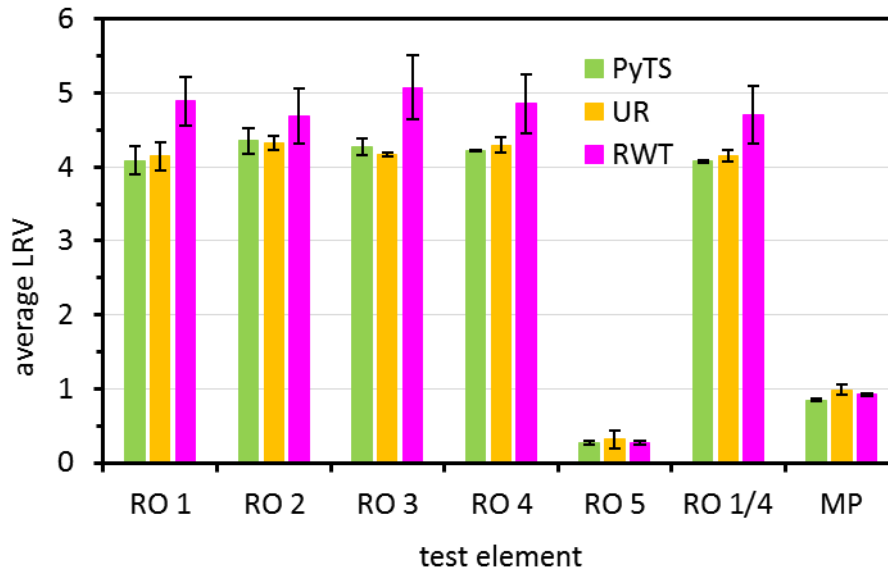


Figure 6.27: Geometric average LRVs for the mixed dye challenge test.

6.5.9 Full-scale MS2 Challenge Test

The results of the MS2 bacteriophage challenge test performed on the system are shown in Figure 6.28 with greater an average $6.46 \pm 0.88 \log_{10}$ LRV obtained across the intact elements. In each case, no MS2 was determined in the permeate samples so the calculated LRV is given by $\log_{10}(\text{feed concentration})$. The inability to observe any MS2 bacteriophage was reported as less than the limit of detection and on that basis the maximum LRV was ascribed to the result. The error associated with the measurement of the MS2 in the feed is also relatively high in comparison to the PMMA nanoparticles and dyes reported previously. A considerable quantity of MS2 passed through the defect in RO5 into the permeate that resulted in less than 1 \log_{10} LRV and subsequently *ca.* 2.5 \log_{10} LRV in the mixed permeate.

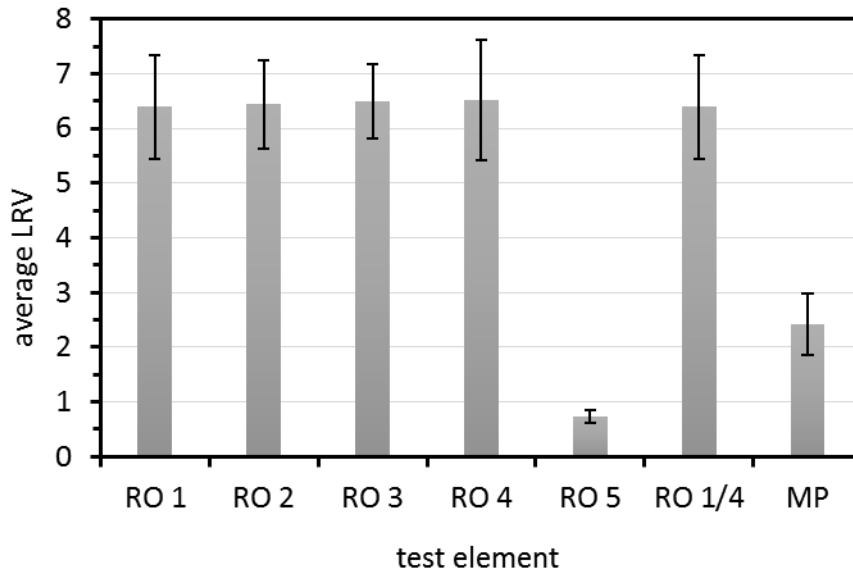


Figure 6.28: Geometric average LRVs for the MS2 challenge test.

Figure 6.29 shows the comparison between the three series of challenge tests and with the exception of the mixed permeate, the trend in LRVs follows MS2 > PMMA nanoparticles > RWT. It is also clear that there is a high error involved in the measurement of the MS2 and this is a result of the multiple serial dilutions needed to enumerate the MS2 in order to obtain measurable plate counts. The observed LRV for fluorescent dyes was lower than that provided by the PMMA nanoparticles. This observation was in accord with the more conservative nature of LRV results obtained by using fluorescent dyes because more of the dye passed through membranes with imperfections that would otherwise reject virus sized nanoparticles.

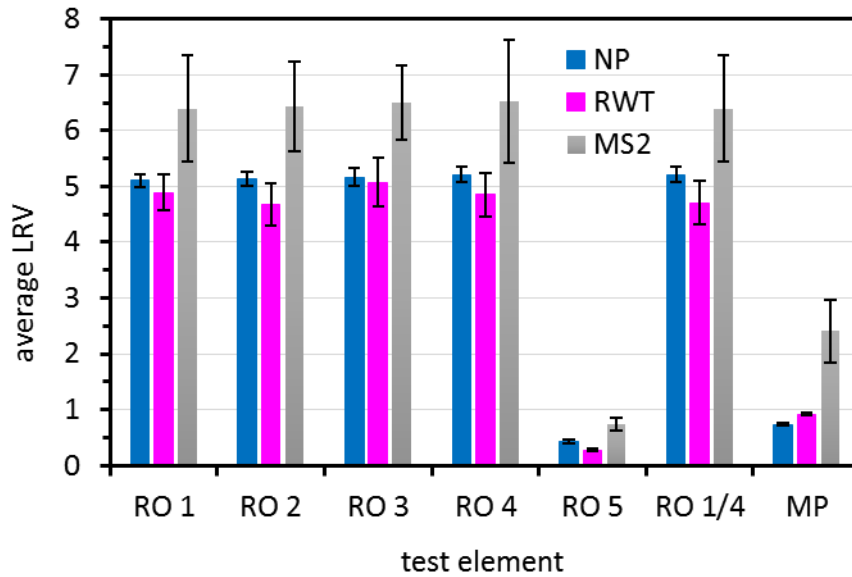


Figure 6.29: Geometric average LRVs for the three challenge tests.

Figure 6.30 illustrates the variability of the LRVs determined for all three challenge tests with a comparison of the LRV data shown in Table 6.6. The RWT dye displayed greater LRV variability compared to that provided by PMMA nanoparticles in terms of LRV across individual membranes and along the membrane array. An increasing LRV trend along the membrane array for the first four membranes should have been evident because the feed concentration of the surrogate increased along the array as the majority of the surrogate was rejected but the volume was reduced by the set recovery rate. The challenge test using PMMA nanoparticles showed the LRV steadily increased along the first four membranes in the array whereas the RWT LRV results were more inconsistent and reported a slight decline in LRV. This erratic behaviour may be the result of an interaction with an increased concentration of salinity or another compound concentrated along the array. This effect was featured by the results from screening results reported in Chapter 3 where the fluorescence was affected by

environmental and chemical exposure. In addition to the erratic LRV across the array reported for the fluorescent dye, the LRV variability for individual membranes was also greater than that reported for the PMMA nanoparticles. These LRV results suggest that challenge tests using dyes may provide greater variability and that the PMMA nanoparticles represent a more stable integrity challenge test.

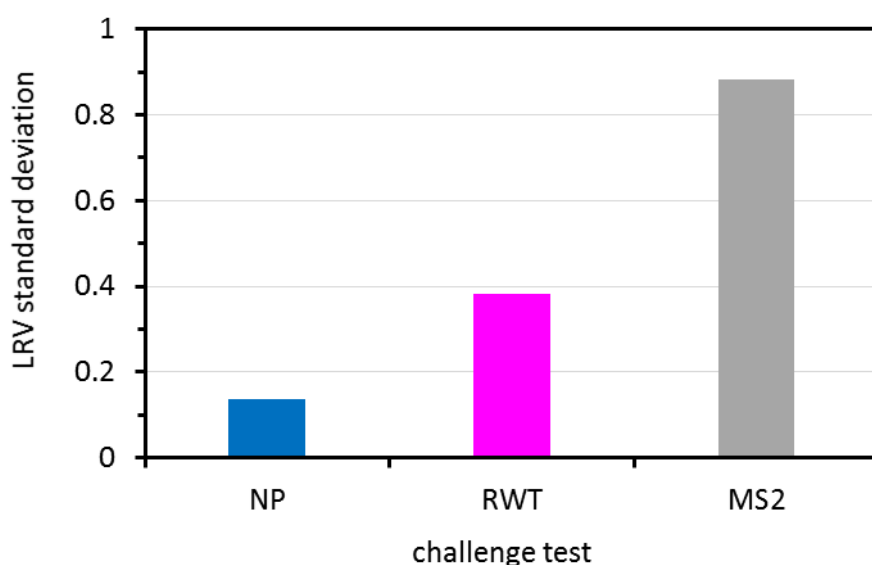


Figure 6.30: LRV standard deviations for the three challenge tests.

Table 6.3: Membrane integrity performance for different surrogates

Challenge Test Surrogate	LRV
MS2 Bacteriophage	6.46 ± 0.88
RWT Fluorescent Dye	4.87 ± 0.38
PMMA nanoparticles	5.15 ± 0.14

Further examination of the data indicated that the LRV reported in the mixed permeate across all of the membranes in the array using RWT was higher than that provided by the integrity test using PMMA nanoparticles. However, the data

for each individual membrane in the array shows that the LRV using RWT was consistently lower than that reported for the PMMA nanoparticle challenge tests. This inconsistency suggests that the reliability and the precision of LRV using RWT may be difficult to interpret performance. If a challenge test was conducted regularly during the day it would be difficult to reconcile whether the variability observed in the data was representative of performance.

Overall, for intact elements, the MS2 challenge test can provide higher LRVs that are considerably greater than the current credits attributed to RO systems. The mixed permeate LRV results indicate that the PMMA nanoparticles provided a more conservative result than that reported for RWT but this is contrary to the LRV reported for each of the five individual membranes where RWT provided more conservative results.

6.5.10 Full-scale Salt Rejection

The RO system design (see Figure 6.8) enabled continuous monitoring of the permeate and feed/concentrate conductivity of each element. The conductivity LRVs were determined at the same time as the samples taken for each challenge test and the results are shown in Figure 6.31. For the intact elements, the results were similar for each challenge test with averaged LRVs between 1.7 and 1.8 \log_{10} and a slightly lower LRV across the four elements. For the mixed permeate and the compromised membrane, the LRVs were considerably lower between 0.7 and 0.9 \log_{10} . This is consistent with the perception that LRVs measured by conductivity offer only a very conservative measure of the system LRV and are not an accurate depiction of the overall integrity of the system.

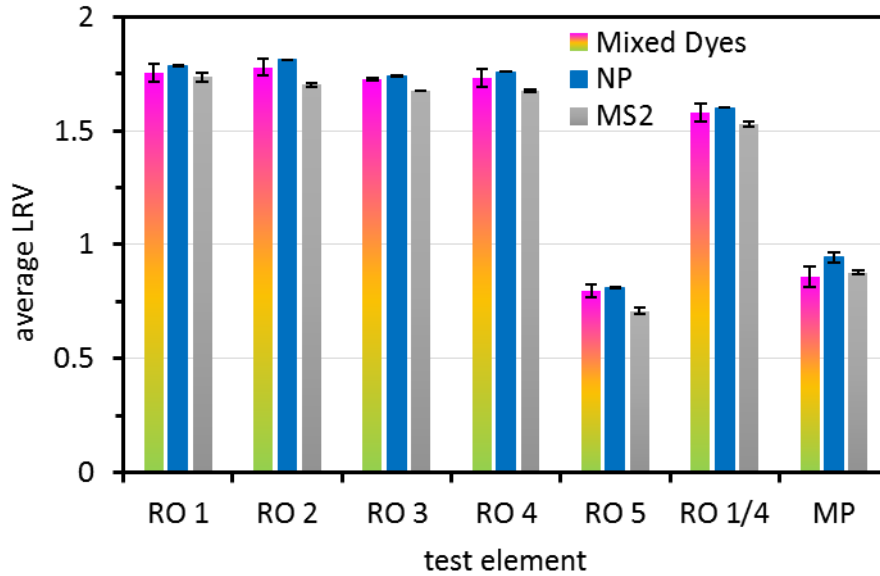


Figure 6.31: Geometric average salt rejection LRVs.

The difference between the LRVs obtained by measuring conductivity or by light scattering of the PMMA nanoparticles is best presented in Figure 6.32. This data clearly demonstrates that conductivity fell well short of the integrity results provided by the three methods tested. Slightly higher LRVs were obtained for the compromised membrane and the mixed permeate and this is due to the lower influent conductivity used in the LRV calculation.

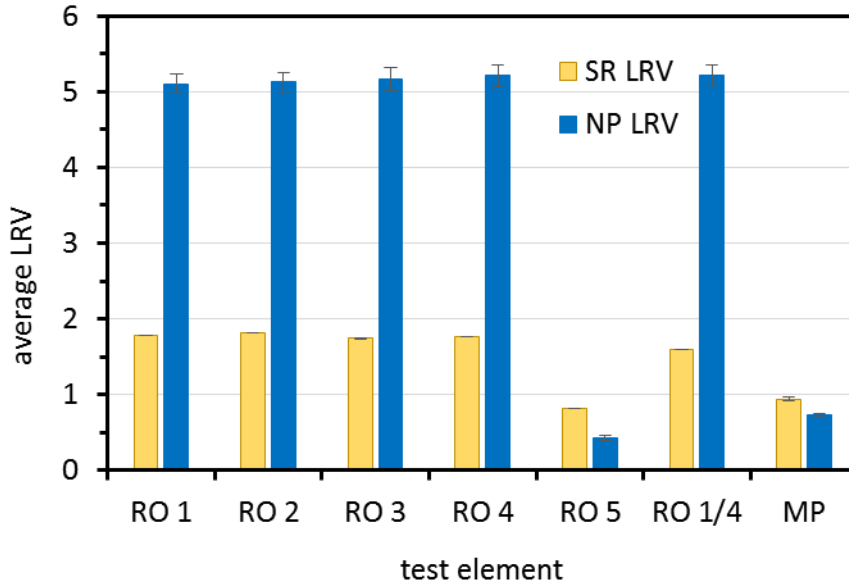


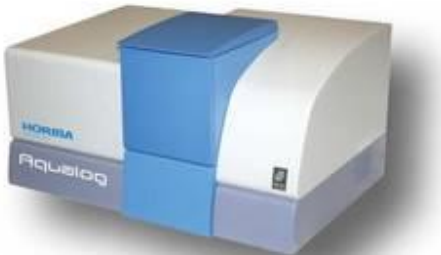
Figure 6.32: Comparison of concurrent LRVs for salt rejection and RS.

6.5.11 Commercial Instruments

The techniques investigated and developed throughout this project have relied on common laboratory scale analytical spectrofluorometers, namely Shimadzu RF-501 and Perkin Elmer LS-50 instruments. These devices are bench-scale laboratory instruments so all testing was performed offline, although whenever possible, samples were tested on the same day as sampling was conducted. The Perkin Elmer instrument was used for the flow-through cell bench-scale tests previously discussed in Chapter 5, but only the Shimadzu device was used to measure the RS data. These instruments are primarily designed to detect fluorescence across a range of wavelengths not to detect scattered light. Additionally, typical laboratory based instruments such as these are not designed for online applications in the field.

There are a limited number of portable field instruments that could potentially be used to measure RS, although some of these are designed with software that specifically subtracts any light scattering signals as “interference”. Table 6.4 lists some of the currently available instruments with their advantages and limitations.

Table 6.4: Potential field instruments for RS detection.

Instrument supplier, details	Advantages, limitations, cost
<p>Stellarnet Scientific (US) c/- Warsash Scientific Pty Ltd (NSW) Portable field instrument</p>  <p>http://www.stellarnet.us/PopularConfigurations_fluorosystem.htm</p>	<ul style="list-style-type: none"> • No EEM capability, need to change out LEDs to alter excitation wavelength • Can apply a flow-through cell • Unit costs: <\$10k
<p>Laser Diagnostic Instruments AS (Estonia) Instant Screener - portable scanning fluorescence spectrophotometer</p>  <p>http://www.lidi.ee/index.php?main=399</p>	<ul style="list-style-type: none"> • Ex/Em wavelength range from 200-750/200-750 nm but increased range is possible • Unit costs: € 24,900, carry case & adapter € 380 (excl. VAT) • Flow through cell integrated with instrument under development • Current availability unknown
<p>Ocean Optics (US) c/- Lastek Pty Ltd (SA) Aqualog, bench top unit</p>  <p>http://www.horiba.com/scientific/products/fluorescence-spectroscopy/steady-state/aqualog/aqualog-r-our-compact-benchtop-fluorometer-for-cdom-13031/</p>	<ul style="list-style-type: none"> • Ex wavelength range 200-650 nm but can be extended up to 800 nm • Applies correction of inner-filter effects and Rayleigh and Raman scattering lines • Unit cost: AUD\$42-50K • Flow through cell for online applications under development

The Stellarnet instrument is the most portable and least expensive option although there is no easy method to perform EEMs without modifying the unit. The Aqualog device is not technically portable but it is widely used to record EEMs and perform quantitative analyses. However, the software has built in functions that remove the Rayleigh scattering lines that are the main feature of the proposed technique. Perhaps the best option in this current list is the Instant Screener that is portable and scans EEMs, and discussions with an Estonian manufacturer indicated that flow-through capabilities could be integrated into the system.

Flow through cells are available and must be integrated with the instrumentation. It is also relatively expensive and there are no local or national suppliers for this device in Australia with limited access available from the manufacturer. Another alternative is to custom build a system based on a high-energy laser and detectors that are widely available that include suppliers like Ocean Optics. The use of high energy lasers and multiple detectors across a range of detection limits can potentially intensify the observed signal leading to even lower detection limits.

Although the final development of the technique will involve the measurement of a “fluorescence” intensity at single or multiple RS wavelength pairs, the ability to also measure EEMs could offer an additional water quality parameter that could be used as a trigger to identify compromised membrane system integrity in full-scale plants in real-time while monitoring permeate flows online. The use of EEM can be used in the same sense that coal miners during the 19th century used canaries to detect the presence of methane gas underground and, therefore, can be seen as the modern day ‘canary’ to provide an indication of a possible breach

in membrane system integrity. Nanoparticles afford better detection of impaired membrane performance that would allow passage of virus whereas fluorescent dyes are at least twenty times smaller and highlight “impairments” in membranes that would otherwise reject virus. Fluorescent dyes can detect membrane impairment developed through aging processes, contact with oxidants, and aggressive CIP regimes that could individually or in combination that would still render the membrane fit for purpose. Including EEM in a membrane integrity surveillance technique could be used as a trigger to initiate an automated challenge test that would increase surveillance security.

Using the same instrument, EEMs could be automatically recorded more frequently and used as a qualitative measure by collecting EEMs into a library and running qualitative comparisons. Increases in the fluorescence intensity in the fDOM regions, for example, may indicate an integrity breach somewhere in the system that could then be isolated by a challenge test. The challenge technique based on PMMA nanoparticles and RS light scattering measurements could be performed intermittently, once a day, week or month for example, to determine the system LRV or could be initiated when the presence of fluorescent fDOM was reported.

6.5.12 Costs to Implement at Full-scale

The cost of materials required to produce 1 kg of PMMA nanoparticles is shown in Table 6.5. Other production costs include water, electricity costs for heating to 70°C, other costs that may be required to concentrate dilute particles, applied labour and production facility utilisation. The cost of commercial fluorescent polystyrene nanoparticles can vary from around \$75 to more than \$500 for a

sample vial containing around 2.5% w/v solids. This represents a cost of between \$4/kL and \$26.70/kL of treated water and that is a huge impost on service providers and consumers alike, and is between two and three orders of magnitude than that established as an acceptable target for a non-microbial surrogate at \$0.02/kL of treated water.

Discussions with a local supplier of industrial chemicals to industry (Challons 2013) indicated that any price reduction for fluorescently tagged nanoparticles would not represent a significant saving because the market supply was small and any additional consumption would require production expansion. Demand would have to be established and assured before producers would invest in expanding production to satisfy a new unproven market demand.

The cost of chemicals to produce PMMA nanoparticles for the experiments have been based on the minimum commercial unit costs provided by Consolidated Chemicals Pty Ltd (based on 2014 costs), and were used to establish the unit cost per kL of treated water. The unit costs identified in Table 6.5 represent the minimum commercial order quantities and will ensure a conservative costing approach as greater quantities of the raw materials will realize lower unit prices through bulk purchasing discounts.

Table 6.5: Cost analysis of PMMA synthesis.

	\$/kg[#]	Minimum quantity (kg)	Cost per kg of PMMA*
MMA monomer	\$8.00	190	\$8.80
Initiator	\$17.20	25	\$0.53
Surfactant	\$16.30	25	\$0.36
Total			\$9.68

*assuming 1:1 reaction plus 10%, #minimum commercial order quantities

One of the objectives of this research was to identify or produce a non- microbial surrogate that would add less than \$0.02/kL of treated water to reduce the direct cost to the service provider and ultimately to the consumer while providing regulators with real-time membrane integrity performance monitoring. In addition to the costs of raw materials, the provision for production costs must be allowed to properly assess the cost per unit volume of treated water. The material costs identified in the table above would typically be increased by 300% to allow for production costs, marketing and margin (Challons 2015).

The cost of the PMMA nanoparticle supply translates to \$0.052/kL to provide a dose of 1 mg/L into the feed at a feed flow rate of 1 ML/h, which is a moderately sized treatment facility equivalent to 24 ML/d or 6.34 MG/d. The choice of feed concentration was based on the sensitivity of the technique and the capacity to measure at least 5 log removal by applying a dose of 10^6 ng/L (1 mg/L) and reporting as little as 10 ng/L. The operating cost associated with the nanoparticle is based on a conservative 75% recovery rate from the membrane plant and a membrane integrity testing schedule of one hour or for 1 ML per day. The cost per day of using a daily membrane integrity test would then become \$0.002/kL, an order of magnitude less than the original objective identified. This would enable the service provider to monitor membrane integrity 40% of the operating day for 10 hours at \$0.02/d, well within the operating budget of any organisation and would not represent a significant impost by regulators on service providers to assure membrane integrity. An important point to note is that membrane integrity surveillance does not occur on such a frequent basis but rather on a daily frequency, or less often, as the case may merit.

In the event that membrane monitoring was conducted for one hour every day the cost of the non-microbial surrogate would only be \$0.002/d. The cost of the analytical instrumentation and sampling array would be depreciated over a five-year period so the initial capital cost of around \$125,000 would translate as \$9/ML based on the following parameters;

- Set the cost of money at 20% over five years,
- Apply a zero residual value after five years,
- Use a plant production rate of 24 ML/d at 75% recovery rate,
- Provide for 95% availability that provides over 18 days for annual maintenance.

It is important to recognise that a membrane integrity monitoring system extends beyond the provision of an appropriate instrument and the synthesised nanoparticles but includes a number of components to be integrated. The capital cost was developed based on the following component items.

- A light scattering instrument using the Laser Diagnostics Instant Screener as a benchmark (A\$40,000 based on a Euro/AUD exchange rate of 0.65 Dec 2015). Provision of an additional \$20,000 was included to provide additional detectors for the different range of intensities provided by more or less material in the continuous sample. The detectors can be damaged if subjected to excessive light intensity so electronic isolation is required to protect each detector.
- Electrical and instrumentation cubicles as a complete assembly that provides IP67 protection against the ingress of water jets and dust (estimated at \$15,000).

- A precision dosing system using stainless steel components and tubing to add the nanoparticles and calibrated solutions (estimated at \$20,000).
- Magnetic flow meters, in line flow element integrated with the light scattering instrument, valving and associated control hardware and software (estimated at \$15,000).
- Galvanised skid fitted with supports for the panel, chemical dosing equipment, non-microbial surrogate storage and inlet feed water valve array (estimated at \$15,000).

This accounts for an additional \$0.009/kL or \$215.76/d as the recurrent cost of owning and operating the integrated membrane integrity system. This satisfies the cost of implementation and recurrent cost associated with the dosing of PMMA as the non-microbial surrogate to monitor high pressure membrane system integrity.

6.6 Conclusions

Successful membrane integrity monitoring requires a sensitive and accurate monitoring technique that can mimic the smallest of viruses quantitatively. Detection of synthesised PMMA nanoparticles that were equal in size with the smallest enteric virus at 30 nm were successfully detected using light scattering intensity and the techniques was demonstrated through pilot and full-scale membrane integrity challenge testing conducted during this study. Synthesised PMMA nanoparticles at the same scale as the 30 nm poliovirus, selected as the target virus, were detected and quantified to determine the system LRV. The technique using PMMA non-microbial surrogates and RS light intensity to quantify the LRV for high pressure membrane systems compared favourably with

challenge tests using fluorescent dyes and provided conservative LRV compared to MS2 bacteriophage. The scattered light membrane integrity monitoring technique has been shown to determine system integrity, rather than just membrane integrity. Integrity testing in real-time was demonstrated using a flow through cell measuring a pulsed dose challenge test with fluorescent dyes at the bench scale. This is a promising development that has the potential to be extended to RS measurements in the future.

The challenge tests performed on the 5 element pilot scale RO system in Australia consisted of continuous dosing of nanoparticles, mixed fluorescent tracer dyes and MS2 bacteriophage. The challenge tests were performed separately under similar flux conditions and LRV results from each challenge test showed that each of the fluorescent dyes in the mixed dye challenge test was able to report greater than 4 LRV while detection of the PMMA nanoparticles reported greater than 5 LRV. These data illustrated the more conservative results obtained using fluorescent dyes compared to virus-sized particles.

The challenge test using MS2 bacteriophage reported greater than 6 log₁₀ LRV but the inability to enumerate any bacteriophage in the permeate for intact membranes resulted in the highest LRV because the denominator was set to unity so the feed concentration was used to calculate LRV. Regardless of this significant limitation, the key issue revolved around the timely production of the rejection capacity of the membrane system which not possible using a biological surrogate. Challenge tests using fluorescent dyes were able to provide real-time information on the performance of the entire membrane system with better than the 4 log₁₀ LRV established threshold value for this research. Using the same

flow through cell technology it is clear that a challenge test using PMMA nanoparticles could deliver rejection performance data in real-time.

The cost to synthesize PMMA nanoparticles that could mimic a small 30 nm virus particle was estimated to be well below the threshold of \$0.02/kL of treated water established as a key objective. In addition, a review of commercially available instruments able to measure scattered light intensity with high sensitivity and resolution identified several instruments currently available, however, modifications were required for complete integration to occur. The cost to develop and implement instrumentation that can measure light scattering intensity coupled to the equipment required to control the application of nanoparticles was developed and shown to be equal to current online instrumentation such as TOC instruments. These instruments can provide an LRV but as has been previously noted the results provide a $2 \log_{10}$ LRV at best.

As expected, the salt rejection LRV results measured concurrently with each challenge test resulted in much lower LRVs due to the relatively low influent salt content and limitations of the detection of conductivity. A comparison of the four challenge tests used during this study is presented in Table 6.6, and shows that the non-microbial surrogate using a synthesised nanoparticle to challenge membrane integrity developed through this research provide the highest LRV provided by non-microbial surrogates. The stability and low variability of the measured LRV was a feature of the PMMA nanoparticles and the ability to recognise a trend in the LRV across membranes in an array was equal to that reported by the challenge test using MS2 bacteriophage. The ability to recognise membrane rejection performance using PMMA nanoparticles has the potential to

equal that provided by dyes and electrical conductivity, however, the stability, reliability, resolution and precision make the use of PMMA nanoparticles the preferred choice as a non-microbial surrogate.

Table 6.6: Challenge test comparison.

Challenge Test	Advantages	Disadvantages
Tracer Dyes	<ul style="list-style-type: none"> • High sensitivity • Rapid fluorescence detection • Low toxicity • More expensive than the targeted cost. 	<ul style="list-style-type: none"> • Sensitive to different chemical and environmental exposure • Sensitive to temperature • Highly absorbent on membrane surface • Not representative of a virus
MS2 Bacteriophage	<ul style="list-style-type: none"> • Good virus surrogate • Widely accepted challenge test 	<ul style="list-style-type: none"> • Live organism, needs specialised operator to test and analyse • Can only measuring live virus • Offline analysis, 24-48 h • Very expensive
Nanoparticle	<ul style="list-style-type: none"> • Good virus surrogate • Rapid measurement, potentially online • High sensitivity • Proof of concept provided high LRV • Lower implementation cost versus other challenge tests 	<ul style="list-style-type: none"> • New technique still under development. • Existing light scattering instrumentation requires modifications
Conductivity	<ul style="list-style-type: none"> • Continuous online measurement • Inexpensive to implement 	<ul style="list-style-type: none"> • Very low LRV capability • Not representative of virus • Variations in temperature affect the response.

The results reported in this Chapter clearly demonstrate that the key objectives of this research have been met and exceeded. The ability to measure small virus scale particles using a synthesised nanoparticle by measuring the scattered light intensity has been demonstrated and compares favourably with the existing methods of membrane integrity testing.

Chapter 7 Conclusions and Recommendations

7.1 The Target

Increasing urbanization, industrial activities and population growth will challenge conventional water supplies and drive producers and consumers towards a world where single use of water is no longer sustainable. Drinking water provided by direct or indirect potable reuse facilities or where challenged surface or groundwater supplies that employ high pressure membrane systems that include NF and RO require high standards of quality assurance, specifically in terms of pathogen removal. Membrane integrity tests are very important as a monitoring and surveillance tool under these circumstances because they can assure the quality of drinking water produced by the operator and delivered to the consumer.

The ability to recognise the true potential of high pressure membranes to reject virus to levels at least $4 \log_{10}$ LRV, or better, in real-time and in a cost effective manner is currently not available. Health regulators currently do not recognise the true barrier potential of high pressure membranes because the current tools used to determine membrane integrity such as electrical conductivity or TOC, provide only up to $2 \log_{10}$ LRV, or only 99% removal. Health regulators demand a high degree of security to reduce risks to public health from compromised water sources and treatment facilities, and the best available technology can only offer security that is at least one hundred fold less than high pressure membrane systems are capable of delivering consistently and reliably.

The aim of this research was to identify, develop and test a real-time membrane integrity monitoring technique that has the capacity to identify impaired

membranes, and their associated system components, that allow passage of the smallest virus, poliovirus, at approximately 30 nm (0.03 μm) into the treated water supply.

Identification of a non-microbial surrogate coupled with appropriate instrumentation was key objectives of this research. The ability to continuously monitor, in real-time, the integrity of high pressure RO and NF membranes required the production of non-microbial surrogates combined with an instrument with high resolution to meet specified targets with the following features.

- Target the smallest virus, poliovirus, with a diameter of 30 nm to define the size and physical nature of the surrogate,
- Reliable and easy method of detection that can be used online and provide real-time feedback,
- Is non-toxic and is environmentally degradable,
- Utilise a relatively inexpensive surrogate that may contribute less than \$0.02/kL of the water treated on a continuous surveillance protocol.
- Can be incorporated into new system designs (greenfield) and existing (brownfield) operational platforms.
- Identify detection devices available in the market that will achieve surrogate detection and provide at least 4 \log_{10} LRV.

The outcomes of this research have led to the development of a novel membrane integrity and surveillance technique that is robust, reliable and meets these challenges. Virus was the key measure for this research because they are

significantly small, at around 30 nm for the poliovirus, and therefore represent a greater integrity challenge for high pressure membrane treatment.

This research was able to identify a monitoring technique that was sensitive to 10 µg/L that enabled the determination of at least 5 log₁₀ LRV that recognised the higher performance capability that membrane systems are capable of providing. Resolution was one factor, but stability and precision are necessary to provide the level of assurance that a low detection limit provided reliable and consistent LRV results.

The low LRV variability using synthesised PMMA nanoparticles and the low detection limit of 10 µg/L were key features of the new integrity test identified as a result of this research. Potential remains for improving sensitivity gains by using coherent light produced by a high energy laser to increase the intensity of RS response.

7.2 Implications from the Findings

Three membrane integrity techniques were explored and assessed to determine whether the performance of intact, impaired or compromised membrane elements, arrays or systems can quantify LRV performance up to and beyond 4 log₁₀. Existing as well as new and innovative techniques were examined and were distilled down to two techniques; namely fluorescence and light scattering. A selection of dyes, fluorescent chemicals, fluorescently tagged nanospheres were assessed to determine whether any could be used as reliable surrogates and provide the level of detection required to meet the objectives of this research.

The key aspect of this research was to identify a non-microbial surrogate for the smallest enteric virus, polio, which is 30 nm in diameter. The development of a polymeric nanoparticle at the same scale as poliovirus coupled with an innovative light scattering measurement technique was explored to determine the capacity to verify membrane system performance of at least 4 log₁₀ LRV. The results of the range of experiments subsequently led to the identification of a new and innovative high pressure membrane integrity monitoring technique.

7.2.1 Chemical Dyes

Eight dyes commonly used in food production and as tracers in environmental studies, identified in Table 3.1, were examined to determine whether they met the established criteria. It became obvious when the absorbance of the dyes was measured and calibration curves were developed that the blue/green dyes were more sensitive than the red/yellow dyes. The higher sensitivity of the blue/green dyes led to the selection of Brilliant Blue (BB) and Fast Green (FG) dyes for further assessment.

Although FG was slightly more sensitive than the BB dye, the limit of detection was relatively poor at around 2 mg/L that would limit the potential LRV measurement to 2 log₁₀ only if a feed dose of 100 mg/L was applied. Clearly, the application of such a significant dose to achieve a modest LRV defeated the objective of measuring at least 4 log₁₀ LRV. The stability of the selected dyes was also challenged by a range of factors, but most notably by UV exposure, the presence of oxidants, pH and temperature. The poor stability of these dyes coupled with their poor sensitivity resulting in poor limits of detection was

sufficient evidence to discount them as potential surrogates for further consideration.

7.2.2 Fluorescent Dyes and Chemicals

A range of fluorescent dyes and chemicals were examined to determine whether they could satisfy the objectives of this research. Vitamin B-12 (RB) and quinine (QN) were the two fluorescent chemicals selected along with Rhodamine WT (RWT), Uranine (UR) and pyrene-tetrasulfonic acid tetrasodium salt (PyTS), three fluorescent dyes, selected for testing against the established criteria.

The RB and QN fluorescent chemicals were shown to be at least one hundred fold less sensitive than the fluorescent chemicals that offered better detection limits. The poor sensitivity with high concentrations required to elicit a strong fluorescence response resulted in the termination of any further screening of these two fluorescent chemicals.

The fluorescent dyes displayed strong fluorescent signatures at very low concentration with PyTS dye consistently showing the highest sensitivity followed by RWT then UR in the bench scale tests. These results are in contrast to those of Frenkel and Cohen (2014) who reported higher sensitivity of UR than RWT. The fluorescent dyes provided effective detection limits greater than 5 µg/L for UR, around 2 µg/L for RWT and <1 µg/L for PyTS satisfying a key consideration of sensitivity. The PyTS dye provided a better sensitivity at moderate fluorescence levels compared to RWT and UR without any environmental or chemical conditions that may suppress the fluorescent response.

The fluorescence response from each of the dyes was tested under different chemical and environmental conditions that included temperature, pH, mono- and divalent salts, oxidants, UV exposure and a mixed matrix provided by RO feed water and permeate sourced from a tertiary wastewater treatment plant using activated sludge and membrane filtration pre-treatment. Each dye was tested under each condition in isolation with the RO feed water and permeate the only situation where the fluorescent dyes were exposed to a mixed matrix.

A temperature change from 10 to 30°C reduced PyTS fluorescence by 18%, the least affected, while the most affected was RWT with a 37% reduction in fluorescence. This response has a seasonal impact unless the source water is affected by industrial discharges such as cooling water from a power station. The reduced fluorescence intensity as temperature increased also has the potential to reduce the LRV. Warmer water may require a greater application of dye to compensate for the lower fluorescence intensity at higher temperature, otherwise a lower LRV will be reported as the sensitivity of permeate fluorescence is reduced.

The RWT and PyTS fluorescence intensities were unaffected across the pH range of 5 to 7.5 but the fluorescence response for UR increased by 235%. While the increase in fluorescence was linear across the pH range, the pH across a membrane can vary depending on temperature and the amount of dissolved carbon dioxide present in the permeate. The ability to calibrate for these complex conditions indicates that the application of UR may be severely limited. The ability to reliably measure pH in low salinity water also challenges the ability to adequately calibrate the fluorescent response across varying pH in permeate.

Frenkel and Cohen (2014) reported that RWT and UR were relatively stable with pH, however, the screening tests conducted in the present study indicated that this is not the case for UR and may significantly limit the use of this dye. The authors (Frenkel and Cohen 2014) also used very high concentrations of dyes at 2.5 mg/L, which depending on the instrument used, may be considered outside the range of quantitative fluorescence. Further, this high concentration may be potentially self-quenching where the lower frequency fluorescent emissions are absorbed and do not have sufficient energy to excite adjacent molecules to fluoresce.

The effect of mono- and di-valent salt solutions on the fluorescent dyes PyTS and RWT were minimal, but the UR fluorescent response increased by 43% in the NaCl solution and by 10% in the CaCl₂ solution. Fluorescence stability at higher NaCl concentrations in feed water may result in a degree of self-quenching that may adversely affect the resulting permeate fluorescence and any LRV results determined using the results.

The presence of oxidants as either free chlorine or monochloramine had a significant impact on the stability of the fluorescence intensity for the dyes. Residual chlorine has a considerable impact on the fluorescence with a nonlinear response. Fortunately, free chlorine is not generally used to disinfect feed water into membrane treatment plants, however, anoxic or anaerobic ground water containing dissolved iron may use chlorine to remove iron before membrane treatment. Under such circumstances, quenching residual chlorine is essential if fluorescent dyes are used to detect membrane impairment.

Performance of the dyes in contact with monochloramine, the more likely oxidant used to reclaim water, produced negligible response from PyTS and RWT, but UR was again significantly affected with an increase in fluorescent intensity by more than 100%. Once again UR is the subject of a poor response that would adversely affect its performance in the event that monochloramine was used to reduce biological fouling.

Exposure to UV light provided a mixed response with a reduction in PyTS fluorescence intensity by 30% after 9 hours and 20% reduction for RWT, but UR remained relatively stable over the test period. The emission/excitation wavelengths for PyTS are closer to the UVA light source so this may be a factor in the degradation of the fluorescent response. Packing, transporting and storing the dyes in opaque containers may reduce the effect of UV exposure. The shelf-life of these dyes must be a consideration if they were purchased and stored for long periods of time or frequently opened and exposed to UV.

Contact with RO feed water and permeate sourced from a tertiary wastewater treatment plant resulted in a slight increase in fluorescence for RWT and PyTS, but a substantial increase of 220% for UR. This fluorescence intensity may adversely affect the performance of UR by potentially self-quenching that may reduce the response of UR in permeate and increase the measured LRV thereby favourably biasing the integrity result. The interaction between UR with organic matter and or sodium present may influence the fluorescence intensity. However, it remains unclear what the fluorescence response will be when these native compounds in the RO feed water are rejected by RO membranes and in a limited way by NF membranes.

Clearly the stability of the fluorescence intensity in response environmental and chemical exposure is a key issue for the fluorescent dyes. Any surrogate must remain stable across a variety of water chemistries expected in feed water. Calibration to overcome certain conditions is only useful where the feed water chemistry remains constant, but this may not be the case across the membrane. An example is that a change in pH may be easily accounted for by preparing multiple calibrations and/or by online measurements, however fluctuations across the membrane because of changes in the concentration of dissolved gases such as CO₂ may reduce the reliability of the integrity results.

Overall, UR appears to be the least stable fluorescent compound where the fluorescence intensity invariably increased substantially across the screening tests, which is contrary to the findings of other researchers. Although PyTS has a better stability profile than RWT across the range of screening tests, access to PyTS is potentially problematic to use for integrity testing because it is part of a proprietary chemical formulation and not readily available commercially.

The performance of the fluorescent dyes tested with membranes that were physically impaired indicated that UR had a higher detection limit in the permeate of 5 µg/L followed by RWT with 2 µg/L and PyTS had the lowest detectability at less than 1 µg/L. The physical size of the dyes appeared to be responsible for the different rejection potential with the molecular diameters estimated by computer simulated models indicating that the size of the molecules from smallest to largest was UR<PyTS<RWT. The molecular diameter reflected the rejection and sensitivity observed during the pulsed dose challenge tests at a pilot scale.

The molecular weight of the compounds in contrast, did not follow in the same pattern where MW from lowest to highest was Ur (378 g/mol) < RWT (532 g/mol) < PyTS (610 g/mol). The MW suggested that PyTS would be rejected before RWT but the larger molecular diameter and more complex structure of RWT made it more likely to be rejected before PyTS.

Overall, PyTS provided the best response to the selection criteria closely followed by RWT, but the use of UR as a surrogate must be seriously challenged. The fluorescent dyes were very sensitive and offered the ability to detect membrane integrity to at least $4 \log_{10}$ LRV, but should not be routinely considered as a viable surrogate for virus because of the implications of the limitations that various environmental and chemical exposure can have on the detection results. The dyes were between 1.1 nm and 1.5 nm in size, more than twenty-fold smaller than the 30 nm target virus and as such can pass through imperfections or impairments in membranes that would otherwise reject virus. Consequently, LRV determined using fluorescent dyes would be lower and therefore more conservative than those achieved using virus sized nanoparticles (Frenkel and Cohen, 2013).

Membrane discoloration was observed during the screening tests and was recognised as the adsorption of the dye by the membrane polymer. Membrane staining was most notable for RWT; however, the extent of the adsorption was not quantitatively determined. The adsorption of dye may adversely affect the sensitivity of the challenge test and reduce the diagnostic capability to locate integrity impairment.

7.2.3 Pulsed Integrity Test

It is clear that PyTS and RWT fluorescent dyes remained relatively stable across a range of environmental and chemical conditions and provided high sensitivity that met or exceeded the objective to provide 4 log₁₀ LRV or better. The application of dyes to measure membrane integrity generally is generally by continuous dosing for a set duration at regular intervals; however, a pulsed application of dye provides an alternative approach. A pulsed application of dye for shorter durations rather than continuous application provided a stepped fluorescence response that diminished until the dye is no longer present. The dynamic change in the permeate fluorescence intensity has the potential to reveal the presence and characteristics of membrane impairment, as well as providing the ability to quantify membrane system performance.

The results of the pulsed dye experiments clearly illustrated that this technique can provide a quantitative measure of integrity of a membrane system. The fluorescent dye was able to detect membrane impairment that would typically reject virus, and was able to provide a response to physical impairment directly imposed on the membrane. The temporal response in conjunction with the size and shape of the peak and tail to the passage of dye has the potential to identify the extent and location of the impairment that can provide operators the opportunity to quickly locate and replace faulty membranes, and reinstate the rejection capacity of the membrane system.

Intuitively, the mass of fluorescent dye used by the pulsed application would be expected to be less than that used for the continuously dosed integrity challenge test. The reality, however, is that the pulsed application challenge test required

10 mg/L of fluorescent dye to be delivered to achieve a suitably sensitive outcome, this represents an order of magnitude higher concentration than that required for the continuous dosing challenge test. While the duration may be up to three times shorter, based on swept volume considerations, the mass of dye can be three times greater than a challenge test using a continuous dose for a longer duration.

The response provided by the pulsed dose challenge tests indicated that this type of integrity challenge might be more time efficient at the expense of more dye used and recognised a higher rejection capacity of the membrane system than the implementation of a continuous challenge test. The potential for this challenge test to provide the rejection capacity by determining LRV in addition to the nature and location of the breach of integrity is a bonus. However, a cautionary note must be made regarding the stability of fluorescent dyes under certain environmental and chemical exposure as identified previously.

7.2.4 Fluorescent Nanoparticles

Fluorescently tagged nano- and micro-spheres were sourced from two specialist suppliers and were subjected to a range of environmental and chemical exposure in the same manner as the fluorescent dyes were screened. Four tagged nanospheres sourced from Sigma responded with very low sensitivity in the range of mg/L rather than µg/L range necessary to provide at least 4 log₁₀ LRV, and so further testing was discontinued for these particles.

The concept of adding a fluorescent tag to the nanoparticles synthesised in a laboratory setting was considered and experiments were conducted to determine whether the addition of a fluorescent tag was possible with improved detection

limits. Nanoparticles synthesised in the presence of a fluorescent dye such as RWT produced a range of diameters between 100 nm and 650 nm, too large for a virus surrogate. Synthesis experiments in the presence of fluorescent compounds resulted very poor detection limits that reaffirmed the results obtained from the commercially available fluorescently tagged particles.

The detection limit and stability remain the key challenges for fluorescently tagged nanoparticles, as the detection limit is at least two orders of magnitude greater than that demonstrated using fluorescent dye compounds. Stability across the range of environmental and chemical conditions that the fluorescently tagged nano- and micro-spheres were exposed to during the screening tests was poor, with each of the tagged particles showing significant variation in fluorescence response to several of the conditions. The potential to quantify nanoparticles *via* light scattering made the quest to further develop a more sensitive fluorescently tagged PMMA nanoparticle, and the associated production costs, less relevant to this research.

The concept of using nanosized particles as a surrogate for enteric virus remains valid but the use of commercially available fluorescently tagged nanoparticles that were tested was shown to be unsuitable due to the sensitivity limitations and the dose required to show 4 log₁₀ removal capacity. Therefore, the fluorescently tagged nanoparticles tested do not offer a plausible replacement for the target virus based on poor sensitivity and stability so they cannot be used as an effective non-microbial surrogate.

7.2.5 New Membrane Integrity Monitoring Technique

A diverse range of polymeric nanoparticles can be readily synthesised in a laboratory setting. Poly(methyl methacrylate) nanoparticles were synthesised and characterised to develop an inexpensive, potentially highly detectable, virus-like, non-microbial surrogate for membrane integrity monitoring. The potential to implement the PMMA nanoparticle detection using RS at an anticipated cost less than the target cost of \$0.02/kL of treated water is unmatched by current surrogates including fluorescent dyes.

Modifications to a standard PMMA synthesis procedure were required before reliable production of consistently sized polymeric nanoparticles was achieved. The formation of stable nanoparticle suspensions was successful in more than 95% of attempts after the synthesis procedure was refined. The particle diameter was influenced by a range of different factors with the addition of surfactant resulting in the smallest size. Importantly, the use of inert nitrogen gas purge was found to be unnecessary offering a potentially substantial production cost saving.

The preparation of uniform sized PMMA nanoparticles was achieved using standard laboratory equipment where smallest particles with a diameter of less than 20 nm were synthesised. The ability to consistently and reliably produce PMMA nanoparticles that were of the same size as the targeted virus at 30 nm diameter was possible and were ideal for use as non-microbial surrogates for membrane integrity testing. Based on these results, it was possible to tailor the size of a required particle by adapting the synthesis procedure during the production of PMMA to satisfy any non-microbial surrogate size for other membrane challenge requirements. The production of PMMA particles on a

larger industrial scale for broader use as a non-microbial surrogate, although outside the scope of this research, could be readily achieved.

Characterization of the PMMA nanoparticles resulted in the observation of some interesting optical properties that were used to develop a measurement method using light scattering phenomenon. Light incident on the PMMA nanoparticles produced a scattering response based on the Rayleigh scattering (RS) phenomenon that was subsequently shown to be capable of detecting and quantifying the synthesised PMMA nanoparticles without adding fluorescent dyes. Light scattering was confirmed in 2D fluorescence EEMs that showed the Rayleigh light scattering phenomenon was sensitive to low concentrations of nanoparticles and could be used as a reliable quantification technique.

Using RS to measure PMMA nanoparticles as a non-microbial surrogate for poliovirus provided a highly sensitive technique that met and exceeded the target LRV detection of at least $4 \log_{10}$. Furthermore, it is possible to integrate a flow-through sensor to provide real-time quantification of the rejection capacity of the membrane and the associated equipment that is integrated to develop a system. The synthesised PMMA nanoparticles that were equal in size with the smallest enteric virus (*ca.* 30 nm) were successfully detected using light scattering intensity as demonstrated through pilot and full-scale membrane integrity challenge testing conducted during this study. Synthesised PMMA nanoparticles were detected and quantified that enabled the system LRV to be determined and the technique compared favourably with challenge tests using fluorescent dyes and MS2 bacteriophage. The RS membrane integrity monitoring technique has

been shown to determine overall system integrity, rather than just single element membrane integrity.

Challenge tests were performed on Australia's first potential DPR scheme that is to be located at Davis Station in the Antarctic. The RO system that formed part of the DPR plant was dosed separately with PMMA nanoparticles, mixed fluorescent tracer dyes and MS2 bacteriophage. The challenge tests were performed under similar flux conditions and LRV results from each challenge test showed that each of the fluorescent dyes in the mixed dye challenge test was able to report greater than 4 log₁₀ LRV with the detection of the PMMA nanoparticles greater than 5 log₁₀ LRV. These data illustrated the more conservative results obtained using fluorescent dyes compared to virus-sized particles.

The challenge test using MS2 bacteriophage reported greater than 6 log₁₀ LRV but the inability to enumerate any bacteriophage in the permeate for intact membranes resulted in the highest LRV because the denominator was set to unity so the feed concentration was used to calculate LRV. Regardless of this significant limitation, the key issue revolved around the timely production of the rejection capacity of the membrane system, which was not possible using a biological surrogate as there is no online technique available. Both the fluorescent dyes and the PMMA nanoparticles were able to provide real-time information on the performance of the entire membrane system with better than the 4 log₁₀ LRV, the established threshold value for this research. As expected, the salt rejection LRV results measured concurrently with each challenge test resulted in much

lower measured LRVs, as the salt rejection characteristics of RO membranes are generally around $2 \log_{10}$ LRV.

The cost to synthesise PMMA nanoparticles that could mimic a small 30 nm virus particle was estimated and was an order of magnitude below the threshold of \$0.02/kL of treated water, established as a key objective. In addition, a review of commercially available instruments able to measure scattered light intensity with high sensitivity and resolution identified several instruments currently available, however, modifications were required for complete integration to occur. The cost to develop and implement instrumentation that can measure light scattering intensity coupled to the equipment required to control the application of nanoparticles was developed and shown to be equal to current online instrumentation such as TOC instruments. The significant difference is that the membrane integrity system using RS to detect the synthesised PMMA nanoparticles is capable of outperforming conventional membrane integrity systems, such as TOC and EC, by at least one hundred fold compared to the current $2 \log_{10}$ detection limits.

The comparison of the four challenge tests used during this study presented in Table 6.6 showed that the technique based on RS using a synthesised nanoparticle provided the best non-microbial integrity results and can be considered as a new membrane integrity test. Although the microbial surrogate, the MS2 bacteriophage, provided a higher LRV, this was tempered by the limitation of the enumeration for uncompromised membranes. The MS2 bacteriophage challenge test provided a higher LRV for an impaired membrane compared to the PMMA nanoparticles but this may have been the result of

enumeration or better rejection performance of MS2 bacteriophage contrary to their smaller diameter (i.e. increased adsorption of bacteriophage compared to nanoparticles).

The summary presented in Table 7.1 compares the research objectives presented in Chapter 1 with the outcomes achieved in this thesis. An additional benefit that this new integrity test can provide is the integration of fluorescence to specifically monitor for the presence of fDOM. Monitoring EEM in addition to RS has the potential to provide an early warning of membrane system impairment and can alert operators to an integrity breach before the next scheduled integrity challenge test. Adding EEM scanning can provide an additional quality assurance measure to increase confidence in membrane system performance.

The ability to detect and quantify PMMA nanoparticles using RS with high sensitivity demonstrated that the key objectives established for this research have been met and exceeded. The ability to measure small virus-scale particles using a synthesised nanoparticle by measuring the scattered light intensity also compares favourably with the existing methods.

Table 7.1: Research Objectives versus Outcomes

Objective of this research	Outcome delivered	
Target the smallest virus, poliovirus with a diameter of 30nm to define the size and physical nature of the surrogate	PMMA nanoparticles ca. synthesized consistently and reliably. PMMA is a stable polymer and is not affected by environmental and chemical exposure.	
Reliable and easy method of detection that can be used online and provide real-time feedback	Light scattering intensity can be measured using instrumentation currently available. Modifications will be required to satisfy full-scale deployment. Integration of a suitable flow through cell is essential to provide real-time integrity monitoring.	
Is non-toxic and is environmentally degradable.	PMMA is used in medical imaging, drug delivery and is compatible with biological systems.	
Utilise a relatively inexpensive surrogate that may contribute less than \$0.02/kL of the water treated on a continuous surveillance protocol.	The cost to produce an apply PMMA nanoparticles can contribute less than an order of magnitude to the delivery cost of treated water.	
Can be incorporated into new system designs (greenfield) and existing (brownfield) operational platforms.	The instrumentation, controls automation, storage and dosing delivery system can be skid mounted and installed on site without interrupting production with connection to individual pressure vessel permeate lines and permeate manifolds the only interface.	
Identify detection devices available in the market that will achieve surrogate detection and provide at least 4 log ₁₀ LRV.	Full-scale tests have confirmed that the integrity test developed through this research has reported at least 4 log ₁₀ LRV	

 Completely meets the objective established for this research.	 Substantially meets the objective established for this research.	 Does not meet the objective established for this research.
--	---	---

7.3 Limitations

While it is clear that the objectives established for this research have been met, it is important to recognise that the outcomes were tempered by a variety of limitations that any study faces. While this study attempted to answer the questions established there are limitations by virtue of the scope, methodological restrictions, and practical realities.

7.3.1 Laboratory Scale Synthesis

The small-scale production of PMMA nanoparticles using laboratory scale equipment challenged the production quantity of PMMA. The number of tests required a ready supply of 30 nm PMMA nanoparticles and there were occasions when insufficient material was available to conclude a series of tests. The testing program resulted in the synthesis of 104 batches of PMMA nanoparticles and although not all resulted in producing the specified size, the tests were all necessary to supply sufficient material to complete the screening and testing of a suitable non-microbial surrogate.

It was not feasible to scale-up the production of PMMA nanoparticles, so limited information was developed to determine whether the synthesis could be economically commercialised. The relatively simple procedure to synthesize PMMA nanoparticles has strong potential for easy production of much larger volumes than were achieved in the laboratory but this remains untested.

7.3.2 Error Analysis

Error analysis on the limit of detection is critical as variations in permeate concentration can significantly affect the reported membrane integrity. The

contribution of errors introduced by dosing systems, measurement, calibration and in serial dilutions used to enumerate MS2 bacteriophage need to be quantified to understand the implications of the reported integrity expressed as LRV. Determining the contribution of errors associated with dosing nanoparticles may represent a small contribution to LRV determination but without the quantification the value of the reported integrity is incomplete. A detailed review of the errors introduced into each of the membrane integrity tests can provide some insight into the variability of the reported LRV and the implications to rejection capacity.

7.3.3 Integrity Monitoring

The reliable characterisation of membrane system integrity is critical to public health safety and can be distorted by operational conditions. Consistent reporting of the conditions under which membrane integrity is measured is critical to establish reliable membrane system rejection capacity. Consequently, a guideline is required to inform operators, health regulators, researchers and the general public what conditions applied prior to implementing an integrity challenge test and what influence these conditions have on the results reported. Condition reporting should form part of an integrity test and include the condition and age of the membranes before the challenge test, the last scheduled CIP event and a reference to the initial membrane performance data such as initial 'clean' operating flux and differential pressure among other parameters. Integrating a condition report introduces transparency and may help identify contributing factors to changes in LRV across a membrane array.

The impact that fouled membranes have on system integrity was not within the scope of this work and was therefore not investigated with respect to the light scattering technique. Membrane fouling has the capacity to “heal” membrane imperfections or minor impairments thereby increasing the apparent rejection capacity of the system but this feature was not explored and so the implications that this has on scheduling integrity tests remains unresolved. Reliable and consistent integrity results can be achieved by identifying the initial condition of the membrane system before commencing an integrity test.

7.3.4 Instrumentation

The Shimadzu RF501 spectrofluorometer was designed to analyse fluorescence rather than scattering although the EEMs reported RS and associated secondary satellite spectra produced by the interaction of the excitation light and the diffraction grating. The default output generated by the spectrofluorometer referenced the secondary spectral lines rather than the Rayleigh scattering spectra. Consequently, some of the calibration was completed using these lines rather than the Rayleigh scattering spectra.

The Shimadzu spectrofluorometer uses a xenon lamp to generate the excitation light source. The xenon lamp in the instrument has a limited lifespan and consequently the intensity of the incident light was not consistent during the prolonged period over which the experiments were conducted. This feature of the light source may have impacted on the intensity of the measured emissions, and better results may have been obtained using a high energy laser light source. Measuring the incident light source energy over time may be necessary to ensure

a consistent approach to reporting LRV using RS as the measurement tool, particularly when using bench-scale spectrofluorometers

The light sources used in the newer more specialised instruments incorporate lasers that produce high intensity coherent light to ensure that measured scattering intensity is higher than that reported in this study. However, the lower incident light intensity provided by the xenon lamp incorporated in the Shimadzu spectrophotometer was capable of providing data with sufficient sensitivity to verify light scattering as a viable technique to determine membrane integrity beyond 4 log₁₀ reduction. Using a high energy laser as the incident light can potentially significantly increase the scattered light intensity that will decrease detection limits and provide greater sensitivity than that achieved through this work.

7.3.5 MS2 Bacteriophage Integrity Test

Using a living biological surrogate does not provide any scope for real-time membrane integrity monitoring. There are a number of limitations associated with using a live biological surrogate including serial dilutions required to enumerate stock and feed samples and the error that introduces. Such serial dilutions, often ten or more, introduce a significant error into the enumeration of the MS2 bacteriophage.

Enumeration only refers to the living surrogate not MS2 bacteriophage that may have been damaged or died because of the stresses associated with passing through an impaired membrane. Unfortunately, it is probably beyond the current science to determine whether this scenario is valid, but it may unduly bias the LRV result by promoting a lower MS2 count in the permeate.

Low MS2 PFU counts in permeate or less than the limit of detection is reported as the log of the feed concentration. This is recognised as a biasing factor but the results are generally always reported as the maximum value using unity for the denominator. Filtering large volumes of sample presents another challenge where the sampling filter may be subject to breach of integrity and therefore the number of MS2 is not representative of the sample collected from the impaired membrane permeate. The preparation for the MS2 challenge test is also extensive and requires skilled personnel to prepare for sample receipt, record management and traceability of results using quality assurance procedures. Enumeration is not a quick process and results can take up to 48 hours to process that does provide the opportunity for operators to take remedial action if necessary but not in a timely manner.

Transporting MS2 bacteriophage after sample collection from an integrity test is a challenge as the samples must remain frozen until received at the laboratory. If they are thawed during transport back to the laboratory they may subsequently die and the enumeration of the bacteriophage will be different to the number that were collected from the permeate and the LRV reported will most likely be biased. The inability to track the MS2 bacteriophage concentration makes the determination of the associated error impossible as the reduction in viable MS2 bacteriophage associated with collection, transport conditions and handling remains unknown.

7.4 Recommendations for Future Directions

The ability to detect the rejection capability of integrated membrane systems using the new integrity monitoring technique developed as a result of this

research presents several opportunities for further work. The results from these projects can only strengthen the capability of this new technique and promote its adoption across the water industry to provide another tool to protect public health when challenged water sources are used.

7.4.1 Low Pressure Membrane Integrity Monitoring

Low pressure membrane systems such as MF and UF already utilise integrity monitoring tests by measuring pressure decay and MS2 challenge test and may benefit from a challenge test that uses nano- and micro-sized particles. The PMMA particles can be tailored to suit specific membrane rejection requirements and detected using the RS technique. The challenge will be to interpret the scattering intensity and the cross over between particle size and the type of light scattering response and whether Mie or RS will dominate.

7.4.2 Particle Size Identification

Rayleigh light scattering is generally measured at 90° to the incident light source but an array of detectors placed around 180° from -90° to 90° in the plane of the incident light can define the nanoparticle shape and size. The ability to identify the size of nanoparticles may provide an additional dataset that may assist in defining the impairment in addition to the rejection capacity of the membrane system.

An alternative to using synthesised polymeric particles is to establish whether the light scattering phenomenon can be used to detect native virus present in the permeate. In addition to detection, the concept of determining the size using an array of detectors across 90° either side of the plane of incident light has the

potential to define the shape and diameter of the nanoparticle. The number of virus particles in the permeate becomes a challenge for detection but the ability to quantify virus rather than a surrogate in real-time would be significant.

7.4.3 Hydraulic Modelling for Integrity Breach Identification

While the application of fluorescent dyes has been shown to provide conservative measurement of the rejection capacity of membrane systems, they also have the potential to identify the type and location of a breach in integrity. The shape and fluorescence intensity response to a pulsed dose of dye into a membrane system has the potential to characterise and locate the impaired membrane element, the contribution by ancillary equipment such as membrane connectors or perhaps the type of membrane impairment itself. Developing a hydraulic modelling tool that can recognise the peak and shape of the resulting response to a pulsed application of dye may provide a real-time diagnostic tool for operators of critical infrastructure and protect public health.

7.4.4 Use and Interpretation of Integrity Challenge Test Results

Recognised as a limitation previously, the absence of any guidelines to promote a consistent approach to the condition of the membrane system prior to conducting an integrity test will add value to the results produced. The guidelines should define the conditions of a membrane system (e.g. following a CIP event) and provide guidance to the likely impact that heavy fouling or scaling can have on the results of an integrity challenge test. This additional layer added to a challenge test as a quality assurance protocol can provide health regulators, operators and the general public greater confidence in capacity of the barrier itself to reject pathogens rather than the added barrier that fouling can contribute.

7.5 The End

The outcomes of this research have the potential to alter the risks associated with the provision of reclaimed water for direct or indirect potable water substitution. Water quality security is the key outcome of an effective and timely membrane integrity monitoring system. In addition, real-time integrity monitoring has the potential to provide greater public confidence in the provision of either direct or indirect potable water substitution.

The use of light scattering to quantify synthesised PMMA nanoparticles to define the rejection capacity of high pressure membrane systems is unique. The application of RS and a non-microbial surrogate that can replicate the size of poliovirus to measure the performance of membrane systems has been proven at full-scale for Australia's first potential direct potable reuse facility.

Real-time performance validation of reclaimed water systems as well as surface water treatment where NF membranes are employed, particularly in catchments with elevated risk factors, can significantly reduce the potential for exposing consumers to microbial contamination. Facility operators will have the capability to maintain very high quality assurance and control over the complete production process, not just the membranes, and promptly identify and isolate compromised elements as well as other system components as a result of the real-time information provided by online membrane integrity surveillance.

The integrity system developed can provide greater confidence in high pressure membrane system performance and come closer to recognising their true performance capability. Equally, this new membrane integrity test can provide

real-time feedback when the membranes are impaired and provide a level of quality assurance that currently does not exist.

When Lord Rayleigh first discovered light scattering behaviour, the concept of synthesized nanoparticles, or nanosized particles in general, would not have been imagined. Integrating light scattering phenomenon first understood in the 19th century with 21st polymer nanoparticle synthesis does suggest **what was once old is new again** and to quote a title from a Hollywood movie, we move **Back to the Future**.

BIBLIOGRAPHY

- Acker CL, Colvin CK, Marinas BJ and Lozier JC** (2001), "Assessing the integrity of reverse osmosis spiral-wound membrane elements with biological and non-biological surrogate indicators", in Membrane Practices for Water Treatment, Denver CO, American Water Works Association, 10: 464-484.
- ACT Environment and Health** (1997), "Wastewater Reuse Guidelines", accessed: November 3, 2011, available at: http://apps.actpla.act.gov.au/tplan/planning_register/register_docs/reuse_gui.pdf.
- ACT Government** (2007), "Water ACT", accessed: November 3, 2011, available at: http://www.thinkwater.act.gov.au/PDFs/water_policy.pdf.
- Adams J** (2009), "Shedding Light on Continuous Water Monitoring", Journal of the American Water Works Association 101(4): 46-48.
- Adham S, Gagliardo P, Smith D, Ross D, Gramith K and Trussell R** (1998a), "Monitoring the integrity of reverse osmosis membranes", Desalination 119(1-3): 143-150.
- Adham SS, Jacangelo JG and Laine JM** (1995), "Low-pressure membranes: assessing integrity", Journal of the American Water Works Association 87(3): 62-75.
- Adham SS, Trussell RS, Gagliardo PF and Trussell RR** (1998b), "Rejection of MS-2 virus by RO membranes", Journal of the American Water Works Association 90(9): 130-135.
- Adu FD** (2005), "The Virology of the Polio Virus", Annals of Ibadan Postgraduate Medicine 3(1): 13-19.
- American Water Works Association** (1999), "Manual of Water Supply Practices (M48): Waterborne Pathogens", AWWA, Denver CO.
- Amoozegar A, Niewoehner C and Lindbo D** (2008), "Water flow from trenches through different soils", Journal of Hydrologic Engineering 13(8): 655-664.
- An Z, Tang W, Hawker CJ and Stucky GD** (2006), "One-Step Microwave Preparation of Well-Defined and Functionalized Polymeric Nanoparticles", Journal of the American Chemical Society 128(47): 15054-15055.
- Andersen CM and Bro R** (2003), "Practical aspects of PARAFAC modeling of fluorescence excitation-emission data", Journal of Chemometrics 17(4): 200-215.

- Anderson GP, Rowe-Taitt CA and Ligler FS** (2000), "RAPTOR: A Portable, Automated Biosensor", proceedings of First Joint Conference on Point Detection for Chemical and Biological Defense, Williamsburg VA, October 23-27.
- Antony A, Blackbeard J and Leslie G** (2012), "Removal Efficiency and Integrity Monitoring Techniques for Virus Removal by Membrane Processes", *Critical Reviews in Environmental Science and Technology* 42(9): 891-933.
- AquaDiagnostic** (2013), "PeCPD™ Laboratory or Field COD Analysis - L100/F100", accessed: September 5, 2013, available at: <http://www.aquadiagnostic.com/downloads/brochures/L100.pdf>.
- Aqualab** (2004), "Rhodamine WT", accessed: January 12, 2010, available at: <http://www.aqualab.com.au/products/rhodamine-wt.html>.
- Arora P, Jain R, Mathur K, Sharma A and Gupta A** (2010), "Synthesis of polymethyl methacrylate (PMMA) by batch emulsion polymerization", *African Journal of Pure and Applied Chemistry* 4(8): 152-157.
- American Society for Testing and Materials**, ASTM E 2456 - 06 (2006), Standard Terminology Relating to Nanotechnology, available at: <http://www.astm.org/Standard/index.shtml>
- American Society for Testing and Materials**, ASTM D 3923 - 08 (2008), Standard Practices for Detecting Leaks in Reverse Osmosis and Nanofiltration Devices, 11.02, available at: <http://www.astm.org/Standards/D3923.htm>.
- American Society for Testing and Materials**, ASTM D 6908 - 06 (2010), Standard Practice for Integrity Testing of Membrane Filtration Systems, 11.02: 20p, available at: <http://www.astm.org/Standards/D6908.htm>.
- Australian Academy of Science** (2006), "Making every drop count", accessed: February 4, 2011, available at: <http://www.science.org.au/nova/095/095print.htm>.
- Australian Water Recycling Centre of Excellence** (2015), "Recycled water for drinking: El Paso, Texas, diversifies water supply with potable reuse", accessed: February 20, 2016, available at: http://www.water360.com.au/wp-content/uploads/2015/07/J003887-El-Paso-fact-sheet_2.pdf.
- AWRCoE** (2011), "Roadmap for a National Validation Framework", accessed: July 19, 2012, available at: http://www.australianwaterrecycling.com.au/coe/images/stories/publications/NatVal_Road_Map_Report_2011.pdf.
- Bahram M, Bro R, Stedmon C and Afkhami A** (2006), "Handling of Rayleigh and Raman scatter for PARAFAC modeling of fluorescence data using interpolation", *Journal of Chemometrics* 20(3-4): 99-105.

- Baker A** (2001), "Fluorescence excitation - Emission matrix characterization of some sewage-impacted rivers", *Environmental Science and Technology* 35(5): 948-953.
- Baker A** (2002a), "Fluorescence excitation-emission matrix characterization of river waters impacted by a tissue mill effluent", *Environmental Science and Technology* 36(7): 1377-1382.
- Baker A** (2002b), "Fluorescence properties of some farm wastes: Implications for water quality monitoring", *Water Research* 36(1): 189-195.
- Banerjee A, Lambertson M, Lozier J and Colvin C** (2001), "Monitoring membrane integrity using high sensitivity laser turbidimetry", *Water Science and Technology: Water Supply* 1(5-6): 273-276.
- Bao J and Zhang A** (2004), "Poly(methyl methacrylate) nanoparticles prepared through microwave emulsion polymerization", *Journal of Applied Polymer Science* 93(6): 2815-2820.
- Bartels CR, Wilf M, Andes K and long J** (2005), "Design considerations for wastewater treatment by reverse osmosis", *Water Science and Technology* 51(6-7): 473-482.
- Becker J** (2012), "Light-Scattering and -Absorption of Nanoparticles", in *Plasmons as Sensors*, Springer Berlin Heidelberg, 2: 5-37.
- Becker MW, Reimus PW and Vilks P** (1999), "Transport and Attenuation of Carboxylate-Modified Latex Microspheres in Fractured Rock Laboratory and Field Tracer Tests", *Ground Water* 37(3): 387-395.
- Bedford EE, Spadavecchia J, Pradier C-M and Gu FX** (2012), "Surface Plasmon Resonance Biosensors Incorporating Gold Nanoparticles", *Macromolecular Bioscience* 12(6): 724-739.
- Behrens H, Beims U, Dieter H, Dietze G, Eikmann T, Grummt T, Hanisch H, Henseling H, Käß W, Kerndorff H, Leibundgut C, Müller-Wegener U, Rönnefahrt I, Scharenberg B, Schleyer R, Schloz W and Tilkes F** (2001), "Toxicological and ecotoxicological assessment of water tracers", *Hydrogeology Journal* 9(3): 321-325.
- Ben AS, Greaves J, Ishida KP, Cooper WJ and Song W** (2011), "Removal of Pharmaceutical and Personal Care Products from Reverse Osmosis Retentate Using Advanced Oxidation Processes", *Environmental Science and Technology* 45: 3665-3671.
- Bennett A** (2008), "Drinking water: Pathogen removal from water - technologies and techniques", *Filtration & Separation* 45(10): 14-16.
- Bernardy N, Romio AP, Barcelos EI, Dal Pizzol C, Dora CL, Lemos-Senna E, Araujo PHH and Sayer C** (2010), "Nanoencapsulation of quercetin via miniemulsion polymerization", *Journal of Biomedical Nanotechnology* 6(2): 181-186.

- Bielefeldt AR, Kowalski K, Schilling C, Schreier S, Kohler A and Summers RS** (2010), "Removal of virus to protozoan sized particles in point-of-use ceramic water filters", *Water Research* 44: 1482-1488.
- Bieroza MZ, Bridgeman J and Baker A** (2010), "Fluorescence spectroscopy as a tool for determination of organic matter removal efficiency at water treatment works", *Drinking Water Engineering and Science* 3(1): 63-70.
- Binet S, Jomard H, Lebourg T, Guglielmi Y, Tric E, Bertrand C and Mudry J** (2007), "Experimental analysis of groundwater flow through a landslide slip surface using natural and artificial water chemical tracers", *Hydrological Processes* 21: 3463-3472.
- Bisoffi M, Hjelle B, Brown DC, Branch DW, Edwards TL, Brozik SM, Bondu-Hawkins VS and Larson RS** (2008), "Detection of viral bioagents using a shear horizontal surface acoustic wave biosensor", *Biosensors and Bioelectronics* 23(9): 1397-1403.
- Bohrerova Z, Bohrer G, Mohanraj SM, Ducoste J and Linden KG** (2005), "Experimental Measurements of Fluence Distribution in a UV Reactor Using Fluorescent Microspheres", *Environmental Science and Technology* 39(22): 8925-8930.
- Borisov SM, Mayr T, Karasyov AA, Klimant I, Chojnacki P, Moser C, Nagl S, Schaeferling M, Stich MI, Kocincova AS and Wolfbeis OS** (2008), "New Plastic Microparticles and Nanoparticles for Fluorescent Sensing and Encoding", in *Springer Series on Fluorescence*, Berlin, Heidelberg, Springer, 4: 431-463.
- Bosma G, Pathmamanoharan C, de Hoog EHA, Kegel WK, van Blaaderen A and Lekkerkerker HNW** (2002), "Preparation of Monodisperse, Fluorescent PMMA–Latex Colloids by Dispersion Polymerization", *Journal of Colloid and Interface Science* 245: 292-300.
- Boudou J-P, Tisler J, Reuter R, Thorel A, Curmi PA, Jelezko F and Wrachtrup J** (2013), "Fluorescent nanodiamonds derived from HPHT with a size of less than 10 nm", *Diamond and Related Materials* 37: 80-86.
- Boulet S** (2015), "Diamonds could help detect early stage cancers, University of Sydney researchers say", accessed: February 12, 2016, available at: <http://www.abc.net.au/news/2015-10-10/diamonds-could-help-detect-early-stage-cancers/6844212>.
- Bourlinos AB, Zboril R, Kubala M, Stathi P, Deligiannakis Y, Karakassides MA, Steriotis TA and Stubos AK** (2011), "Fabrication of fluorescent nanodiamond@C core-shell hybrids via mild carbonization of sodium cholate-nanodiamond complexes", *Journal of Materials Science* 46(24): 7912-7916.
- Brar SK and Verma M** (2011), "Measurement of nanoparticles by light-scattering techniques", *Trends in Analytical Chemistry* 30(1): 4-17.

- Byrne B, Stack E, Gilmartin N and O'Kennedy R** (2009), "Antibody-Based Sensors: Principles, Problems and Potential for Detection of Pathogens and Associated Toxins", *Sensors* 9(6): 4407-4445.
- Byungchul J, Peiyan C, Chevalier A, Ellington A and Hassibi A** (2009), "A CMOS fluorescent-based biosensor microarray", proceedings of Solid-State Circuits Conference, San Francisco CA, February 8-12.
- Cai Z, Chen G, Huang X and Ma M** (2011a), "Determination of lysozyme at the nanogram level in chicken egg white using Resonance Rayleigh-scattering method with Cd-doped ZnSe quantum dots as probe", *Sensors and Actuators B: Chemical* 157(2): 368-373.
- Cai Z, Yu H and Ma M** (2011b), "Determination of lysozyme at the nanogram level in food sample using Resonance Rayleigh-scattering method with Au nanoparticles as probe", *Spectrochimica Acta Part A: Molecular and Biomolecular Spectroscopy* 78(4): 1266-1271.
- California Department of Public Health** (2001), "California Surface Water Treatment Rule, Alternative Filtration Technology Demonstration Report", accessed: May 12, 2014, available at: http://www.waterboards.ca.gov/drinking_water/certlic/drinkingwater/documents/dwdocuments/aftr6_2001.pdf.
- Camli ST, Buyukserin F, Balci O and Budak GG** (2010a), "Size controlled synthesis of sub-100nm monodisperse poly(methylmethacrylate) nanoparticles using surfactant-free emulsion polymerization", *Journal of Colloid and Interface Science* 344: 528-532.
- Camli ST, Buyukserin F, Yavuz MS and Budak GG** (2010b), "Fine-tuning of functional poly(methylmethacrylate) nanoparticle size at the sub-100 nm scale using surfactant-free emulsion polymerization", *Colloids and Surfaces A: Physicochemical and Engineering Aspects* 366(1-3): 141-146.
- Carr B and Wright M** (2013), "Nanoparticle Tracking Analysis. A Review of Applications and Usage 2010 – 2012", NanoSight Ltd.
- Carstea EM, Baker A, Bierozza M and Reynolds D** (2010), "Continuous fluorescence excitation–emission matrix monitoring of river organic matter", *Water Research* 44(18): 5356-5366.
- Casani S, Hansen TB, Christensen J and Knøchel S** (2005), "Comparison of Methods for Assessing Reverse Osmosis Membrane Treatment of Shrimp Process Water", *Journal of Food Protection* 68(4): 801-807.
- Causserand C, Aimar P, Vilani C and Zambelli T** (2002), "Study of the effects of defects in ultrafiltration membranes on the water flux and the molecular weight cut-off", *Desalination* 149(1-3): 485-491.
- Challons R** (2013), personal communication: discussion of pricing of fluorescently tagged nanoparticles, October 15, 2013.

- Challons R** (2015), personal communication: discussion of pricing of chemicals to synthesise PMMA, February 10, 2015.
- Chen C-W, Chen C-Y and Lin C-L** (2011), "Preparation of monodisperse poly(methyl methacrylate) microspheres: effect of reaction parameters on particle formation, and optical performances of its diffusive agent application", *Journal of Polymer Research* 18: 587-594.
- Chen J, Zhang P and Yi P** (2010a), "Preparation of Fluorescence Tunable Polymer Nanoparticles by One-step Mini-emulsion", *Journal of Macromolecular Science, Part A: Pure and Applied Chemistry* 47(11): 1135-1141.
- Chen M-Q, Kishida A, Serizawa T and Akashi M** (2000), "Nanosphere formation in copolymerization of methyl methacrylate with poly(ethylene glycol) macromonomers", *Journal of Polymer Science Part A: Polymer Chemistry* 38(10): 1811-1817.
- Chen W, Liu X, Liu Y, Bang Y and Kim H-I** (2010b), "Synthesis of PMMA and PMMA/PS nanoparticles by microemulsion polymerization with a new vapor monomer feeding system", *Colloids and Surfaces A: Physicochemical and Engineering Aspects* 364(1-3): 145-150.
- Chiu T-P and Don T-M** (2008), "Synthesis and characterization of poly(methyl methacrylate) nanoparticles by emulsifier-free emulsion polymerization with a redox-initiated system", *Journal of Applied Polymer Science* 109(6): 3622-3630.
- Choi SH, Yang J, Suh C and Cho J** (2011), "Use of fluorescent silica particles for checking the integrity of microfiltration membranes", *Journal of Membrane Science* 367(1-2): 306-313.
- Chua LHC, Robertson AP, Yee WK, Shuy EB, Lo EYM, Lim TT and Tan SK** (2007), "Use of Fluorescein as a Ground Water Tracer in Brackish Water Aquifers", *Ground Water* 45(1): 85-88.
- Colvin CK, Acker CL, Marinas BJ and Lozier JC** (2000), "Microbial removal by NF/RO", presented at American Water Works Association Annual Conference, Denver CO, June 11-15.
- Colvin VL** (2003), "The potential environmental impact of engineered nanomaterials", *Nature Biotechnology* 21(10): 1166-1170.
- Cote P, Janson A and Adams N** (2001), "Method and apparatus for testing the integrity of filtering membranes", Patent # WO 01/45829 A1, 31 pp.
- Cote P, Janson A and Adams N** (2004), "Method and Apparatus for Testing the Integrity of Filtering Membranes", Patent # EP 1 194 217 B1, 18 pp.
- Cross SE, Innes B, Roberts MS, Tsuzuki T, Robertson TA and McCormick P** (2007), "Human Skin Penetration of Sunscreen Nanoparticles: In-vitro

Assessment of a Novel Micronized Zinc Oxide Formulation", *Skin Pharmacology and Physiology* 20(3): 148-154.

Crozes GF, Sethi S, Mi B, Curl J and Mariñas B (2002), "Improving membrane integrity monitoring indirect methods to reduce plant downtime and increase microbial removal credit", *Desalination* 149(1-3): 493-497.

CTG Marine Systems (2002), "Dye Tracing Procedure", accessed: August 29, 2011, available at: <http://www.chelsea.co.uk/aqua-tracka#download>.

Cui Z, Hu X, Liu S and Liu Z (2011), "A dual-wavelength overlapping resonance Rayleigh scattering method for the determination of chondroitin sulfate with Nile blue sulfate", *Spectrochimica Acta Part A: Molecular and Biomolecular Spectroscopy* 83(1): 1-7.

Cupaioli FA, Zucca FA, Boraschi D and Zecca L (2014), "Engineered nanoparticles. How brain friendly is this new guest?", *Progress in Neurobiology* 119-120: 20-38.

D'Amato R, Venditti I, Russo MV and Falconieri M (2006), "Growth control and long-range self-assembly of poly(methyl methacrylate) nanospheres", *Journal of Applied Polymer Science* 102(5): 4493-4499.

Dan Y, Yang Y and Chen S (2002), "Synthesis and Structure of the Poly(methyl methacrylate) Microlatex", *Journal of Applied Polymer Science* 85: 2839-2844.

DeCarolis J, Adham S, Hirani Z and Pearce W (2006a), "Integrity evaluation of new generation reverse osmosis membranes during municipal wastewater reclamation", presented at Water Quality Technology Conference, Denver CO, November 5-9.

DeCarolis J, Adham S, Kumar M and Hirani Z (2006b), "Reverse Osmosis Membrane Integrity", Montgomery Watson Internal Report.

DeCarolis J, Adham S, Kumar M, Pearce B and Wasserman L (2005), "Integrity and performance evaluation of new generation desalting membranes during municipal wastewater reclamation", proceedings of Water Environment Federation (WEFTEC 2005), Washington DC, October 29-November 2.

Deluhery J and Rajagopalan N (2008), "Use of paramagnetic particles in membrane integrity testing", *Journal of Membrane Science* 318(1-2): 176-181.

Department of Health & Human Services Victoria (2015), "Class A recycled or reclaimed water", accessed: February 21, 2016, available at: <https://www2.health.vic.gov.au/public-health/water/alternative-water-supplies/class-a-recycled-reclaimed-water>.

- Dettrick D and Gallagher S** (2002), "Environmental Guidelines for the use of Recycled Water in Tasmania", accessed: July 12, 2013, available at: <http://epa.tas.gov.au/epa/water>.
- Diouani MF, Helali S, Hafaid I, Hassen WM, Snoussi MA, Ghram A, Jaffrezic-Renault N and Abdelghani A** (2008), "Miniaturized biosensor for avian influenza virus detection", *Materials Science and Engineering C* 28(5–6): 580-583.
- Dolnicar S and Schäfer AI** (2006), "Public perception of desalinated versus recycled water in Australia", proceedings of AWWA Desalination Symposium, Honolulu, Hawaii, May 7-9.
- Dong JX, Wen W, Li NB and Luo HQ** (2012), "Determination of dopamine at the nanogram level based on the formation of Prussian blue nanoparticles by resonance Rayleigh scattering technique", *Spectrochimica Acta Part A: Molecular and Biomolecular Spectroscopy* 86: 527-532.
- Dreher KL** (2004), "Health and environmental impact of nanotechnology: Toxicological assessment of manufactured nanoparticles", *Toxicological Sciences* 77(1): 3-5.
- Dullens RPA, Claesson EM and Kegel WK** (2004), "Preparation and Properties of Cross-Linked Fluorescent Poly(methyl methacrylate) Latex Colloids", *Langmuir* 20(3): 658-664.
- Eriksson P and Mueller P** (2003), "Vacuum Decay test of Membrane Systems with Spiral wound Elements", presented at AWWA Membrane Technology Conference, Atlanta GA, March 2-5.
- Fan X, Peng J, Yan S and He Y** (2011), "Study on the Interaction Between Water-Soluble CdTe Quantum Dots and Ovalbumin by Optical Spectroscopy", *Spectroscopy Letters* 44(5): 318-327.
- Fane T** (2009), "Monitoring Membrane Processes for Improved Performance", presented at AWA Membranes and Desalination Specialty Conference, Sydney NSW, February 11-13.
- Farquar G and Leif R** (2009), "Biocompatible fluorescent microspheres: Safe particles for material penetration studies, Report LLNL-TR-414873", accessed: May 16, 2012, available at: <https://www.etde.org/etdeweb/purl.cover.jsp?purl=/966915-mg8vXE/>.
- Feng M and Li P** (2006), "Amine-containing core-shell nanoparticles as potential drug carriers for intracellular delivery", *Journal of Biomedical Materials Research Part A* 80A(1): 184-193.
- Fluorescent Microsphere Center** (1999), "Manual for Using Fluorescent Microspheres to Measure Regional Organ Perfusion", accessed: April 2, 2013, available at: <http://fmrc.pulmcc.washington.edu/DOCUMENTS/FMRCMAN.pdf>.

- Flury M and Fluehler H** (1995), "Tracer characteristics of Brilliant Blue FCF", *Soil Science Society of America Journal* 59(1): 22-27.
- Flury M and Fluehler H** (1994), "Brilliant Blue FCF as a dye tracer for solute transport studies - a toxicological overview", *Journal of Environmental Quality* 23(5): 1108-1112.
- Ford DE and Thornton KW** (1983), "Lissamine FF fluorescent dye", *Journal of Environmental Engineering* 109(4): 952-955.
- Freedman RA, Geller R and Kaufmann WJ** (2014), "Universe", W.H.Freeman & Co Ltd, New York.
- Frenkel VS and Cohen Y** (2014), "New Techniques for Real-Time Monitoring of Reverse Osmosis (RO) Membrane Integrity", accessed: April 15, 2014, available at: <https://watereuse.org/watereuse-research/new-techniques-for-real-time-monitoring-of-membrane-integrity-for-virus-removal-pulsed-marker-membrane-integrity-monitoring-system/>.
- Galinha CF, Carvalho G, Portugal CAM, Guglielmi G, Reis MAM and Crespo JG** (2011), "Two-dimensional fluorescence as a fingerprinting tool for monitoring wastewater treatment systems", *Journal of Chemical Technology and Biotechnology* 86(7): 985-992.
- Germán-Heins J and Flury M** (2000), "Sorption of Brilliant Blue FCF in soils as affected by pH and ionic strength", *Geoderma* 97(1-2): 87-101.
- Geszke M, Murias M, Balan L, Medjahdi G, Korczynski J, Moritz M, Lulek J and Schneider R** (2011), "Folic acid-conjugated core/shell ZnS:Mn/ZnS quantum dots as targeted probes for two photon fluorescence imaging of cancer cells", *Acta Biomaterialia* 7(3): 1327-1338.
- Gholivand MB, Ghasemi JB, Saaidpoura S and Mohajeri A** (2008), "Spectrophotometric study of the effects of surfactants and ethanol on the acidity constants of fluorescein", *Spectrochimica Acta Part A: Molecular and Biomolecular Spectroscopy* 71: 1158-1165.
- Giglia S and Krishnan M** (2008), "High sensitivity binary gas integrity test for membrane filters", *Journal of Membrane Science* 323(1): 60-66.
- Giglia S and Krishnan M** (2011), "New binary gas integrity test improves membrane quality assurance", *BioPharm International* 24(4): 24-28.
- Gitis V, Adin A, Nasser A, Gun J and Lev O** (2002), "Fluorescent dye labeled bacteriophages—a new tracer for the investigation of viral transport in porous media: 1. Introduction and characterization", *Water Research* 36(17): 4227-4234.
- Gitis V, Haught RC, Clark RM, Gun J and Lev O** (2006), "Application of nanoscale probes for the evaluation of the integrity of ultrafiltration membranes", *Journal of Membrane Science* 276(1-2): 185-192.

- Gold Coast City Council** (2008), "Recycled Water Class A – Class C", accessed: August 1, 2009, available at: <http://www.goldcoast.qld.gov.au/environment/recycled-water-for-industry-7900.html>.
- Government of Western Australia** (2010), "Recycled Water Sampling Technique", accessed: May 16, 2012, available at: <http://www.public.health.wa.gov.au>.
- Greenlee LF, Lawler DF, Freeman BD, Marrot B and Moulin P** (2009), "Reverse osmosis desalination: Water sources, technology, and today's challenges", *Water Research* 43(9): 2317-2348.
- Griest WH, Wise MB, Hart KJ, Lammert SA, Hryncewich AP and Sickenberger DW** (2000), "The Block II Chemical Biological Mass Spectrometer – Point Detection for Both Chemical and Biological Warfare Agents", proceedings of First Joint Conference on Point Detection for Chemical and Biological Defense, Williamsburg VA, October 23-27.
- Gu Z-Z, Chen H, Zhang S, Sun L, Xie Z and Ge Y** (2007), "Rapid synthesis of monodisperse polymer spheres for self-assembled photonic crystals", *Colloids and Surfaces A: Physicochemical and Engineering Aspects* 302(1-3): 312-319.
- Guanming Q, Changhao Y, Chunfang G, Wenwuan W and Ming Z** (2007), "Study on Properties and Synthesis of Fluorescence PMMA", *Journal of Rare Earths* 25(Suppl): 5-8.
- Guo H, Wyart Y, Perot J, Nauleau F and Moulin P** (2010), "Application of magnetic nanoparticles for UF membrane integrity monitoring at low-pressure operation", *Journal of Membrane Science* 350(1-2): 172-179.
- Hambly A, Henderson RK, Baker A, Stuetz RM and Khan SJ** (2010a), "Probabilistic analysis of fluorescence signals for monitoring dual reticulation water recycling schemes", *Water Science and Technology* 62(9): 2059-2065.
- Hambly AC, Henderson RK, Storey MV, Baker A, Stuetz RM and Khan SJ** (2010b), "Fluorescence monitoring at a recycled water treatment plant and associated dual distribution system - Implications for cross-connection detection", *Water Research* 44 5323-5333.
- Hammer A, Grüttner C and Schumann R** (2001), "New biocompatible tracer particles: use for estimation of microzooplankton grazing, digestion, and growth rates", *Aquatic Microbial Ecology* 24: 153-161.
- Harden HS, Chanton JP, Rose JB, John DE and Hooks ME** (2003), "Comparison of sulfur hexafluoride, fluorescein and rhodamine dyes and the bacteriophage PRD-1 in tracing subsurface flow", *Journal of Hydrology* 277(1-2): 100-115.

- Havlik J, Petrakova V, Rehor I, Petrak V, Gulka M, Stursa J, Kucka J, Ralis J, Rendler T, Lee S-Y, Reuter R, Wrachtrup J, Ledvina M, Nesladek M and Cigler P** (2013), "Boosting nanodiamond fluorescence: towards development of brighter probes", *Nanoscale* 5(8): 3208-3211.
- He G, Pan Q and Rempel GL** (2003a), "Synthesis of Poly(methyl methacrylate) Nanosize Particles by Differential Microemulsion Polymerization", *Macromolecular Rapid Communications* 24: 585-588.
- He L, Ozdemir SK, Zhu J, Kim W and Yang L** (2011), "Detecting single viruses and nanoparticles using whispering gallery microlasers", *Nature Nanotechnology* 6(7): 428-432.
- He LM, Kear-Padilla LL, Lieberman SH and Andrews JM** (2003b), "Rapid in situ determination of total oil concentration in water using ultraviolet fluorescence and light scattering coupled with artificial neural networks", *Analytica Chimica Acta* 478(2): 245-258.
- He Y, Liu S, Liu Q, Liu Z and Hu X** (2005), "Absorption, fluorescence and resonance Rayleigh scattering spectral characteristics of interaction of gold nanoparticle with safranin T", *Science in China Series B: Chemistry* 48(3): 216-226.
- Henderson RK, Baker A, Murphy KR, Hambly A, Stuetz RM and Khan SJ** (2009), "Fluorescence as a potential monitoring tool for recycled water systems: A review", *Water Research* 43(4): 863-881.
- Herrmann J, Escher B, Jämting Å and Neale PA** (2012), "The fate of engineered nanoparticles in wastewater: Literature Review", accessed: October 30, 2012, available at: <http://www.waterra.com.au/project-details/135>.
- Hill D** (2006), "Basic Microbiology for Drinking Water Personnel", American Water Works Association, Denver, CO.
- Homola J, Yee SS and Gauglitz G** (1999), "Surface plasmon resonance sensors: review", *Sensors and Actuators B: Chemical* 54(1-2): 3-15.
- Horticulture Australia Limited** (2006), "Water Recycling in Australia", accessed: May 16, 2012, available at: <http://www.recycledwater.com.au/>.
- Hu S, Bai P, Sun J and Cao S** (2010), "Fluorescent carbon nanoparticles: recent achievements and technical challenges", *Progress in Chemistry* 22(2/3): 345-351.
- Huang X and Brittain WJ** (2001), "Synthesis and Characterization of PMMA Nanocomposites by Suspension and Emulsion Polymerization", *Macromolecules* 34(10): 3255-3260.
- Hurlimann A** (2007), "Recycling Water for Australia's Future – The Case of Two Victorian Cities", proceedings of State of Australian Cities Conference, Adelaide SA, November 28-30.

- Hydranautics** (2012), "Procedure for Pressure Vessel Probing, Technical Service Bulletin TSB114.03", accessed: November 19, 2012, available at: <http://www.membranes.com/docs/tsb/tsb114.pdf>.
- iitkgp.vlab.co.in** (2013), "Charging effect on non conducting sample and its elimination", accessed: February 16, 2016, available at: <http://iitkgp.vlab.co.in/?sub=40&brch=263&sim=1596&cnt=3340>.
- Irudayaraj J** (2009), "Pathogen sensors", *Sensors* 9(11): 8610-8612.
- International Standards Organization** TS 27687 (2008), Nanotechnologies - Terminology and definitions for nano objects - nanoparticle, nanofibre and nanoplate, available at: http://www.iso.org/iso/iso_catalogue.htm.
- Ivnitski D, Abdel-Hamid I, Atanasov P and Wilkins E** (1999), "Biosensors for detection of pathogenic bacteria", *Biosensors and Bioelectronics* 14: 599-624.
- Jacangelo JG, Brown NLP, Madec A, Schwab K, Huffman D, Amy G, Mysore C, Leparc J and Prescott A** (2006), "Micro- and ultrafiltration performance specifications based on microbial removal", accessed: November 1, 2007, available at: <http://www.iwapublishing.com/books/9781843399759/micro-and-ultrafiltration-performance-specifications-based-microbial-removal>.
- Jacangelo JG, Cran M, Gray S, Knoell T, Bashai J, Dunkin N and Schwab K** (2015), "Microbial Seeding Studies for Demonstration of Log Removal in DPR: A Review of Methodology and Field Applications", presented at 30th Annual Water Reuse Symposium, Seattle WA, September 13-16.
- Jacangelo JG, Laine JM, Carns KE, Cummings EW and Mallevalle J** (1991), "Low-pressure membrane filtration for removing Giardia and microbial indicators", *Journal of the American Water Works Association* 83(9): 97-106.
- Jardine RS and Bartlett P** (2002), "Synthesis of non-aqueous fluorescent hard-sphere polymer colloids", *Colloids and Surfaces A: Physicochemical and Engineering Aspects* 211(2-3): 127-132.
- Jhaveri SB and Carter KR** (2007), "Triggered decomposition of polymeric nanoparticles", *Macromolecules* 40(22): 7874-7877.
- Jiang W, Yang W, Zeng X and Fu S** (2004), "Structure and Properties of Poly(methyl methacrylate) Particles Prepared by a Modified Microemulsion Polymerization", *Journal of Polymer Science Part A: Polymer Chemistry* 42: 733-741.
- JMar** (2011), "Contamination Warning and Process Control Device for Waterborne Microorganisms", accessed: September 6, 2013, available at: http://www.jmar.com/wordpress/?page_id=329.

- Johnson DW, Callis JB and Christian GD** (1977), "Rapid Scanning Fluorescence Spectroscopy", *Analytical Chemistry* 49(8): 747A-757A.
- Jones G and Rahman MA** (1994), "Fluorescence Properties of Coumarin Laser Dyes in Aqueous Polymer Media. Chromophore Isolation in Poly(methacrylic acid) Hypercoils", *Journal of Physical Chemistry* 98(49): 13028-13037.
- Jons SD** (2011), "Method of Testing the Integrity of Spiral Wound Modules", Patent # WO 2011/0497790 A1, 22 pp.
- Jons SD, Haynes TN and Nathan JS** (2005), "Sensitive Integrity Test for RO/NF Elements, Paper: IWC-05-16", proceedings of International Water Conference, Orlando FL, October 9-13.
- Jons SD, Johnson JE and Fialkowski MA** (2010), "Method for testing separation modules", Patent # 7,698,928 B2, 26 pp.
- Juck DF, Whissell G, Steven B, Pollard W, McKay CP, Greer CW and Whyte LG** (2005), "Utilization of Fluorescent Microspheres and a Green Fluorescent Protein-Marked Strain for Assessment of Microbiological Contamination of Permafrost and Ground Ice Core Samples from the Canadian High Arctic", *Applied and Environmental Microbiology* 71(2): 1035-1042.
- Kaplan DA, Lytle CD, Routson LB and Myers MR** (1999), "Issues associated with using fluorescent microspheres to evaluate the barrier integrity of natural rubber latex films", *Journal of Rubber Research* 2: 131-139.
- Kasteel R, Vogel HJ and Roth K** (2002), "Effect of non-linear adsorption on the transport behaviour of Brilliant Blue in a field soil", *European Journal of Soil Science* 53(2): 231-240.
- Ketelsen H and Meyer-Windel S** (1999), "Adsorption of brilliant blue FCF by soils", *Geoderma* 90(1-2): 131-145.
- Kitis M, Lozier JC, Kim JH, Mi B and Marinas BJ** (2003a), "Evaluation of biologic and non-biologic methods for assessing virus removal by and integrity of high pressure membrane systems", *Water Science and Technology: Water Supply* 3(5-6): 81-92.
- Kitis M, Lozier JC, Kim JH, Mi B and Marinas BJ** (2003b), "Microbial removal and integrity monitoring of RO and NF membranes", *Journal of the American Water Works Association* 95(12): 105-119.
- Knappenberger KL, Wong DB, Romanyuk YE and Leone SR** (2007), "Excitation Wavelength Dependence of Fluorescence Intermittency in CdSe/ZnS Core/Shell Quantum Dots", *Nano Letters* 7(12): 3869-3874.
- Koh I and Josephson L** (2009), "Magnetic Nanoparticle Sensors", *Sensors* 9: 8130-8145.

- Kramer MF and Lim DV** (2004), "A rapid and automated fiber optic-based biosensor assay for the detection of Salmonella in spent irrigation water used in the sprouting of sprout seeds", *Journal of Food Protection* 67(1): 46-52.
- Kreuter J** (2000), "Poly(Methyl Methacrylate) Nanoparticles As Vaccine Adjuvants", in *Methods in Molecular Medicine, Vol 42: Vaccine Adjuvants: Preparation Methods and Research Protocols*, Totowa, NJ, Humana Press, Inc.: 105-119.
- Kruithof JC, Kamp PC, Folmer HC, Nederlof MM and van Hoof SCJM** (2001), "Development of a membrane integrity monitoring strategy for the UF/RO Heemskerk drinking water treatment plant", *Water Science and Technology: Water Supply* 1(5-6): 261-271.
- Kumar M, Adham S and DeCarolis J** (2007), "Reverse osmosis integrity monitoring", *Desalination* 214(1-3): 138-149.
- Ladner DA, Lee BW and Clark MM** (2007), "Laser scanning cytometry for enumeration of fluorescent microspheres", *Journal of the American Water Works Association* 99(3): 110-117.
- Laenen A and Bencala KE** (2001), "Transient storage assessments of dye-tracer injections in rivers of the Willamette Basin, Oregon", *Journal of the American Water Resources Association* 37(2): 367-377.
- Lakowicz JR** (2006), "Instrumentation for Fluorescence Spectroscopy", in *Principles of Fluorescence Spectroscopy*, Springer, Chapter 2: 27-61.
- Land & Water Australia** (2009), "Using Recycled Water for Irrigation: An overview of the issues, opportunities and challenges", accessed: May 6, 2013, available at: <http://npsi.gov.au/products/pn30123>.
- Langlet J, Gaboriaud F and Gantzer C** (2007), "Effects of pH on plaque forming unit counts and aggregation of MS2 bacteriophage", *Journal of Applied Microbiology* 103(5): 1632-1638.
- Larsson T, Wedborg M and Turner D** (2007), "Correction of inner-filter effect in fluorescence excitation-emission matrix spectrometry using Raman scatter", *Analytica Chimica Acta* 583(2): 357-363.
- Lawler W, Antony A, Cran M, Duke M, Leslie G and Le-Clech P** (2013), "Production and characterisation of UF membranes by chemical conversion of used RO membranes", *Journal of Membrane Science* 447: 203-211.
- Lee C-F, Young T-H, Huang Y-H and Chiu W-Y** (2000), "Synthesis and properties of polymer latex with carboxylic acid functional groups for immunological studies", *Polymer* 41: 8565-8571.

- Lee WE and Thompson HG** (1996), "Detection of Newcastle disease virus using an evanescent wave inamno-based biosensor", *Canadian Journal of Chemistry* 74: 707-712.
- Leskinen SD and Lim DV** (2008), "Rapid ultrafiltration concentration and biosensor detection of Enterococci from large volumes of Florida recreational water", *Applied and Environmental Microbiology* 74(15): 4792-4798.
- Li Y, Liu X and Lin Z** (2012), "Recent developments and applications of surface plasmon resonance biosensors for the detection of mycotoxins in foodstuffs", *Food Chemistry* 132(3): 1549-1554.
- Liang A, Zhou L, Qin H, Zhang Y, Ouyang H and Jiang Z** (2011), "A highly sensitive aptamer-nanogold catalytic resonance scattering spectral assay for melamine", *Journal of Fluorescence* 21(5): 1907-1912.
- Liang Q, Ma W, Shi Y, Li Z and Yang X** (2013), "Easy synthesis of highly fluorescent carbon quantum dots from gelatin and their luminescent properties and applications", *Carbon* 60: 421-428.
- Liao X, Lin X and Liu B** (2004), "Functional fluorescent microspheres", *Colloid and Polymer Science* 282: 1279-1281.
- Lim DV** (2003), "Detection of microorganisms and toxins with evanescent wave fiber-optic biosensors", *Proceedings of the IEEE* 91(6): 902-907.
- Lindner H, Fritz G and Glatter O** (2001), "Measurements on Concentrated Oil in Water Emulsions Using Static Light Scattering", *Journal of Colloid and Interface Science* 242(1): 239-246.
- Liu H, Ye H, Lin T and Zhou T** (2008), "Synthesis and characterization of PMMA/Al₂O₃ composite particles by in situ emulsion polymerization", *Particuology* 6: 207-213.
- Liu J-H, Yang S-T, Chen X-X and Wang H** (2012), "Fluorescent carbon dots and nanodiamonds for biological imaging: preparation, application, pharmacokinetics and toxicity", *Current Drug Metabolism* 13(8): 1046-1056.
- Liu S, Chen Y, Liu Z, Hu X and Wang F** (2006), "A Highly Sensitive Resonance Rayleigh Scattering Method for the Determination of Vitamin B1 with Gold Nanoparticles Probe", *Microchimica Acta* 154(1-2): 87-93.
- Liu SP, He YQ, Liu ZF, Kong L and Lu QM** (2007), "Resonance Rayleigh scattering spectral method for the determination of raloxifene using gold nanoparticle as a probe", *Analytica Chimica Acta* 598(2): 304-311.
- Liu Z, Zhao G, Yu J, Zhang J, Ma X and Han G** (2011), "Preparation and properties of chitosan-graft-poly(methyl methacrylate) nanoparticles using potassium diperiodatocuprate (III) as an initiator", *Journal of Applied Polymer Science* 120(5): 2707-2715.

- Lohwacharin J and Takizawa S** (2009), "Effects of nanoparticles on the ultrafiltration of surface water", *Journal of Membrane Science* 326(2): 354-362.
- Long X, Bi S, Ni H, Tao X and Gan N** (2004), "Resonance Rayleigh scattering determination of trace amounts of Al in natural waters and biological samples based on the formation of an Al(III)-morin-surfactant complex", *Analytica Chimica Acta* 501(1): 89-97.
- Loudon R** (1983), "The quantum theory of light", Oxford University Press, New York.
- Lozier J, Kitis M, Colvin C, Kim J-H, Mi B and Marinas B** (2003), "Microbial Removal and Integrity Monitoring of High-Pressure Membranes", accessed: July 1, 2011, available at: <http://www.iwapublishing.com/books/9781843398509/microbial-removal-and-integrity-monitoring-high-pressure-membranes>.
- Lozier JC, Edwards B and Scholes E** (2013), "Use and suitability of dye-based pathogen integrity testing of RO systems within advanced water recycling schemes", proceedings of AWA Water Recycling Conference, Brisbane QLD, July 1-4.
- Lozier JC, Zornes GL and Jansen E** (2011), "Validation testing of a full-scale RO system for pathogen removal", proceedings of IDA World Congress, Perth WA, September 4-9.
- Luin S, Pellegrini V, Pinczuk A, Dennis BS, Pfeiffer LN and West KW** (2004), "Resonant Rayleigh scattering from quantum phases of cold electrons in semiconductor heterostructures", arXiv preprint cond-mat/0606289.
- Luo HQ, Liu SP, Liu ZF, Liu Q and Li NB** (2001), "Resonance Rayleigh scattering spectra for studying the interaction of heparin with some basic phenothiazine dyes and their analytical applications", *Analytica Chimica Acta* 449(1-2): 261-270.
- Ma Y, Li NB and Luo HQ** (2009a), "Novel and sensitive methods for the determination of dopamine based on the resonance Rayleigh scattering, second-order scattering and frequency doubling scattering quenching effects", *Spectrochimica Acta Part A: Molecular and Biomolecular Spectroscopy* 73(4): 747-751.
- Ma Y, Nian BL and Hong QL** (2009b), "Resonance Rayleigh scattering of $K_2Zn_3[Fe(CN)_6]_2$ nanoparticles and its application for the determination of vitamin C", *Instrumentation Science and Technology* 37(3): 345-358.
- Magal E, Weisbrod N, Yakirevich A and Yechieli Y** (2008), "The use of fluorescent dyes as tracers in highly saline groundwater", *Journal of Hydrology* 358(1-2): 124-133.

- Mairhofer J, Roppert K and Ertl P** (2009), "Microfluidic systems for pathogen sensing: a review", *Sensors* 9(6): 4804-4823.
- Martin L** (2014), "Texas Leads The Way With First Direct Potable Reuse Facilities In U.S.", accessed: February 20, 2016, available at: <http://www.wateronline.com/doc/texas-leads-the-way-with-first-direct-potable-reuse-facilities-in-u-s-0001>.
- Matthews BJH, Jones AC, Theodorou NK and Tudhope AW** (1996), "Excitation-emission-matrix fluorescence spectroscopy applied to humic acid bands in coral reefs", *Marine Chemistry* 55: 317-332.
- Mi B, Eaton CL, Kim J-H, Colvin CK, Lozier JC and Marinas BJ** (2004), "Removal of biological and non-biological viral surrogates by spiral-wound reverse osmosis membrane elements with intact and compromised integrity", *Water Research* 38(18): 3821-3832.
- Miller-Chou BA and Koenig JL** (2003), "A review of polymer dissolution", *Progress in Polymer Science* 28: 1223-1270.
- Min C, Bo Y, Shuxue Z and Limin W** (2006), "Preparation of raspberry-like PMMA/SiO₂ nanocomposite particles", *Frontiers in Chemistry - China* 3: 340-344.
- Mochalin VN and Gogotsi Y** (2009), "Wet Chemistry Route to Hydrophobic Blue Fluorescent Nanodiamond", *Journal of the American Chemical Society* 131(13): 4594-4595.
- Molecular Probes Inc.** (2004), "Working With FluoSpheres® Fluorescent Microspheres", accessed: October 11, 2010, available at: <http://www.invitrogen.com/site/us/en/home/Products-and-Services/Services/Assay-Development-Services/Custom-Microspheres.html>.
- Mon J, Flury M and Harsh JB** (2006), "A quantitative structure-activity relationships (QSAR) analysis of triarylmethane dye tracers", *Journal of Hydrology* 316(1-4): 84-97.
- Montgomery Watson** (1997), "Water Re-purification Project: Final Report on Membrane Prequalification Pilot Study", Montgomery Watson (internal report).
- Morris C, Mooney SJ and Young SD** (2008), "Sorption and desorption characteristics of the dye tracer, Brilliant Blue FCF, in sandy and clay soils", *Geoderma* 146(3-4): 434-438.
- Mukundan H, Anderson AS, Grace WK, Grace KM, Hartman N, Martinez JS and Swanson BI** (2009), "Waveguide-based biosensors for pathogen detection", *Sensors* 9(7): 5783-5809.
- Murphy KR, Hambly A, Singh S, Henderson RK, Baker A, Stuetz R and Khan SJ** (2011), "Organic Matter Fluorescence in Municipal Water

Recycling Schemes: Toward a Unified PARAFAC Model", Environmental Science and Technology 45(7): 2909-2916.

MWH (2007), "City of San Diego Advanced Water Treatment Research Studies, Aqua 2030 Research Center", accessed: May 16, 2012, available at: <http://www.sandiego.gov/water/pdf/purewater/advancedfinalrpt.pdf>.

Myat DT, Roddick F, Wilson S, Chan A, Arabatzoudis C, Zhu B, Muthukumaran S and Duke M (2013), "Study of RO pretreatment of secondary effluent using Coagulation/Ozonation and Ceramic Microfiltration recycled wastewater", presented at IMSTEC13, Melbourne, Australia, November 26-28.

Nagao D, Anzai N, Kobayashi Y, Gu S and Konno M (2006), "Preparation of highly monodisperse poly(methyl methacrylate) particles incorporating fluorescent rhodamine 6G for colloidal crystals", Journal of Colloid and Interface Science 298(1): 232-237.

Naismith J (2005), "Membrane integrity - direct turbidity measurement of filtrate from MF membrane modules at an operating potable water treatment plant", Desalination 179(1-3): 25-30.

Nanduri V, Kim G, Morgan M, Ess D, Hahm B-K, Kothapalli A, Valadez A, Geng T and Bhunia A (2006), "Antibody Immobilization on Waveguides Using a Flow-Through System Shows Improved *Listeria monocytogenes* Detection in an Automated Fiber Optic Biosensor: RAPTOR™", Sensors 6(8): 808-822.

NanoSight (2013), "Measuring Concentration with Nanoparticle Tracking Analysis", accessed: May 11, 2013, available at: <http://www.nanosight.com/technology/nta-software/concentration-measurement>.

Narkis M (1979), "Sintering behavior of poly(methyl methacrylate) particles", Polymer Engineering and Science 19(13): 889-892.

Natural Heritage Trust (2010), "Guidelines for developing recycled water schemes in horticulture", accessed: May 16, 2012, available at: <https://www.environment.gov.au/resource/guidelines-developing-recycled-water-schemes-horticulture>.

Nave R (2016), "HyperPhysics", accessed: February 10, 2016, available at: <http://hyperphysics.phy-astr.gsu.edu/hbase/hframe.html>.

Ni X (2008), "Photoluminescent, water-soluble Mn-doped ZnS quantum dots", accessed: April 2, 2012, available at: <http://nanotechweb.org/cws/article/lab/37256>.

Nobbmann U and Morfesis A (2009), "Light scattering and nanoparticles", Materials Today 12(5): 52-54.

- Nobles MM, Wilding LP and Lin HS** (2010), "Flow pathways of bromide and Brilliant Blue FCF tracers in caliche soils", *Journal of Hydrology* 393(1-2): 114-122.
- Nobles MM, Wilding LP and McInnes KJ** (2004), "Submicroscopic measurements of tracer distribution related to surface features of soil aggregates", *Geoderma* 123(1-2): 83-97.
- Norakankorn C, Pan Q, Rempel GL and Kiatkamjornwong S** (2007), "Synthesis of Poly(methyl methacrylate) Nanoparticles Initiated by 2,2'-Azobisobutyronitrile via Differential Microemulsion Polymerization", *Macromolecular Rapid Communications* 28(9): 1029-1033.
- Northern Territory Government** (2009), "Guidelines for Management of Recycled Water Systems", accessed: May 16, 2012, available at: http://www.health.nt.gov.au/environmental_health/wastewater_management/index.aspx.
- NSW Government** (2008), "Interim NSW Guidelines for Management of Private Recycled Water Schemes", accessed: November 3, 2010, available at: https://www.metrowater.nsw.gov.au/sites/default/files/publication-documents/Private_Recycled_Water_guideMay2008.pdf.
- O'Malley E** (2015), "Fate and toxicity of engineered nanomaterials in treated wastewater", *Water: Journal of the Australian Water Association* 42(7): 66-70.
- Optimos Solutions** (2012), "Solutions / ZAPS Technologies", accessed: October 10, 2013, available at: http://www.optimos.com.au_zaps-liquid.php.
- Ostarcevic E** (1991), "A Study of Advanced Wastewater Treatment Plants in the USA, Inland Wastewater Treatment Division", Sydney Water.
- Ostarcevic E, Cran M and Gray S** (2013), "Screening fluorescent chemicals and nanoparticles as potential surrogates for real-time reverse osmosis integrity monitoring", proceedings of AWA Water Recycling Conference, Brisbane QLD, July 1-4.
- Osterhus CJ** (2013), "Fluorescence", accessed: February 20, 2016, available at: <http://laserclassroom.com/slimy-glowing-cupcakes/fluorescence/>.
- Pan K and Yi D** (2006), "Synthesis of well-defined poly(methyl methacrylate) nanoparticles by reverse atom transfer radical polymerization in a microemulsion", *Journal of Applied Polymer Science* 101(6): 3670-3676.
- Pandey S, Verma P and Pandey AC** (2006), "Synthesis of Highly Luminescent Manganese Doped ZnS Nanophosphor", proceedings of ASID '06, New Delhi, October 8-12.
- Paul DR** (2004), "Reformulation of the solution-diffusion theory of reverse osmosis", *Journal of Membrane Science* 241(2): 371-386.

- Pearce B, DeCarolis J and Wetterau G** (2012), "Evaluation of Performance Monitoring Methods for Advanced Water Purification Processes: City of San Diego", presented at 16th Annual WateReuse & Desalination Research Conference, San Diego CA, June 4-5.
- Peiris RH, Hallé C, Budman H, Moresoli C, Peldszus S, Huck PM and Legge RL** (2010), "Identifying fouling events in a membrane-based drinking water treatment process using principal component analysis of fluorescence excitation-emission matrices", *Water Research* 44(1): 185-194.
- Pejcic B, De Marco R and Parkinson G** (2006), "The role of biosensors in the detection of emerging infectious diseases", *Analyst* 131(10): 1079-1090.
- Peng B, van der Wee E, Imhof A and van Blaaderen A** (2012), "Synthesis of Monodisperse, Highly Cross-Linked, Fluorescent PMMA Particles by Dispersion Polymerization", *Langmuir* 28(17): 6776-6785.
- Peng J-J, Liu S-P, Wang L and He Y-Q** (2010), "Studying the interaction between CdTe quantum dots and Nile blue by absorption, fluorescence and resonance Rayleigh scattering spectra", *Spectrochimica Acta Part A: Molecular and Biomolecular Spectroscopy* 75(5): 1571-1576.
- Pirillo S, Cornaglia L, Ferreira ML and Rueda EH** (2008), "Removal of Fluorescein using different iron oxides as adsorbents: Effect of pH", *Spectrochimica Acta Part A: Molecular and Biomolecular Spectroscopy* 71 636-643.
- Polysciences Inc.** (2009), "Polybead® Polystyrene Microspheres: Frequently Asked Questions", accessed: May 16, 2012, available at: <http://www.polysciences.com>.
- Pontius FW, Amy GL and Hernandez MT** (2009), "Fluorescent microspheres as virion surrogates in low-pressure membrane studies", *Journal of Membrane Science* 335 (1): 43-50.
- Pype M-L, Patureau D, Wery N, Poussade Y and Gernjak W** (2013), "Monitoring reverse osmosis performance: Conductivity versus fluorescence excitation–emission matrix (EEM)", *Journal of Membrane Science* 428(1): 205-211.
- Quinten M** (2011), "Optical Properties of Nanoparticle Systems", Wiley-VCH Verlag GmbH & Co. KGaA.
- Racaniello V** (2004), "Poliovirus", accessed: February 1, 2016, available at: <http://www.virology.ws/2004/08/18/poliovirus/>.
- Radcliffe JC** (2008), "Australian water recycling today – the big issues", presented at National Water Recycling and Reuse Conference, Melbourne VIC, May 27.

- Rao JP and Geckeler KE** (2011), "Polymer nanoparticles: Preparation techniques and size-control parameters", *Progress in Polymer Science* 36(7): 887-913.
- Reinken G, Kale SP and Fuehr F** (1996), "Distribution pattern of organic carbon in soils and its role in preferential movement of brilliant blue in a structured silty soil", *Sciences of Soils* <http://www.hintze-online.com/sos/1996/Articles/Art2>.
- Ridgway HF, Gale JD, Hughes ZE, Stewart MB, Orbell JD and Gray SR** (2013), "Molecular Scale Modeling of Membrane Water Treatment Processes", in *Functional Nanostructured Materials and Membranes for Water Treatment*, Wiley-VCH Verlag GmbH & Co. KGaA, 10: 249-299.
- Rinnan Å and Andersen CM** (2005), "Handling of first-order Rayleigh scatter in PARAFAC modelling of fluorescence excitation–emission data", *Chemometrics and Intelligent Laboratory Systems* 76(1): 91-99.
- Rocha-Gaso MI, March-Iborra C, Montoya-Baides A and Arnau-Vives A** (2009), "Surface generated acoustic wave biosensors for the detection of pathogens: a review", *Sensors* 9(7): 5740-5769.
- Sabnis RW** (2015), "1,3,6,8-Pyrenetetrasulfonic acid tetrasodium salt", in *Handbook of Fluorescent Dyes and Probes*, John Wiley & Sons, Inc, 130: 352-354.
- Sahoo PK and Mohapatra R** (2003), "Synthesis and kinetic studies of PMMA nanoparticles by non-conventionally initiated emulsion polymerization", *European Polymer Journal* 39: 1839-1846.
- Salata OV** (2004), "Applications of nanoparticles in biology and medicine", *Journal of Nanobiotechnology* 2(3): 1-6.
- Sandin R, Ferrero E, Repolles C, Navea S, Bacardit J, Espinos JP and Malfeito JJ** (2013), "Reverse osmosis membranes oxidation by hypochlorite and chlorine dioxide: spectroscopic techniques vs. Fujiwara test", *Desalination and Water Treatment* 51(1-3): 318-327.
- Sanvicens N, Pastells C, Pascual N and Marco MP** (2009), "Nanoparticle-based biosensors for detection of pathogenic bacteria", *Trends in Analytical Chemistry* 28(11): 1243-1252.
- Schijven JF and Hassanizadeh SM** (2000), "Removal of Viruses by Soil Passage: Overview of Modeling, Processes, and Parameters", *Critical Reviews in Environmental Science and Technology* 30(1): 49-127.
- Schneider RI, Balan L and Aldeek F** (2011), "Synthesis, Characterization and Biological Applications of Water-Soluble ZnO Quantum Dots", in *Nanomaterials*, InTech, 2: 27-42.

- Schwartz RC, McInnes KJ, Juo ASR and Cervantes CE** (1999), "The vertical distribution of a dye tracer in a layered soil", *Soil Science* 164(8): 561-573.
- Seah H** (2012), "NEWater: Regulatory framework in Singapore", presented at International Conference on Water Reuse for Drinking Purposes, Umhlanga, KwaZulu-Natal, October 9-11.
- Seinfeld JH and Pandis SN** (2012), "Interaction of Aerosols with Radiation", in *Atmospheric Chemistry and Physics : From Air Pollution to Climate Change*, Hoboken, Wiley, 15: 691-719.
- Sene JA, Pinheiro MVB, Krambrock K and Barbeira PJS** (2009), "Quantification of fullerene nanoparticles suspensions in water based on optical scattering", *Talanta* 78(4-5): 1503-1507.
- Senga Y and Minami S** (1991), "Excitation-Emission Matrix Scanning Spectrofluorometer", *Applied Spectroscopy* 45(10): 1721-1725.
- Seqwater** (2013), "Purified recycled water", accessed: February 20, 2016, available at: <http://www.seqwater.com.au/water-supply/water-treatment/purified-recycled-water>.
- Shiau B-J, Sabatini DA and Harwell JH** (1993), "Influence of Rhodamine WT Properties on Sorption and Transport in Subsurface Media", *Ground Water* 31(6): 913-920.
- Shim SE, Lee H and Choe S** (2004), "Synthesis of Functionalized Monodisperse Poly(methyl methacrylate) Nanoparticles by a RAFT Agent Carrying Carboxyl End Group", *Macromolecules* 37: 5565-5571.
- Shirasaki N, Matsushita T, Matsui Y, Kobuke M and Ohno K** (2009), "Comparison of removal performance of two surrogates for pathogenic waterborne viruses, bacteriophage Q[beta] and MS2, in a coagulation-ceramic microfiltration system", *Journal of Membrane Science* 326(2): 564-571.
- Sigma-Aldrich Pty. Ltd.** (2011), "Polystyrene Latex Beads, Product Information", accessed: January 6, 2011, available at: <http://www.sigmaaldrich.com/catalog/substance/latexbeadspolystyrene1234598765?lang=en®ion=AU>.
- Singapore PUB** (2010), "Ensuring Water Sustainability", accessed: February 20, 2016, available at: <http://www.pub.gov.sg/Pages/default.aspx>.
- Singh S, Henderson RK, Baker A, Stuetz RM and Khan SJ** (2009), "Distinguishing stage 1 and 2 reverse osmosis permeates using fluorescence spectroscopy", *Water Science and Technology* 60(8): 2017-2023.
- Singh S, Henderson RK, Baker A, Stuetz RM and Khan SJ** (2012), "Characterisation of reverse osmosis permeates from municipal recycled

water systems using fluorescence spectroscopy: Implications for integrity monitoring", *Journal of Membrane Science* 421–422: 180-189.

Smart PL and Laidlaw IMS (1977), "An Evaluation of Some Fluorescent Dyes for Water Tracing", *Water Resources Research* 13(1): 15-33.

Song A, Zhang J, Zhang M, Shen T and Tang Ja (2000), "Spectral properties and structure of fluorescein and its alkyl derivatives in micelles", *Colloids and Surfaces A: Physicochemical and Engineering Aspects* 167: 253-262.

Song WW, Li NB and Luo HQ (2012), "Gemini surfactant applied to the heparin assay at the nanogram level by resonance Rayleigh scattering method", *Analytical Biochemistry* 422(1): 1-6.

Stanbro WD and Pyrch DA (1979), "Stability of rhodamine WT in saline waters", *Water Resources Research* 15(6): 1631-1632.

Stanek LG, Heilmann SM and Gleason WB (2006), "Preparation of monodisperse PMMA microspheres using 2-vinyl-4,4'-dimethylazlactone as a particle Stabilizer", *Colloid and Polymer Science* 284: 586-595.

Stedmon CA, Markager S and Bro R (2003), "Tracing dissolved organic matter in aquatic environments using a new approach to fluorescence spectroscopy", *Marine Chemistry* 82(3-4): 239-254.

Stokes GG (1852), "On the Change of Refrangibility of Light", *Philosophical Transactions of the Royal Society of London* 142: 463-562.

Strutt J (1871), "On the light from the sky, its polarization and colour", *Philosophical Magazine* 4(41): 107-120, 274-279.

Sunintaboon P, Duangphet S and Tangboriboonrat P (2009), "Polyethyleneimine-functionalized poly(methyl methacrylate) colloidal nanoparticles for directly coating natural rubber sheet", *Colloids and Surfaces A: Physicochemical and Engineering Aspects* 350 114–120.

Surawanvijit S, Thompson J, Rahardianto A, Frenkel V and Cohen Y (2015), "Pulsed marker method for real-time detection of reverse osmosis membrane integrity loss", *Desalination* 370: 25-32.

Sutton DJ, Kabala ZJ, Francisco A and Vasudevan D (2001), "Limitations and potential of commercially available rhodamine WT as a groundwater tracer", *Water Resources Research* 37(6): 1641-1656.

Szabelski M, Gryczynski Z and Gryczynski I (2010), "Photophysical properties of novel fluorescein derivative and its applications for time-resolved fluorescence spectroscopy", *Chemical Physics Letters* 493: 399-403.

Taitt CR, Anderson GP and Ligler FS (2005), "Evanescent wave fluorescence biosensors", *Biosensors and Bioelectronics* 20(12): 2470-2487.

- Tan D, Zhou S, Xu B, Chen P, Shimotsuma Y, Miura K and Qiu J** (2013), "Simple synthesis of ultra-small nanodiamonds with tunable size and photoluminescence", *Carbon* 62: 374-381.
- Tang M, Wen G, Luo Y, Liang A and Jiang Z** (2015), "A simple resonance Rayleigh scattering method for determination of trace CA125 using immuno-AuRu nanoalloy as probe via ultrasonic irradiation", *Spectrochimica Acta Part A: Molecular and Biomolecular Spectroscopy* 135: 1032-1038.
- Texas Water Development Board** (2015), "Water Reuse", accessed: February 20, 2016, available at: <http://www.twdb.texas.gov/publications/shells/WaterReuse.pdf>.
- Tjandraatmadja G and Diaper C** (2006), "Sources of critical contaminants in domestic wastewater: a literature review", accessed: March 23, 2011, available at: <http://www.clw.csiro.au/publications/waterforahealthycountry/2006/wfhc-criticalcontaminants-sources-domesticwastewater.pdf>.
- Tu R, Liu B, Wang Z, Gao D, Wang F, Fang Q and Zhang Z** (2008), "Amine-Capped ZnS–Mn²⁺ Nanocrystals for Fluorescence Detection of Trace TNT Explosive", *Analytical Chemistry* 80(9): 3458-3465.
- Turner Designs Solutions** (1998), "Fluorescein: Bulletin No. 103", accessed: November 11, 2010, available at: http://www.turnerdesigns.com/t2/doc/appnotes/998_5103.pdf.
- U.S. Environmental Protection Agency** (2005), "Membrane Filtration Guidance Manual, EPA 815-R-06-009", accessed: June 29, 2011, available at: http://www.epa.gov/safewater/disinfection/lt2/pdfs/guide_lt2_membranefiltration_final.pdf.
- U.S. Environmental Protection Agency** (2009), "Final Report: Online Water Monitoring Utilizing an Automated Microarray Biosensor Instrument, EPA Contract # EPD09016", accessed: September 6, 2013, available at: http://cfpub.epa.gov/ncer_abstracts/index.cfm/fuseaction/display.abstractDetail/abstract/8951/report/F.
- van Hoof SCJM, Broens L, Nahrstedt A, Panglisch S and Gimbel R** (2003), "Development of a new integrity testing system", *Water Science and Technology: Water Supply* 3(5-6): 101-108.
- Verity B and Bigger SW** (1996), "The dependence of quinine fluorescence quenching on ionic strength", *International Journal of Chemical Kinetics* 28(12): 919-923.
- Victorian Government Department of Health** (2013), "Guidelines for validating treatment processes for pathogen reduction. Supporting Class A recycled water schemes in Victoria", accessed: March 7, 2013, available at: <http://www.health.vic.gov.au/water/alternative/recycling.htm>.

- Vollmer F** (2010), "Optical microresonators: label-free detection down to single viral pathogens", SPIE Newsroom.
- Vollmer F, Arnold S and Keng D** (2008), "Single virus detection from the reactive shift of a whispering-gallery mode", Proceedings of the National Academy of Sciences 105(52): 20701-20704.
- Wang C, Yan J, Cui X, Cong D and Wang H** (2010), "Preparation and characterization of magnetic hollow PMMA nanospheres via in situ emulsion polymerization", Colloids and Surfaces A: Physicochemical and Engineering Aspects 363: 71-77.
- Wang D-j, Wang X-q, Jia D-d, Luo Q, Zhen Z and Liu X-h** (2004), "Preparation of cauliflower-like PMMA particles and their formation mechanism", Chinese Journal of Polymer Science 22(3): 295-297.
- Wang Q, Liu Z-F, Kong L and Liu S-P** (2007), "Absorption and Resonance Rayleigh Scattering Spectra of the Interaction for Copper Nanoparticles with Vitamin B1", Chinese Journal of Analytical Chemistry 35(3): 365-369.
- Wang X-M, Xu S-P and Xu W-Q** (2011a), "Luminescent properties of dye-PMMA composite nanospheres", Physical Chemistry Chemical Physics 13(4): 1560-1567.
- Wang X, Xu S, Liang C, Li H, Sun F and Xu W** (2011b), "Enriching PMMA nanospheres with adjustable charges as novel templates for multicolored dye@PMMA nanocomposites", Nanotechnology 22(275608).
- WaterReuse** (2015), "Framework for Direct Potable Reuse", accessed: February 20, 2016, available at: <https://watereuse.org/watereuse-research/framework-for-direct-potable-reuse/>.
- Wee T-L, Mau Y-W, Fang C-Y, Hsu H-L, Han C-C and Chang H-C** (2009), "Preparation and characterization of green fluorescent nanodiamonds for biological applications", Diamond and Related Materials 18(2-3): 567-573.
- Wei D, Oyarzabal OA, Huang T-S, Balasubramanian S, Sista S and Simonian AL** (2007), "Development of a surface plasmon resonance biosensor for the identification of *Campylobacter jejuni*", Journal of Microbiological Methods 69(1): 78-85.
- Weller M** (2005), "Optical microarray biosensors", Analytical and Bioanalytical Chemistry 381(1): 41-43.
- Wilbert MC and Linton K** (2000), "Methods for Monitoring the Integrity of Reverse Osmosis and Nanofiltration Membrane Systems, Denver Colorado", accessed: August 7, 2013, available at: <http://www.usbr.gov/research/AWT/reportpdfs/report055.pdf>.

- WWAP** (2015), "United Nations World Water Assessment Programme. The United Nations World Water Development Report 2015: Water for a Sustainable World. Paris, UNESCO", accessed: December 3, 2015, available at: <http://www.unesco.org/new/en/natural-sciences/environment/water/wwap/wwdr/2015-water-for-a-sustainable-world/>.
- Yan Y, Li H and Myrick ML** (2000), "Fluorescence Fingerprint of Waters: Excitation-Emission Matrix Spectroscopy as a Tracking Tool", *Applied Spectroscopy* 54(10): 1539-1542.
- Yang C, Shao Q, He J and Jiang B** (2010), "Preparation of Monodisperse Magnetic Polymer Microspheres by Swelling and Thermolysis Technique", *Langmuir* 26(7): 5179-5183.
- YSI Environmental** (2001), "Water Tracing, *In Situ* Dye Fluorometry and the YSI 6130 Rhodamine WT Sensor", accessed: February 3, 2012, available at: <http://www.ysi.com>.
- Yu G-H, Wu M-J, Luo Y-H, Yang X-M, Ran W and Shen Q-R** (2011), "Fluorescence excitation–emission spectroscopy with regional integration analysis for assessment of compost maturity", *Waste Management* 31(8): 1729-1736.
- ZAPS Technologies Inc.** (2012a), "Raw Water Monitoring and Event Detection", accessed: October 10, 2013, available at: <http://www.zapstechnologies.com/wp-content/uploads/2012/05/ZAPS-RW-Monitoring-and-Event-Detection.pdf>.
- ZAPS Technologies Inc.** (2012b), "Real-Time *E. coli* Monitoring with the Liquid Station", accessed: October 10, 2013, available at: <http://www.zapstechnologies.com/wp-content/uploads/2012/07/Monitoring-E.coli-in-the-Creek.pdf>.
- ZAPS Technologies Inc.** (2013a), "Automated Online Water Quality Monitoring", accessed: October 10, 2013, available at: <http://www.zapstechnologies.com/wp-content/uploads/2013/02/Liquid-2013-Product-Brochure.pdf>.
- ZAPS Technologies Inc.** (2013b), "Technical Specification Sheet: The Liquid™ Station", accessed: October 10, 2013, available at: <http://www.zapstechnologies.com/wp-content/uploads/2012/05/Liquid-Tech-Specifications-July-2013.pdf>.
- Zeiger EH, Ho B and Williams KD** (2003), "A fluorescent technology to ensure RO antiscalant performance", *Ultrapure Water* 20(7): 36-43.
- Zepp RG, Sheldon WM and Moran MA** (2004), "Dissolved organic fluorophores in southeastern US coastal waters: correction method for eliminating Rayleigh and Raman scattering peaks in excitation–emission matrices", *Marine Chemistry* 89(1-4): 15-36.

- Zhang B-H, Wu F-Y, Wu Y-M and Zhan X-S** (2010), "Fluorescent Method for the Determination of Sulfide Anion with ZnS:Mn Quantum Dots", *Journal of Fluorescence* 20(1): 243-250.
- Zhang C-y and Hu J** (2010), "Single Quantum Dot-Based Nanosensor for Multiple DNA Detection", *Analytical Chemistry* 82(5): 1921-1927.
- Zhang C-Y, Yeh H-C, Kuroki MT and Wang T-H** (2005), "Single-quantum-dot-based DNA nanosensor", *Nature Materials* 4(11): 826-831.
- Zhang P and Liu W** (2010), "ZnO QD@PMAA-co-PDMAEMA nonviral vector for plasmid DNA delivery and bioimaging", *Biomaterials* 31(11): 3087-3094.
- Zheng J, Zhu R, He Z, Cheng G, Wang H and Yao K** (2010), "Synthesis and characterization of PMMA/SiO₂ nanocomposites by in situ suspension polymerization", *Journal of Applied Polymer Science* 115: 1975-1981.
- Zhou J-F, Li N-B and Luo H-Q** (2011), "Analytical Application of Resonance Rayleigh Scattering, Frequency Doubling Scattering, and Second-Order Scattering Spectra for the Sodium Alginate-CTAB System", *Analytical Letters* 44(4): 637-647.
- Zhu J, Li J-j and Zhao J-w** (2011), "Tuning the wavelength drift between resonance light absorption and scattering of plasmonic nanoparticle", *Applied Physics Letters* 99(10): 101901-101903.
- Zhu J, Ozdemir SK, Xiao Y-F, Li L, He L, Chen D-R and Yang L** (2010), "On-chip single nanoparticle detection and sizing by mode splitting in an ultrahigh-Q microresonator", *Nature Photonics* 4(1): 46-49.
- Zornes GE, Jansen E and Lozier JC** (2010), "Validation testing of the reverse osmosis system at Gippsland Water Factory", proceedings of WaterReuse and WSAA Speciality Conference, Sydney NSW, November 15-16.

APPENDIX A

Summary of PMMA synthesis variables (Chapter 5).

Run #	Reaction time (min)	Stirring speed (rpm)	Temp (°C)	Water volume (mL)	MMA volume (mL)	% MMA	Initiator	Initiator %	*Additive %	Size (nm)	Comments
1	40	1200	70	16	3	16%	Azobis	0.1%			
2	40	1200	70	16	3	16%	Azobis	0.1%			
3	40	1200	70	16	3	16%	Azobis	0.1%			
4	40	1200	70	32	6	16%	Azobis	0.1%			evaporated to dryness, repeated (#17)
5	40	1200	70	16	3	16%	Azobis	2.6%			change in initiator
6	40	1200	70	16	3	16%	Azobis	2.6%			monomer residual present
7	40	1000	70	16	3	16%	Azobis	2.6%			
8	40	1200	60	16	3	16%	Azobis	2.6%			poor images, seems fused
9	40	1200	80	16	3	16%	Azobis	2.6%		500	uniform charged particles
10	40	1200	65	16	3	16%	Azobis	2.6%			
11	40	1200	75	16	3	16%	Azobis	2.6%			
12	40	1200	70	16	4	20%	Azobis	2.5%			
13	40	1200	70	16	4.5	22%	Azobis	2.4%		500	uniform charged particles
14	40	1200	70	16	2.5	13%	Azobis	2.7%			
15	40	1200	70	16	2	11%	Azobis	2.8%			

Run #	Reaction time (min)	Stirring speed (rpm)	Temp (°C)	Water volume (mL)	MMA volume (mL)	% MMA	Initiator	Initiator %	*Additive %	Size (nm)	Comments
16	40	1200	70	16	3	16%	Azobis	2.6%			
17	40	1200	70	32	6	16%	Azobis	2.6%			similar to #27
18	40	1000	70	32	6	16%	Azobis	2.6%			
19	40	1200	60	32	6	16%	Azobis	2.6%			totally fused
20	40	1200	65	32	6	16%	Azobis	2.6%			
21	40	1200	75	32	6	16%	Azobis	2.6%			
22	40	1200	80	32	6	16%	Azobis	2.6%		90-430	
23	40	1200	70	32	4	11%	Azobis	2.8%			
24	40	1200	70	32	5	13%	Azobis	2.7%			
25	40	1200	70	32	7	18%	Azobis	2.6%			
26	40	1200	70	32	8	20%	Azobis	2.5%			
27	40	1200	70	32	6	16%	Azobis	2.6%			similar to #17, charged & fused
28	40	1200	70	32	6	16%	Azobis	2.6%		range	partial fusion
29	40	1200	70	32	6	16%	Azobis	2.6%		range	partial fusion
30	40	1200	70	32	6	16%	Azobis	2.6%			initiator added in stages over 20 min, residual monomer
31	40	1200	70	32	6	16%	Azobis	2.6%			residual monomer, poor emulsion, uniform particles
32	40	1200	70	32	6	16%	Azobis	2.6%			
33	40	1200	70	32	6	16%	Azobis	2.6%		260-830	pH 2, charged particles

Run #	Reaction time (min)	Stirring speed (rpm)	Temp (°C)	Water volume (mL)	MMA volume (mL)	% MMA	Initiator	Initiator %	*Additive %	Size (nm)	Comments
34	40	1200	70	32	6	16%	Azobis	2.6%		190-420	pH 10.5
35	40	1200	70	32	6	16%	Azobis	2.6%			initiator added before heating
36	40	1200	70	32	6	16%	Azobis	2.6%			same as #34, glue like pieces
37	240	1200	70	32	6	16%	Azobis	2.6%			4 hour run, uniform with some bigger spheres, no monomer
38	40	1200	70	32	6	16%	Azobis	2.6%			all reactants added and heated
39	180	1200	70	32	6	16%	Azobis	2.6%			2 hour run, different sizes, charged or fused, no monomer
40	90	1200	70	16	3	16%	Azobis	2.6%		250	1.5 hour run, uniform, smaller particles, no monomer
41	75	1200	70	16	3	16%	Azobis	2.6%			1.25 hour run, some monomer odour
42	90	1200	70	20	3	13%	Azobis	2.2%			charged or fused, different sizes, changed to 1.5 hour runs
43	120	1200	70	16	3	16%	APS	15.5%			change to new initiator (APS), residual monomer
44	120	1200	70	16	3	16%	APS	2.6%			residual monomer, very good emulsion
45	120	1200	70	16	1.5	9%	APS	2.8%		350-420	residual monomer

Run #	Reaction time (min)	Stirring speed (rpm)	Temp (°C)	Water volume (mL)	MMA volume (mL)	% MMA	Initiator	Initiator %	*Additive %	Size (nm)	Comments
46	120	1200	70	16	1	6%	APS	2.9%			residual monomer
47	120	1200	70	16	0.5	3%	APS	3.0%		140-180	residual monomer
48	120	1200	70	16	0.5	3%	APS	3.0%			initiator added in stages, no residual monomer
49	120	1200	70	16	1.5	9%	APS	2.8%	A 40%		large particles, some fused mostly very small particles
50	120	1200	70	16	1.5	9%	APS	2.8%	A 40%	70-490	residual monomer
51	120	1200	70	16	0.5	3%	APS	3.0%	A 40%	70-80	residual acetone, some larger pieces
52	120	1200	70	16	1.5	9%	APS	2.8%	A 10%	80-360	residual acetone, new APS, different sizes
53	120	200	70	16	1.5	9%	APS	2.8%	A 10%	360	residual acetone, uniform spheres
54	120	400	70	16	1.5	9%	APS	2.8%	A 10%		very uniform
55	120	600	70	16	1.5	9%	APS	2.8%	A 10%		high order, very few big particles
56	120	800	70	16	1.5	9%	APS	2.8%	A 10%		few very small ones
57	120	1000	70	16	1.5	9%	APS	2.8%	A 10%		few smaller ones
58	120	400	70	16	1.5	9%	APS	2.8%	A 40%	110-740	new heating plate
59	120	1000	70	16	1.5	9%	APS	2.8%	A 40%		different sizes, temperature problems
60	120	1000	69-71	16	1.5	9%	APS	2.8%	A 40%		different sizes
61	120	750	70	16	1.5	9%	APS	2.8%	A 40%		porous particles

Run #	Reaction time (min)	Stirring speed (rpm)	Temp (°C)	Water volume (mL)	MMA volume (mL)	% MMA	Initiator	Initiator %	*Additive %	Size (nm)	Comments
62	120	750	68-71	24	1.5	6%	APS	2.0%	A 10%		very uniform and high order
63	120	750	70	16	1.5	9%	APS	2.8%	A 10%		temperature drop of 5 degrees at 90 minutes
64	120	750	70	24	1.5	6%	APS	2.0%	A 10%	300	uniform particles
65	120	1200	70	16	1.5	9%	APS	2.8%	A 10%	350	separated, high order, uniform spheres
66	120	750	70	16	0.5	3%	APS	3.0%	A 11%		temperature drop of 8 degrees at 60 minutes, change in heating plate
67	120	750	70	16	0.5	3%	APS	3.0%			charged particles
68	120	750	70	16	1.5	9%	APS	2.8%	A 20%	350	some very small particles, mainly uniform
69	120	750	70	16	1.5	9%	APS	2.8%	S 0.5%	<50	changed to high stirring speed, better results
70	120	1200	70	16	1.5	9%	APS	2.8%	S 0.5%	<50	
71	120	1200	70	16	1.5	9%	APS	2.8%	S 1.0%	<50	
72	120	1200	70	16	1.5	9%	APS	1.4%	S 0.25%	<50	
73	120	1200	70	24	0.5	2%	APS	1.0%	A 10%	<200	
74	120	1200	70	16	1.5	9%	APS	1.4%	S 1.0%		
75	120	1200	70	16	1.5	9%	APS	1.4%		50	same as #74
76	120	1200	70	16	1.5	9%	APS	1.4%	S 0.25%, A 10%		
77	120	1200	70	16	1.5	9%	APS	1.4%	S 0.25%		

Run #	Reaction time (min)	Stirring speed (rpm)	Temp (°C)	Water volume (mL)	MMA volume (mL)	% MMA	Initiator	Initiator %	*Additive %	Size (nm)	Comments
78	120	1200	70	16	1.5	9%	APS	1.4%	S 2.25%		
79	120	1200	70	16	0.5	3%	APS	1.5%	S 1.50%		
80	120	1200	70	16	1.5	9%	APS	1.4%	S 0.25%		no nitrogen purge
81	120	1500	70	16	0.5	3%	APS	1.5%	S 1.50%		
82	120	1200	70	16	1.5	9%	APS	1.4%			quinine added, range of sizes
83	120	1200	70	16	0.5	3%	APS	1.5%			RWT added
84	120	1200	70	15.3	2.7	15%	APS	1.4%			
85	120	1200	70	15.75	2.25	12%	APS	1.4%			
86	120	1200	70	16.2	1.8	10%	APS	1.4%			
87	120	1200	70	16.65	1.35	7%	APS	1.4%			
88	120	1200	70	17.1	0.9	5%	APS	1.4%			
89	120	1200	70	17.55	0.45	2%	APS	1.4%			
90	120	1200	70	16.5	1.5	8%	APS	1.4%			
91	120	1200	70	16.05	1.5	9%	APS	1.4%	A 2.5%		
92	120	1200	70	15.6	1.5	9%	APS	1.5%	A 5%		
93	120	1200	70	14.7	1.5	9%	APS	1.5%	A 10%		
94	120	1200	70	13.8	1.5	10%	APS	1.6%	A 15%		
95	120	1200	70	12.9	1.5	10%	APS	1.7%	A 20%		
96	120	1200	70	11.1	1.5	12%	APS	2.0%	A 30%		
97	120	1200	70	16.5	1.5	8%	APS	1.4%			new monomer

Run #	Reaction time (min)	Stirring speed (rpm)	Temp (°C)	Water volume (mL)	MMA volume (mL)	% MMA	Initiator	Initiator %	*Additive %	Size (nm)	Comments
98	120	1200	70	16.5	1.5	8%	APS	1.4%			
99	120	1200	70	16.2	1.8	10%	APS	1.4%	S 0.42%		
100	120	1200	70	16.65	1.35	7%	APS	1.4%	S 0.56%		
101	120	1200	70	17.1	0.9	5%	APS	1.4%	S 0.83%		
102	120	1200	70	17.55	0.45	2%	APS	1.4%	S 1.67%		
103	120	1200	70	17.82	0.18	1%	APS	1.4%	S 4.17%		
104	120	1200	70	160	15	9%	APS	2.8%	S 0.50%		upscale of #70

*S = surfactant, A = acetone

Selected SEM images are shown in the following pages.

